



Lee, Ho Sum Jason (2023) *Buckling and first-ply failure of mechanically coupled composite structures*. PhD thesis.

<https://theses.gla.ac.uk/83935/>

Copyright and moral rights for this work are retained by the author

A copy can be downloaded for personal non-commercial research or study, without prior permission or charge

This work cannot be reproduced or quoted extensively from without first obtaining permission in writing from the author

The content must not be changed in any way or sold commercially in any format or medium without the formal permission of the author

When referring to this work, full bibliographic details including the author, title, awarding institution and date of the thesis must be given

Enlighten: Theses

<https://theses.gla.ac.uk/>
research-enlighten@glasgow.ac.uk



University
of Glasgow

BUCKLING AND FIRST-PLY FAILURE OF
MECHANICALLY COUPLED COMPOSITE STRUCTURES

HO SUM JASON LEE

Submitted in fulfilment of the requirements for the

Degree of Doctor of Philosophy

Aerospace Sciences Research Division

School of Engineering

College of Science and Engineering

University of Glasgow

October 2023

© Ho Sum Jason Lee, October 2023

ABSTRACT

Double angle-ply or 'Double-Double' (DD) laminates offer new design possibilities in laminated composite materials design, permitting non-standard ply orientations with new layup configurations. DD laminates can be viewed as an alternative to so-called 'Variable Angle Tow' (VAT) laminates. The latter allow each ply within the laminate to possess constantly changing fibre directions and ply thicknesses. In contrast, double angle-ply technology uses straight fibres (with non-standard ply orientations and may confer similar benefits to VAT laminates, but without the added design complexity associated with a continuously changing fibre orientation and ply thicknesses, or indeed without the added manufacturing complexity and equipment costs involved in producing VAT laminates. This research focuses on the use of a lamination parameter design space as a way of designing laminated composite materials with both conventional and DD configurations.

Design spaces of compression and shear buckling of finite length *Bend-Twist* (*B-T*) coupled laminates manufactured from traditional ply orientations (containing 0° , 90° and $\pm 45^\circ$ ply orientations), with simply supported edges, are investigated. Both local and global optima of compression and shear buckling are shown in the lamination parameter design space, with practical design rules applied. Shear buckling contour maps demonstrate significant improvements in shear buckling performance with the presence of *B-T* coupling.

Buckling and First-Ply Failure (FPF) performances of DD laminates are discussed and compared to standard laminate configurations through stiffness matching. Polar plots have demonstrated that DD designs with coupled properties offer comparable FPF strength to standard laminates when off-axis orientation is applied to maximise anisotropy or *Extensional-Shear* (*E-S*) coupling. It is demonstrated that DD laminates with *B-T* coupling can provide significant improvement in FPF strength over traditional laminates without reducing the buckling load.

CONTENTS

ABSTRACT	I
LIST OF FIGURES	XI
LIST OF TABLES	XV
ACKNOWLEDGEMENTS	XVII
DECLARATION	XVIII
NOMENCLATURE	XXI
1 INTRODUCTION	1
1.1 BACKGROUND	1
1.2 LITERATURE REVIEW ON THE FUNDAMENTALS OF ADVANCED COMPOSITES	4
1.2.1 BACKGROUND KNOWLEDGE OF COMPOSITE LAMINATE MECHANICS	4
1.2.2 CLASSICAL LAMINATION THEORY (CLT)	5
1.2.3 ELASTIC COUPLING	6
1.2.4 CLASSIFICATION OF COMPOSITE LAMINATES	10
1.2.5 LAMINATION PARAMETERS	14
1.2.6 BUCKLING	19

1.2.7	FIRST PLY FAILURE (FPF)	23
1.2.8	VARIABLE-STIFFNESS LAMINATES	27
1.2.9	DOUBLE ANGLE-PLY LAMINATES (DOUBLE-DOUBLE, DD)	30
1.3	THESIS OUTLINE	34
1.4	RESEARCH OBJECTIVES	34
1.5	PUBLICATIONS	35
2	THEORY AND EXAMPLE CALCULATIONS AND FEA MODELLING	36
2.1	CLASSICAL LAMINATE THEORY (CLT)	36
2.1.1	THEORY	36
2.1.2	EXAMPLE 1. CALCULATION OF THE ABD MATRIX FROM MECHANICAL PROPERTIES OF THE LAMINATE	37
2.2	LAMINATION PARAMETERS, NON-DIMENSIONAL PARAMETERS AND ABD MATRIX	39
2.2.1	THEORY	40
2.2.2	EXAMPLE 2. CALCULATION OF THE ABD MATRIX FROM NON-DIMENSIONAL PARAMETERS	44
2.2.3	EXAMPLE 3. CALCULATION OF ABD MATRIX FROM THE LAMINATION PARAMETERS	47
2.3	BUCKLING	49
2.3.1	THEORY	49
2.3.2	EXAMPLE 4. CALCULATION OF BUCKLING LOAD AND BUCKLING FACTOR OF A SQUARE LAMINATE SUBJECT TO A UNIFORM AXIAL LOAD	50
2.4	FINITE ELEMENT ANALYSIS MODELLING	51

3	COMPRESSION AND SHEAR BUCKLING PERFORMANCE OF FINITE LENGTH PLATES WITH BENDING-TWISTING COUPLING	55
3.1	INTRODUCTION AND MOTIVATION TO LAMINATE BUCKLING LOAD OPTIMISATION USING LAMINATION PARAMETER DESIGN SPACE	55
3.2	DESIGN SPACE INTERROGATION	57
3.2.1	STIFFNESS AND LAMINATION PARAMETER RELATIONS	62
3.2.2	EFFECT OF DESIGN HEURISTICS ON THE LAMINATION PARAMETER DESIGN SPACE	63
3.3	BUCKLING PERFORMANCE OF FINITE LENGTH PLATES	65
3.3.1	CONTOUR MAPPING FOR COMPRESSION BUCKLING	66
3.3.2	CONTOUR MAPPING FOR SHEAR BUCKLING	78
3.3.3	SURFACE CONTOUR MAPPING FOR COMPRESSION AND SHEAR BUCKLING	83
3.4	CONCLUSION	91
4	DOUBLE ANGLE-PLY (DD) LAMINATES	93
4.1	INTRODUCTION AND MOTIVATION TO DOUBLE ANGLE-PLY LAMINATES AND OFF-AXIS ALIGNMENT	93
4.2	METHODOLOGY	96
4.3	DESIGN SPACES OF DOUBLE ANGLE-PLY LAMINATE DESIGNS	100
4.4	OFF-AXIS ALIGNMENT	111
4.5	COMPRESSION TEST	123
4.6	CONCLUSION	132
5	COUPLING EFFECTS	133
5.1	INTRODUCTION	133
5.2	BENDING-TWISTING COUPLING	135

5.3	STIFFNESS MATCHING	138
5.3.1	FIRST PLY FAILURE OF DD LAMINATES WITH BENDING-TWISTING COUPLING	140
5.4	COMPRESSION BUCKLING	154
5.5	CONCLUSION	161
6	CONCLUSION AND FUTURE WORK	162
6.1	CONCLUSION	162
6.2	FUTURE WORK	165
6.2.1	DESIGN SPACES AND CONTOUR MAPS	165
6.2.2	BOUNDARY CONDITION	166
6.2.3	SHEAR BUCKLING	166
6.2.4	FIRST PLY FAILURE STRENGTH	167
6.2.5	EXPERIMENTAL WORK	167
	BIBLIOGRAPHY	178
	APPENDIX	179
A1	ABAQUS INPUT CODES FOR COMPRESSION BUCKLING WITH ABD MATRIX INPUT	179
A2	EXTRACTS OF ABAQUS INPUT CODES FOR COMPRESSION BUCKLING WITH STACKING SEQUENCE	181
A3	EXTRACTS OF ABAQUS INPUT CODES FOR SHEAR LOADING	182
A4	STACKING SEQUENCES	184
A5	24PLYDDRESULTS-FULL	198
A6	20-PLY DD LAMINATES RESULTS	202

LIST OF FIGURES

1.1	Components on Airbus airliners made from composite from 1970's to 2000's [2].	2
1.2	Composite structures used on aircraft from 1975 to 2010 [5].	2
1.3	Illustration of a laminate in (a): x-z plane and (b): x-y plane [10].	5
1.4	A box model illustrating a <i>B-T</i> coupled wing structure or a wind turbine blade, showing (a) general box configuration; (b) the deformation of the top and bottom skin and; (c) the B-T coupled deformation [15].	7
1.5	An <i>Extension-Shear</i> coupled laminate [21].	9
1.6	An <i>Bend-Twist</i> Coupled laminate [22].	9
1.7	Illustration of a laminated plate before and after buckling deformation from [6].	19
1.8	Illustration of (a) plate and (b) column buckling [49].	19
1.9	Illustrations of buckling curves for: (a) Compression and (b) Shear buckling [52]	21
1.10	Compression buckling contours from [54]: (a) $\zeta_9 - \zeta_{10}$ where ζ_{11} and $\zeta_{12} = 0$ and; (b) $\zeta_{11} - \zeta_{12}$ where $\zeta_9 = 0.5$ and $\zeta_{10} = -0.2$.	22
1.11	Illustration of VAT laminates with fibre angles varying along (a) longitudinal and (b) vertical axes [71].	28
1.12	Thickness variation illustration of (a) AFP and (b) CTS technologies [9].	30
2.1	The relationship between non-dimensional parameters, lamination parameters and ABD matrix.	44

2.2	Illustration of the procedure of finding the lamination parameter using non-dimensional parameters.	45
2.3	Illustration of the FEA model mesh.	52
2.4	Illustration of the buckling pattern for (a) ABD matrix and (b) stacking sequence inputs with corresponding eigenvalues.	53
2.5	Illustration of the shear buckling pattern from FEA model compared to literature.	54
3.1	Lamination parameter design spaces for symmetric Bend-Twist coupled laminates with up to 21 plies, with 10% rule and ply contiguity constraints (≤ 3) applied, corresponding to point clouds for: (a) extensional stiffness (ξ_1, ξ_2), including ply percentage mapping; (b) three-dimensional representation of the lamination parameter design space for bending stiffness with 20 randomly chosen points, and; (c) 3-D representation of the lamination parameter design space highlighting the planes with $\xi_{11} = 0$ and $\xi_{11} = 0.5$.	59
3.2	Orthographic projections (a): plan, (b) front elevation and (c) side views of point clouds for bending stiffness ($\xi_9, \xi_{10}, \xi_{11}$), corresponding to symmetric <i>Bend-Twist</i> coupled laminates with up to 21 plies, with 10% rule and ply contiguity constraints (≤ 3) applied.	61
3.3	Orthographic projections (a): plan, (b) front elevation and (c) side views of point clouds for bending stiffness ($\xi_9, \xi_{10}, \xi_{11}$), corresponding to Quasi-Isotropic laminates.	64
3.4	Compression buckling Garland curves for $\xi_{11} = 0$ (solid lines) and $\xi_{11} = 0.5$ (broken lines). The corresponding lamination parameter coordinates ($\xi_{0.5}$) are given alongside each curve.	68
3.5	Compression buckling contours $k_x (= N_x b^2 / \pi^2 D_{Iso})$ for $\xi_{11} = 0.0$, with: (a) $a/b = 1.0$ (including parabolic bounds after Ref. [54]; (b) $a/b = 1.5$ and; (c) $a/b = 2.0$.	69
3.6	Compression buckling contours map construction for $a/b = 2.0$, involving superposition of contour maps for each buckling mode, representing $m = 1, 2, 3$ and 4 in Eqn. 1.18. Shading illustrates the extent of each mode region, corresponding to minimum k_x .	72

- 3.7 Compression buckling contours, $k_x (= N_x b^2 / \pi^2 D_{Iso})$, for $\xi_{11} = 0.5$ with: (a) $a/b = 1.0$; (b) $a/b = 1.5$ and (c) $a/b = 2.0$. 77
- 3.8 Illustration of the plate axis system, positive shear load, positive fibre orientation with respect to the x-axis, and aspect ratio (a/b). 78
- 3.9 Positive and Negative Shear buckling factor contours, $k_{xy} (= N_{xy} b^2 / \pi^2 D_{Iso})$, for $\xi_{11} = 0.0$ with: (a) $a/b = 1.0$; (b) $a/b = 1.5$, and (c) $a/b = 2.0$. 79
- 3.10 Negative Shear buckling factor contours, $k_{xy} (= N_{xy} b^2 / \pi^2 D_{Iso})$, for $\xi_{11} = 0.5$ with: (a) $a/b = 1.0$; (b) $a/b = 1.5$ and (c) $a/b = 2.0$. 80
- 3.11 Positive Shear buckling factor contours, $k_{xy} (= N_{xy} b^2 / \pi^2 D_{Iso})$, for $\xi_{11} = 0.5$ with: (a) $a/b = 1.0$; (b) $a/b = 1.5$ and (c) $a/b = 2.0$. 81
- 3.12 Lamination parameter design space surface contours for Compression buckling factor, $k_x (= N_x b^2 / \pi^2 D_{Iso})$, with $a/b = 1$, corresponding to: (a) Left (sloping) face; (b) Front (sloping) face; (c) Right (sloping) face and; Rear (sloping) face. 84
- 3.13 Lamination parameter design space surface contours for Compression buckling factor, $k_x (= N_x b^2 / \pi^2 D_{Iso})$, with $a/b = 1.5$, corresponding to: (a) Left (sloping) face; (b) Front (sloping) face; (c) Right (sloping) face and; Rear (sloping) face. 85
- 3.14 Lamination parameter design space surface contours for Compression buckling factor, $k_x (= N_x b^2 / \pi^2 D_{Iso})$, with $a/b = 2$, corresponding to: (a) Left (sloping) face; (b) Front (sloping) face; (c) Right (sloping) face and; Rear (sloping) face. 86
- 3.15 Lamination parameter design space surface contours for Positive Shear buckling factor, $k_{xy} (= N_{xy} b^2 / \pi^2 D_{Iso})$, with $a/b = 1$, corresponding to: (a) Left (sloping) face; (b) Front (sloping) face; (c) Right (sloping) face and; Rear (sloping) face. 88
- 3.16 Lamination parameter design space surface contours for Positive Shear buckling factor, $k_{xy} (= N_{xy} b^2 / \pi^2 D_{Iso})$, with $a/b = 1.5$, corresponding to: (a) Left (sloping) face; (b) Front (sloping) face; (c) Right (sloping) face and; Rear (sloping) face. 89
- 3.17 Lamination parameter design space surface contours for Positive Shear buckling factor, $k_{xy} (= N_{xy} b^2 / \pi^2 D_{Iso})$, with $a/b = 2$, corresponding to: (a) Left (sloping) face; (b) Front (sloping) face; (c) Right (sloping) face and; Rear (sloping) face. 90

-
- 4.1 Illustration of the off-axis alignment on the x-y axis. 94
- 4.2 Lamination parameter design spaces for laminate **d** from Table 4.1 corresponding to (a) extension stiffness and; (b) bending stiffness, with the lines of constant compression buckling factor $k_x = 4.0$. Compression buckling contour maps for aspect ratio (c) $a/b = 1.0$ and; (d) $a/b = 1.5$. 102
- 4.3 Feasible design space for (a) extension stiffness and; (b) bending stiffness, for the angles switched DD laminate **d** with bold lines that pass through the blue points representing constant compression buckling factor, $k_x = 4.0$. 103
- 4.4 Illustration of: (a) a bubble plot with comparison of a full size bubble at $(\xi_1, \xi_2) = (1, 1)$; (b) a 3-D conversion of the bubble plot for laminate **d** and (c) comparisons between 6 failure criteria with ψ , and ϕ ranging from 0° to 12° . 105
- 4.5 Strength comparisons for fully uncoupled Standard laminates (satisfying 10% rule) and DD laminates for stacking sequences **a** to **d** with angles: (a) as listed in Table 4.1; (b) switched; stacking sequences **e** and **f** with angles: (c) as listed in Table 4.1; (d) switched. Standard laminates are superimposed on designs **a** to **f** with angles: (e) listed in Table 4.1 and; (f) switched. Strength values are indicated by bubble area, normalized against maximum (100%) strength for 0° ply laminate shown at $(\xi_1, \xi_2) = (1, 1)$. 107
- 4.6 The bending stiffness design space for the laminates with normal angle configurations (a): **a**; (b): **b**; (c): **c**; (d): **d**; (e): **e** and (f): **f**. 109
- 4.7 The bending stiffness design space for the laminate with angle switched configurations (a): **a**; (b): **b**; (c): **c**; (d): **d**; (e): **e** and (f): **f**. 110
- 4.8 Strength comparisons for off-axis orientation β between a full envelope of 24 plies: (a) Isotropic laminate; DD laminate design: (b) **a**; (c) **b**; (d) **c**; (e) **d**; (f) **e** and (g) **f**; (h) superimposed laminates **a** to **f**; (i) Balanced and symmetric; (j) Extension-Shearing coupled (only) design and; (k) Superimposed laminate **d** and Extension-Shearing coupled design, all subject to equal compressive force resultant (N_x). 113

-
- 4.9 Illustration of the extensional stiffness design spaces of the 6 DD laminate designs with and without off-axis alignment, and bubbles indicating the normalized FPF strength 116
- 4.10 Illustration of the extension stiffness design spaces of the 6 angle switched DD laminate designs with and without off-axis alignment, and bubbles indicating the normalized FPF strength 118
- 4.11 Strength comparisons for off-axis orientation β between a full envelope of 24 ply: (a) Isotropic laminate; (b) DD laminate design *d*; (c) Balanced and symmetric; (d) *E-S* coupled (only) design and; (e) Superimposed laminate *d* and *E-S* coupled design, normalised to equal compressive force resultant (N_x) of 5027N. 120
- 4.12 The relationship between the extensional ξ_{1-4} and bending stiffness lamination parameters ξ_{9-12} and β for DD laminate designs: (a) *a*; (b) *b*; (c) *c*; (d) *d*; (e) *e* and (f) *f*.
122
- 4.13 Manufactured DD laminates. 124
- 4.14 Manufactured DD laminates. 125
- 4.15 Samples after failure for (a) all *E-S* laminates and (b) a zoomed in capture of one of the laminates after failure. 127
- 4.16 Stress-strain curves of specimens for (a): Isotropic; (b): DD design *d*; (c): *Extension-Shear* and; (d): Balanced and Symmetric laminates. 130
- 5.1 Illustration of the 2-D extensional stiffness design space of 24-ply design sub-group [16/8]₁₅. 142
- 5.2 Illustration of the 4-D bending stiffness design space of 24-ply design sub-group [16/8]₁₅. 143
- 5.3 Illustration of the 2-D extensional stiffness design space of 20-ply design sub-group [12/8]₁₃. 145
- 5.4 Illustration of the 4-D bending stiffness design space of the 20-ply design sub-group [12-8]₆. 146

5.5	Illustration of the 2-D extensional stiffness design space of 20-ply design sub-group [8/12] ₆ .	147
5.6	Illustration of the 4-D bending stiffness design space of the 20-ply design sub-group [8-12] ₆ .	148
5.7	Illustration of the 2-D extensional stiffness design space of 16-ply design sub-group [8/8] ₄ .	150
5.8	Illustration of the 4-D bending stiffness design space of the 16-ply design sub-group [8-8] ₄ .	151
5.9	Illustration of the 2-D extensional stiffness design space of 12-ply design sub-group [4/8] ₁ .	152
5.10	Illustration of the 4-D bending stiffness design space of the 12-ply design sub-group [4-8] ₁ .	153
6.1	(a) Top view and; (b) bottom view of the 12-ply laminate made from woven fabric.	168

LIST OF TABLES

1.1	Material properties that can be improved with composite materials.	3
1.2	Illustration of different combinations of coupling behaviour for B matrix.	8
2.1	Illustration of the transformed reduced stiffness for -45° , 45° , 0° and 90° layers.	38
3.1	Effect of ply continuity constraints ($1, \leq 2, \leq 3$) on the number of stacking sequence solutions for each ply number grouping (n), balanced and symmetric representing <i>Bend-Twist</i> coupled designs from databases with the 10% rule applied.	60
3.2	Buckling coefficients for Eqn. 2.15, for all discrete mode regions of Fig. 3.5c, with $\xi_{11} = 0$ and $a/b = 2.0$.	73
3.3	Coefficients for Eqn. 3.3, representing mode boundaries in Fig. 3.5c, with $\xi_{11} = 0$ and $a/b = 2.0$.	74
4.1	Stacking sequences for fully uncoupled double angle-ply laminates with 24 layers. The listed angles (ϕ , ψ) produce bending isotropy.	98
4.2	Engineering properties of T300/5208 graphite/epoxy.	99
4.3	Plate width (mm), b , corresponding to 24-ply DD design with coincident buckling and first ply failure.	123
4.4	Width-to-thickness ratio, b/H , corresponding to optimal 24 ply DD designs in Table 4.3.	123
4.5	Measured dimensions of manufactured laminate designs.	126

4.6	Resulted failure strength, maximum stress, strain and modulus obtained from using measured dimensions.	128
4.7	Resulted failure strength, maximum stress, strain and modulus obtained from using designed dimensions.	129
4.8	First ply Failure load predictions of the fully isotropic, DD design d with $\beta=-46.1^\circ$, E - S coupled and balanced and symmetric designs $\beta=37.3^\circ$ under compressive load.	129
5.1	The bending stiffness lamination parameters relationships of standard and DD laminates in 2-D and 3-D design spaces.	134
5.2	Thickness, stacking sequence and the bending stiffness of the standard quads laminates.	136
5.3	Thickness, stacking sequence and the bending stiffness of the DD laminates with equivalent ζ_9 and ζ_{10} .	136
5.4	List of combination of arbitrary B - T coupling applied to the standard and DD laminate designs.	136
5.5	Buckling factors of standard quads and DD designs under the ζ_{11} and ζ_{12} combinations listed in Table 5.4 for $AR = 1.0$.	137
5.6	Buckling factors of standard quads and DD designs under the ζ_{11} and ζ_{12} combinations listed in Table 5.4 for $AR = 1.5$.	137
5.7	Buckling factors of standard quads and DD designs under the ζ_{11} and ζ_{12} combinations listed in Table 5.4 for $AR = 2.0$.	137
5.8	Number of DD laminate designs that match the design constraints for each laminate thickness.	139
5.9	Buckling and first ply failure performances of the fully uncoupled laminate designs with standard configurations listed in Table 5.2.	140
5.10	24-ply designs, stacking sequences and ψ_{\pm} , ϕ_{\pm} values that produce bending stiffness that matches $(\zeta_9, \zeta_{10}) = (-0.045, -0.967)$.	141

-
- 5.11 20-ply designs, stacking sequences and ψ_{\pm}, ϕ_{\pm} values that produce bending stiffness that matches $(\zeta_9, \zeta_{10}) = (-0.102, -0.692)$. 144
- 5.12 16-ply designs, stacking sequences and ψ_{\pm}, ϕ_{\pm} values that produce bending stiffness that matches $(\zeta_9, \zeta_{10}) = (-0.070, -0.852)$. 149
- 5.13 12-ply designs, stacking sequences and ψ_{\pm}, ϕ_{\pm} values that produce bending stiffness that matches $(\zeta_9, \zeta_{10}) = (-0.083, -0.815)$. 152
- 5.14 Number of individual designs from sub-groups of 24, 20 and 16 plies laminate with improved FPF strength. 154
- 5.15 List of stacking sequences of 10 designs from 24-ply *B-T* coupled DD laminate design sub-group $[16/8]_{15}$. All designs possess identical extensional stiffness $(\zeta_1, \zeta_2, \zeta_3, \zeta_4) = (0.295, -0.365, 0, 0)$ and bending stiffness $(\zeta_9, \zeta_{10}) = (-0.007, -0.926)$. 155
- 5.16 List of stacking sequences of 10 designs from 20-ply *B-T* coupled DD laminate design sub-group $[8/12]_6$. All designs possess identical extensional stiffness $(\zeta_1, \zeta_2, \zeta_3, \zeta_4) = (0.252, -0.466, 0, 0)$ and bending stiffness $(\zeta_9, \zeta_{10}) = (-0.102, -0.692)$. 156
- 5.17 List of stacking sequences of 10 designs from 20-ply *B-T* coupled DD laminate design sub-group $[12/8]_8$. All designs possess identical extensional stiffness $(\zeta_1, \zeta_2, \zeta_3, \zeta_4) = (0.252, -0.466, 0, 0)$ and bending stiffness $(\zeta_9, \zeta_{10}) = (-0.102, -0.692)$. 157
- 5.18 List of stacking sequences of 10 designs from 16 ply *B-T* coupled DD laminate design sub-group $[4/8]_4$. All designs possess identical extensional stiffness $(\zeta_1, \zeta_2, \zeta_3, \zeta_4) = (0.228, -0.579, 0, 0)$ and bending stiffness $(\zeta_9, \zeta_{10}) = (-0.070, -0.850)$. 158
- 5.19 Buckling and first ply failure performance comparison between 24-ply standard quad and 10 designs from $[16/8]_{15}$ *Bend-Twist* coupled double angle-ply sub-group. 159
- 5.20 Buckling and first ply failure performance comparison between 20-ply standard quad and 10 designs from $[8/12]_6$ *Bend-Twist* coupled double angle-ply sub-group. 159
- 5.21 Buckling and first ply failure performance comparison between 20-ply standard quad and 10 designs from $[12/8]_8$ *Bend-Twist* coupled double angle-ply sub-group. 160

-
- 5.22 Buckling and first ply failure performance comparison between 16-ply standard quad and 10 designs from $[8/8]_4$ *Bend-Twist* coupled double angle-ply sub-group. 160
- A1 Stacking sequences and Lamination Parameter coordinates for Quasi Isotropic laminates for 16 ply laminates, i.e. $(\zeta_1, \zeta_2) = (0, 0)$. Here the 10% rule has been applied, which corresponds to the minimum number of plies in each of the standard ply orientations. Ply contiguity constraints have also been applied, which limits the maximum of number of adjacent plies with the same orientation to 3, as is now common design practice. The listings are grouped by matching orthotropic bending stiffness (ζ_9, ζ_{10}) and ordered by increasing Bending-Twisting coupling, ζ_{11} . Symbols +, - \circ and \bullet represent standard ply angles 0° , 90° and $\pm 45^\circ$, respectively. 184
- A2 24-ply designs, stacking sequences and ψ_\pm, ϕ_\pm values that produce bending stiffness that matches that $(\zeta_9, \zeta_{10}) = (-0.045, -0.967)$. 198
- A3 20-ply designs, stacking sequences and ψ_\pm, ϕ_\pm values that produce bending stiffness that matches that $(\zeta_9, \zeta_{10}) = (-0.102, -0.692)$. 202

ACKNOWLEDGEMENTS

Four years is a long journey, especially with what happened for the past 4 years. It would not be possible without the support I received, in all the different ways.

First and foremost, I would like to thank my supervisors, Associate Prof Christopher York and Dr Philip Harrison for their invaluable advice, continuous support, and patience throughout my PhD study. They have encouraged and enlightened me with their immense knowledge and experience have encouraged, not only academically but also my personal life, I feel very lucky to be their student. Although Associate Prof York left the University of Glasgow and moved to Singapore for a better opportunity, he never stop supporting and giving me guidance throughout the entire 4 years, his insight and knowledge always amaze me. He also invited me to his lab at the Singapore Institution of Technology (SIT) to carry out manufacturing and experimental work, but the trip did not proceed because of COVID. Secondly, Dr Harrison was not my primary supervisor at the beginning of my PhD study, but he agreed to take me as his PhD student after Prof York left. I am very grateful, as he tried his best to understand and learn about my research even though his area of research is in the manufacturing area. He always gave me meaningful feedback and advice with his knowledge and experience, which I never thought of.

Towards the end of the study, Dr Periyasamy Manikandan, whom I never met Mani in person, and Prof York helped me to conduct some experiments that I have not been able to do. Mani also answered all the questions that I had very patiently.

I also want to thank a few individuals that help and supported me in this journey, without them I would not be able to complete this 4-year study. Firstly, Paul Mori, from the University of Glasgow counselling service. During COVID, I suffered from depression, primarily because of the endless delay of the Singapore experimental trip, Dr. Harrison suggested seeking help from the counselling service at the university. Paul taught me ways to deal with the depression and

helped me get back on track with my work, without help from Paul who knows if I would be able to complete my study.

Finally, thank you to my girlfriend, family and friends, who supported me throughout the journey. It had been a rough time during the pandemic, luckily my girlfriend was there with me. I haven't seen my family since 2019 because of the pandemic, but they had been very understanding and supportive. Also, to everyone else who helped and supported me, Thank you.

DECLARATION

I declare that the presented thesis is the result of my own personal work and does not include work forming part of a thesis presented successfully for another degree, any joint work and contributions of others are clearly indicated.

Ho Sum Jason Lee

October 2023

NOMENCLATURE & ABBREVIATIONS

NOMENCLATURE

All units of measurement throughout this thesis conform to the *Système Internationale*, with deviations from this rule noted where appropriate.

A_{ij}	Extensional stiffness matrix and elements
B_{ij}	Extensional-bending couple
D_{ij}	Bending stiffness matrix and elements
a	Length of laminate (mm)
b	Width of laminate (mm)
β	Off-axis alignment ($^{\circ}$)
C_{ij}	Stiffness coefficients
\bar{C}	Stiffness matrix of material in Cartesian coordinate system
$E_{1,2}$	In-plane longitudinal and transverse Young's moduli
G_{12}	In-plane shear modulus
H	Total thickness of laminate (mm)
$k_{x,xy}$	Compression and shear buckling factors
$M_{x,y,xy}$	Bending moments in x , y and xy directions
N_x	Applied load (N/mm)
N_{xy}	Shear load (N/mm)
n	Number of plies in laminate
P	Applied compression load (N)
Q_{ij}	Reduced stiffnesses
\bar{Q}_{ij}	Transformed reduced stiffnesses

S_{ij}	Material compliance
t	Thickness of one ply (mm)
U_i	Laminate invariants
X_t, X_c	Allowable tensional and compressional stresses in x direction
Y_t, Y_c	Allowable tensional and compressional stresses in y direction
$z_{k,k-1}$	Location of the interfaces for layer k
$\epsilon_{x,y,xy}$	Direct and shear strain in x and y directions
λ	Eigenvalue from FEA
n_+, n_-, n_o, n_\bullet	Non-dimensional parameters for extensional stiffness
$\chi_+, \chi_-, \chi_o, \chi_\bullet$	Non-dimensional parameters for coupling stiffness
$\zeta_+, \zeta_-, \zeta_o, \zeta_\bullet$	Non-dimensional parameters for bending stiffness
ν_{ij}	Poisson's ratio
θ	Angle ply orientation of laminate
ξ_1, ξ_2 or ξ_{1-2}^A	Lamination parameters for orthotropic extensional stiffness
ξ_3, ξ_4 or ξ_{3-4}^A	Lamination parameters for coupled extensional stiffness
ξ_{5-8} or ξ_{1-4}^B	Lamination parameters for in-plane and out-of-plane coupling stiffness
ξ_9, ξ_{10} or ξ_{1-2}^D	Lamination parameters for orthotropic bending stiffness
ξ_{11}, ξ_{12} or ξ_{3-4}^D	Lamination parameters for coupled bending stiffness
$\epsilon_{x,y,xy}$	Direct and shear strain in x and y directions
$\kappa_{x,y,xy}$	Curvature in x and y directions
ϕ_{\pm}, ϕ_{\pm}	Ply orientation for double angle-ply laminates
σ	Direct stress
τ	Shear stress
ϵ	Strain
γ	Shear strain

SUBSCRIPTS

S Symmetric

Iso Isotropic

r	Repeat
T	Total
F	Finite
0	Zero

ABBREVIATION

AFP	Automatic Fibre Placement
<i>a/b</i>	Aspect Ratio
B-T	Bending-Twisting coupling
CFRP	Carbon Fibre Reinforced Polymer
CLT	Classical lamination theory
CTS	
DD	Double angle-ply/ Double-double
E-S	Extension-Shearing coupling
E-S-B-T	Extension-Shearing and Bending-Twisting coupling
FEA	Finite Element Analysis
FPF	First ply failure
GA	Genetic algorithm
NCF	Non-crimped fabric
Pre-preg	Pre-impregnated composite
Quads	Quasi-isotropic
VAT	Variable angle tow
<i>x, y, z</i>	Principal axes

CHAPTER 1

INTRODUCTION

1.1 BACKGROUND

The use of composite materials on aircraft component has increased due to the rapid advance in materials technology. Polymer composites, CFRP in particular, have become the primary material of modern aircraft manufacturing, accounting for half of the total materials. In 1903, the Wright brothers flew the first powered aircraft made from wood. Since then, composite materials have been implemented in the construction of aircrafts. Fibrous composites were used in another aircraft built by the Wright Brothers. In the late 1930s, plastic-impregnated wood materials were used in an eight engine Duramold aircraft known as the Space Goose, which was constructed by Hughes Aircraft Co. Glass fibre was developed and applied on an aircraft reportedly in the late 1940s. However, composite materials were not used in major aircraft component constructions until the invention of carbon fibre in mid 1960s [1]. Military technology was the first to use carbon fibre reinforced materials in the aeronautical industry to construct certain components of the aircraft, i.e., rudders, doors and spoilers. The primary material of aircraft advanced from wood to alloys, like steel and aluminium, then to advanced composite materials. For commercial aircraft, the use of composite materials has gradually increased from 5% in structural weight on an A300 aircraft in the early 1980s to approximately 53% on a modern A350 and 50% on a B787 aircraft [2, 3, 4]. The components that are made from composite materials on the Airbus airliners, and the percentage of composite structures used on aircraft are shown in Figure 1.1 and 1.2 [2, 5]. The application of carbon composites in aircraft structures is believed to be increased further and this domination will likely to be continued for a long period of time as the technology continues to develop, and new designs and manufacturing methods continue to drive improvements in

composite materials.

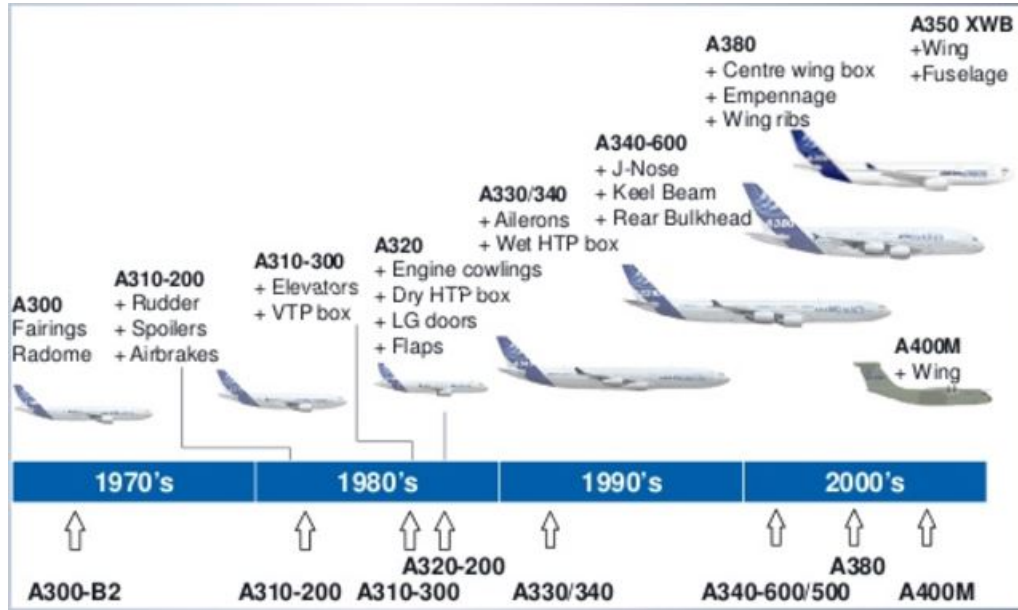


FIGURE 1.1: Components on Airbus airliners made from composite from 1970's to 2000's [2].

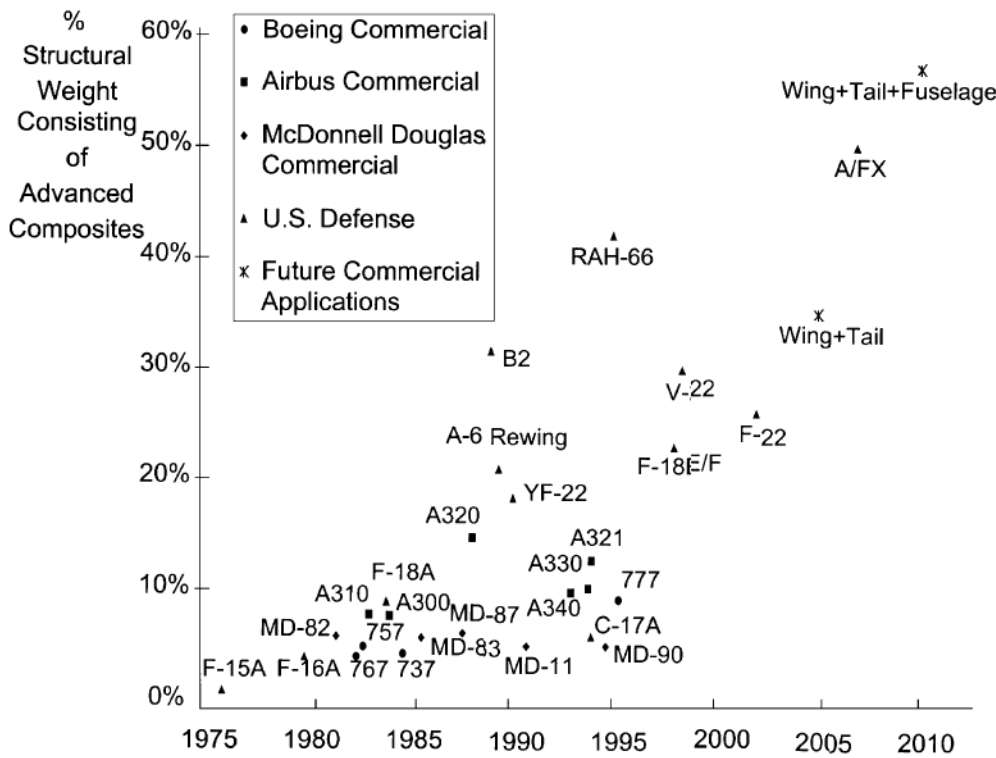


FIGURE 1.2: Composite structures used on aircraft from 1975 to 2010 [5].

The definition of composite means a mixture of two or more materials to create a more useful material in terms of strength, weight, or any other advantageous function. Similar to composite, an alloy is a metallic substance that consists of two or more metals, or a metal or alloy with other elements. While composite materials consist of two or more components that are not necessarily

metal. The two constituents are called the ‘matrix’ and the ‘reinforcement’ parts. For polymer composites in particular, the resin can be a vinyl ester, epoxy or polyester while the reinforcement part could be any kind of fibres such as glass and carbon.

The advantage of composite materials is that they maintain the best properties that the components possess and the properties that the components are not strong can be improved. Typically, the material properties that can be improved by producing composite material are shown in Table 1.1 [6].

TABLE 1.1: Material properties that can be improved with composite materials.

	Physical	Mechanical
Weight	Thermal insulation	Strength
Attractiveness	Thermal-dependent behaviour	Wear resistance
Corrosive resistance	Acoustical insulation	Fatigue
Thermal conductivity		Stiffness

On the other hand, composite materials have high costs due to the high raw material costs, fabrication and assembly costs, recycling and repairing are hard the design and manufacture process are much more complicated and require more considerations compare to conventional materials like metals. The mechanical performance of composite materials out of plane can be significantly different to their in-plane properties.

Composite laminates are usually manufactured as very thin panels. Therefore, composite laminates are easily buckled, this makes buckling one of the most important design requirements for composite plates [7], in particular: aircraft wing and fuselage panels. As buckling is one of the most major design criteria for thin composite laminates, it is also vital to understand the first-ply failure (FPF) behaviour of such materials.

1.2 LITERATURE REVIEW ON THE FUNDAMENTALS OF ADVANCED COMPOSITES

Composite materials are a relatively new technology, current understanding of composites is just tip of the iceberg. Traditional design approaches only make use of the fundamental advantages of composite. Recent research has shown further potential to improve on the performances of composite structures by developing new manufacture techniques. For example, Variable Angle Tow (VAT) technology offers new design possibilities in laminated composite materials design and construction, permitting each layer of the laminate to possess constantly changing fibre directions [8]. However, new technique comes with new challenges. VAT laminates can produce gaps and overlaps during the manufacturing process. The technology is now understood, gaps and overlaps can be avoided through tow-shearing, albeit with a resulting ply thickness variation [9].

1.2.1 BACKGROUND KNOWLEDGE OF COMPOSITE LAMINATE MECHANICS

This part gives an introduction to the basic mechanics of composites is necessary in order to understand the subsequent content of this thesis, some terminology and notations are first introduced.

Laminated structures consist of stacking of a number of layers of material, which make the length, width and the thickness of a laminate the primary dimensions. Because of this, a regular global Cartesian coordinate system is often used, which is also called the structural coordinate system, in which the x and y axes represent the length and width in the plane of the laminate layer and the z axis refers to the thickness of the laminate perpendicular to the x - y plane. However, z does not start at the bottom of the laminate, but the mid-point of the total laminate thickness H , and positive z direction is downwards. While z starts from the midplane of the laminate, the numbering of layers starts from the layer with the most negative z value, counting towards the N^{th} layer, with the $z_{\text{textitk}}^{\text{th}}$ layer being the layer at any arbitrary location within a laminate. In addition, the interface layers are defined with a subscripted z , e.g. z_0 refers to the top surface of a laminate and z_1 represents the lower surface of layer 1. Finally, the fibre angle, denoted by θ , of a lamina is the angle between the fibre direction and the x axis. For example, a 0° layer means the fibre direction is parallel to the x axis and a fibre angle of 90° represents a layer with fibre directions paral-

parallel to the y axis. Figure shows the x - z plane demonstration and the fibre direction in x - y plane [10].

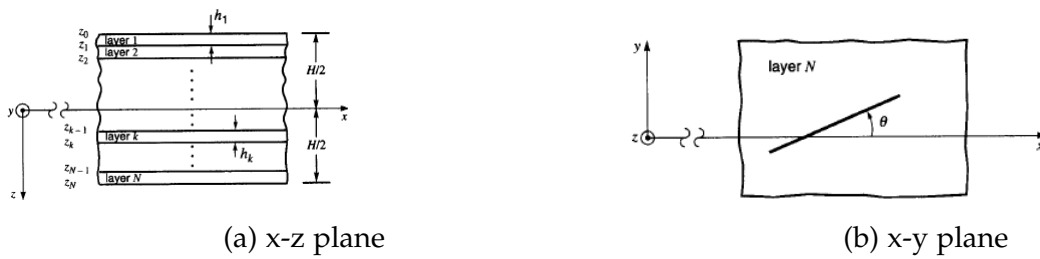


FIGURE 1.3: Illustration of a laminate in (a): x - z plane and (b): x - y plane [10].

The configuration of a laminate can be described with a stacking sequence. A stacking sequence defines the fibre orientation of a laminate from the 1st to the N^{th} layer, written from left to right. For example, a $[+45/0/90/90/0/+45]$ laminate indicates a 6 layers laminate, with the first layer being 45° , layer 2 with 0° ply etc., until layer N^{th} , which is layer 6. In addition, subscripts are also used to describe a stacking sequence of a laminate. A subscript T is often positioned at the end of a stacking sequence, which represents 'Total', to specify a complete laminate, in which the stacking sequence mentioned above can be written as $[+45/0/90/90/0/+45]_T$. Subscript S is also used to for 'symmetric' between the upper and lower half of the laminate, in which the same laminate can be written as $[+45/0/90]_S$. Finally, a subscripted number indicates a repeat of certain times. For example, a stacking sequence of $[\pm 45/90]_2$ represents a 6 ply laminate with the following layout: $[\pm 45/90/\pm 45/90]_T$. And the subscripts can be used together.

1.2.2 CLASSICAL LAMINATION THEORY (CLT)

Classical Laminate Theory (CLT) is vastly used to treat composite structures like thin plates and shells. CLT describes the stress distribution within a laminate and relates the force and moment resultants to the strain and curvature with the well-known 'ABD' stiffness matrix. The theory can be used to predict the deformation of a laminate, to assess the performance of a simple block of material (such as a square or a rectangular block), a laminate and even a complete laminated structure. The ABD matrix refers to a 6 by 6 stiffness matrix that relates in-plane and out-of-plane loading to in-plane strains and out of plane curvatures and is important because it is the simplest and most common way to express the mechanical response of advanced composite laminates. It can be used for both buckling and first-ply failure performances predictions. The derivation of the

CLT is provided in Chapter 2 with detailed example calculations, but the resulting relationship is given here as [10]:

$$\begin{bmatrix} N_x \\ N_y \\ N_{xy} \\ M_x \\ M_y \\ M_{xy} \end{bmatrix} = \begin{bmatrix} A_{11} & A_{12} & A_{16} & B_{11} & B_{12} & B_{16} \\ A_{21} & A_{22} & A_{26} & B_{21} & B_{22} & B_{26} \\ A_{61} & A_{62} & A_{66} & B_{61} & B_{62} & B_{66} \\ B_{11} & B_{12} & B_{16} & D_{11} & D_{12} & D_{16} \\ B_{21} & B_{22} & B_{26} & D_{21} & D_{22} & D_{26} \\ B_{61} & B_{62} & B_{66} & D_{61} & D_{62} & D_{66} \end{bmatrix} \begin{bmatrix} \epsilon_x \\ \epsilon_y \\ \epsilon_{xy} \\ \kappa_x \\ \kappa_y \\ \kappa_{xy} \end{bmatrix} \quad (1.1)$$

which can also be represented in a simplified notation as:

$$\begin{bmatrix} N \\ M \end{bmatrix} = \begin{bmatrix} A & B \\ B & D \end{bmatrix} \begin{bmatrix} \epsilon \\ \kappa \end{bmatrix} \quad (1.2)$$

Here A_{ij} refers to the extensional stiffnesses; B_{ij} refers to the extensional-bending coupling stiffnesses and D_{ij} represents the bending stiffnesses. A_{ij} and D_{ij} can also be found for metallic structures while B_{ij} only occurs in composite structures. The calculation and validation of the ABD matrix individual terms are provided in Chapter 2, to ensure that the equations are implemented correctly and accurate to use in the rest of the investigation.

1.2.3 ELASTIC COUPLING

The reaction of composite laminates to thermal and mechanical loading, usually refers to the coupling behaviour within the laminate. Coupling refers to the interaction of combinations of simple material deformation, such as bending, extension, shear, twisting, etc. these do not occur in conventional materials [11]. Research has been conducted on the application of coupled laminates to practical designs such as passive adaptive wings or rotating blades [12, 13, 14, 15, 16]. A passive adaptive wing or a wind turbine blade can be imagined as a box structure, as demonstrated in 1.4 [15].

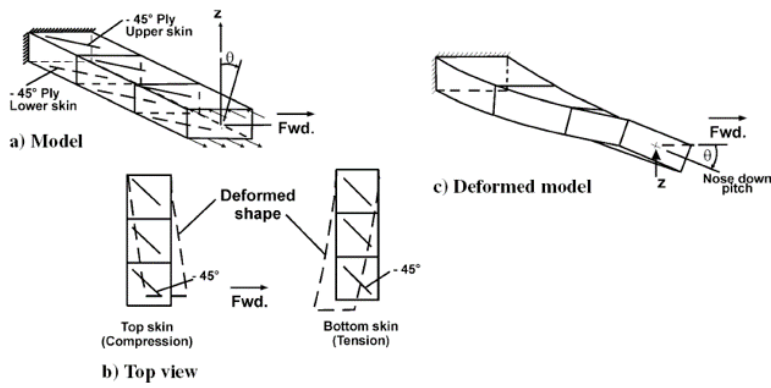


FIGURE 1.4: A box model illustrating a *B-T* coupled wing structure or a wind turbine blade, showing (a) general box configuration; (b) the deformation of the top and bottom skin and; (c) the *B-T* coupled deformation [15].

The application of coupled laminates has extended to manned from only unmanned air vehicles, for instance, Volocopters and Multicopters, in which the blades with Extension-Twist coupling offer the potential to increase the lift characteristics through the change in rotor speed [16].

The combination of coupling properties depends on the configuration of the laminate, which determines the ABD matrix of the laminate and hence its buckling and FPF performance. In general, coupling behaviours occur between:

- In-plane (extension or membrane) and out-of-plane (bending or flexure) loading, or when a laminate has a non-zero [B] matrix [17]. The combination of coupling and their characteristics are listed below [18, 19, 20].

TABLE 1.2: Illustration of different combinations of coupling behaviour for B matrix.

Notation	Designation and labelling	Laminate configuration	Matrix form
B_1	<i>Extension-Bend</i>	<i>E-B</i>	$\begin{bmatrix} B_{11} & 0 & 0 \\ 0 & B_{22} & 0 \\ 0 & 0 & 0 \end{bmatrix}$
B_t	<i>Extension-Twisting and Shearing-Bending</i>	<i>E-T, S-B</i>	$\begin{bmatrix} 0 & 0 & B_{16} \\ 0 & 0 & B_{26} \\ B_{16} & B_{26} & 0 \end{bmatrix}$
B_{it}	<i>Extension-Bending, Extension-Twisting and Shearing-Bending</i>	<i>E-B, E-T, S-B</i>	$\begin{bmatrix} B_{11} & 0 & B_{16} \\ 0 & B_{22} & B_{26} \\ B_{16} & B_{26} & 0 \end{bmatrix}$
B_s	<i>Extension-Bending, and Shearing-Twisting</i>	<i>E-B, S-T</i>	$\begin{bmatrix} B_{11} & B_{12} & 0 \\ B_{12} & B_{22} & 0 \\ 0 & 0 & B_{66} \end{bmatrix}$
B_F	<i>Extension-Bending, and Shearing-Bending, Extension-Twisting, Shearing-Twisting (or fully coupled)</i>	<i>E-B, S-B, E-T, S-T</i>	$\begin{bmatrix} B_{11} & B_{12} & B_{16} \\ B_{12} & B_{22} & B_{26} \\ B_{16} & B_{26} & B_{66} \end{bmatrix}$

where the subscripts: l represents the leading diagonal elements B_{11} and B_{22} are non-zero; t means the transverse elements are B_{16} and B_{26} non-zero; S refers to simple, uncoupled i.e. B_{16} and B_{26} equal to zero and; F implies that all the elements are finite.

- In-plane *shear* and *extension*, where A_{16} and A_{26} are non-zero (for which the $[A]$ matrix can be written as A_F). Figure 11 illustrates a laminate that possesses coupling between extension and shear.

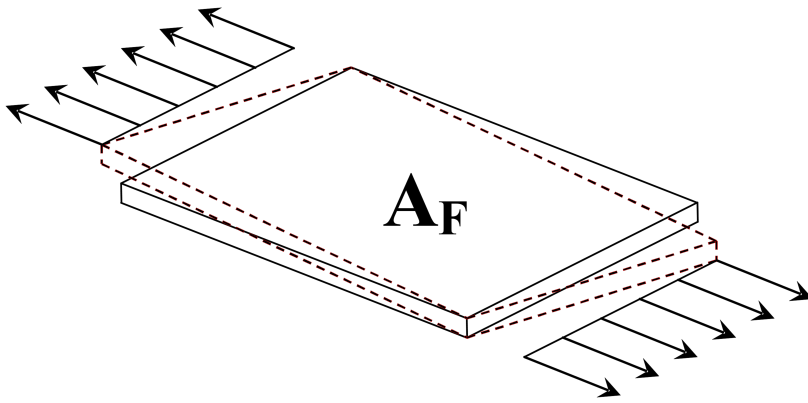


FIGURE 1.5: An *Extension-Shear* coupled laminate [21].

- Out-of-plane *bending* and *twisting*, where D_{16} and D_{26} are non-zero (D_F).

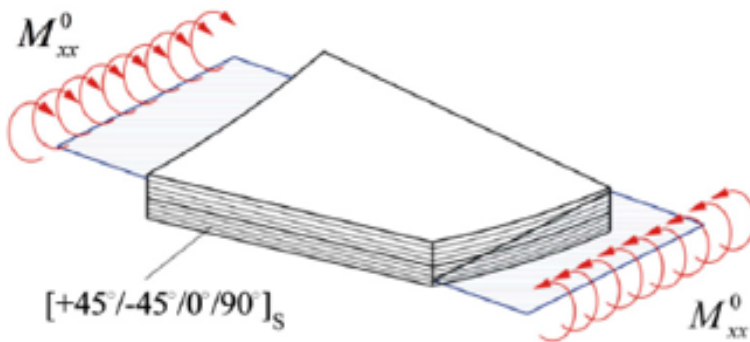


FIGURE 1.6: An *Bend-Twist* Coupled laminate [22].

In industry, symmetric and uncoupled laminates are mostly used because these types of laminate are guaranteed to be free of thermal warping and distortion free i.e. the $[B]$ matrix is zero. Nevertheless, research has been conducted on fully uncoupled, Extension-Shear and Bend-Twist coupled laminates to show that these types of laminates can also avoid thermal warping [23, 24, 20, 25]. This finding expands the potential of composite laminates applicable for aircraft applications. Moreover, the introduction of coupling behaviour expands the size of the

overall design space of composite laminates, allowing more options to be explored and potential improvements in performance to be made.

1.2.4 CLASSIFICATION OF COMPOSITE LAMINATES

Composite laminates are usually classified in terms of stacking sequence. The difference in stacking sequence leads to a huge difference in the ABD matrix and hence the performance of a laminate. The form of the individual ABD stiffness matrices of a laminate can be described using various subscripts notations: F represents a matrix with all elements being finite, i.e. non-zero; 0 means all the elements within the matrix are zero; S for specially orthotropic, where the 16 and 26 elements of the matrix are zero and; I for isotropic [18, 19, 21]. Composite laminates are typically classified as:

- Isotropic laminate

Isotropic laminate is a unique type of laminate where the material properties are identical in every direction and independent of the orientation. The ABD matrix of an isotropic layer of thickness H is:

$$\begin{bmatrix} A & \nu A & 0 & 0 & 0 & 0 \\ \nu A & A & 0 & 0 & 0 & 0 \\ 0 & \frac{1-\nu}{2}A & 0 & 0 & 0 & 0 \\ 0 & 0 & 0 & D & \nu D & 0 \\ 0 & 0 & 0 & \nu D & D & 0 \\ 0 & 0 & 0 & 0 & 0 & \frac{1-\nu}{2}D \end{bmatrix} \quad (1.3)$$

where $A = \frac{EH}{1-\nu}$ and $D = \frac{EH^3}{12(1-\nu^2)}$

For an isotropic material:

$$\begin{aligned} A_{11} &= A_{22} = A \\ A_{66} &= \frac{A_{11} - A_{22}}{2} \\ D_{ij} &= \frac{A_{ij}H^2}{12} \end{aligned} \quad (1.4)$$

For composite laminates that possess isotropic properties:

$$\begin{aligned} \nu &= \frac{Q_{11} + Q_{22} + 6Q_{12} - 4Q_{66}}{3Q_{11} + 3Q_{22} + 2Q_{12} + 4Q_{66}} \\ G &= \frac{Q_{11} + Q_{22} - 2Q_{12} + 4Q_{66}}{8} \\ E &= 2(1 + \nu)G \end{aligned} \quad (1.5)$$

This is an unusual type of response for a composite laminate because composite materials are usually orthotropic, where the material properties are different in 3 mutually perpendicular directions and are orientation dependent.

- Anisotropic laminate

On the other hand, composite materials are often anisotropic, here the material properties are different in all directions, anisotropic laminates have a fully non-zero ABD matrix:

$$\begin{bmatrix} A_{11} & A_{12} & A_{16} & B_{11} & B_{12} & B_{16} \\ A_{21} & A_{22} & A_{26} & B_{21} & B_{22} & B_{26} \\ A_{61} & A_{62} & A_{66} & B_{61} & B_{62} & B_{66} \\ B_{11} & B_{12} & B_{16} & D_{11} & D_{12} & D_{16} \\ B_{21} & B_{22} & B_{26} & D_{21} & D_{22} & D_{26} \\ B_{61} & B_{62} & B_{66} & D_{61} & D_{62} & D_{66} \end{bmatrix} \quad (1.6)$$

- Balanced laminate

A laminate is said to be balanced if all the layers have a specific 'pair' within the laminate, i.e. with the same material properties, thickness but opposite in fibre directions. For example, a $[0/\pm 45/0]_T$ laminate. A balanced laminate always has the extensional stiffness element A_{16} and A_{26} equal to zero and can be referred as $A_S B_0 D_F$. The ABD matrix of a balanced

laminate would be:

$$\begin{bmatrix} A_{11} & A_{12} & 0 & 0 & 0 & 0 \\ A_{21} & A_{22} & 0 & 0 & 0 & 0 \\ 0 & 0 & A_{66} & 0 & 0 & 0 \\ 0 & 0 & 0 & D_{11} & D_{12} & D_{16} \\ 0 & 0 & 0 & D_{21} & D_{22} & D_{26} \\ 0 & 0 & 0 & D_{61} & D_{62} & D_{66} \end{bmatrix} \quad (1.7)$$

■ Symmetric laminate

A laminate is said to be symmetric if the stacking sequence is mirrored at the midplane of the laminate, with each pair sharing identical material properties and thickness. For example, a stacking sequence of $[90/\pm 45]_S$ represent a symmetric laminate with a configuration of $[90/+45/-45/-45/+45/90]$. The B_{ij} matrix of a symmetric laminate a is always zero, with a notation of $A_F B_0 D_F$, and the ABD matrix would be:

$$\begin{bmatrix} A_{11} & A_{12} & A_{16} & 0 & 0 & 0 \\ A_{21} & A_{22} & A_{26} & 0 & 0 & 0 \\ A_{16} & A_{26} & A_{66} & 0 & 0 & 0 \\ 0 & 0 & 0 & D_{11} & D_{12} & D_{16} \\ 0 & 0 & 0 & D_{21} & D_{22} & D_{26} \\ 0 & 0 & 0 & D_{61} & D_{62} & D_{66} \end{bmatrix} \quad (1.8)$$

■ Balanced and Symmetric laminate

A balanced and symmetric laminate is the combination of the two types of laminates above, the stacking sequence must be both symmetrical about the midplane of the laminate and every layer must be paired with an opposite layer. The designation of a balance and

symmetric laminate is $A_S B_0 D_F$ and the ABD matrix becomes:

$$\begin{bmatrix} A_{11} & A_{12} & 0 & 0 & 0 & 0 \\ A_{21} & A_{22} & 0 & 0 & 0 & 0 \\ 0 & 0 & A_{66} & 0 & 0 & 0 \\ 0 & 0 & 0 & D_{11} & D_{12} & D_{16} \\ 0 & 0 & 0 & D_{21} & D_{22} & D_{26} \\ 0 & 0 & 0 & D_{61} & D_{62} & D_{66} \end{bmatrix} \quad (1.9)$$

Balanced and symmetric laminates are widely used in practice and industry because they are guaranteed to be immune to thermal warping during the high temperature curing process, and the ABD matrix is considerably simplified. One of the most important simplifications is that the B matrix is zero, which eliminates the 'coupling' behaviour that is unique to advanced composite materials,. Non-symmetric designs commonly possess thermal warping problems that arise during the fabrication process,, or in terms of the ABD matrix, when B_{ij} are non-zero [7], making the analysis technique non-linear and making the prediction process less accurate. However, research have shown that non-symmetric laminates can be immune to thermal warping, when [B] equals zero [18, 19].

- Specially orthotropic or Cross-ply laminates Cross-ply refers to layers with either 0° and 90° fibre orientations, and a cross-ply laminate indicates a laminate consisting of only 0° and 90° ply laminates [26]. The characteristics of this type of laminate is that the transformed reduced stiffnesses \tilde{Q}_{16} and \tilde{Q}_{26} are zero, therefore all A_{16} , A_{26} , B_{16} , B_{26} , D_{16} and D_{26} elements in the ABD matrix and also B_{12} and B_{66} are zero, which results in the following form:

$$\begin{bmatrix} A_{11} & A_{12} & 0 & B_{11} & 0 & 0 \\ A_{21} & A_{22} & 0 & 0 & B_{22} & 0 \\ 0 & 0 & A_{66} & 0 & 0 & 0 \\ B_{11} & 0 & 0 & D_{11} & D_{12} & 0 \\ 0 & B_{22} & 0 & D_{21} & D_{22} & 0 \\ 0 & 0 & 0 & 0 & 0 & D_{66} \end{bmatrix} \quad (1.10)$$

- Symmetric Cross-ply laminate A symmetric cross-ply laminate contains only 0° and 90° ply

laminates, and the laminate is symmetric about the midplane. Beside the 16 and 26 terms, the entire [B] matrix is zero, the ABD matrix becomes:

$$\begin{bmatrix} A_{11} & A_{12} & 0 & 0 & 0 & 0 \\ A_{21} & A_{22} & 0 & 0 & 0 & 0 \\ 0 & 0 & A_{66} & 0 & 0 & 0 \\ 0 & 0 & 0 & D_{11} & D_{12} & 0 \\ 0 & 0 & 0 & D_{21} & D_{22} & 0 \\ 0 & 0 & 0 & 0 & 0 & D_{66} \end{bmatrix} \quad (1.11)$$

1.2.5 LAMINATION PARAMETERS

In lay-up optimisation problems, the traditional approach is to design laminates by rotating the fibre direction or changing the stacking sequence, which often involves optimising the ABD matrix using a genetic algorithm [27, 28, 29, 30]. For an optimisation problem, the minimum number of terms required to describe a laminate using the ABD matrix is 8 for a fully uncoupled laminate, i.e. A_{11} , A_{12} , A_{22} , A_{66} , D_{11} , D_{12} , D_{22} and D_{66} , and up to a maximum of 21 for a fully coupled laminate, in which the ABD matrix also depends on the engineering constants. Also, design problems optimised by rotating the fibre orientation are non-convex, which means the optimised results are often found to be local optima rather than global. Moreover, the order of layer stacking combined with the fibre orientations, makes the optimisation process complicated, and this complexity increases with the number of layers, which significantly increases the computation cost of optimisation.

Optimisation of composite laminate layup has evolved significantly over the past 40 years. Another, albeit less popular way to carry out optimisation design problems, is to use trigonometric functions called 'lamination parameters', a method first introduced by Tsai [31, 32]. Much research on designing composite laminates using lamination parameters has since been conducted [33, 34, 35, 36, 37, 38]. Lamination parameters consist of 12 variables, ξ_{1-12} , with 4 parameters representing each of the [A], [B] and [D] matrices, or ξ_{1-4}^A , ξ_{1-4}^B and ξ_{1-4}^D . These parameters only depend on the stacking sequence and the number of plies, but not on the thickness of each ply. By using lamination parameters, less variables are needed to describe a laminate.

For example, using the ABD matrix needs 8 variable to describe a fully uncoupled laminate, while using lamination parameters requires only 4 variables, making it a more efficient way of optimising composite laminates [39]. The design can also become a convex problem, and the feasible design region described using lamination parameters can be convex [40]. As the stiffness terms are related linearly with the lamination parameters, everything is defined within a convex space, which means optimum results obtained using this approach are global, rather than local optima. Lamination parameters offer an advantage for optimisation of laminate design as the stiffness terms are given as linear variables. The latter are often treated as independent design variables constrained by inequality relationships that determine a feasible design space. For example, lamination parameter design spaces are often drawn using buckling factors, the patterns that are created in these plots can then be used to find the most buckle-resistant design for a given laminate. In industry, aircraft skins, spars and stiffeners are usually designed with typical lamination parameter values, represented by a fixed point in the lamination parameter plots. Stacking sequences that fit the specific point can then be found and the buckling and FPF performance of the different configurations can be compared. Moreover, using lamination parameters as the optimisation tool is also beneficial as the results can be easily related to the ply percentages, corresponding stacking sequences can be determined directly from the results of the lamination parameter optimisation problem.

Lamination parameters are used to present the feasible design space of composite laminates. This process first requires the derivation of the relationships between the lamination parameters. Miki (1982) and Mike and Sugiyama (1993) were some of the earliest to use lamination parameters as the design variables for optimising composite laminates [41, 42]. Miki (1993) stated that 2 in-plane (ξ_1 and ξ_2) or 2 out-of-plane (ξ_9 and ξ_{10}) lamination parameters are needed to describe the feasible design space of an orthotropic laminate graphically, using the following relationship [41]:

$$2(\xi_1^j)^2 - 1 \leq \xi_2^j \quad (1.12)$$

where $j = A$ or D Later on in 1992, the feasible design space of 4 in-plane (ξ_{1-4}) and 4 out-of-plane

(ξ_{9-12}) lamination parameters was developed [43]:

$$\begin{aligned} (x_1^j)^2 + (\xi_3^j)^2 &\leq 1 \\ 2(1 + \xi_2^j)\xi_3^j - 4\xi_1^j\xi_3^j\xi_4^j + (\xi_4^j)^2 &\leq (\xi_2^j - 2\xi_1^j + 1)(1 - \xi_2^j) \end{aligned} \quad (1.13)$$

After that, the relationship between the in-plane and out-of-plane lamination parameters was derived [40]:

$$\frac{1}{4}(\xi_i^A + 1)^3 - 1 \leq \xi_i^D \leq \frac{1}{4}(\xi_i^A - 1)^3 + 1 \quad (1.14)$$

There is a range of value for ξ_i^D for any value of ξ_i^A , except when $\xi_i^A = \xi_i^D$ for $\xi_i^A = \pm 1$. Then Diaconu et al. (2002) derived the relationship between the in-plane, coupling and out-of-plane lamination parameters [44] as:

$$\begin{aligned} (\xi_i^A + 1)^4 + 3(\xi_i^B)^2 &\leq 4(\xi_i^A + 1)^3(\xi_i^D + 1) \\ (\xi_i^A - 1)^4 + 3(\xi_i^B)^2 &\leq 4(\xi_i^A - 1)^3(\xi_i^D - 1) \end{aligned} \quad (1.15)$$

The 12 lamination parameters can be related to the non-dimensional parameters, the stacking

sequence and the number of plies are given in [32] as:

$$\begin{aligned}
\bar{\zeta}_1 &= \frac{[n_+ \cos(2\theta_+) + n_- \cos(2\theta_-) + n_\circ \cos(2\theta_\circ) + n_\bullet \cos(2\theta_\bullet)]}{n} \\
\bar{\zeta}_2 &= \frac{[n_+ \cos(4\theta_+) + n_- \cos(4\theta_-) + n_\circ \cos(4\theta_\circ) + n_\bullet \cos(4\theta_\bullet)]}{n} \\
\bar{\zeta}_3 &= \frac{[n_+ \sin(2\theta_+) + n_- \sin(2\theta_-) + n_\circ \sin(2\theta_\circ) + n_\bullet \sin(2\theta_\bullet)]}{n} \\
\bar{\zeta}_4 &= \frac{[n_+ \sin(4\theta_+) + n_- \sin(4\theta_-) + n_\circ \sin(4\theta_\circ) + n_\bullet \sin(4\theta_\bullet)]}{n} \\
\bar{\zeta}_5 &= \frac{[\chi_+ \cos(2\theta_+) + \chi_- \cos(2\theta_-) + \chi_\circ \cos(2\theta_\circ) + \chi_\bullet \cos(2\theta_\bullet)]}{\chi} \\
\bar{\zeta}_6 &= \frac{[\chi_+ \cos(4\theta_+) + \chi_- \cos(4\theta_-) + \chi_\circ \cos(4\theta_\circ) + \chi_\bullet \cos(4\theta_\bullet)]}{\chi} \\
\bar{\zeta}_7 &= \frac{[\chi_+ \sin(2\theta_+) + \chi_- \sin(2\theta_-) + \chi_\circ \sin(2\theta_\circ) + \chi_\bullet \sin(2\theta_\bullet)]}{\chi} \\
\bar{\zeta}_8 &= \frac{[\chi_+ \sin(4\theta_+) + \chi_- \sin(4\theta_-) + \chi_\circ \sin(4\theta_\circ) + \chi_\bullet \sin(4\theta_\bullet)]}{\chi} \\
\bar{\zeta}_9 &= \frac{[\zeta_+ \cos(2\theta_+) + \zeta_- \cos(2\theta_-) + \zeta_\circ \cos(2\theta_\circ) + \zeta_\bullet \cos(2\theta_\bullet)]}{\zeta} \\
\bar{\zeta}_{10} &= \frac{[\zeta_+ \cos(4\theta_+) + \zeta_- \cos(4\theta_-) + \zeta_\circ \cos(4\theta_\circ) + \zeta_\bullet \cos(4\theta_\bullet)]}{\zeta} \\
\bar{\zeta}_{11} &= \frac{[\zeta_+ \sin(2\theta_+) + \zeta_- \sin(2\theta_-) + \zeta_\circ \sin(2\theta_\circ) + \zeta_\bullet \sin(2\theta_\bullet)]}{\zeta} \\
\bar{\zeta}_{12} &= \frac{[\zeta_+ \sin(4\theta_+) + \zeta_- \sin(4\theta_-) + \zeta_\circ \sin(4\theta_\circ) + \zeta_\bullet \sin(4\theta_\bullet)]}{\zeta}
\end{aligned} \tag{1.16}$$

where n , χ and ζ represent the **non-dimensional parameters** for extension, coupling and bending stiffness respectively.

For traditional laminates (containing 0, 90 and ± 45 degree orientations) these are given by:

$$\begin{aligned}
n_+ &= \sum (z_k - z_{k-1})_+ & \chi_+ &= 2 \times \sum (z_k^2 - z_{k-1}^2)_+ & \zeta_+ &= 4 \times \sum (z_k^3 - z_{k-1}^3)_+ \\
n_- &= \sum (z_k - z_{k-1})_- & \chi_- &= 2 \times \sum (z_k^2 - z_{k-1}^2)_- & \zeta_- &= 4 \times \sum (z_k^3 - z_{k-1}^3)_- \\
n_\circ &= \sum (z_k - z_{k-1})_\circ & \chi_\circ &= 2 \times \sum (z_k^2 - z_{k-1}^2)_\circ & \zeta_\circ &= 4 \times \sum (z_k^3 - z_{k-1}^3)_\circ \\
n_\bullet &= \sum (z_k - z_{k-1})_\bullet & \chi_\bullet &= 2 \times \sum (z_k^2 - z_{k-1}^2)_\bullet & \zeta_\bullet &= 4 \times \sum (z_k^3 - z_{k-1}^3)_\bullet
\end{aligned} \tag{1.17}$$

The non-dimensional parameters (n_+ , n_- , n_\circ , n_\bullet , χ_+ , χ_- , χ_\circ , χ_\bullet , ζ_+ , ζ_- , ζ_\circ and ζ_\bullet) are required to calculate the lamination parameters, the subscripts +, -, \circ and \bullet are the notation for $+45^\circ$, -45° , 0° and 90° ply orientations.

Foldager et al. (1998) looked at the convexity of composite laminate compliance optimisation

using lamination parameters [45] and later the feasible design space was actually proven to be convex [40]. Hammer et. al. (1997) used lamination parameters to optimise the compliance of a composite laminate under in-plane single and multiple loadings [34] and Setoodeh et. al. (2006) attempted to design minimum compliance variable-stiffness laminates under both in-plane and out-of-plane loadings using lamination parameters [33]. Optimisation of orthotropic and non-orthotropic laminated plates under shear loading was done by Grenestedt (1991) [46]. The difference in buckling load predictions when using lamination parameters versus using a genetic algorithm (GA) as the optimisation tool, for balanced and symmetric laminates with different aspect ratios was compared [47]. Results showed that lamination parameters predicted very similar buckling loads as the approach using GA. The pros and cons of using lamination parameters as an optimisation tool are listed below [48].

To summarise, the advantages of using lamination parameters means that:

- Less design variables are required, which ensures lower computational costs, greater robustness and consequently improved computational efficiency.
- Lamination parameters can be linearly related to the ABD matrix which has the advantage of enabling a simpler optimisation process than optimising using fibre angles.
- The analysis is presented in terms of a convex design space with a single global maximum (as opposed to a non-convex design space that often occurs when using fibre angle as the optimisation tool).

and the disadvantages of using lamination parameters are that:

- The development of the relationship between the 12 lamination parameters can be difficult as it becomes a 4-dimensional problem.
- Including strength in the optimisation problem is not easy as any particular point in the lamination parameter design space could have more than one stacking sequence with different ply angles, which leads to different strength values.

The method of using lamination parameters to design composite laminates is adopted as the primary design approach for this project as it is shown to be a more efficient approach to carry out optimisation of composite laminates, at least when the buckling load is the primary concern, see Section 1.2.6). Equations and example calculations are presented in Chapter 2.

1.2.6 BUCKLING

Composite laminates are mostly manufactured as thin panels, which makes buckling the primary design factor for many composite laminates and structures. Unlike column buckling, where a lateral deflection grows along the column length, plate buckling involves one or more, two-dimensional out-of-plane sine wave deflections in the load direction, where the number of sine waves (or modes) along the length of the structure developed during the buckling process depends on the length, a , of the plate [6].

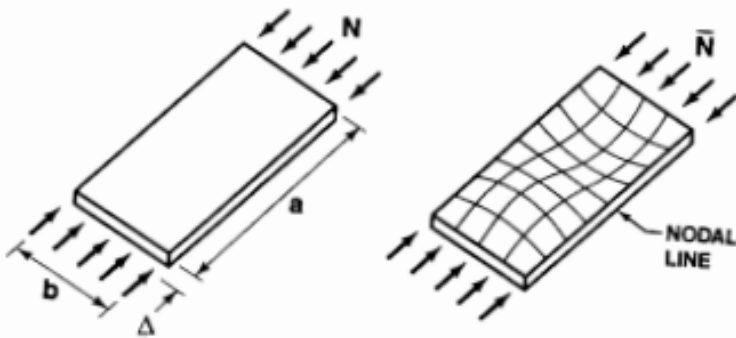


FIGURE 1.7: Illustration of a laminated plate before and after buckling deformation from [6].

When the applied load increases, the plate shortens in the load direction and stays flat until a critical buckling load is reached. The plate becomes unstable, and the deformation bifurcates, jumping from the old unstable path to a new stable path. A buckled plate is able to carry extra loading, beyond the buckling load, in its post-buckled configuration, but at the moment of buckling its stiffness is suddenly reduced. In contrast, column buckling indicates that the structure simply fails and will collapse at the buckling load. Demonstration of plate and column buckling is shown in Figure 7 [49].

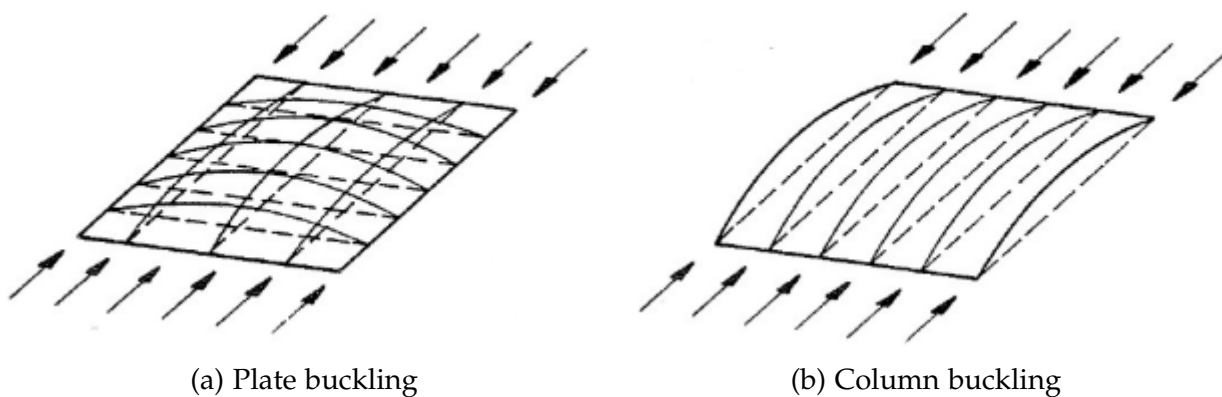


FIGURE 1.8: Illustration of (a) plate and (b) column buckling [49].

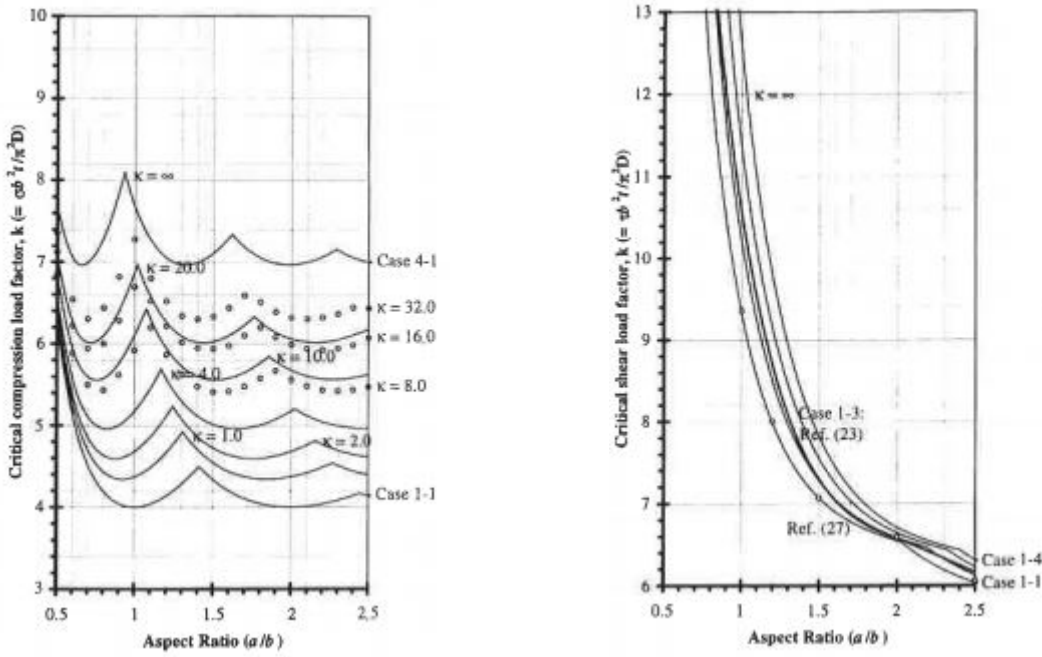
Plate buckling analysis under in-plane loads can be performed by solving an eigenvalue problem, in which the pre-buckling displacement is ignored. A closed form solution can be developed for fully uncoupled laminates. The compression buckling load, N_x , for simply supported edge boundary condition can be obtained exactly as [6]:

$$N_x = \pi^2 [D_{11} \left(\frac{m}{a}\right)^2 + 2(D_{11} + 2D_{66}) \left(\frac{n^2}{b^2}\right) + D_{22} \left(\frac{n^4}{b^4}\right) \left(\frac{a}{m}\right)^2] \quad (1.18)$$

from knowledge of the bending stiffness, D_{ij} , plate length, a , and width, b , and the buckling half-wave parameter in x and y directions, m and n ($=1, 2, 3, \dots$), it is possible to find the lowest critical force resultant N_x . (Worked examples is provided in Chapter 2). However, as emphasised previously, Equation 1.18 and the analysis presented above, is only applicable to fully uncoupled laminates, in which $D_{16} = D_{26} = 0$. Consequently, using this analysis the buckling performance for a general balanced and symmetric laminate, where D_{16} and $D_{26} \neq 0$, can result in a significant overestimate of the buckling load (unsafe). For more general cases of the buckling performance of a laminate that possesses any kind of coupling behaviour Finite Element Analysis (FEA) is required. Furthermore, although closed form solutions of buckling behaviour for infinitely long plates subject to compression or shear buckling exist [50, 51], closed form solutions for short plates are only applicable to compression buckling, shear buckling behaviour must also be performed using FEA.

Other than simply supported, there are other boundary conditions like free, clamped, re-strained, etc. This project focuses on simply supported laminates, other boundary conditions are considered and can be modelled with slight modification in the finite element model. This project primarily looks at laminates just under a simply supported condition to better explore different areas of interest concerning composite laminate behaviour.

York (2000) used FEA to model and analyse rectangular isotropic laminates subject to several different boundary conditions [52]. Compression and shear buckling results of plates with aspect ratio (a/b) ranging from 0.5 to 2.5 were presented in the form of buckling (or Garland) curves. Example results from the simply supported case are shown below.



(a) Compression buckling

(b) Shear buckling

FIGURE 1.9: Illustrations of buckling curves for: (a) Compression and (b) Shear buckling [52]

A Garland curve shows the buckling factors for a laminate across a range of aspect ratios and are adopted in this project as a way to show buckling results. The buckling factor, or buckling coefficient, (k) represents the normalised buckling load against the D_{iso} of the laminate, given as:

$$k = \frac{Nb^2}{\pi^2 D_{iso}} \tag{1.19}$$

where D_{iso} is the bending stiffness of the equivalent isotropic laminate, defined by:

$$D_{iso} = \frac{E_{iso}H^3}{12(1 - \nu_{iso}^2)} = \frac{U_1H^3}{12} \tag{1.20}$$

U_i is called the material invariant, given by:

$$U_1 = \frac{3Q_{11} + 3Q_{22} + 2Q_{12} + 4Q_{66}}{8} \tag{1.21}$$

More details on the actual theory and formulations are provided in Chapter 2 with worked examples showing how to use them.

For aspect ratio (a/b) = 1.0, the compression buckling factor, N_x , is 4.0, which is the classical buckling factor of an simply supported isotropic square plate. While the classical shear buckling

factor, K_S , for a simply supported square panel is 9.35, which was proved by Stein and Neff [53]. The classical compression and shear buckling factors are used for validation of the FEA model predictions found in this project.

Fukunaga et. al used lamination parameters as design variables, to increase the buckling load of composite laminates [54]. Square and rectangular symmetric Bend-Twist coupled laminates were loaded in both compression and shear. The buckling performance of the laminates was analysed and contour maps of buckling factors were plotted. Optimal lamination parameters for maximum buckling load are found within the feasible ranges of the 4 lamination parameters ζ_{9-12} (note that these 4 lamination parameters are the only ones that influence the buckling load). Examples of compression design space contour maps for simply supported square laminates are shown in Figure 1.10.

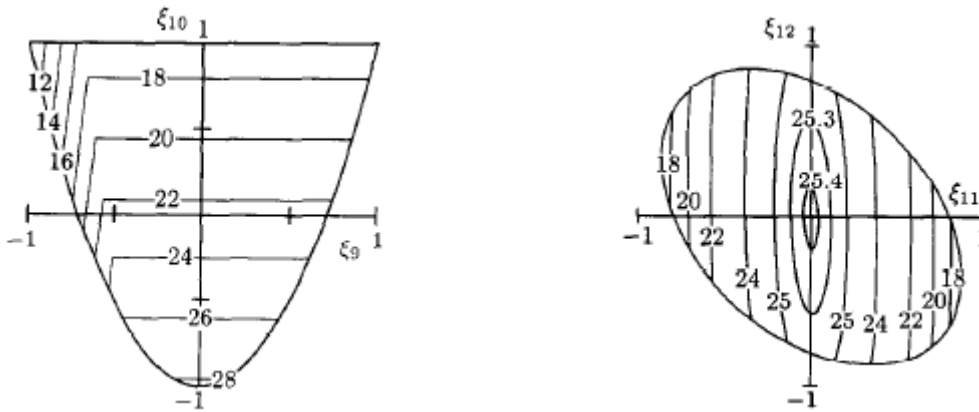


FIGURE 1.10: Compression buckling contours from [54]: (a) $\zeta_9 - \zeta_{10}$ where ζ_{11} and $\zeta_{12} = 0$ and; (b) $\zeta_{11} - \zeta_{12}$ where $\zeta_9 = 0.5$ and $\zeta_{10} = -0.2$.

A contour map shows a lamination parameter design space, which can also illustrate the relationship between lamination parameters and any relevant results such and buckling factors or buckling loads, with each line on the graphs representing a constant value. For instance, the contour lines in Figure 8 represent the normalised compressive buckling load.

Uncoupled laminates are normally used in industry because this type of laminate provides resistance to all different kinds of coupling behaviours. However, interest in coupled laminates has increased in the past few decades [17, 53, 54, 55, 56, 57], as the introduction of coupling increases the size of the design space and hence more options can be explored, potentially for better designs. Design spaces and contour maps are the major way of presenting the results obtained in this project, it is therefore important to understand the fundamentals.

1.2.7 FIRST PLY FAILURE (FPF)

First ply failure (FPF), is used to assess the failure performance of laminate designs in this project. First ply failure means that any one of the layers within a laminated plate fails first and the whole laminate is assumed to be failed at that point. This is a convenient and conservative way to determine the failure strength of a composite structure using CLT. The stress in different directions in the principal coordinate system of each ply is calculated using CLT, then the stresses are used to determine the first ply failure strength of the laminate by applying different failure criteria, which is straightforward. There are various methods to evaluate the strength performance of composite laminates under different types of loading such as compression and shear loads. Different failure criteria have been developed to predict failure strength. Each of the failure criteria predict strength differently, with their own advantages and limitations. These predictions have been evaluated using experimental data. However, none of the criteria provides definitive predictions under all loading conditions, due to the complexity of the interactions within the matrix and the fibre materials within the laminate, the stacking sequence and the orientations of the plies within the laminate. Therefore, multiple failure criteria can be considered and compared to experimental tests to determine the best available failure criteria for a given loading scenario and laminate. Some of the commonly used failure criteria that are used in this project are listed below, note that $X_{t,c}$ and $Y_{t,c}$ represents the allowable stress values of the material in x and y directions. Overall, there are four generic types of failure criteria: (I) independent or non-interactive, (II) partially interactive, (III) fully interactive and (IV) new criteria. Their predictions can be compared against experimental results to determine the criterion that performs best for use in this project.

I. Independent condition (or limit) criteria

Independent criteria simply compare the lamina stress or strains in the 1 and 2 directions with the compression, tensile or shear strength of the material to determine the failure load and mode without considering any interactions between the stresses or strains.

- Maximum Stress Criterion

The maximum stress criterion predicts the failure of a laminate by looking into the stresses individually, interactions between the tension and compressive stresses are ignored [6, 58].

$$\begin{aligned} \frac{\sigma_1}{\sigma_{X_t}} \text{ or } \frac{\sigma_1}{\sigma_{X_c}} &= 1 \\ \text{or} \\ \frac{\sigma_2}{\sigma_{Y_t}} \text{ or } \frac{\sigma_2}{\sigma_{Y_c}} &= 1 \\ \text{or} \\ \frac{|\sigma_6|}{\sigma_Q} &= 1 \end{aligned} \tag{1.22}$$

- Maximum Strain Criterion

The maximum strain criterion function is similar to the maximum stress criterion, but instead of stresses, this approach uses strains to predict the failure strength of a laminate [6, 58].

$$\begin{aligned} \frac{\varepsilon_1}{\varepsilon_{X_t}} \text{ or } \frac{\varepsilon_1}{\varepsilon_{X_c}} &= 1 \\ \text{or} \\ \frac{\varepsilon_2}{\varepsilon_{Y_t}} \text{ or } \frac{\varepsilon_2}{\varepsilon_{Y_c}} &= 1 \\ \text{or} \\ \frac{|\varepsilon_6|}{\varepsilon_Q} &= 1 \end{aligned} \tag{1.23}$$

II. Partially Interactive (or Separative) Criteria

Partially interactive criteria consider the matrix and fibre failure separately. Here interactions between stresses are considered but the matrix and fibre failure modes are considered separately.

- Puck-Modified Criterion

The Puck-modified criterion is an updated version of the simple Puck criterion. The modified version considers interactions between the stress in compression and in tension, normal to the

fibre direction [58, 59, 60].

$$\begin{aligned} \frac{\sigma_1}{X_t} \text{ or } \frac{\sigma_1}{X_c} &= 1 \\ \text{or} & \\ \frac{\sigma_2^2}{Y_t Y_c} + \sigma_2 \left(\frac{1}{Y_t} - \frac{1}{Y_c} \right) + \left(\frac{\sigma_6}{Q} \right)^2 &= 1 \end{aligned} \quad (1.24)$$

- Hashin-Rotem Criterion

The Hashin-Rotem failure criterion considers the matrix and fibre failure modes separately. Interactions between the various stress components are also considered [61].

$$\begin{aligned} \text{Fibre failure: } \frac{\sigma_1}{X} &= 1 \\ \text{Matrix failure: } \left(\frac{\sigma_2}{Y} \right)^2 + \left(\frac{\sigma_6}{Q} \right)^2 &= 1 \end{aligned} \quad (1.25)$$

- Hashin Criteria

The Hashin failure criterion is a modification of Hashin-Rotem criterion, which involves the interactions between the stresses for both fibre and matrix failure [62].

$$\begin{aligned} \text{Fibre failure in tension: } \left(\frac{\sigma_1}{X_t} \right)^2 + \left(\frac{\sigma_6}{Q} \right)^2 &= 1 \\ \text{Fibre failure in compression: } \frac{\sigma_1}{X_c} &= 1 \\ \text{Matrix failure: } \left(\frac{\sigma_2}{Y_t} \right)^2 + \left(\frac{\sigma_6}{Q} \right)^2 &= 1 \end{aligned} \quad (1.26)$$

III. Fully Interactive Criteria

Here the failure load and failure modes are predicted with one single equation, considering all the stresses or strains.

- Tsai-Wu Failure Criterion

Compared to the independent and partially-interactive criteria, the Tsai-Wu criterion gives a more comprehensive prediction by considering the interaction between the compressive and tensile strengths. However, the criterion does not indicate whether the laminate failure occurs in the fibre or matrix material. Like the previously mentioned criteria, the Tsai-Wu criterion is predicted

using a single expression. Moreover, assumptions are made to generalise the von Mises criterion, giving the A_{12} term [58, 32].

$$F_1\sigma_1 + 2F_2\sigma_2 + F_{11}\sigma_1^2 + F_{22}\sigma_2^2 + F_{66}\tau_{12}^2 - \sqrt{F_{11}F_{22}}\sigma_1\sigma_2 = 1 \quad (1.27)$$

where

$$\begin{aligned} F_1 &= \frac{1}{\sigma_1^T} + \frac{1}{\sigma_1^C} & F_2 &= \frac{1}{\sigma_2^T} \frac{1}{\sigma_2^C} \\ F_{11} &= -\frac{1}{\sigma_1^T\sigma_1^C} & F_{22} &= -\frac{1}{\sigma_2^T\sigma_2^C} & F_{66} &= \left(\frac{1}{\tau_{12}^F}\right)^2 \end{aligned} \quad (1.28)$$

■ Tsai-Hill Failure Criterion

Similar to the Tsai-Wu criterion, the Tsai-Hill criterion determines the strength with one single expression, without indicating whether the failure occurs in the fibre or matrix material. The Tsai-Hill criteria is applicable to the case of a single homogeneous orthotropic layer [58].

$$\left(\frac{\sigma_1}{X}\right)^2 - \frac{\sigma_1\sigma_2}{X^2} + \left(\frac{\sigma_2}{Y}\right)^2 + \left(\frac{\sigma_6}{Q}\right)^2 = 1 \quad (1.29)$$

■ Puppo-Evensen Criterion

The Puppo-Evensen criterion is proposed to carry out strength assessment for an entire laminate, although it can also be utilized for a single layer. The criterion considers a more thorough interaction between the tensile and compressive stress than the Tsai-Hill criterion and requires simpler testing requirements than the Tsai-Wu criterion [58, 63]. However, adjustments are needed according to the sign of the stresses, which makes it more cumbersome to use than the Tsai-Wu failure criterion.

$$\left(\frac{\sigma_1}{X}\right)^2 - \phi \frac{X\sigma_1\sigma_2}{X^2Y} + \phi \left(\frac{\sigma_2}{Y}\right)^2 + \left(\frac{\sigma_6}{Q}\right)^2 = 1 \quad (1.30)$$

where

$$\phi = \frac{3Q^2}{X_t Y_t}$$

IV. New failure criteria

Other than the ones mentioned above, which have been used in industry for a long time, there are now several new failure criteria that have been recently developed:

- Omni Strain

Omni strain criterion is an invariant based failure criterion proposed by Tsai and Melo [64], which introduces a modified approach to include the stiffness of a material and can be classify into the group fully interactive criterion.

A survey from AIAA journal in 1983 about the popularity of different failure criteria was conducted and results show that 80% of the representatives used either the Maximum stress, Maximum strain, Tsai-Wu or Tsai-Hill failure criteria, and the remaining 20% used either the Hashin, Hashin-Rotem or other criteria [65]. Sun et. al. [66] compared the six failure criteria mentioned in the survey and another review of the six criteria was also conducted by Paris [67]. Hinton et. al. compared 14 different failure criteria using both predictions and experimental data to determine the overall effectiveness of the various theories [68].

To determine the failure mode, some of the criteria mentioned above require adjustments in the strength values, while others require 2 or more equations, depending on whether the applied stress is positive or negative (tensile or compression). On the other hand, the Tsai-Wu failure criteria is designed to account for both positive and negative stresses, hence only one equation is needed and no adjustments to the strength values are required. Beside the suggested equations, it is found that A_{12} is insignificant for the majority of failure theories [69], indeed setting A_{12} to zero provides prediction accuracy sufficient for many engineering problems [70].

1.2.8 VARIABLE-STIFFNESS LAMINATES

A relatively new concept of manufacturing composite laminates called 'variable stiffness laminates', 'variable angle tow' (VAT) or 'steered-fibre' laminates was proposed by Gurdal and Olemedo in the early 1990s [8]. The most important characteristic of VAT laminates is that the fibre orientation of each ply varies constantly as a wave along the longitudinal or transverse directions, hence the stiffness properties also change, illustrations are provided in Fig. 1.11 [71]. The engineering properties and transverse stresses of symmetric square VAT laminates were improved compared to straight fibre laminates, approximate closed form solutions of a variable stiffness panel under 3 different boundary conditions along the transverse edges were also derived, i.e. free, fixed and free but straight [8].

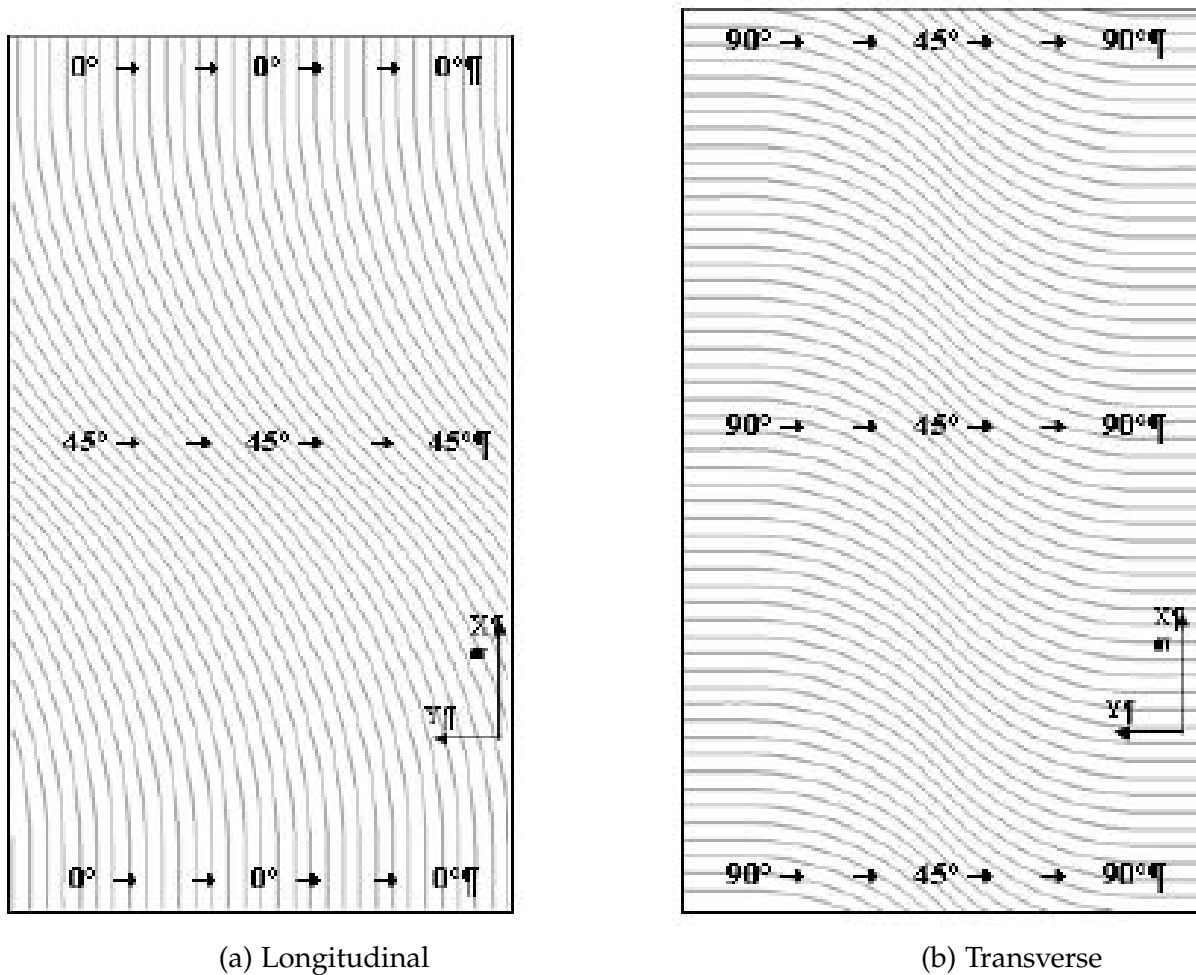


FIGURE 1.11: Illustration of VAT laminates with fibre angles varying along (a) longitudinal and (b) vertical axes [71].

Buckling analysis of variable stiffness laminates have been performed many times previously [72, 73, 74, 75]. Weaver et al. conducted experimental buckling tests on VAT laminates and compared the results with FEA and with similar experiments on straight fibre laminates [71]. Both longitudinal and transverse ply laminates were used. Results showed that variable stiffness laminates offer improvements in buckling performance but there was a 10 to 20 percent difference between the experimental results and the computational predictions. The difference might have been due to load misalignment or inaccurate modelling of the thickness change across the VAT laminates in FEA. Buckling analysis of stiffened VAT panels using a generalised Rayleigh-Ritz procedure was studied and compared with FEA [76, 77]. Raju et al. used a two-level approach to optimising VAT laminates using lamination parameters [78]. First, optimal lamination parameters that gave the maximum buckling load were found using a gradient based mathematical program and second, the fibre angles and stacking sequence were determined with fixed lamination parameters. Buckling results between the 2-level laminate parameter approach and the direct

genetic algorithm approach provided very similar predictions, and buckling performance was shown to improve compared to conventional straight fibre laminates. However, thickness changes across the VAT laminates were not considered.

Research has also shown improvements in the post-buckling performance of VAT laminates [79]. Wu et al. used a genetic algorithm to optimise VAT laminate design and also showed that the postw-buckling performance was improved compared to straight fibre laminates [80]. Wu et al. designed VAT laminates using lamination parameters and the feasible region of lamination parameters was examined [81].

Traditionally, manufacturing of variable stiffness laminates uses automatic fibre placement (AFP) machines. The lay-up process involves a tow-placement head that rotates freely and follows the centreline of the tow path of each ply [82]. Shifting methods are often used, as additional paths are required to cover the area of the laminate. However, tow overlaps can occur when adjacent tow paths are created as the paths move outward from the centreline and tow gaps can also occur as adjacent tow-paths diverge as the tow-paths move inwards due to in-plane bending deformation [83]. The defects lead to gaps and abrupt local changes in thickness across the laminate, affecting the properties of the structure. New manufacturing methods have been developed such as continuous tow shearing (CTS) to avoid overlaps and gaps, which allow thickness changes within VAT laminates to be predicted [84], the thickening pattern of AFP and CTS are illustrated in Figure 1.12 [9].

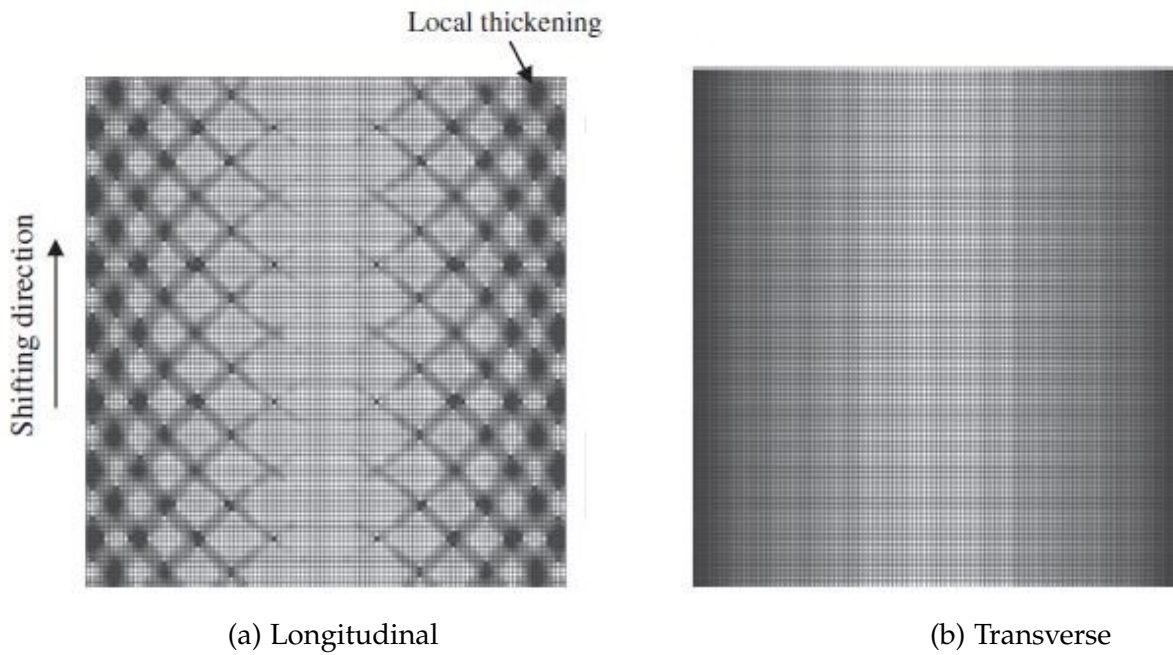


FIGURE 1.12: Thickness variation illustration of (a) AFP and (b) CTS technologies [9].

1.2.9 DOUBLE ANGLE-PLY LAMINATES (DOUBLE-DOUBLE, DD)

After understanding the basics of the more traditional technology related to composite laminates (see Sections 1.2.2 - 1.2.8), it is also of interest to learn about new developments within the area, this leads to an important area of study in this research project, namely, 'Double angle-ply laminates'. Conventional laminates usually incorporate just 4 ply-angles (quad laminates), namely, 0° , 90° and $\pm 45^\circ$, which has limited design space. The design of conventional laminates in industry typically follows a number of rules [85, 86]: (i) mid-plane symmetric to prevent thermal warping; (ii) balanced to prevent any mechanical couplings, (iii) the 10 percent rule, which means that each of the 4 plies must take up at least 10% of the total number of plies and (iv) ply contiguity of no more than 3 plies, to reduce delamination.

A new layup method of composite laminate was introduced by Tsai in 2017, called double angle-ply, or double-double (DD) laminates [87]. A DD laminate is a novel idea for designing laminates involving two pairs of sub-laminates. These replace conventional fixed ply angles (i.e. 0° , 90° , $\pm 45^\circ$), in which the two pairs of fibre angles can theoretically be arbitrary. DD laminates offers great potential for improvements over standard quad laminates, as listed below:

- DD laminates have been shown to offer potential improvements in first ply failure strength [88]

- Rather than being limited to 4 fixed angles for standard quad designs, ϕ and ψ in DD laminates can be any arbitrary angle between 0° to 90° . This offers a significantly larger design space compared to standard ply laminates.
- Ease of manufacturability: DD plies enhance the compatibility between the sub-laminates, which reduces the chance of wrinkle defects during the forming process, hence a higher production rate and lowering the requirement of manufacturing knockdown factors [89].
- As ϕ and ψ can be arbitrary angles, unlike the set angles found in quads, the fibre potential is allowed to be utilised fully with optimised combinations. Less layers are therefore needed to obtain the same performance as standard laminates of the same mass, which means reductions in the weight of the resulting structure [90].
- Mid-plane symmetric is not required with DD laminates because ϕ and ψ always comes with a positive and negative pair and always repeats, which allows DD laminates to be homogenised more quickly than standard quad laminates [91, 92]. A homogenised laminate refers to a laminate that has repeated properties throughout its thickness.
- The design and manufacture processes of homogenised laminates is simple, tailoring is also more straightforward and less prone to delamination [93].
- Layup speed of DD laminates can be up to 6 times quicker than quad laminates and with less scrap [93].
- Tapering can be achieved using a single ply drop-off at each step, rather than two drop-offs, as required with quad laminates [93].
- Ply termination of a DD laminate can be done anywhere on the laminate [93].
- DD laminates have a less serious problem of blending [93], which refers to a design methodology where a panel or laminate is divided into different regions, single ply drop off is allowed from one region to the adjacent region according to the load concentration of each region [94].
- More aggressive tapering can be achieved, up to a ratio of 10:1 between the centre and the edge. This can lead to further weight savings [95, 87].

Double angle ply laminates utilize the same design techniques as standard laminates and the

lamination parameters method can also be used for optimisation. Here the stacking sequence can be determined from the desired lamination parameters coordinates, i.e. the position within a lamination parameter design space. Moreover, the required lamination parameter values can be determined by stiffness matching; matching the lamination parameter coordinates of standard -ply designs for extensional (ξ_{1-4}) and bending stiffness (ξ_{9-10}) with those of DD laminates. For example, York used a stiffness matching approach to design double angle ply laminates and compared these with standard quads and also performed buckling analysis on the double angle ply laminates [96]. Here, lamination parameters were used for optimisation of the buckling performance of the DD laminates.

It should be noted that the notations for double angle ply laminates must be slightly modified from that of quad laminates. The symbols \circ , \bullet , $+$ and $-$ are replaced with $(+\phi/-\phi)$, $(-\phi/+\phi)$, $(+\psi/-\psi)$ and $(-\psi/+\psi)$ respectively. The relationships between the lamination parameters and the laminate configuration become:

$$\begin{aligned}
\bar{\xi}_1 &= \frac{n_{+\phi} \cos 2\theta_{+\phi} + n_{-\phi} \cos 2\theta_{-\phi} + n_{+\psi} \cos 2\theta_{+\psi} + n_{-\psi} \cos 2\theta_{-\psi}}{n} \\
\bar{\xi}_2 &= \frac{n_{+\phi} \cos 4\theta_{+\phi} + n_{-\phi} \cos 4\theta_{-\phi} + n_{+\psi} \cos 4\theta_{+\psi} + n_{-\psi} \cos 4\theta_{-\psi}}{n} \\
\bar{\xi}_3 &= \frac{n_{+\phi} \sin 2\theta_{+\phi} + n_{-\phi} \sin 2\theta_{-\phi} + n_{+\psi} \sin 2\theta_{+\psi} + n_{-\psi} \sin 2\theta_{-\psi}}{n} \\
\bar{\xi}_4 &= \frac{n_{+\phi} \sin 4\theta_{+\phi} + n_{-\phi} \sin 4\theta_{-\phi} + n_{+\psi} \sin 4\theta_{+\psi} + n_{-\psi} \sin 4\theta_{-\psi}}{n} \\
\bar{\xi}_5 &= \frac{\chi_{+\phi} \cos 2\theta_{+\phi} + \chi_{-\phi} \cos 2\theta_{-\phi} + \chi_{+\psi} \cos 2\theta_{+\psi} + \chi_{-\psi} \cos 2\theta_{-\psi}}{\chi} \\
\bar{\xi}_6 &= \frac{\chi_{+\phi} \cos 4\theta_{+\phi} + \chi_{-\phi} \cos 4\theta_{-\phi} + \chi_{+\psi} \cos 4\theta_{+\psi} + \chi_{-\psi} \cos 4\theta_{-\psi}}{\chi} \\
\bar{\xi}_7 &= \frac{\chi_{+\phi} \sin 2\theta_{+\phi} + \chi_{-\phi} \sin 2\theta_{-\phi} + \chi_{+\psi} \sin 2\theta_{+\psi} + \chi_{-\psi} \sin 2\theta_{-\psi}}{\chi} \\
\bar{\xi}_8 &= \frac{\chi_{+\phi} \sin 4\theta_{+\phi} + \chi_{-\phi} \sin 4\theta_{-\phi} + \chi_{+\psi} \sin 4\theta_{+\psi} + \chi_{-\psi} \sin 4\theta_{-\psi}}{\chi} \\
\bar{\xi}_9 &= \frac{\zeta_{+\phi} \cos 2\theta_{+\phi} + \zeta_{-\phi} \cos 2\theta_{-\phi} + \zeta_{+\psi} \cos 2\theta_{+\psi} + \zeta_{-\psi} \cos 2\theta_{-\psi}}{\zeta} \\
\bar{\xi}_{10} &= \frac{\zeta_{+\phi} \cos 4\theta_{+\phi} + \zeta_{-\phi} \cos 4\theta_{-\phi} + \zeta_{+\psi} \cos 4\theta_{+\psi} + \zeta_{-\psi} \cos 4\theta_{-\psi}}{\zeta} \\
\bar{\xi}_{11} &= \frac{\zeta_{+\phi} \sin 2\theta_{+\phi} + \zeta_{-\phi} \sin 2\theta_{-\phi} + \zeta_{+\psi} \sin 2\theta_{+\psi} + \zeta_{-\psi} \sin 2\theta_{-\psi}}{\zeta} \\
\bar{\xi}_{12} &= \frac{\zeta_{+\phi} \sin 4\theta_{+\phi} + \zeta_{-\phi} \sin 4\theta_{-\phi} + \zeta_{+\psi} \sin 4\theta_{+\psi} + \zeta_{-\psi} \sin 4\theta_{-\psi}}{\zeta}
\end{aligned} \tag{1.31}$$

Note that [B] is kept to zero at all times during this project to prevent thermal warping or any

coupling behaviour between the in-plane and out-of-plane loading, which means ζ_{5-8} are also zero. For balanced double angle-ply pairings, + and - ϕ and ψ are the equal, hence the expressions for extension and bending stiffnesses simply to:

$$\begin{aligned}
\bar{\zeta}_1 &= \frac{n_{\pm\phi} \cos 2\theta_{\pm\phi} + n_{\pm\psi} \cos 2\theta_{\pm\psi}}{n} & \bar{\zeta}_2 &= \frac{n_{\pm\phi} \cos 4\theta_{\pm\phi} + n_{\pm\psi} \cos 4\theta_{\pm\psi}}{n} \\
\bar{\zeta}_3 &= \frac{n_{\pm\phi} \sin 2\theta_{\pm\phi} + n_{\pm\psi} \sin 2\theta_{\pm\psi}}{n} & \bar{\zeta}_4 &= \frac{n_{\pm\phi} \sin 4\theta_{\pm\phi} + n_{\pm\psi} \sin 4\theta_{\pm\psi}}{n} \\
\bar{\zeta}_5 &= \frac{\chi_{\pm\phi} \cos 2\theta_{\pm\phi} + \chi_{\pm\psi} \cos 2\theta_{\pm\psi}}{\chi} & \bar{\zeta}_6 &= \frac{\chi_{\pm\phi} \cos 4\theta_{\pm\phi} + \chi_{\pm\psi} \cos 4\theta_{\pm\psi}}{\chi} \\
\bar{\zeta}_7 &= \frac{\chi_{\pm\phi} \sin 2\theta_{\pm\phi} + \chi_{\pm\psi} \sin 2\theta_{\pm\psi}}{\chi} & \bar{\zeta}_8 &= \frac{\chi_{\pm\phi} \sin 4\theta_{\pm\phi} + \chi_{\pm\psi} \sin 4\theta_{\pm\psi}}{\chi} \\
\bar{\zeta}_9 &= \frac{\zeta_{\pm\phi} \cos 2\theta_{\pm\phi} + \zeta_{\pm\psi} \cos 2\theta_{\pm\psi}}{\zeta} & \bar{\zeta}_{10} &= \frac{\zeta_{\pm\phi} \cos 4\theta_{\pm\phi} + \zeta_{\pm\psi} \cos 4\theta_{\pm\psi}}{\zeta} \\
\bar{\zeta}_{11} &= \frac{\zeta_{\pm\phi} \sin 2\theta_{\pm\phi} + \zeta_{\pm\psi} \sin 2\theta_{\pm\psi}}{\zeta} & \bar{\zeta}_{12} &= \frac{\zeta_{\pm\phi} \sin 4\theta_{\pm\phi} + \zeta_{\pm\psi} \sin 4\theta_{\pm\psi}}{\zeta}
\end{aligned} \tag{1.32}$$

For bending stiffness matching, $n_{\pm\psi}$ and $\zeta_{\pm\phi}$ can be written as $n - n_{\pm\phi}$ and $\zeta - \zeta_{\pm\phi}$, and by substituting $\alpha = \cos 2\phi$, $\beta = \sin 2\psi$, $\gamma = \frac{\zeta_{\pm\phi}}{\zeta}$ and the double angle trigonometric relationship $\cos 4\phi = 2\cos^2 2\phi - 1$, the bending stiffness lamination parameters, $\bar{\zeta}_9$ and $\bar{\zeta}_{10}$, become [97]:

$$\bar{\zeta}_9 = \frac{\zeta_{\pm\phi}}{\zeta} \alpha + \left(1 - \frac{\zeta_{\pm\phi}}{\zeta}\right) \beta \quad \bar{\zeta}_{10} = \frac{\zeta_{\pm\phi}}{\zeta} (2\alpha^2 - 1) + \left(1 - \frac{\zeta_{\pm\phi}}{\zeta}\right) (2\beta^2 - 1) \tag{1.33}$$

Also, β can be expressed by the following quadratic solution [97]:

$$\beta = -\frac{\bar{\zeta}_{10} + 1 - 2\alpha^2}{4(\alpha - \bar{\zeta}_9)} + \sqrt{\left(\frac{\bar{\zeta}_{10} + 1 - 2\alpha^2}{4(\alpha - \bar{\zeta}_9)}\right)^2 - \frac{2\alpha^2 \bar{\zeta}_9 - \alpha - \bar{\zeta}_{10} \alpha}{2(\alpha - \bar{\zeta}_9)}} \tag{1.34}$$

Finally using the obtained target value of β , the solution for α can be obtained iteratively until Eqn. 1.34 is balanced, where the target coordinates of $\bar{\zeta}_9$ and $\bar{\zeta}_{10}$ are used. Finally, the values of ψ and ϕ can be calculated.

Furthermore, stiffness matching for the extensional stiffness ($\bar{\zeta}_1$ and $\bar{\zeta}_2$) can also be performed in a similar way, to determine the ply percentages and the exact values of ψ and ϕ .

Previous work has been done on bending stiffness matching [97], where the stiffness of the DD laminates were matched to standard laminate configurations. A new database of DD laminate configurations, containing specific mechanical coupling characteristics was developed. The stiffness matching approach is also used in the current investigation to develop designs with

bending isotropy. Off-axis orientations can then be modified in order to introduce Extension-Shear coupling for first ply failure assessment.

1.3 THESIS OUTLINE

The remainder of this thesis is split into six chapters as follows:

- Chapter 2 provides the detailed theoretical derivations behind classical laminate theory and closed form buckling solutions. Multiple approaches are applied to ensure that the equations are implemented correctly using numerical examples. The details behind creation of a Finite Element Analysis model for buckling simulations is also presented.
- Chapter 3 provides an overview of the design of composite laminates with traditional orientations. Techniques for optimising standard laminates using lamination parameters are introduced. Results predicted under both compression and shear loading are presented, and design spaces of uncoupled standard laminates are plotted.
- Chapter 4 introduces a method of designing composite laminates with new DD configurations. The buckling and strength performance of DD laminates are examined, and their design spaces are plotted.
- Chapter 5 looks into the effect of different coupling behaviours on the buckling and FPF performance for both standard and DD laminate configurations are investigated. The 4-dimensional design space of laminates possessing coupling behaviours is also investigated further. Design spaces for fully coupled laminates are presented.
- Chapter 6 concludes the research and potential future work is also presented.

1.4 RESEARCH OBJECTIVES

The aim of this research is to design and optimise composite laminates with improved buckling and first-ply failure performance using an alternative design approach, which allows improved design of composite laminates without any concerns related to thickness changes that can occur in VAT laminates. In industry, symmetric and uncoupled laminates are mostly used because this type of laminate is guaranteed to be free of thermal warping and distortion. However, this rather conservative design approach is overly restrictive and can preclude the design of

better optimised laminates and structures. With better understanding of the technology, the potential of composite laminates can be better utilised with improved performance in buckling and FPF behaviour, with greater weight saving and with more flexible laminates possessing aero-elastic coupling behaviours. This point leads to one of the main motivations behind this project; namely, to examine the influence of non-symmetric and coupled laminates on buckling and FPF performance. To facilitate this goal, novel laminate design spaces will be developed and utilized to obtain an enhanced understanding of mechanically coupled laminates, involving bending and twisting.

To summarise, the goals for the current study are:

- To explore the lamination parameter design space for standard quad and DD laminates under compression and shear loading and to use the lamination parameter design space as a way of designing laminates.
- To design laminates using newly developed DD lamination configurations
- To examine possible improvements of DD laminates in terms of buckling and FPF performance.
- To examine the effect of coupling behaviours on the buckling and FPF performance of composite laminates, and to understand how the design spaces changes with coupling behaviours.

1.5 PUBLICATIONS

Journal Article

Lee, H.S. Jason. and York, C. B. (2020). Compression and shear buckling performance of finite length plates with bending-twisting coupling. *Composite Structures*, 241, 112069. **In Conference**

Proceedings

Lee, H.S. Jason. and York, C.B. (2019). Design Procedures for Improved Laminate Performance in Bending and Extension. 22nd International Conference on Composite Materials 2019 (ICCM 22), Melbourne, Australia, 11-16 Aug 2019.

CHAPTER 2

THEORY AND EXAMPLE CALCULATIONS AND FEA MODELLING

For completeness, this chapter provides theory and equations that are used during the investigation. Worked examples are also presented for clarity.

2.1 CLASSICAL LAMINATE THEORY (CLT)

2.1.1 THEORY

Classical laminate theory was briefly introduced in 1.2.2, which is given by:

$$\begin{bmatrix} N \\ M \end{bmatrix} = \begin{bmatrix} A & B \\ B & D \end{bmatrix} \begin{bmatrix} \epsilon \\ \kappa \end{bmatrix} \quad (2.1)$$

Here A_{ij} refers to the extensional stiffnesses; B_{ij} refers to the extensional-bending coupling stiffnesses and D_{ij} represents the bending stiffnesses. A_{ij} and D_{ij} can also be found on metallic structures while only occurs in composite structures. The individual terms in the ABD matrix are the integrals given as:

$$\begin{aligned} A_{ij} &= \int_{-\frac{H}{2}}^{+\frac{H}{2}} \bar{Q}_{ij} dz = \sum_{k=1}^N \bar{Q}_{ijk} (z_k - z_{k-1}) \\ B_{ij} &= \int_{-\frac{H}{2}}^{+\frac{H}{2}} \bar{Q}_{ij} z dz = \frac{1}{2} \sum_{k=1}^N \bar{Q}_{ijk} (z_k^2 - z_{k-1}^2) \\ D_{ij} &= \int_{-\frac{H}{2}}^{+\frac{H}{2}} \bar{Q}_{ij} z^2 dz = \sum_{k=1}^N \bar{Q}_{ijk} (z_k^3 - z_{k-1}^3) \end{aligned} \quad (2.2)$$

where \bar{Q}_{ij} are the transformed reduced stiffnesses given by:

$$\begin{aligned}
 \bar{Q}_{11} &= m^4 Q_{11} + 2m^2 n^2 (Q_{12} + 2Q_{66}) + n^4 Q_{22} \\
 \bar{Q}_{12} &= n^2 m^2 (Q_{11} + Q_{22} - 4Q_{66}) + (n^4 + m^4) Q_{12} \\
 \bar{Q}_{16} &= nm(m^2(Q_{11} - Q_{12} - 2Q_{66}) + n^2(Q_{12} - Q_{22} + 2Q_{66})) \\
 \bar{Q}_{22} &= n^4 Q_{11} + 2m^2 n^2 (Q_{12} + 2Q_{66}) + m^4 Q_{22} \\
 \bar{Q}_{26} &= nm(n^2(Q_{11} - Q_{12} - 2Q_{66}) + m^2(Q_{12} - Q_{22} + 2Q_{66})) \\
 \bar{Q}_{66} &= n^2 m^2 (Q_{11} + Q_{22} - 2Q_{12} - 2Q_{66}) + (m^4 + n^4) Q_{66}
 \end{aligned} \tag{2.3}$$

and Q_{ij} are the reduced stiffnesses that are related to the engineering constants as:

$$Q_{11} = \frac{E_1}{1 - \nu_{12}\nu_{21}} \quad Q_{12} = \frac{\nu_{12}E_2}{1 - \nu_{12}\nu_{21}} = \frac{\nu_{21}E_1}{1 - \nu_{12}\nu_{21}} \quad Q_{22} = \frac{E_2}{1 - \nu_{12}\nu_{21}} \quad Q_{66} = G_{12} \tag{2.4}$$

2.1.2 EXAMPLE 1. CALCULATION OF THE ABD MATRIX FROM MECHANICAL PROPERTIES OF THE LAMINATE

A 24-ply graphite/epoxy T300/5208 fully isotropic plate is used to illustrate the calculations of the ABD matrix with the 3 approaches mentioned using the following properties: Young's moduli $E_1 = 181.0$ GPa and $E_2 = 10.3$ GPa, shear modulus $G_{12} = 7.17$ GPa, Poisson ratio $\nu_{12} = 0.28$ and lamina thickness $t = 0.1397$ mm. The stacking sequence of the plate is: $[-/\bullet/\circ/+/\circ/+/\bullet/+/-/\circ/-/\bullet/-/\bullet/+/\bullet/\circ/-/\circ/+/\circ/+/-/\bullet]_T$, where subscripts +, -, \circ and \bullet are the notation for $+45^\circ$, -45° , 0° and 90° ply orientations respectively. First of all, the method of using the reduced stiffness starts with applying Eqn. 2.4:

$$\begin{aligned}
 Q_{11} &= \frac{E_1}{1 - \nu_{12}\nu_{21}} = \frac{181,000}{1 - 0.3 \times 0.01593} = 181,811 \text{ N/mm}^2 \\
 Q_{12} &= \frac{(\nu_{12}E_2)}{1 - \nu_{12}\nu_{21}} = \frac{0.28 \times 10,300}{1 - 0.3 \times 0.01593} = 2,897 \text{ N/mm}^2 \\
 Q_{22} &= \frac{E_2}{1 - \nu_{12}\nu_{21}} = \frac{10,300}{1 - 0.3 \times 0.01593} = 10,346 \text{ N/mm}^2 \\
 Q_{66} &= G_{12} = 7170 \text{ N/mm}^2
 \end{aligned}$$

The transformed reduced stiffnesses are calculated by using Eqn. 2.3 and shown in Table 2.1.

TABLE 2.1: Illustration of the transformed reduced stiffness for -45° , 45° , 0° and 90° layers.

θ°	\bar{Q}_{11}	\bar{Q}_{12}	\bar{Q}_{16}	\bar{Q}_{22}	\bar{Q}_{26}	\bar{Q}_{66}
-45	56,658	42,318	-42,866	56,658	-42,866	46,591
45	56,658	42,318	42,866	56,658	42,866	46,591
0	181,811	2,897	0	10,346	0	7,170
90	10,346	2,897	0	181,811	0	7,170

By applying Eqn. 2.2, and using A_{11} as example:

$$\begin{aligned}
A_{11} &= \sum_{k=1}^N \bar{Q}_{11}(z_k - z_{k-1}) \\
&= ((\bar{Q}_{11})_{-45} \times (12 \times 0.1397 - 11 \times 0.1397) + (\bar{Q}_{11})_{90} \times (11 \times 0.1397 - 10 \times 0.1397) \\
&+ (\bar{Q}_{11})_0 \times (10 \times 0.1397 - 9 \times 0.1397) + (\bar{Q}_{11})_{45} \times (9 \times 0.1397 - 8 \times 0.1397) \\
&+ (\bar{Q}_{11})_0 \times (8 \times 0.1397 - 7 \times 0.1397) + (\bar{Q}_{11})_{45} \times (7 \times 0.1397 - 6 \times 0.1397) \\
&+ (\bar{Q}_{11})_{90} \times (6 \times 0.1397 - 5 \times 0.1397) + (\bar{Q}_{11})_{45} \times (5 \times 0.1397 - 4 \times 0.1397) \\
&+ (\bar{Q}_{11})_{-45} \times (4 \times 0.1397 - 3 \times 0.1397) + (\bar{Q}_{11})_0 \times (3 \times 0.1397 - 2 \times 0.1397) \\
&+ (\bar{Q}_{11})_{-45} \times (2 \times 0.1397 - 1 \times 0.1397) + (\bar{Q}_{11})_{90} \times (1 \times 0.1397 - 0 \times 0.1397) \\
&+ (\bar{Q}_{11})_{-45} \times (0 \times 0.1397 - (-1) \times 0.1397) + (\bar{Q}_{11})_{90} \times (-2 \times 0.1397 - (-2) \times 0.1397) \\
&+ (\bar{Q}_{11})_{45} \times (-2 \times 0.1397 - (-3) \times 0.1397) + (\bar{Q}_{11})_{90} \times (-4 \times 0.1397 - (-4) \times 0.1397) \\
&+ (\bar{Q}_{11})_0 \times (-4 \times 0.1397 - (-5) \times 0.1397) + (\bar{Q}_{11})_{-45} \times (-6 \times 0.1397 - (-6) \times 0.1397) \\
&+ (\bar{Q}_{11})_0 \times (-6 \times 0.1397 - (-7) \times 0.1397) + (\bar{Q}_{11})_{45} \times (-8 \times 0.1397 - (-8) \times 0.1397) \\
&+ (\bar{Q}_{11})_0 \times (-8 \times 0.1397 - (-9) \times 0.1397) + (\bar{Q}_{11})_{45} \times (-10 \times 0.1397 - (-10) \times 0.1397) \\
&+ (\bar{Q}_{11})_{-45} \times (-10 \times 0.1397 - (-11) \times 0.1397) + (\bar{Q}_{11})_{90} \times (-11 \times 0.1397 - (-12) \times 0.1397) \\
&= 256,047N/mm
\end{aligned}$$

Repeating the process with the rest of the ABD matrix element gives:

$$\begin{bmatrix} A_{11} & A_{12} & A_{16} \\ A_{21} & A_{22} & A_{26} \\ A_{61} & A_{62} & A_{66} \end{bmatrix} = \begin{bmatrix} 256,047 & 75,798 & 0 \\ 75,798 & 256,047 & 0 \\ 0 & 0 & 90,125 \end{bmatrix} N/mm$$

$$\begin{bmatrix} D_{11} & D_{12} & D_{16} \\ D_{21} & D_{22} & D_{26} \\ D_{61} & D_{62} & D_{66} \end{bmatrix} = \begin{bmatrix} 239,858 & 71,005 & 0 \\ 71,005 & 239,858 & 0 \\ 0 & 0 & 84,426 \end{bmatrix} N/mm$$

Classical laminate theory is very important as the ABD matrix is used for buckling and first-ply failure assessment throughout this project. Therefore, it is vital that the ABD matrix is correctly calculated. In addition to using classical laminate theory, the ABD matrix can be obtained by other approaches that produce identical results. The approaches are listed below and are used to cross check and mutually verify results. In so doing it is ensured that all the different approaches used in this investigation are correctly implemented.

- Lamination parameters
- Non-dimensional parameters

2.2 LAMINATION PARAMETERS, NON-DIMENSIONAL PARAMETERS AND ABD MATRIX

This section provides the theory behind lamination parameters. These are used as an important design optimisation tool in this project. They are used to draw design spaces and to calculate the ABD matrix (which is required for buckling analysis). The form and presentation of lamination parameters has evolved since the theory was first introduced by Tsai in 1968 [31, 32]. The relationship between the lamination parameters and ABD matrix is discussed below. Examples of the use of lamination parameters are provided to demonstrate the method.

2.2.1 THEORY

The derivation process of the lamination parameters starts with evaluating Eqn. 2.2:

$$A_{ij} = \int_{-\frac{H}{2}}^{+\frac{H}{2}} \bar{Q}_{ij} dz \quad B_{ij} = \int_{-\frac{H}{2}}^{+\frac{H}{2}} \bar{Q}_{ij} z dz \quad D_{ij} = \int_{-\frac{H}{2}}^{+\frac{H}{2}} \bar{Q}_{ij} z^2 dz$$

By expanding the transformed reduced stiffnesses, \bar{Q}_{ij} , with Eqn. 2.3, the ABD matrix relationship becomes:

$$\begin{aligned} A_{11} &= \int_{-\frac{H}{2}}^{+\frac{H}{2}} (m^4 Q_{11} + 2m^2 n^2 (Q_{12} + 2Q_{66}) + n^4 Q_{22}) dz \\ A_{12} &= \int_{-\frac{H}{2}}^{+\frac{H}{2}} (n^2 m^2 (Q_{11} + Q_{22} - 4Q_{66}) + (n^4 + m^4) Q_{12}) dz \\ A_{16} &= \int_{-\frac{H}{2}}^{+\frac{H}{2}} (nm(m^2 (Q_{11} - Q_{12} - 2Q_{66}) + n^2 (Q_{12} - Q_{22} + 2Q_{66}))) dz \\ A_{22} &= \int_{-\frac{H}{2}}^{+\frac{H}{2}} (n^4 Q_{11} + 2m^2 n^2 (Q_{12} + 2Q_{66}) + m^4 Q_{22}) dz \\ A_{26} &= \int_{-\frac{H}{2}}^{+\frac{H}{2}} (nm(n^2 (Q_{11} - Q_{12} - 2Q_{66}) + m^2 (Q_{12} - Q_{22} + 2Q_{66}))) dz \\ A_{66} &= \int_{-\frac{H}{2}}^{+\frac{H}{2}} (n^2 m^2 (Q_{11} + Q_{22} - 2Q_{12} - 2Q_{66}) + (m^4 + n^4) Q_{66}) dz \end{aligned} \quad (2.5)$$

By expanding m and n and grouping the terms, the expression becomes:

$$\begin{aligned} A_{11} &= \int_{-\frac{H}{2}}^{+\frac{H}{2}} \left(\frac{3Q_{11} + 3Q_{22} + 2Q_{12} + 4Q_{66}}{8} + \left(\frac{Q_{11} - Q_{22}}{2} \right) \cos 2\theta \right. \\ &\quad \left. + \left(\frac{Q_{11} + Q_{22} - 2Q_{12} - 4Q_{66}}{8} \right) \cos 4\theta \right) dz \\ A_{12} &= \int_{-\frac{H}{2}}^{+\frac{H}{2}} \left(\frac{Q_{11} + Q_{22} + 6Q_{12} - 4Q_{66}}{8} - \left(\frac{Q_{11} + Q_{22} - 2Q_{12} - 4Q_{66}}{8} \right) \cos 4\theta \right) dz \\ A_{16} &= \int_{-\frac{H}{2}}^{+\frac{H}{2}} \left(\frac{2Q_{11} - 2Q_{22}}{8} + \left(\frac{Q_{11} + Q_{22} - 2Q_{12} - 4Q_{66}}{8} \right) \sin 4\theta \right) dz \\ A_{22} &= \int_{-\frac{H}{2}}^{+\frac{H}{2}} \left(\frac{3Q_{11} + 3Q_{22} + 2Q_{12} + 4Q_{66}}{8} - \left(\frac{Q_{11} - Q_{22}}{2} \right) \cos 2\theta \right. \\ &\quad \left. + \left(\frac{Q_{11} + Q_{22} - 2Q_{12} - 4Q_{66}}{8} \right) \cos 4\theta \right) dz \\ A_{26} &= \int_{-\frac{H}{2}}^{+\frac{H}{2}} \left(\frac{2Q_{11} - 2Q_{22}}{8} - \left(\frac{Q_{11} + Q_{22} - 2Q_{12} - 4Q_{66}}{8} \right) \sin 4\theta \right) dz \\ A_{66} &= \int_{-\frac{H}{2}}^{+\frac{H}{2}} \left(\frac{Q_{11} + Q_{22} - 2Q_{12} + 4Q_{66}}{8} - \left(\frac{Q_{11} + Q_{22} - 2Q_{12} - 4Q_{66}}{8} \right) \cos 4\theta \right) dz \end{aligned} \quad (2.6)$$

By repeating the same process for [B] and [D] matrices, and substituting 2 new variables U_i and ξ_{ij} , the relationships is simplified to:

$$\begin{aligned}
A_{11} &= (U_1 + \xi_1 U_2 + \xi_2 U_3) \times H & A_{12} &= A_{21} = (-\xi_2 U_3 + U_4) \times H \\
A_{16} &= A_{61} = \left(\frac{\xi_3 U_2}{2} + \xi_4 U_3\right) \times H & A_{22} &= (U_1 - \xi_1 U_2 + \xi_2 U_3) \times H \\
A_{26} &= A_{62} = \left(\frac{\xi_3 U_2}{2} - \xi_4 U_3\right) \times H & A_{66} &= (-\xi_2 U_3 + U_5) \times H \\
B_{11} &= \frac{(\xi_5 U_2 + \xi_6 U_3) \times H^2}{4} & B_{12} &= B_{21} = \frac{(-\xi_6 U_3 + U_4) \times H^2}{4} \\
B_{16} &= B_{61} = \frac{(\frac{\xi_7 U_2}{2} + \xi_8 U_3)^2}{4} & B_{22} &= \frac{\xi_5 U_2 + \xi_6 U_3}{4} \times H^2 \\
B_{26} &= B_{62} = \frac{(\frac{\xi_7 U_2}{2} - \xi_8 U_3) \times H^2}{4} & B_{66} &= \frac{(-\xi_6 U_3 + U_5) \times H^2}{4} \\
D_{11} &= \frac{(U_1 + \xi_9 U_2 + \xi_{10} U_3) \times H^3}{12} & D_{12} &= \frac{(U_4 - \xi_{10} U_3) \times H^3}{12} \\
D_{16} &= D_{61} = \frac{(\frac{\xi_{11} U_2}{2} + \xi_{12} U_3) \times H^3}{12} & D_{22} &= \frac{(U_1 - \xi_9 U_2 + \xi_{10} U_3) \times H^3}{12} \\
D_{26} &= D_{62} = \frac{(\frac{\xi_{11} U_2}{2} - \xi_{12} U_3) \times H^3}{12} & D_{66} &= \frac{(-\xi_{10} U_3 + U_5) \times H^3}{12}
\end{aligned} \tag{2.7}$$

where U_i are called the material invariants or Tsai-Pagano parameters that depend on the reduced stiffnesses, given as:

$$\begin{aligned}
U_1 &= \frac{3Q_{11} + 3Q_{22} + 2Q_{12} + 4Q_{66}}{8} \\
U_2 &= \frac{Q_{11} - Q_{22}}{2} \\
U_3 &= \frac{Q_{11} + Q_{22} - 2Q_{12} - 4Q_{66}}{8} \\
U_4 &= \frac{Q_{11} + Q_{22} + 6Q_{12} - 4Q_{66}}{8} \\
U_5 &= \frac{Q_{11} + Q_{22} - 2Q_{12} + 4Q_{66}}{8}
\end{aligned} \tag{2.8}$$

and $\tilde{\zeta}_{ij}$ are called the **lamination parameters**, give as:

$$\begin{aligned}
\tilde{\zeta}_1 &= \int_{-\frac{H}{2}}^{+\frac{H}{2}} \cos 2\theta dz & \tilde{\zeta}_5 &= \int_{-\frac{H}{2}}^{+\frac{H}{2}} \cos 2\theta z dz & \tilde{\zeta}_9 &= \int_{-\frac{H}{2}}^{+\frac{H}{2}} \cos 2\theta z^2 dz \\
\tilde{\zeta}_2 &= \int_{-\frac{H}{2}}^{+\frac{H}{2}} \cos 4\theta dz & \tilde{\zeta}_6 &= \int_{-\frac{H}{2}}^{+\frac{H}{2}} \cos 4\theta z dz & \tilde{\zeta}_{10} &= \int_{-\frac{H}{2}}^{+\frac{H}{2}} \cos 4\theta z^2 dz \\
\tilde{\zeta}_3 &= \int_{-\frac{H}{2}}^{+\frac{H}{2}} \sin 2\theta dz & \tilde{\zeta}_7 &= \int_{-\frac{H}{2}}^{+\frac{H}{2}} \sin 2\theta z dz & \tilde{\zeta}_{11} &= \int_{-\frac{H}{2}}^{+\frac{H}{2}} \sin 2\theta z^2 dz \\
\tilde{\zeta}_4 &= \int_{-\frac{H}{2}}^{+\frac{H}{2}} \sin 4\theta dz & \tilde{\zeta}_8 &= \int_{-\frac{H}{2}}^{+\frac{H}{2}} \sin 4\theta z dz & \tilde{\zeta}_{12} &= \int_{-\frac{H}{2}}^{+\frac{H}{2}} \sin 4\theta z^2 dz
\end{aligned} \tag{2.9}$$

Expanding the integrals and grouping the same angle orientations, the relationship between the 12 lamination parameters and the non-dimensional parameters, the stacking sequence and the number of plies are given in [32] as:

$$\begin{aligned}
\tilde{\zeta}_1 &= \frac{[n_+ \cos(2\theta_+) + n_- \cos(2\theta_-) + n_o \cos(2\theta_o) + n_\bullet \cos(2\theta_\bullet)]}{n} \\
\tilde{\zeta}_2 &= \frac{[n_+ \cos(4\theta_+) + n_- \cos(4\theta_-) + n_o \cos(4\theta_o) + n_\bullet \cos(4\theta_\bullet)]}{n} \\
\tilde{\zeta}_3 &= \frac{[n_+ \sin(2\theta_+) + n_- \sin(2\theta_-) + n_o \sin(2\theta_o) + n_\bullet \sin(2\theta_\bullet)]}{n} \\
\tilde{\zeta}_4 &= \frac{[n_+ \sin(4\theta_+) + n_- \sin(4\theta_-) + n_o \sin(4\theta_o) + n_\bullet \sin(4\theta_\bullet)]}{n} \\
\tilde{\zeta}_5 &= \frac{[\chi_+ \cos(2\theta_+) + \chi_- \cos(2\theta_-) + \chi_o \cos(2\theta_o) + \chi_\bullet \cos(2\theta_\bullet)]}{\chi} \\
\tilde{\zeta}_6 &= \frac{[\chi_+ \cos(4\theta_+) + \chi_- \cos(4\theta_-) + \chi_o \cos(4\theta_o) + \chi_\bullet \cos(4\theta_\bullet)]}{\chi} \\
\tilde{\zeta}_7 &= \frac{[\chi_+ \sin(2\theta_+) + \chi_- \sin(2\theta_-) + \chi_o \sin(2\theta_o) + \chi_\bullet \sin(2\theta_\bullet)]}{\chi} \\
\tilde{\zeta}_8 &= \frac{[\chi_+ \sin(4\theta_+) + \chi_- \sin(4\theta_-) + \chi_o \sin(4\theta_o) + \chi_\bullet \sin(4\theta_\bullet)]}{\chi} \\
\tilde{\zeta}_9 &= \frac{[\zeta_+ \cos(2\theta_+) + \zeta_- \cos(2\theta_-) + \zeta_o \cos(2\theta_o) + \zeta_\bullet \cos(2\theta_\bullet)]}{\zeta} \\
\tilde{\zeta}_{10} &= \frac{[\zeta_+ \cos(4\theta_+) + \zeta_- \cos(4\theta_-) + \zeta_o \cos(4\theta_o) + \zeta_\bullet \cos(4\theta_\bullet)]}{\zeta} \\
\tilde{\zeta}_{11} &= \frac{[\zeta_+ \sin(2\theta_+) + \zeta_- \sin(2\theta_-) + \zeta_o \sin(2\theta_o) + \zeta_\bullet \sin(2\theta_\bullet)]}{\zeta} \\
\tilde{\zeta}_{12} &= \frac{[\zeta_+ \sin(4\theta_+) + \zeta_- \sin(4\theta_-) + \zeta_o \sin(4\theta_o) + \zeta_\bullet \sin(4\theta_\bullet)]}{\zeta}
\end{aligned} \tag{2.10}$$

where n , χ and ζ represent the **non-dimensional parameters** for extension, coupling and bending stiffness respectively.

For traditional laminates (containing 0, 90 and ± 45 degree orientations) these are given by:

$$\begin{aligned}
 n_+ &= \sum (z_k - z_{k-1})_+ & \chi_+ &= 2 \times \sum (z_k^2 - z_{k-1}^2)_+ & \zeta_+ &= 4 \times \sum (z_k^3 - z_{k-1}^3)_+ \\
 n_- &= \sum (z_k - z_{k-1})_- & \chi_- &= 2 \times \sum (z_k^2 - z_{k-1}^2)_- & \zeta_- &= 4 \times \sum (z_k^3 - z_{k-1}^3)_- \\
 n_o &= \sum (z_k - z_{k-1})_o & \chi_o &= 2 \times \sum (z_k^2 - z_{k-1}^2)_o & \zeta_o &= 4 \times \sum (z_k^3 - z_{k-1}^3)_o \\
 n_\bullet &= \sum (z_k - z_{k-1})_\bullet & \chi_\bullet &= 2 \times \sum (z_k^2 - z_{k-1}^2)_\bullet & \zeta_\bullet &= 4 \times \sum (z_k^3 - z_{k-1}^3)_\bullet
 \end{aligned} \tag{2.11}$$

The non-dimensional parameters (n_+ , n_- , n_o , n_\bullet , χ_+ , χ_- , χ_o , χ_\bullet , ζ_+ , ζ_- , ζ_o and ζ_\bullet) are required to calculate the lamination parameters, the subscripts +, -, o and \bullet are the notation for +45°, -45°, 0° and 90°ply orientations. While the non-dimensional parameters n , χ and ζ (without a subscript) represent the sum of all parameters with the same subscripts, and the non-dimensional parameters for total coupling, χ and bending stiffnesses, ζ can also be expressed in terms of the n , which are given by:

$$\begin{aligned}
 n &= n_+ + n_- + n_o + n_\bullet \\
 \chi &= \chi_+ + \chi_- + \chi_o + \chi_\bullet \\
 \zeta &= \zeta_+ + \zeta_- + \zeta_o + \zeta_\bullet
 \end{aligned} \tag{2.12}$$

The non-dimensional parameters for extensional stiffness (n_+ , n_- , n_o , n_\bullet) can also be found by inspection of the laminate stacking sequence, it is simply the number of +, -, o and \bullet plies within the laminate, e.g. $n_o = 4$ in the following laminate $[0/90/+45/-45/90/0]_2$, which is equivalent to the summation of $(z_k - z_{k-1})$ for each ply orientation, where z_k is the distance of the k^{th} layer to the midplane normalised against thickness, t . The non-dimensional parameters for extensional stiffness (n_o , n_+ , n_- , n_\bullet) are simply a summation of the number of plies in each of the standard ply orientations, which can be expressed as a proportion of the total number of plies, n , and are commonly expressed as ply percentages.

Note that different types of laminates have different relationships between their non-dimensional parameters. For example, *Bend-Twist (B-T)* coupled laminates have equal n_+ and n_- and *extension-shear (E-S)* coupled laminates have equal ζ_+ and ζ_- . *Extension-shear and bend-twist (E-S-B-T)* coupled laminates have $n_+ \neq n_-$ and $\zeta_+ \neq \zeta_-$ [98].

Finally, the non-dimensional parameters (Eqn. 2.11) be used to calculate either the lamination parameters, or to calculate the ABD matrix directly, if the lamination parameters are not required, Figure 2.1 shows the relationship between the three.

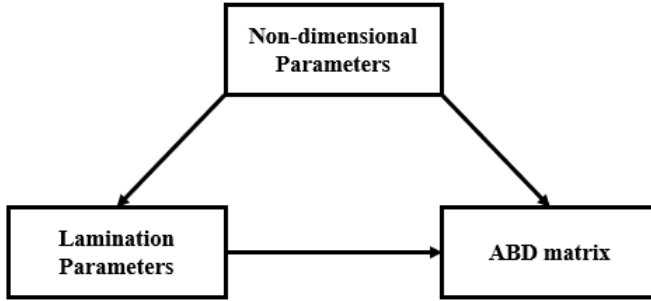


FIGURE 2.1: The relationship between non-dimensional parameters, lamination parameters and ABD matrix.

Note that the non-dimensional parameters can be used to directly calculate the ABD matrix without finding the lamination parameters, which is useful when lamination parameters are not necessary. The relationship between the non-dimensional parameters and the ABD matrix is:

$$\begin{aligned}
 A_{ij} &= (n_+(\bar{Q}_{ij})_+ + n_-(\bar{Q}_{ij})_- + n_o(\bar{Q}_{ij})_o + n_\bullet(\bar{Q}_{ij})_\bullet) \times t \\
 B_{ij} &= \frac{(\chi_+(\bar{Q}_{ij})_+ + \chi_-(\bar{Q}_{ij})_- + \chi_o(\bar{Q}_{ij})_o + \chi_\bullet(\bar{Q}_{ij})_\bullet) \times t^2}{4} \\
 D_{ij} &= \frac{(\zeta_+(\bar{Q}_{ij})_+ + \zeta_-(\bar{Q}_{ij})_- + \zeta_o(\bar{Q}_{ij})_o + \zeta_\bullet(\bar{Q}_{ij})_\bullet) \times t^3}{12}
 \end{aligned} \tag{2.13}$$

Examples are provided below for demonstration purposes.

2.2.2 EXAMPLE 2. CALCULATION OF THE ABD MATRIX FROM NON-DIMENSIONAL PARAMETERS

Using the same 24-ply fully isotropic laminate as used in Example 2.1.2, with $[-/\bullet/\circ/+/\circ/+/\bullet/+/-/\circ/-/\bullet/-/\bullet/+/\bullet/\circ/-/\circ/+/\circ/+/-/\bullet]_T$, the procedure of determining first the non-dimensional parameters is shown in Fig. 2.2, and from there these non-dimensional parameters are used to find the ABD matrix. The first 2 columns of Table 5 represent the ply order starting from the top surface of the laminate and the correspond ply orientation. The next columns are the summation of the number of each ply orientation within the laminate for the A, B and D

matrices, i.e. $(z_k - z_{k-1})$, $(z_k^2 - z_{k-1}^2)$ and $(z_k^3 - z_{k-1}^3)$, where z_k is the distance of the k^{th} layer to the mid plane. For the non-dimensional parameters of the extension stiffness matrix [A], the number of positive angle ply, $n_+(A\Sigma_+)$, number of negative angle plies, $n_-(A\Sigma_-)$, the number of 0° cross-ply, $n_o(A\Sigma_o)$ and the number of 90° cross plies, $n_\bullet(A\Sigma_\bullet)$ are all equals to 6. The sum of the bending-extension stiffness matrix [B] the non-dimensional parameters, ${}_B\Sigma_i$ are zero, which indicates that $B_{ij} = 0$. Finally for the bending stiffness matrix, [D]: the bending stiffness parameters, $\zeta_+ = \zeta_- = \zeta_o = \zeta_\bullet = (4_D\Sigma_+ = 4 \times 864) = 3456$ and $n^3 = 18^3 = 5,832$.

ply	Θ	A				B				D					
		$z_k - z_{k-1}$	$n_+ = A\Sigma_+$	$n_- = A\Sigma_-$	$n_o = A\Sigma_o$	$n_\bullet = A\Sigma_\bullet$	$z_k^2 - z_{k-1}^2$	$\chi_+ = B\Sigma_+$	$\chi_- = B\Sigma_-$	$\chi_o = B\Sigma_o$	$\chi_\bullet = B\Sigma_\bullet$	$z_k^3 - z_{k-1}^3$	$\zeta_+ = D\Sigma_+$	$\zeta_- = D\Sigma_-$	$\zeta_o = D\Sigma_o$
		6	6	6	6		0	0	0	0		864	864	864	864
1	-	1				-23		-23			397		397		
2	•	1				-21				-21	331				331
3	o	1			1	-19			-19		271			271	
4	+	1	1			-17	-17				217	217			
5	o	1			1	-15			-15		169			169	
6	+	1	1			-13	-13				127	127			
7	•	1				-11				-11	91				91
8	+	1	1			-9	-9				61	61			
9	-	1		1		-7		-7			37		37		
10	o	1			1	-5			-5		19			19	
11	-	1		1		-3		-3			7		7		
12	•	1				-1				-1	1				1
13	-	1		1		1		1			1		1		
14	•	1				3				3	7				7
15	+	1	1			5	5				19	19			
16	•	1				7				7	37				37
17	o	1			1	9			9		61			61	
18	-	1		1		11		11			91		91		
19	o	1			1	13			13		127			127	
20	+	1	1			15	15				169	169			
21	o	1			1	17			17		217			217	
22	+	1	1			19	19				271	271			
23	-	1		1		21		21			331		331		
24	•	1				23				23	397				397

FIGURE 2.2: Illustration of the procedure of finding the lamination parameter using non-dimensional parameters.

Using the same laminate as above with the stacking sequence with Eqn. 2.13:

$$\begin{aligned}
 A_{11} &= (n_+(\bar{Q}_{11})_+ + n_-(\bar{Q}_{11})_- + n_o(\bar{Q}_{11})_o + n_\bullet(\bar{Q}_{11})_\bullet) \times t \\
 &= (6 \times 56,658 + 6 \times 56,658 + 6 \times 181,811 + 6 \times 10,346) \times 0.1397 = 256,047 \text{ N/mm} \\
 B_{11} &= \frac{(\chi_+(\bar{Q}_{11})_+ + \chi_-(\bar{Q}_{11})_- + \chi_o(\bar{Q}_{11})_o + \chi_\bullet(\bar{Q}_{11})_\bullet) \times t^2}{4} \\
 &= \frac{(0 \times 56,658 + 0 \times 56,658 + 0 \times 181,811 + 0 \times 10,346) \times 0.1397^2}{4} = 0 \text{ N/mm} \\
 D_{11} &= \frac{(\zeta_+(\bar{Q}_{11})_+ + \zeta_-(\bar{Q}_{11})_- + \zeta_o(\bar{Q}_{11})_o + \zeta_\bullet(\bar{Q}_{11})_\bullet) \times t^3}{12} \\
 &= \frac{(3,456 \times 56,658 + 3,456 \times 56,658 + 3,456 \times 181,811 + 3,456 \times 10,346) \times 0.1397^3}{12} \\
 &= 239,858 \text{ N/mm}
 \end{aligned}$$

The rest of the ABD matrix then becomes:

$$\begin{aligned}
 \begin{bmatrix} A_{11} & A_{12} & A_{16} \\ A_{21} & A_{22} & A_{26} \\ A_{61} & A_{62} & A_{66} \end{bmatrix} &= \begin{bmatrix} 256,047 & 75,798 & 0 \\ 75,798 & 256,047 & 0 \\ 0 & 0 & 90,125 \end{bmatrix} \text{ N/mm} \\
 \begin{bmatrix} B_{11} & B_{12} & B_{16} \\ B_{21} & B_{22} & B_{26} \\ B_{61} & B_{62} & B_{66} \end{bmatrix} &= \begin{bmatrix} 0 & 0 & 0 \\ 0 & 0 & 0 \\ 0 & 0 & 0 \end{bmatrix} \text{ N/mm} \\
 \begin{bmatrix} D_{11} & D_{12} & D_{16} \\ D_{21} & D_{22} & D_{26} \\ D_{61} & D_{62} & D_{66} \end{bmatrix} &= \begin{bmatrix} 239,858 & 71,005 & 0 \\ 71,005 & 239,858 & 0 \\ 0 & 0 & 84,426 \end{bmatrix} \text{ N/mm}
 \end{aligned}$$

Note that the values of the ABD matrix calculated in Example 2.2.2 are identical to those determined in Example 2.1.2, validating the implementation of both approaches.

Once again use of lamination parameters to calculate the ABD matrix provides mutual verification to ensure the correct implementation of the equations used in each approach. But more importantly, this also allows the use of the lamination parameter design space to optimise laminate behaviour (the advantages of this approach over direct use of the fibre orientation were discussed in Section 1.2.5). Nevertheless, the ABD matrix can be found from the lamination parameters and used for buckling analysis. Stacking sequences that can produce the desired ABD

matrix can also be obtained by applying CLT, allowing optimisation of composite laminates. This process is illustrated in the following example.

2.2.3 EXAMPLE 3. CALCULATION OF ABD MATRIX FROM THE LAMINATION PARAMETERS

Using the same laminate example as before, by applying Eqn. 2.10, the lamination parameters are calculated as follow:

$$\begin{aligned}\bar{\zeta}_1 &= \frac{[n_+ \cos(2\theta_+) + n_- \cos(2\theta_-) + n_o \cos(2\theta_o) + n_\bullet \cos(2\theta_\bullet)]}{n} \\ &= \frac{6 \cos(2 \times 45) + 6 \cos(2 \times -45) + 6 \cos(2 \times 0) + 6 \cos(2 \times 90)}{24} = 0\end{aligned}$$

$$\begin{aligned}\bar{\zeta}_2 &= \frac{[n_+ \cos(4\theta_+) + n_- \cos(4\theta_-) + n_o \cos(4\theta_o) + n_\bullet \cos(4\theta_\bullet)]}{n} \\ &= \frac{6 \cos(4 \times 45) + 6 \cos(4 \times -45) + 6 \cos(4 \times 0) + 6 \cos(4 \times 90)}{24} = 0\end{aligned}$$

$$\begin{aligned}\bar{\zeta}_3 &= \frac{[n_+ \sin(2\theta_+) + n_- \sin(2\theta_-) + n_o \sin(2\theta_o) + n_\bullet \sin(2\theta_\bullet)]}{n} \\ &= \frac{6 \sin(2 \times 45) + 6 \sin(2 \times -45) + 6 \sin(2 \times 0) + 6 \sin(2 \times 90)}{24} = 0\end{aligned}$$

$$\begin{aligned}\bar{\zeta}_4 &= \frac{[n_+ \sin(4\theta_+) + n_- \sin(4\theta_-) + n_o \sin(4\theta_o) + n_\bullet \sin(4\theta_\bullet)]}{n} \\ &= \frac{6 \sin(4 \times 45) + 6 \sin(4 \times -45) + 6 \sin(4 \times 0) + 6 \sin(4 \times 90)}{24} = 0\end{aligned}$$

$$\begin{aligned}\bar{\zeta}_9 &= \frac{[\zeta_+ \cos(2\theta_+) + \zeta_- \cos(2\theta_-) + \zeta_o \cos(2\theta_o) + \zeta_\bullet \cos(2\theta_\bullet)]}{\zeta} \\ &= \frac{3,456 \cos(2 \times 45) + 3,456 \cos(2 \times -45) + 3,456 \cos(2 \times 0) + 3,456 \cos(2 \times 90)}{24^3} = 0\end{aligned}$$

$$\begin{aligned}\bar{\zeta}_{10} &= \frac{[\zeta_+ \cos(4\theta_+) + \zeta_- \cos(4\theta_-) + \zeta_o \cos(4\theta_o) + \zeta_\bullet \cos(4\theta_\bullet)]}{\zeta} \\ &= \frac{3,456 \cos(4 \times 45) + 3,456 \cos(4 \times -45) + 3,456 \cos(4 \times 0) + 3,456 \cos(4 \times 90)}{24^3} = 0\end{aligned}$$

$$\begin{aligned}\bar{\zeta}_{11} &= \frac{[\zeta_+ \sin(2\theta_+) + \zeta_- \sin(2\theta_-) + \zeta_o \sin(2\theta_o) + \zeta_\bullet \sin(2\theta_\bullet)]}{\zeta} \\ &= \frac{3,456 \sin(2 \times 45) + 3,456 \sin(2 \times -45) + 3,456 \sin(2 \times 0) + 3,456 \sin(2 \times 90)}{24^3} = 0\end{aligned}$$

$$\begin{aligned}\bar{\zeta}_{12} &= \frac{[\zeta_+ \sin(4\theta_+) + \zeta_- \sin(4\theta_-) + \zeta_o \sin(4\theta_o) + \zeta_\bullet \sin(4\theta_\bullet)]}{\zeta} \\ &= \frac{3,456 \sin(4 \times 45) + 3,456 \sin(4 \times -45) + 3,456 \sin(4 \times 0) + 3,456 \sin(4 \times 90)}{24^3} = 0\end{aligned}$$

The procedure continues by calculating the laminate invariants:

$$\begin{aligned}
 U_1 &= \frac{3Q_{11} + 3Q_{22} + 2Q_{12} + 4Q_{66}}{8} \\
 &= \frac{3 \times 181,811 + 3 \times 10,346 + 2 \times 2,897 + 4 \times 7,170}{8} = 76,368 \\
 U_2 &= \frac{Q_{11} - Q_{22}}{2} \\
 &= \frac{181,811 - 10,346}{2} = 85,732 \\
 U_3 &= \frac{Q_{11} + Q_{22} - 2Q_{12} - 4Q_{66}}{8} \\
 &= \frac{181,811 + 10,346 - 2 \times 2,897 - 4 \times 7,170}{8} = 19,710 \\
 U_4 &= \frac{Q_{11} + Q_{22} + 6Q_{12} - 4Q_{66}}{8} \\
 &= \frac{181,811 + 10,346 + 6 \times 2,897 - 4 \times 7,170}{8} = 22,607 \\
 U_5 &= \frac{Q_{11} + Q_{22} - 2Q_{12} + 4Q_{66}}{8} \\
 &= \frac{181,811 + 10,346 - 6 \times 2,897 + 4 \times 7,170}{8} = 26,880
 \end{aligned}$$

Using the lamination parameters and laminate invariants, the ABD matrices are:

$$\begin{aligned}
 A_{11} &= (U_1 + \xi_1 U_2 + \xi_2 U_3) \times H \\
 &= (76,368 + 0 \times 85,733 + 0 \times 19,710) \times 3.3528 = 256,047 \text{ N/mm} \\
 B_{11} &= \frac{(\xi_5 U_2 + \xi_6 U_3) \times H^2}{4} \\
 &= \frac{(0 \times 85,733 + 0 \times 19,710) \times 3.3528^2}{4} = 0 \text{ N/mm} \\
 D_{11} &= \frac{(U_1 + \xi_9 U_2 + \xi_{10} U_3) \times H^3}{12} \\
 &= \frac{(76,368 + 0 \times 85,733 + 0 \times 19,710) \times 3.3528^3}{12} = 239,858 \text{ N/mm}
 \end{aligned}$$

The final ABD matrix is:

$$\begin{bmatrix} A_{11} & A_{12} & A_{16} \\ A_{21} & A_{22} & A_{26} \\ A_{61} & A_{62} & A_{66} \end{bmatrix} = \begin{bmatrix} 256,047 & 75,798 & 0 \\ 75,798 & 256,047 & 0 \\ 0 & 0 & 90,125 \end{bmatrix} N/mm$$

$$\begin{bmatrix} B_{11} & B_{12} & B_{16} \\ B_{21} & B_{22} & B_{26} \\ B_{61} & B_{62} & B_{66} \end{bmatrix} = \begin{bmatrix} 0 & 0 & 0 \\ 0 & 0 & 0 \\ 0 & 0 & 0 \end{bmatrix} N/mm$$

$$\begin{bmatrix} D_{11} & D_{12} & D_{16} \\ D_{21} & D_{22} & D_{26} \\ D_{61} & D_{62} & D_{66} \end{bmatrix} = \begin{bmatrix} 239,858 & 71,005 & 0 \\ 71,005 & 239,858 & 0 \\ 0 & 0 & 84,426 \end{bmatrix} N/mm$$

The ABD matrix obtained from lamination parameters is identical to the one obtained from non-dimensional parameters in example calculation 2.1.2 and using CLT in example 2.2.2. All the method gives the same results for the ABD matrix, which confirms that the calculations are correct and can be used for the rest of the project. The different methods of obtaining the ABD matrix are implemented with Excel.

2.3 BUCKLING

2.3.1 THEORY

As mentioned in Section 1.2.6, the compression buckling load, N_x , can be obtained exactly by Eqn. 1.18 [6]:

$$N_x = \pi^2 [D_{11} \left(\frac{m}{a}\right)^2 + 2(D_{11} + 2D_{66}) \left(\frac{n}{b}\right)^2 + D_{22} \left(\frac{n}{b}\right)^4 \left(\frac{a}{m}\right)^2]$$

For verification purposes, another numerical way of calculating the buckling load is to apply the equation and data from ESDU 80023 datasheet [99], which is given as:

$$N_{xb} = \frac{K_0 \sqrt{(D_{11} D_{12})}}{b^2} + \frac{C \pi^2 D_{66}}{b^2} \quad (2.14)$$

Finally, the buckling factor is given by:

$$K_x = \frac{N_x b^2}{\pi^2 D_{Iso}} \quad (2.15)$$

where D_{iso} is the bending stiffness of the equivalent isotropic laminate with the same thickness and material properties, it is defined by:

$$D_{iso} = \frac{U_1 H^3}{12} \quad (2.16)$$

The buckling factor is an important parameter in determining the optimum buckling behaviour of a laminate and can be determined by substituting either Eqn. 1.18 or 2.14 into Eqn. 2.15. However, the closed form solution is only applicable to fully uncoupled laminates, laminates with any kind of coupled behaviour must be analysed with Finite Element Analysis.

2.3.2 EXAMPLE 4. CALCULATION OF BUCKLING LOAD AND BUCKLING FACTOR OF A SQUARE LAMINATE SUBJECT TO A UNIFORM AXIAL LOAD

The procedure for obtaining the compression buckling factor starts by applying the closed form buckling solution i.e. Eqn. 1.18. Using the ABD matrix of the same isotropic laminate in the above calculation, the buckling load is:

$$\begin{aligned} N_x &= \pi^2 [D_{11} \left(\frac{m}{a}\right)^2 + 2(D_{11} + 2D_{66}) \left(\frac{n}{b}\right)^2 + D_{22} \left(\frac{n}{b}\right)^4 \left(\frac{a}{m}\right)^2] \\ &= \left\{ \pi^2 [239,858 \left(\frac{1}{300}\right) + 2(239,858 + 2 \times 84,426) \left(\frac{1}{300}\right)^2 + 239,858 \left(\frac{1}{300}\right)^4 \left(\frac{300}{1}\right)^2] \right\} \\ &= 105.214 \text{ N/mm} \end{aligned}$$

Hence using Eqn. 2.15, the buckling factor is:

$$\begin{aligned} K_x &= \frac{N_x b^2}{\pi^2 D_{Iso}} \\ &= \frac{105.214 \times 300^2}{\pi^2 \times 239,860} = 4.0 \end{aligned}$$

Next, the buckling load and buckling factor can be checked by using the ESDU 80023 datasheet [99]. By applying Eqn. 2.14 and $K_0 = 19.7$ from the datasheet of aspect ratio 1, the buckling load

N_{xb} is:

$$\begin{aligned} N_{xb} &= \frac{K_0 \sqrt{(D_{11} D_{12})}}{b^2} + \frac{C \pi^2 D_{66}}{b^2} \\ &= \frac{19.7(239,858 \times 239,858)^{0.5}}{1000^2 \times 0.3^2} + \frac{2 \times \pi^2(71005 + 2 \times 84426)}{1000^2 \times 0.3^2} \\ &= 52.50 + 52.61 = 105.11 \text{ N/mm} \end{aligned}$$

and the buckling factor:

$$K_x = \frac{105.11 \times 3,002}{\pi^2 \times 239,860} = 3.996$$

Both methods match the classical compressive buckling coefficient of 4.0 for an isotropic laminate.

2.4 FINITE ELEMENT ANALYSIS MODELLING

Since the buckling performance of laminates with coupling behaviour cannot be predicted with closed form equations, Finite Element Analysis must be used. The FEA model is explained in this section. The FEA software ABAQUS is used for buckling simulations throughout this project. Input file editing is used instead of the user interface to create the model of a laminate. The input requires either the stacking sequence or the ABD matrix of the laminate, both ways should produce the same result. Both approaches are tested for cross verification and the input files for both are provided in Appendix. Conventional shell elements are used to create the model because the thickness of thin laminated structures is very small compared to their length and width, hence the transverse shear flexibility is considered negligible in the element formulation. A conventional stress/displacement shell element with 8 nodes and 5 degrees of freedom, S8R5, is used for modelling laminates in this project [100]. Comparing to a more general-purpose shell element, S4R for instance, S8R5 only focuses on thin plates whereas S4R is applicable for both thick and thin plates. However, S8R5 requires less refined mesh, which is a more efficient option and requires less running time [98, 101]. 2-D rather than 3-D models are generated by the input code. Here the thickness and lay-up are not shown. The mesh of the Abaqus model is shown in Figure 17.

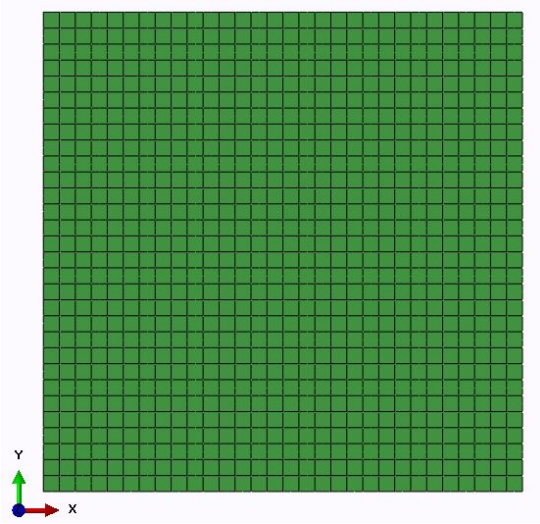
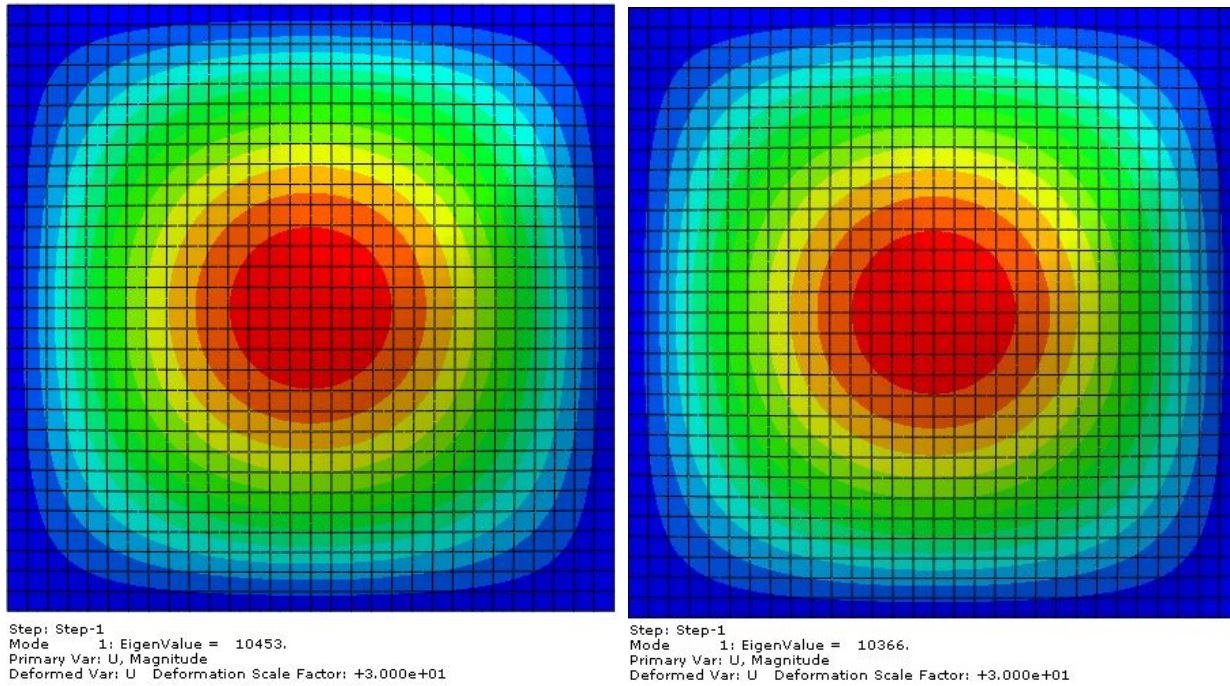


FIGURE 2.3: Illustration of the FEA model mesh.

The example is a square plate that contains 30 elements in each direction, where each element is 10 mm x 10 mm. This sums up to a 300 mm x 300 mm plate containing 3,600 nodes and 900 shell elements.

The buckling analysis from Abaqus is an eigenvalue problem, the eigenvalues obtained are then converted to the corresponding buckling loads and buckling factors. The converted buckling factors from FEA should be identical to the ones obtained with the closed form solution, i.e. 4.0 (see Section 1.2.6). The predicted buckling shape of the plate for the given ABD matrix and stacking sequence are shown in Figure 18. The same 24-ply laminate as that used in Examples 2.1.2, 2.2.2 and 2.2.3 is used to ensure that the FEA model produces the same results as using the closed form solution. The resulting K_x values, obtained using the two different input techniques (i.e. the ABD matrix or the stacking sequence) are 3.991 and 3.946 respectively, revealing differences of 0.125% and 1.25% from the closed form solution. Since the values obtained using the ABD matrix input is closer to the closed form solution than the stacking sequence input, the ABD matrix is used as the input for all FEA in the remainder of this project and extracts of codes used for the FEA in ABD and stacking sequence are included in A1 and A2.



(a) ABD matrix

(b) Stacking sequence

FIGURE 2.4: Illustration of the buckling pattern for (a) ABD matrix and (b) stacking sequence inputs with corresponding eigenvalues.

Moreover, the closed form solution is only applicable to compressive buckling, therefore FEA must be used for shear buckling analysis. The input code for shear buckling is similar to that used for compression buckling, the only difference is the load condition, here the loading direction is changed to both x and y directions instead of the x direction only. Extract of the shear loading codes is included in A3. The same 24-ply laminate as that used in Examples 2.1.2 - 2.2.3 is once used again for demonstration purposes. The predicted shear buckling pattern is shown in Figure 2.5a, which reveals a similar pattern compared to that presented by York [52] in Figure 2.5b.

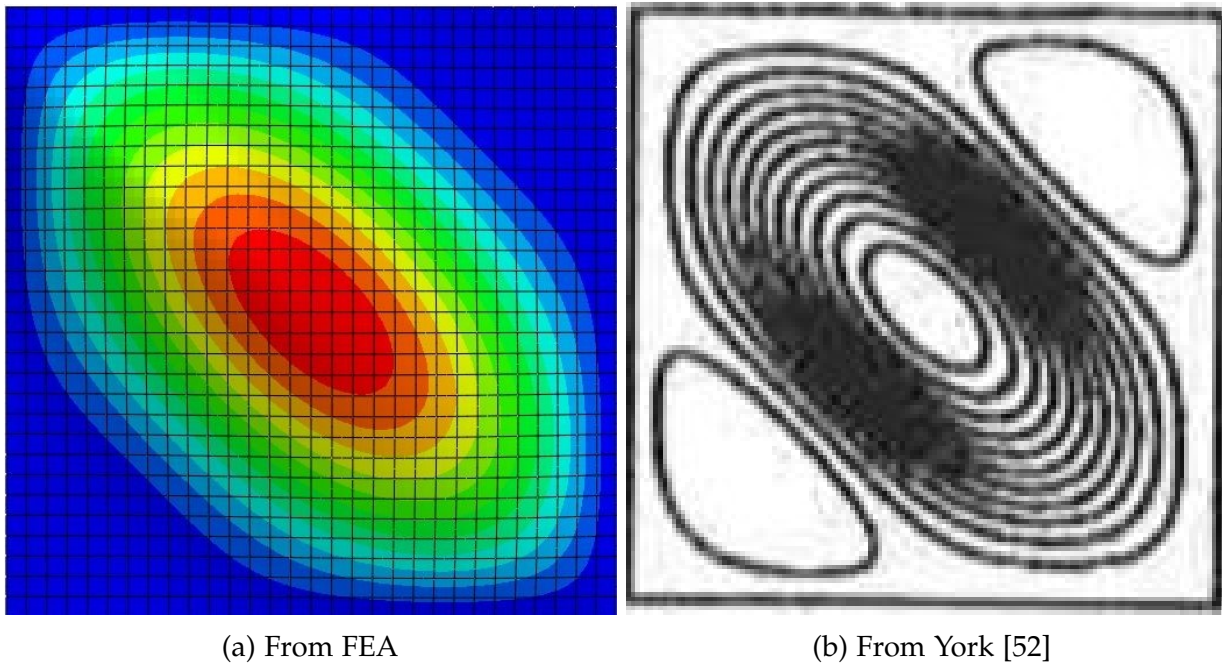


FIGURE 2.5: Illustration of the shear buckling pattern from FEA model compared to literature.

The converted buckling factor from the Abaqus eigenvalue gives 9.297, which is 0.41% away from the classical shear buckling factor value of 9.35 (from Stein and Neff [53]). The FEA model is therefore considered to be accurate enough for shear modelling in this project.

The theory and equations discussed in this chapter are used throughout this thesis in order to fulfil the objectives mentioned in Chapter 1.4. The CLT and lamination parameters are used to for design and optimisation of composite laminates with both standard and DD configurations. The compression closed form buckling solution is used for uncoupled laminate designs while FEA is used for any design that possesses any coupling behaviours.

The next chapter applies the theory in practice, starting by the investigation of compression and shear buckling performances of finite length laminates with standard ply orientations.

CHAPTER 3

COMPRESSION AND SHEAR BUCKLING PERFORMANCE OF FINITE LENGTH PLATES WITH BENDING-TWISTING COUPLING

3.1 INTRODUCTION AND MOTIVATION TO LAMINATE BUCKLING LOAD OPTIMISATION USING LAMINATION PARAMETER DESIGN SPACE

The aim of the work in this chapter is to explore buckling performance across the lamination parameter design space of laminated composite materials with both standard (as opposed to double angle) and straight (as opposed to steered) fibre orientations. Buckling performance is projected on the feasible design space to facilitate direct comparisons between any location within the design space. By indicating the buckling factors on the design space plots, locations with the highest laminate strength can easily be seen. This allows designers to know the buckling load at any location in the design space of applications that have typical values of lamination parameters, such as aircraft skins, spars and stiffeners. This chapter acts as the foundation of the entire study, laminates with more complicated designs will be investigated in later chapters.

Reduction in the buckling performance of composite plates or panel structures can occur whenever the material exhibits *Bend-Twist* coupling [102, 25], which commonly arises in symmetric laminate designs under compressive loading but not necessarily for shear. However, the effect of *Bend-Twist* coupling continues to be ignored on the basis that the effects dissipate for laminates comprised of many plies. However, fuselage panels typically have between 12 and 16 plies and wing panels may have less than 17 plies in buckling critical regions. In these cases, the compression buckling load may be overestimated (unsafe) and shear buckling load may be either

overestimated or underestimated (over-designed) if the effects of *Bend-Twist* coupling are ignored.

Optimisation of buckling performance can be performed by various methods. An earlier study on the effect of *Bend-Twist* coupling on finite length plates with simply supported edges adopted non-dimensional parameters [103], as indeed did the most recent study [22]. However, the latter differed from the lamination parameters approach to aid optimum design, used in this research, and by others [46, 54]. Furthermore, the buckling factor results presented in those studies were normalised by a bending stiffness parameter, which varies across the design space, hence buckling performance was not directly comparable. The advantages of using lamination parameters over non-dimensional parameters in buckling optimisation are outlined in Section 1.2.5.

Laminate databases containing *Extension-Shear* [104] and/or *Bend-Twist* coupling [25] properties demonstrate that the design spaces contain predominantly non-symmetric stacking sequences. Heuristic design rules are applied to these databases [85], including the adoption of symmetric stacking sequences, ply percentages and contiguity constraints to provide practical rather than purely theoretical designs, from which meaningful buckling performance characteristics can be assessed.

A set of high-fidelity orthographic projections of the lamination parameter design space can provide information on the significance of ply percentages and contiguity constraints. These are discussed later in this chapter in the context of the effect that in-plane material constraints have on the out-of-plane design space, with specific reference to *Bend-Twist* coupling.

Finally, new insights into compression and shear buckling performance are provided in this chapter via buckling factor contour maps, which are superimposed onto the lamination parameter design spaces. Contour mapping is applied to cross-sections through the design space, to allow detailed interrogation of the effects of *Bend-Twist* coupling on buckling performance. The mapping is also applied to external surfaces of the feasible domain of lamination parameters, on which some of the designs are found, since these bounding surfaces also correspond to bounds on buckling load. The results are applicable to finite length plates, across a range of aspect ratios, and complement a similar study on infinitely long plates with simply supported edges [86]. The latter provides lower bound solutions to the finite length plate results. The results of this chapter are useful for preliminary design, where optimised lamination parameters can be quickly matched to practical designs.

The effect of different combinations of simple supports and other boundary conditions is now well understood [52] and is covered extensively in the literature, albeit predominantly for metallic (isotropic) plates. This chapter therefore adopts an equivalent isotropic laminate datum to bridge the gap between metallic and composite behaviour, by comparing the buckling results of metallic and composite materials.

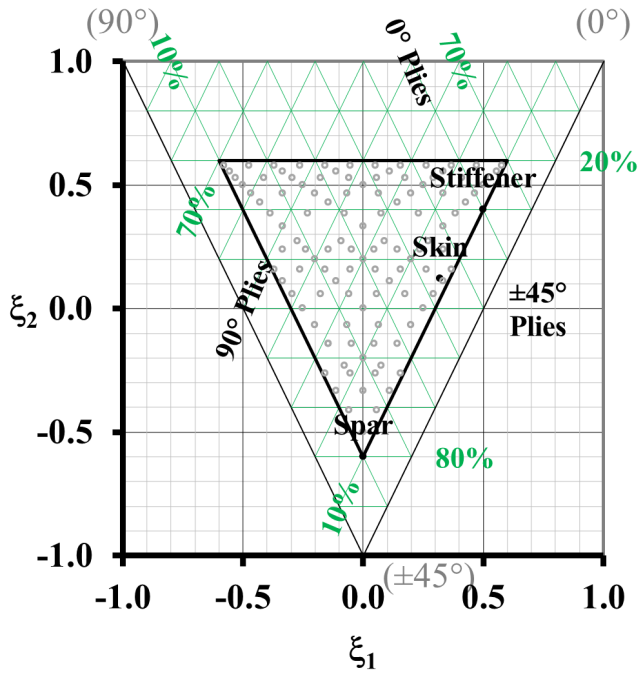
There are also many published results dealing with the minimum mass design or optimisation of laminated composite plate assemblies or built-up structures subject to buckling constraints. Optimisation procedures for stiffened panels generally lead to coincident buckling modes, i.e., the global and local modes share the same buckling load [105]. An exception to this is when constraints are applied to the stiffener height, here global modes develop at loads far below the local buckling load [106]. However, buckling behaviour cannot be generalized in such cases because it is configuration dependent. Results from the current study, assuming finite length plates, and from the earlier study, assuming infinitely long plates, are applicable where plate assemblies exhibit local buckling of the individual flat plates between stiffeners. Hence the influence of aspect ratio on the reduction in buckling load, resulting from poor laminate design choice, is a primary focus of this study. The behaviour of finite length plates is found to be very different from that of infinitely long panels, where buckling loads of infinitely long plates represents the lower bound.

3.2 DESIGN SPACE INTERROGATION

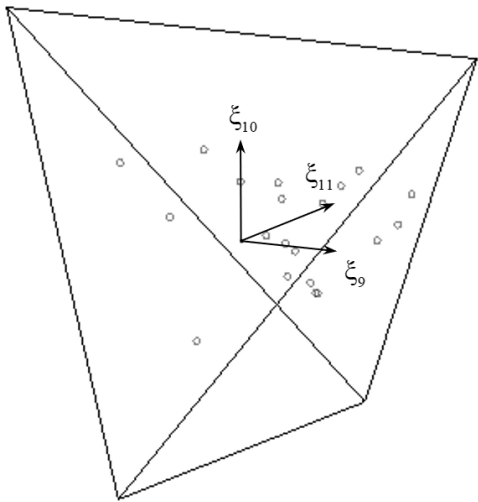
The database for Bend-Twist coupled designs with up to 21 plies is presented graphically in Figs. 3.1 and 3.2. Figure 3.1a represents the lamination parameter design space for extensional stiffness (ξ_1, ξ_2) with ply percentage mapping of straight fibre ply orientation. As mentioned in Chapter 5.1, ξ_{1-4} represent the extensional stiffness, ξ_{5-8} represent the coupling (in & out of plane) stiffness and ξ_{9-12} represent the bending stiffness, each set has its own feasible design region. The lamination parameter point cloud for extensional stiffness is illustrated by 112 points (grey circles) in Fig. 3.1a. Here $\xi_3 = \xi_4 = 0$, the coupling stiffness $\xi_{5-8} = 0$, and the bending stiffness $\xi_{12} = 0$, while ξ_9, ξ_{10} and ξ_{11} are all non-zero. Each of the 112 unique points represents many individual laminate designs sharing the same proportion of standard ply orientations, i.e. $0^\circ, 90^\circ$ and $\pm 45^\circ$ plies, but with different stacking sequences that result in different bending stiffnesses

(i.e. different values of ζ_9 , ζ_{10} and ζ_{11}). The contents of the database are also summarized in Table 3.1. The larger black triangle in Fig. 3.1a represents the feasible region of the design space when the extensional stiffness is uncoupled (i.e. A_{16} and A_{26} are zero). Note that the 10% rule has been applied, which means that each design consists of at least 10% of each of the standard ply orientations, this defines a smaller triangle (a sub-region) within the uncoupled design space corresponding to this constraint. Ply contiguity further constrains the available design space, which is set to a maximum of 3 adjacent plies with the same orientation, as is now common design practice. Ply contiguity is used to prevent 'ply blocking', which refers to a large numbers of consecutive repeating plies with the same fibre angle, that would increase the likelihood of delamination occurring [85]. This condition further shrinks the available design space. The smaller black triangle in Fig 1a is defined by the application of both these two types of constraint. The green grid lines represent constant ply percentage values for 0° , 90° and $\pm 45^\circ$ plies, ranging from 0 to 100% in intervals of 10%, where the top, left and right lines of the triangular design space represent purely 0° , 90° and $\pm 45^\circ$ plies respectively. To give an example of how to read this graph, the blue point in Fig. 3.1a at $(\zeta_1, \zeta_2) = (-0.7, 0.8)$ contains (0/ ± 45 /90) ply percentages of (10/10/80), as indicated by the green grid lines. Typical locations of aircraft wing skins, spars and stiffeners in this design space are indicated by the red points in Fig 1a. The results in Table 1 reveal that applying the contiguity constraint alone creates results that closely match predictions when applying the 10% rule constraint alone, across all ply number groupings. Figure 3.1b shows 20 points in a three-dimensional design space for bending stiffness defined by ζ_9 , ζ_{10} and ζ_{11} . The points are randomly selected from all available designs correspond to the points shown in Fig. 3.1a.

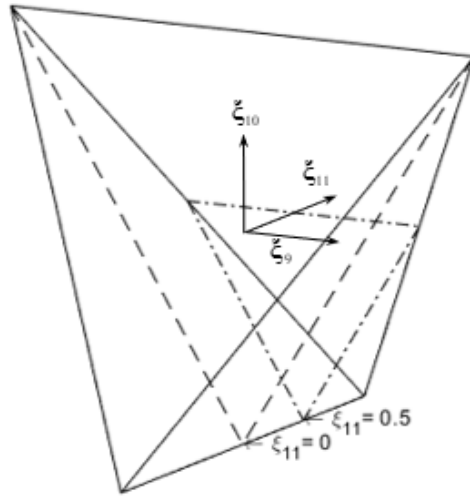
Finally, Fig 3.1c shows the location of the planes defined by $\zeta_{11} = 0$ (bounded by the dashed line) and $\zeta_{11} = 0.5$ (bounded by the dashed-dotted line) in the bending stiffness design space. These 2-D cross-sections are used later in Ch. 3, 4 and 5, where a 15-point grid of sample points is used to develop closed form buckling equations, as discussed in Section 3.1. ζ_{11} represents the out-of-plane coupling, with 0.5 being the most extreme value for this type of coupling used by industry. By using this value, the knock-down in buckling performance due to out-of-plane coupling can be assessed, while the size of the design space is reduced, making the optimisation more feasible.



(a)



(b)



(c)

FIGURE 3.1: Lamination parameter design spaces for symmetric Bend-Twist coupled laminates with up to 21 plies, with 10% rule and ply contiguity constraints (≤ 3) applied, corresponding to point clouds for: (a) extensional stiffness (ξ_1, ξ_2), including ply percentage mapping; (b) three-dimensional representation of the lamination parameter design space for bending stiffness with 20 randomly chosen points, and; (c) 3-D representation of the lamination parameter design space highlighting the planes with $\xi_{11} = 0$ and $\xi_{11} = 0.5$.

TABLE 3.1: Effect of ply continuity constraints (1, ≤ 2 , ≤ 3) on the number of stacking sequence solutions for each ply number grouping (n), balanced and symmetric representing *Bend-Twist* coupled designs from databases with the 10% rule applied.

n	Ply contiguity only			10% rule only
	1	≤ 2	≤ 3	
7	4	4	4	4
8	-	6	6	6
9	10	14	18	18
10	-	20	20	24
11	14	30	44	48
12	-	96	104	128
13	68	164	242	260
14	-	392	422	534
15	240	676	980	1,080
16	-	1,572	1,790	2,302
17	690	2,736	4,184	4,612
18	-	6,000	7,142	9,324
19	4,108	10,846	16,842	18,720
20	-	13,532	15,860	19,994
21	5,114	32,116	49,282	53,224

Note that, each point in the $\xi_1 - \xi_2$ design space has multiple possible design layups in the ξ_{9-11} design space, leading to over around 50,000 designs as shown in 3.1. If the constraints on ξ_{11} (0 and 0.5) are not applied, then the whole set of data is extremely large. For example, the full data set in the ξ_{9-11} design space can be plotted, as shown in Fig. 3.2. The lamination parameter point clouds for bending stiffness are illustrated in the orthographic projections in Fig. 3.2. The point clouds correspond to symmetric *Bend-Twist* coupled laminates with up to 21 plies, with 10% rule and ply contiguity constraints (≤ 3) applied. Here, the effect of the 10% rule is seen to have limited impact, since the point cloud extends to the bounds of the feasible region.

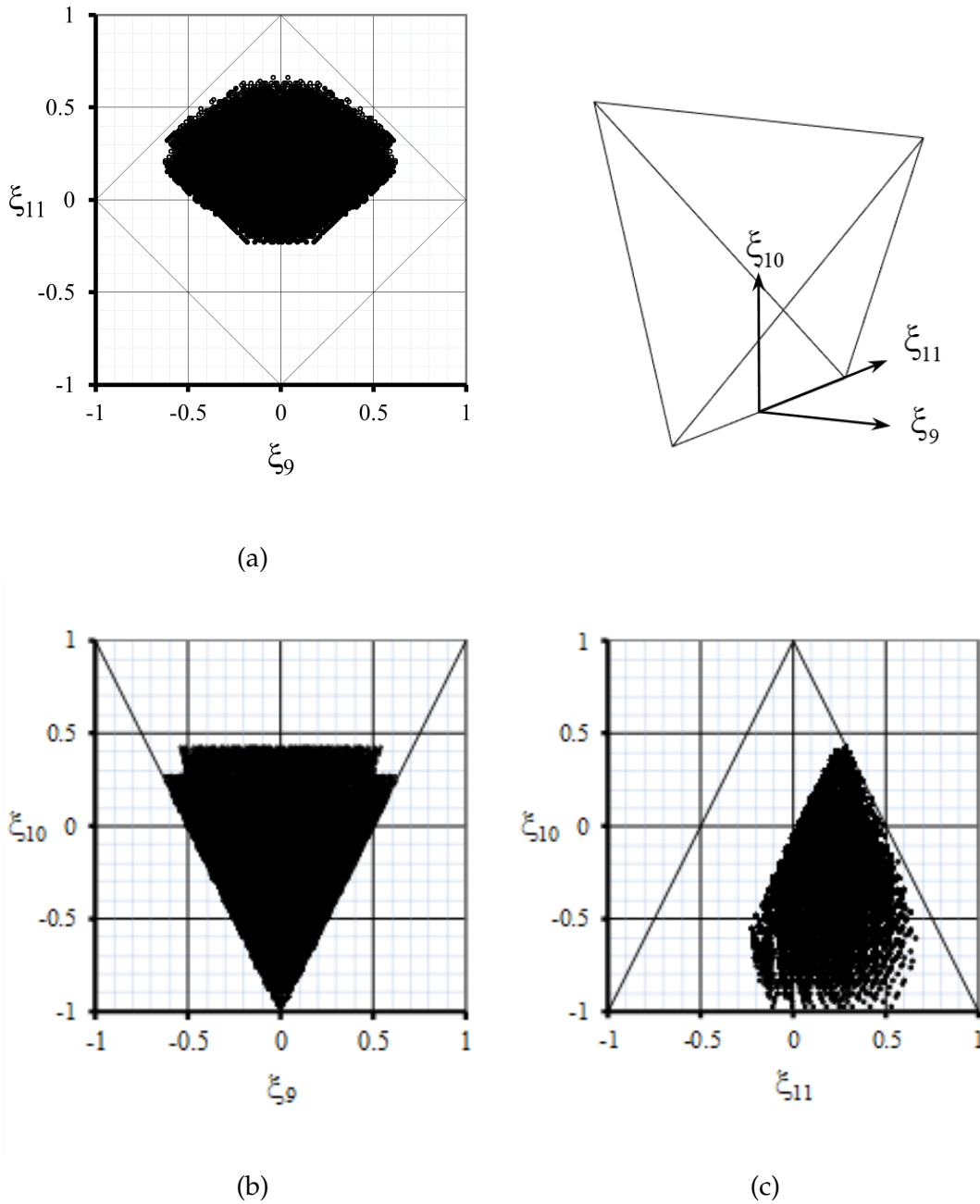


FIGURE 3.2: Orthographic projections (a): plan, (b) front elevation and (c) side views of point clouds for bending stiffness ($\xi_9, \xi_{10}, \xi_{11}$), corresponding to symmetric *Bend-Twist* coupled laminates with up to 21 plies, with 10% rule and ply contiguity constraints (≤ 3) applied.

Whilst the use of standard ply orientations was chosen primarily because they conform to common design practice, this also permits an otherwise 4-dimensional design space for non-standard ply orientations [54] to be represented in 3-dimensions, resulting in a design space defined by a regular tetrahedron, see Fig. 3.1b.

In the original derivation of the database, all stacking sequence designs possess a single outer

surface angle ply (e.g. +45°), as is a common design practice, to improve damage tolerance. This also serves to eliminate the possibility of generating cross-ply only designs. The resulting design space therefore appears to be skewed toward the positive region of the lamination parameter design space, defined by the lamination parameter ζ_{11} , representing the magnitude of *Bend-Twist* coupling, as seen in the plan view of Fig. 3.2a. If the signs of all the angle plies are switched, such that there is now a negative outer surface angle ply, the design space will be skewed towards the negative region. Designs that represent merely a switch in the sign of the ply angles are not unique and since the stacking sequences are listed in symbolic form (+/ -/ o/ ●), the designer has complete freedom to choose both the sign and the value of the ply angles. For the compression buckling design charts that follow, the results are unaffected by a sign switch in the angle plies, but for the corresponding shear buckling design charts a sign switch is equivalent to reversing the shear load direction, hence both positive and negative shear buckling charts are illustrated.

3.2.1 STIFFNESS AND LAMINATION PARAMETER RELATIONS

Ply angle dependent lamination parameters are now commonly adopted in design practice since they allow extensional and bending stiffness to be expressed as a set of linear design variables within convenient bounds. However, optimized lamination parameters must still be matched to a corresponding laminate configuration within the feasible region, and this is aided by graphical representations and laminate listings provided in an earlier article [25].

The general stiffness and lamination parameter relationship is discussed in chapter 1.2.5 and 2.2.1, given by Eqn. 2.10, while some simplification is introduced here. Namely, for standard ply orientations (+/ -/ o/ ●) = (45°/-45°/0°/90°), lamination parameter $\zeta_{12} = 0$. Note also that for balanced laminates, the extensional stiffness parameter $n_+ = n_- = n_{\pm}/2$, thus Eqn. 2.10 reduce to:

$$\begin{aligned}\zeta_1 &= \frac{n_{\pm} \cos(2\theta_+) + n_o \cos(2\theta_o) + n_{\bullet} \cos(2\theta_{\bullet})}{n} \\ \zeta_2 &= \frac{n_{\pm} \cos(4\theta_+) + n_o \cos(4\theta_o) + n_{\bullet} \cos(4\theta_{\bullet})}{n}\end{aligned}\quad (3.1)$$

Lamination parameters are provided for all stacking sequence data in the this chapter and the associated electronic annexe.

3.2.2 EFFECT OF DESIGN HEURISTICS ON THE LAMINATION PARAMETER DESIGN SPACE

Ply percentages are often used to account for design uncertainties relating to in-plane properties [103] and can be readily applied to the associated in-plane lamination parameter design space [89]. However, the effect of these constraints on the bending stiffness properties has not previously been investigated.

Ply percentages for standard ($0^\circ/\pm 45^\circ/90^\circ$) orientations are mapped onto the lamination parameter design space of Fig. 3.1a, and are related directly to orthotropic lamination parameters, ζ_1 and ζ_2 . Typical aircraft components, such as a Spar, Skin and Stiffener, can be represented by ($0/\pm 45/90$) ply percentages (10/80/10), (44/44/12) and (60/30/10), which are in turn related to the equivalent in-plane (ζ_1, ζ_2) lamination parameters (0, -0.6), (0.32, 0.12) and (0.5, 0.4), respectively.

These typical aircraft components are plotted together with 112 unique points representing symmetrically laminated designs, with up to 21 plies, possessing *Bend-Twist* coupling. All are contained within the 10% design rule and correspond to a ply contiguity constraint of up to 3 adjacent plies with identical orientation. Restricting the design space to a maximum of 21 plies is justified by the fact that it represents a natural limit for symmetric designs with the design heuristics applied here, i.e. with $[45_3/-45_3/0_3/90_3/0_3/-45_3/45_3]_T$. Beyond this, repeating sub-laminates lead to homogenisation of the stiffness properties and a reduction in the magnitude of Bend-Twist coupling.

The corresponding lamination parameter point cloud for bending stiffness is illustrated in the orthographic projections of Fig. 3.2, there is no discernible difference between this and the design space representing the entire database [25]. Each point within this 3-dimensional design space represents a coordinate from which the bending stiffness properties can be calculated directly, and to which a stacking sequence from the laminate database can readily be matched. There are 3,404 solutions with duplicate bending stiffness properties, meaning that designs with identical bending stiffness can and do possess different extensional stiffness properties. Of course, it is well-known that designs sharing the same extensional stiffness, i.e. ply angle percentages, possess different bending stiffness properties depending on the stacking sequence. The size of the dataset

can also be dramatically reduced if other constraints are applied, for example in Fig. 3.3 the data points in the ζ_{9-11} design space for just quasi-isotropic laminates are plotted, note that all these laminate designs share a single point in the ζ_{1-2} design space, i.e. $\zeta_1, \zeta_2 = 0, 0$ in the lamination parameter design space for extensional stiffness.

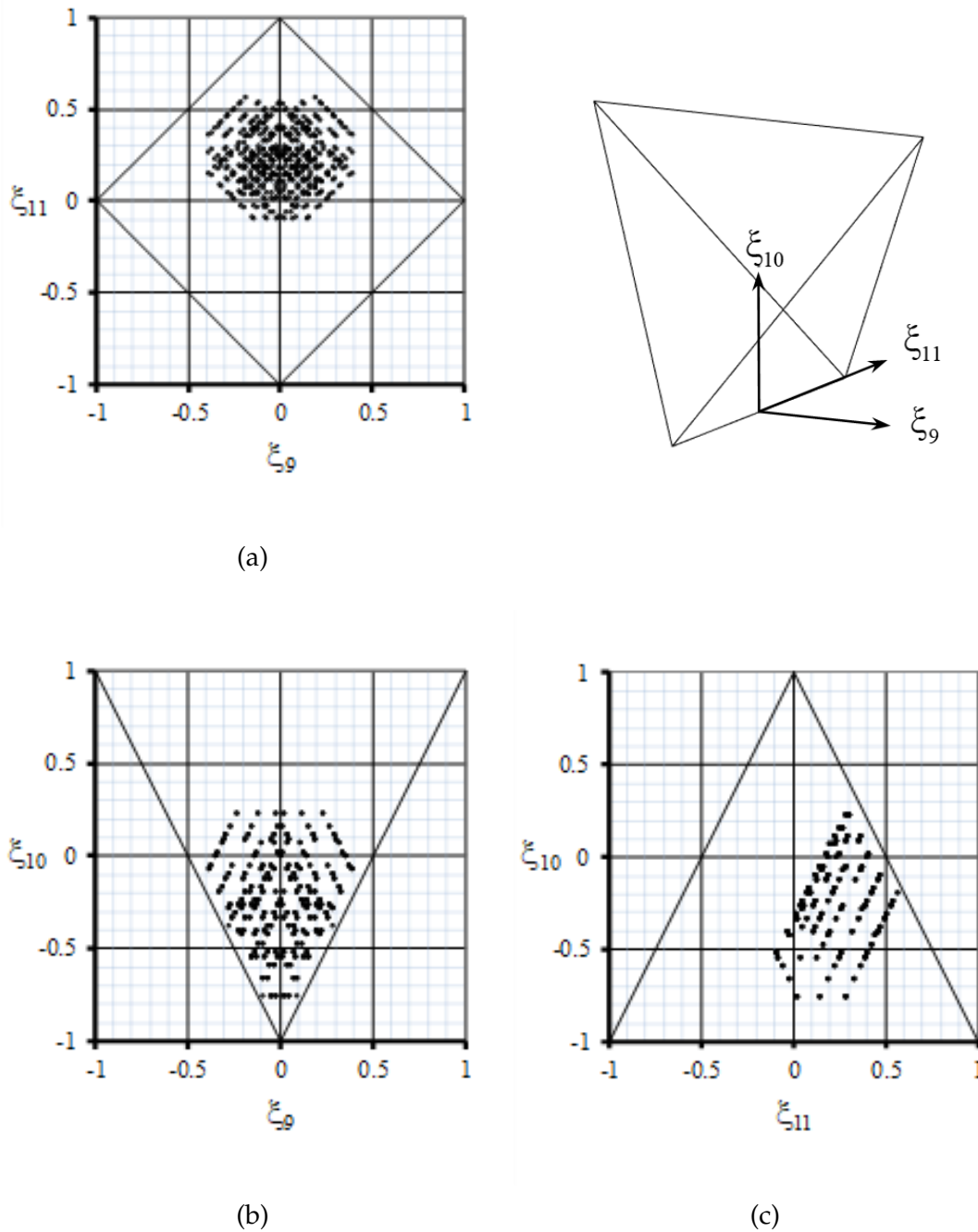


FIGURE 3.3: Orthographic projections (a): plan, (b) front elevation and (c) side views of point clouds for bending stiffness ($\zeta_9, \zeta_{10}, \zeta_{11}$), corresponding to Quasi-Isotropic laminates.

Such designs are often used for benchmarking due to the simplification of in-plane properties, but the simplification should never be assumed to extend to bending stiffness properties. For the

symmetric stacking sequences considered here, quasi-isotropic properties are found exclusively within 8 and 16 plies laminates, for which there are 6 and 536 solutions. The stacking sequence listings for 16 plies laminates can be found in Table A4 of the electronic annexe, together with their lamination parameter coordinates. They are grouped by matching orthotropic bending stiffness to reveal significant differences in *Bend-Twist* coupling magnitude, where each group contains between 2 and 6 stacking sequences.

Of the 93,536 designs, only 25,922 possess unique orthotropic bending stiffness properties, which corresponds to the number of points illustrated on the front elevation of the orthographic projection of Fig. 3.2. The entire design space is contained on 5,731 discrete parallel planes. This allows the effect of *Bend-Twist* coupling to be studied systematically, by comparing laminates with matching orthotropic properties. The plan view of Fig. 3.2 reveals that the vast majority of practical *Bend-Twist* coupled designs are contained within the design space defined by $\xi_{11} \leq 0.5$, which informs the study on buckling performance that follows.

3.3 BUCKLING PERFORMANCE OF FINITE LENGTH PLATES

The effect of *Bend-Twist* coupling on the buckling performance of finite length plates with simply supported edges has previously been investigated for both compression [103] and/or shear loading [107, 108] of hypothetical designs. However, the application of design heuristics to the database of *Bend-Twist* coupled laminates [86, 25] now permits an assessment of the buckling performance of practical design configurations. To assess the vast number of designs contained in the laminate database, a closed form solution of compression buckling is necessary. Eqn. 1.18 gives:

$$N_x = \pi^2 [D_{11} \left(\frac{m}{a}\right)^2 + 2(D_{11} + 2D_{66}) \left(\frac{n^2}{b^2}\right) + D_{22} \left(\frac{n^4}{b^4}\right) \left(\frac{a}{m}\right)^2]$$

from knowledge of the bending stiffness, D_{ij} , plate length, a , and width, b , and the buckling half-wave parameter, m ($= 1, 2, 3, \dots$), which produces the lowest critical force resultant N_x . However, Eqn. 1.18 is only applicable to fully uncoupled laminates, in which $D_{16} = D_{26} = 0$, and the buckling load for a general balanced and symmetric laminate, in which $D_{16}, D_{26} \neq 0$, can therefore be significantly overestimated (unsafe). Furthermore, there is no equivalent closed form solution for finite length plates under shear loading. New equations must therefore be developed to assess the relative buckling performance of finite length *Bend-Twist* coupled laminates. The following

sections therefore develops new equations applicable to both compression and shear buckling assessment of finite length rectangular plates, with simply supported boundary conditions, to complement the lower-bound solutions of the infinitely long plate [86]. The equations are then used to develop contour maps of buckling factors, which are superimposed on the lamination parameter design space to facilitate preliminary design. The contour mapping is readily applied to any cross-section throughout the design space, with constant ζ_{11} , to allow detailed interrogation of the effects of increasing Bend-Twist coupling on buckling performance.

3.3.1 CONTOUR MAPPING FOR COMPRESSION BUCKLING

For orthotropic laminates, the following buckling equation, represented by a 2-dimensional, 4th order polynomial, can be solved estimated using buckling loads obtained from the exact closed form buckling solution at 15 equally spaced points across the lamination parameter design space, as illustrated by the example cross section in Fig. 3.1c, when $\zeta_{11} = 0$:

$$\begin{aligned}
 k_x = & c_1 + c_2\zeta_9 + c_3\zeta_{10} + c_4\zeta_9^2 + c_5\zeta_{10}^2 + c_6\zeta_9\zeta_{10} + c_7\zeta_9^3 + c_8\zeta_{10}^3 + c_9\zeta_9\zeta_{10}^2 \\
 & + c_{10}\zeta_9^2\zeta_{10} + c_{11}\zeta_9^4 + c_{12}\zeta_{10}^4 + c_{13}\zeta_9\zeta_{10}^3 + c_{14}\zeta_9^2\zeta_{10}^2 + c_{15}\zeta_9^3\zeta_{10}
 \end{aligned} \quad (3.2)$$

where k_x is defined by Eqn. 2.15:

$$k_x = \frac{N_x b^2}{\pi^2 D_{Iso}}$$

This normalization ensures that buckling factor results are comparable across the design space, since the relative change in buckling factor, k_x , is the same as the relative change in the critical force resultant, N_x . In this study, IM7/8552 carbon-fibre/epoxy material is used, with Young's moduli $E_1 = 161.0$ GPa and $E_2 = 11.38$ GPa, shear modulus $G_{12} = 5.17$ GPa and Poisson ratio $\nu_{12} = 0.38$.

In contrast to the infinite plate results investigated previously [86], mode changes complicate the contour maps for finite length plates. Hence Eq. 3.2 is no longer a continuous function across the design space. The mode change boundaries must therefore first be determined, and separate equations must be derived for each mode region. To help further understand the buckling mode changes across the lamination parameter design space, classical Garland curves are first presented across a range of aspect ratios (a/b) in Fig. 3.4 Garland curves show the relationship between

buckling factor and the aspect ratios of laminates. These correspond to simply supported plates subject to uniaxial compression. Here, the solid black lines represent the buckling load factor of uncoupled laminate designs, whilst the broken black lines represent the buckling load factor when $\tilde{\zeta}_{11} = 0.5$ (corresponding to the limit for practical designs), comparison of the two sets of lines illustrates the effect of introducing a *Bend-Twist* coupling. The individual curves of Fig. 3.4, with circled labels 1 – 5, and 11 - 15 represent discrete coordinate points along the boundary of the $\tilde{\zeta}_9, \tilde{\zeta}_{10}$ lamination parameter design space, while curves 6-10 represent points along the middle line of the $\tilde{\zeta}_9, \tilde{\zeta}_{10}$ design space, as indicated by the corresponding label locations in Fig. 3.5. Points on the same curve also represent points with the same location on design spaces across a range of aspect ratios (a/b) from 0.5 to 2.5, the coordinates of the points on the design spaces are indicated by the coordinates under each curve. For example, the lowest curve, curve 1, in Fig. 3.4a represents the buckling factor of laminates with lamination parameters $(\tilde{\zeta}_9, \tilde{\zeta}_{10}) = (-1, 1)$, in which the $a/b = 1.0$ case is shown on Fig. 3.5a. The curves are split into 3 separate graphs in Fig. 3.4 to avoid confusion that might be caused by crowding overlapping curves. Fine dotted black lines connect the cusps on the uncoupled ($\tilde{\zeta}_{11} = 0$) and coupled ($\tilde{\zeta}_{11} = 0.5$) curves demonstrate the effect of coupling on the location of mode change in terms of aspect ratio. Only 3 coupled curves with $\tilde{\zeta}_{11} = 0.5$ are presented in Fig. 3.5a - 3.5c because the design space shrinks as the value of $\tilde{\zeta}_{11}$ increases, therefore no feasible data points are available for points located with $\tilde{\zeta}_{10} > 0$ for $\tilde{\zeta}_{11} = 0.5$.

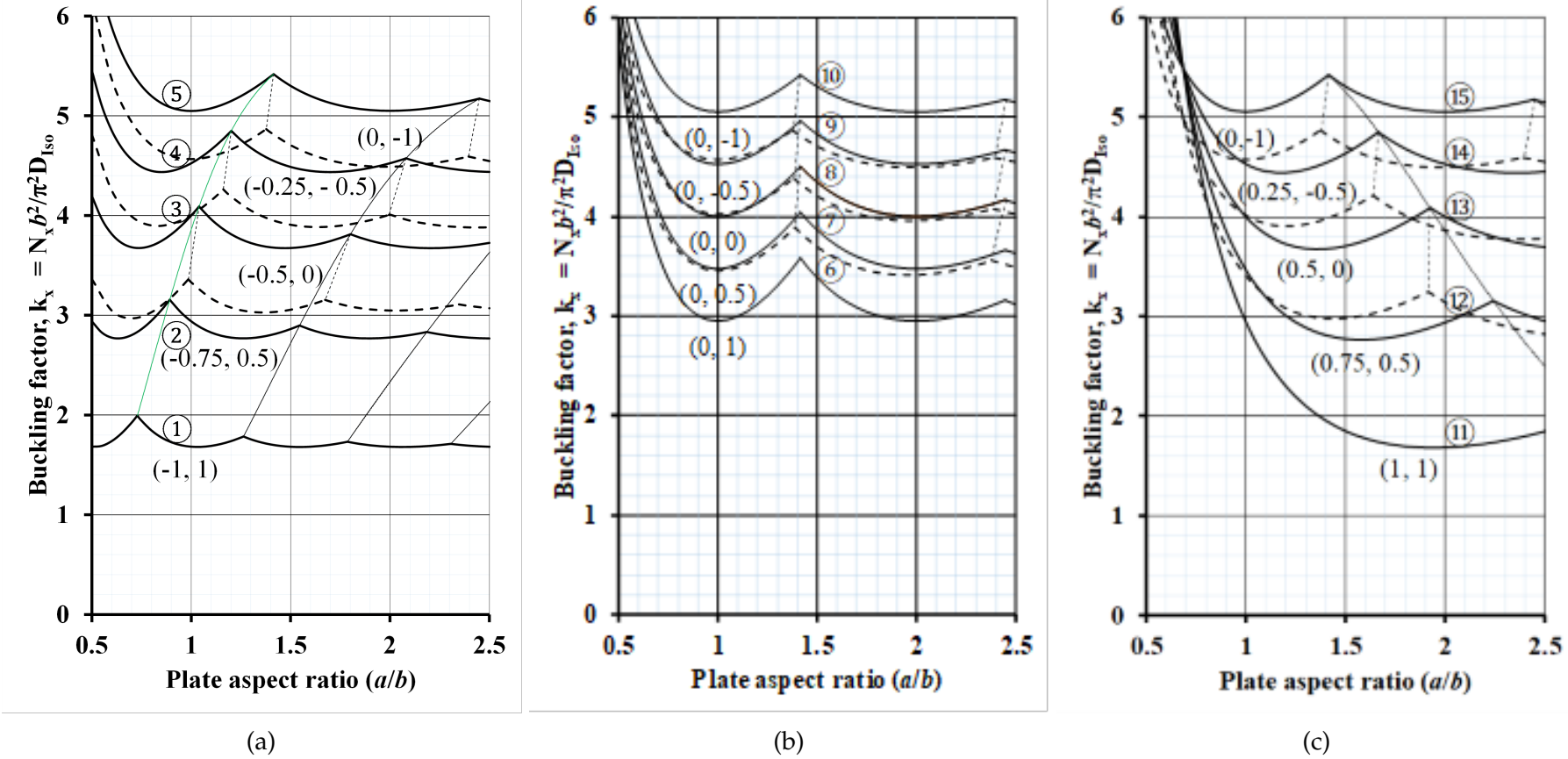


FIGURE 3.4: Compression buckling Garland curves for $\zeta_{11} = 0$ (solid lines) and $\zeta_{11} = 0.5$ (broken lines). The corresponding lamination parameter coordinates $(\zeta_{0.5})$ are given alongside each curve.

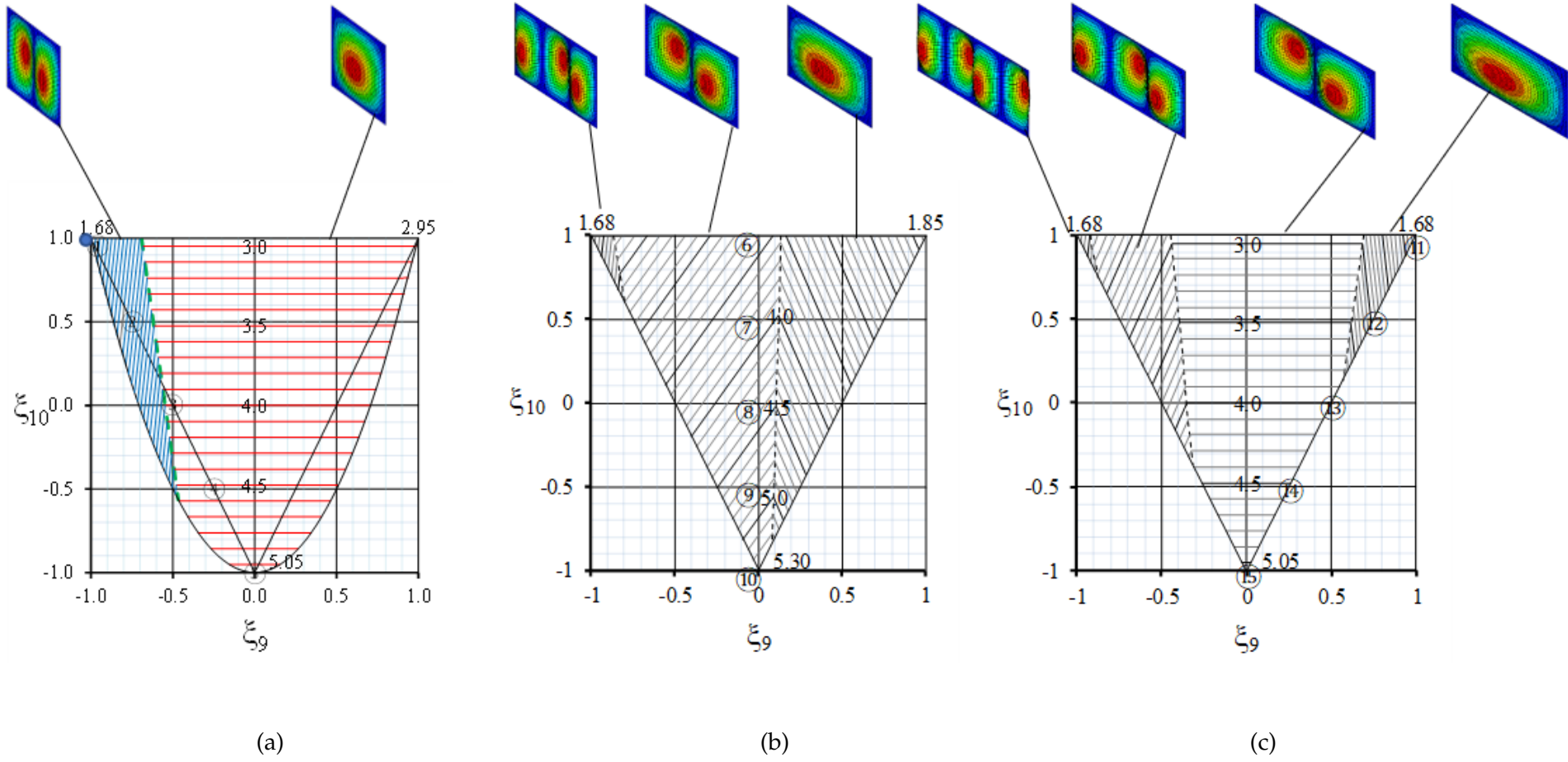


FIGURE 3.5: Compression buckling contours $k_x (= N_x b^2 / \pi^2 D_{Iso})$ for $\zeta_{11} = 0.0$, with: (a) $a/b = 1.0$ (including parabolic bounds after Ref. [54]); (b) $a/b = 1.5$ and; (c) $a/b = 2.0$.

Figure 3.5 illustrates contour maps with different aspect ratios ($a/b = 1, 1.5$ and 2), where distinct different styles of parallel-line in-fill patterns, represent different buckling mode regions (indicated by the inset images above Fig 5 3.5). The value of the buckling load for the contours is indicated by the numbers in the figure. Boundaries between these regions correspond to the cusps in Fig. 3.4. In Fig. 3.5a, the 'mode change line' (highlighted in one instance in Fig. 3.4 and also in Fig. 3.5 by a green line) separates two regions representing modes with one and two longitudinal half-waves, i.e. wavelength parameters $m = 1$ (red lines) and $m = 2$ (blue lines). This mode change is also apparent in Fig. 3.4a, between curves 2 and 3 at aspect ratio $a/b = 1.0$. Such boundary lines are readily determined whenever Eq. 1.18 is applicable, by fixing one lamination parameter coordinate and solving for the other by simply equating $N_{x,m=1}$ and $N_{x,m=2}$. The locations of the mode change at the boundaries in Fig. 3.4a correspond to $(\xi_9, \xi_{10}) = (-0.567, 0.134)$ and $(-0.691, 1)$, with buckling factor $k_x = 3.86$ and 2.95 , respectively. The same procedure can be used to confirm the shape of the mode change line.

Figure 3.4a represents the buckling factor contour map for constant aspect ratio ($a/b = 1.0$) plates with uncoupled orthotropic bending stiffness. Similarly, labels on the Garland curves of Figs. 3.4b and 3.4c correspond to those on the contour maps of Figs. 3.5b and 3.5c for aspect ratios, $a/b = 1.5$ and 2.0 , respectively. Hence, for a fixed aspect ratio, the isolines of constant buckling factor, k_x , are seen to vary with respect to the lamination parameter coordinates, or bending stiffness, as defined by Eqn. 2.15.

The centre of the contour map represents a fully isotropic laminate, with $(\xi_9, \xi_{10}) = (0, 0)$, and corresponds to curve 8 on Fig. 3.4b where $k_x = 4.0$ for aspect ratio $a/b = 1, 2, 3, \dots, \infty$. The cusps that arise from changes in buckling mode also occur at $a/b = \sqrt{2}, \sqrt{6}, \dots$ as in metallic plates [52]. However, for composite materials, the cusp locations are now strongly influenced by orthotropic bending stiffness properties; and further still by the introduction of *Bend-Twist* coupling.

For *Bend-Twist* coupled laminates, Eqn. 1.18 is no longer valid and therefore a different approach must be adopted. Buckling factor (k_x) results are established at 15 sample points across the feasible region of the design space, corresponding to the grid point intersections of the triangulation illustrated by the cross-section of Fig. 3.1c, from which the coefficients $c_1 - c_{15}$ in Eqn. 2.15 can then be derived for each buckling mode.

The finite element analysis software ABAQUS [100] was used to generate buckling factor results, using the same relative grid point geometry for any cross-section throughout the lamination parameter design space with constant magnitude of *Bend-Twist* coupling, $\tilde{\zeta}_{11}$. Lamination parameters $\tilde{\zeta}_{11} = 0$ and $\tilde{\zeta}_{11} = 0.5$ are compared in this chapter since these represent the bounds for practical laminate designs. Note that $-\tilde{\zeta}_{11}$ and $+\tilde{\zeta}_{11}$ yield the same compression buckling factor, k_x , hence only $+\tilde{\zeta}_{11}$ are given. The process of developing the contour maps is now briefly described with specific reference to Fig. 3.5c, representing plate aspect ratio $a/b = 2.0$; chosen because it contains four buckling mode regions. Here, individual buckling contours maps, illustrated in Fig. 3.6, represent the four modes of interest, each generally requires the calculation of a large number of eigenvalues at each grid point to ensure that the specific modes are found. The individual contour maps therefore represent continuous functions and, in general, all the coefficients $c_1 - c_{15}$ in Eq. 3.2 are non-zero. Fig. 3.5c is therefore comprised of the shaded regions from each of the individual contour maps, i.e., regions containing the lowest buckling factor contours from any of the four modes. The coefficients used to generate each mode region ($m = 1, 2, 3,$ and 4) in Fig 3.5c, are listed in Table 3.2. Note that the number of significant figures in the coefficients has been reduced but is sufficient to maintain a buckling factor accurate to 2 decimal places.

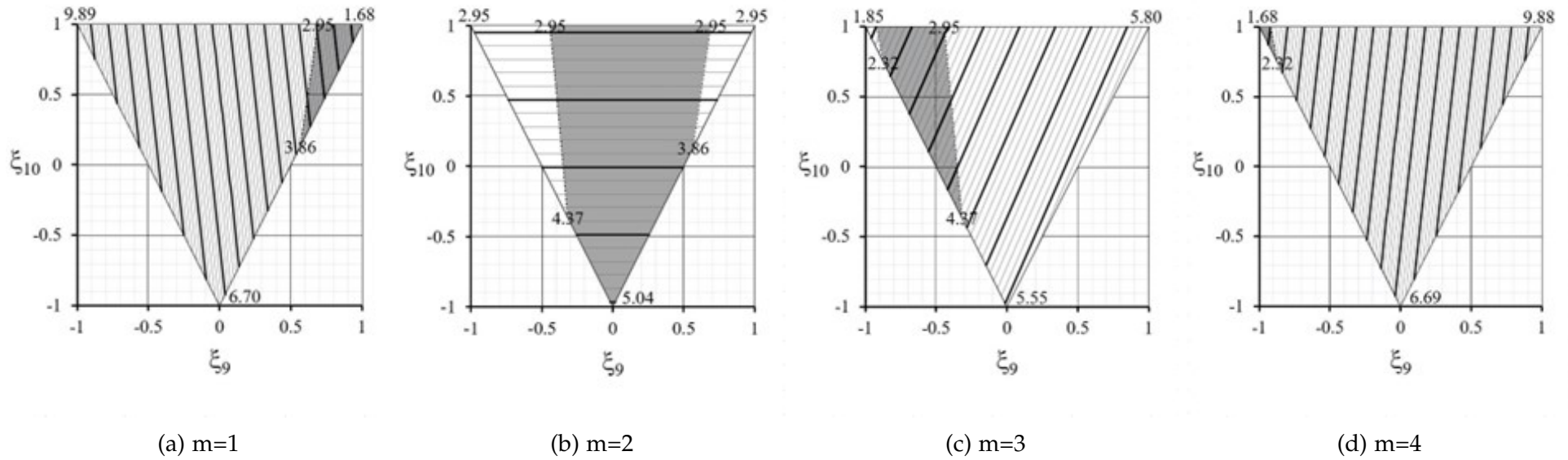


FIGURE 3.6: Compression buckling contours map construction for $a/b = 2.0$, involving superposition of contour maps for each buckling mode, representing $m = 1, 2, 3$ and 4 in Eqn. 1.18. Shading illustrates the extent of each mode region, corresponding to minimum k_x .

TABLE 3.2: Buckling coefficients for Eqn. 2.15, for all discrete mode regions of Fig. 3.5c, with $\zeta_{11} = 0$ and $a/b = 2.0$.

m	1	2	3	4
c_1	6.2445	3.9946	4.6875	6.2395
c_2	-4.1056	0.0002	1.9754	4.0991
c_3	-0.4533	-1.0428	-0.8605	-0.4529
c_4	-0.0010	-0.0007	-0.0015	-0.0040
c_5	-0.0014	-0.0020	-0.0021	-0.0018
c_6	0.0013	0.0000	-0.0002	-0.0007
c_7	-0.0014	-0.0004	-0.0001	0.0003
c_8	-0.0002	-0.0003	0.0000	0.000
c_9	-0.0029	-0.004	0.0000	0.0004
c_{10}	-0.0023	0.0004	0.0003	0.0001
c_{11}	-0.0011	0.0000	-0.0002	-0.0006
c_{12}	-0.0003	0.0001	0.0000	-0.0005
c_{13}	0.0013	0.0003	0.0001	-0.0005
c_{14}	0.0008	-0.0002	0.0000	0.0000
c_{15}	0.0015	0.0004	0.0000	-0.0004

Individual points on the boundary lines between mode regions are found from Eqn. 2.15 by generating two equations using the coefficients from adjacent mode regions, m and $(m + 1)$ and then equating for a fixed lamination parameter ζ_{10} , to solve for the variable lamination parameter ζ_9 . Points on the boundary lines were also verified by individually calculating $k_{x,m}$, corresponding to the mode numbers, m , of interest, at 5 sample points along edges of the feasible region, from which two simpler polynomial equations of the following general form:

$$k_1 = c_1 + c_2\zeta_9 + c_3\zeta_9^2 + c_4\zeta_9^3 + c_5\zeta_9^4 \quad (3.3)$$

Points can be generated and equated to reveal the location, ζ_9 , of coincident buckling modes, $k_{x,m} = k_{x,(m+1)}$. Equation 3.3 has also been used to generate the lines of each mode boundary in Fig. 3.5c, using the coefficients listed in Table 3.3.

TABLE 3.3: Coefficients for Eqn. 3.3, representing mode boundaries in Fig. 3.5c, with $\zeta_{11} = 0$ and $a/b = 2.0$.

Coefficient	$m_1 = m_2$	$m_2 = m_3$	$m_3 = m_4$
c_1	-3.8053	-3.8280	-10.0172
c_2	-6.9129	-11.0256	-32.8008
c_3	0.1197	-0.6705	-45.9682
c_4	-0.1282	-1.2113	-34.0498
c_5	0.0513	-0.8160	-9.4571

The accuracy of Eqn. 2.15, was the verified by seeding each mode region with 15 new sample points and recalculating the coefficients. This is an alternative approach to establishing the mode regions but requires multiple re-seeding steps to achieve convergence.

Generating buckling factor contours for finite length plates is therefore more involved than for the equivalent infinitely long plate, which requires only a single continuous function [25]:

$$k_{x,\infty} = 4.000 - 1.049\zeta_{10} - 1.217\zeta_9^2 + 0.340\zeta_{10}\zeta_9^2 - 0.360\zeta_9^4 - 0.034\zeta_{10}^2\zeta_9^2 \quad (3.4)$$

which was previously printed with an error [25].

Figure 3.4 reveals that the mode changes occur at lower aspect ratios for Bend-Twist coupled laminates in comparison to their uncoupled counterparts. The buckling curves (dotted lines) for *Bend-Twist* coupled laminates are also seen to descend with increasing aspect ratio and, uniquely for curve 3 with lamination parameter coordinates $(\zeta_9, \zeta_{10}, \zeta_{11}) = (-0.5, 0, 0.5)$, ascending curves are also revealed. This is in stark contrast to the curves for uncoupled laminates (solid lines), for which the lowest point between cusps is always coincident with the asymptotic value, corresponding to the buckling load factor of the infinitely long plate.

Figure 3.5a contains a special comparison between triangular bounds for the standard ply laminates considered in this study and parabolic bounds obtained from the literature [54], corresponding to free form angles, where fibre angles are arbitrary. For non-standard or free form fibre directions with arbitrary values, the design space changes from a 3-dimensional to a 4-dimensional relationship, which significantly complicates the mapping procedure. There is also

a further reduction in the buckling factor when the fibre orientations are changed from standard to non-standard angles, since ξ_{12} becomes non-zero. This can be demonstrated through a pseudo quasi-homogeneous quasi-isotropic *Bend-Twist* coupled design: $[45/0/90/45/90/-45_2/0]_S$ for which all lamination parameters are zero, except $\xi_{11} = 0.4$. For finite length plates, with aspect ratios $a/b = 1.0, 1.5$ and 2.0 , when the fibre directions are changed from standard $\pm 45^\circ$ plies to non-standard $\pm 30^\circ (\pm 60^\circ)$ plies, the buckling factors are reduced by a further 5.2% (5.2%), 4.2% (12.1%) and 3.8% (6.0%). However, this is primarily because the lamination parameters representing orthotropic stiffnesses become non-zero, i.e. $(\xi_9, \xi_{10}) = (\pm 0.25, 0.25)$. The coupling stiffnesses remain at similar magnitudes: for $\pm 30^\circ$, $\xi_{11} = \xi_{12} = -0.34$ and; for $\pm 60^\circ$, $\xi_{11} = -\xi_{12} = -0.34$. This comparison does not therefore reveal the true influence of ξ_{12} . However, if ξ_{12} is introduced artificially, to give $(\xi_9, \xi_{10}, \xi_{11}, \xi_{12}) = (0, 0, 0.4, \pm 0.4)$, the resulting buckling factor is reduced by a further 0.6% (0.5%), -0.1% (1.1%) and -1.9% (3.5%) at aspect ratios $a/b = 1.0, 1.5$ and 2.0 , respectively.

The choice of aspect ratios presented here was strongly influenced by the plethora of results reported in the literature for isotropic plates which represent only a single point in the centre of the lamination parameter design space. The square and rectangular plate, with $a/b = 2$, give identical compression buckling results only when the design is representative of the (equivalent) isotropic laminate, i.e., curve 8 of 3.4b, or indeed for square symmetric properties, i.e., curves 6–10 of Fig. 3.4b. The results are also identical to the lower-bound solution corresponding to the infinitely long plate. For *Bend-Twist* coupled designs, there is a very large difference in the degradation in buckling load between these two aspect-ratios, as shown by curve 13 of Fig. 3.4c. The rectangular plate configuration with $a/b = 1.5$ is also commonly presented in this chapter. However, this aspect ratio has special significance in composite materials testing because of the requirement for compression strength after impact assessment in the ASTM standard [109], with an anti-buckling requirement and for which the boundary conditions of the test are simple supports. The ASTM guidelines recommend a stacking sequence of: $[45/0/-45/90]_{rS}$, , but the variable number of repeats, $r = 1, 2, 3, \dots$, can be seen to possess significantly varying magnitude of *Bend-Twist* coupling, i.e., $(\xi_9, \xi_{10}, \xi_{11}) = (0.28, -0.38, 0.47), (0.16, -0.19, 0.21)$ and $(0.12, -0.13, 0.14)$, respectively.

Finally, Fig. 3.7 represents the buckling factor contour map for constant aspect ratio ($a/b = 1.0$,

1.5 and 2.0) plates with *Bend-Twist* coupled orthotropic bending stiffness where $\xi_{11} = 0.5$. The buckling performances of *Bend-Twist* coupled laminates across different aspect ratios is illustrated in Fig. 3.4. The Garland curves for the coupled plates are related to the curves with the same ξ_9 , ξ_{10} design space cross section coordinates but uncoupled ($\xi_{11} = 0$) with dotted lines. Figure 3.7 also reveals that the *Bend-Twist* coupled laminates have reduced buckling performances compared to uncoupled laminates with the same location in the design space.

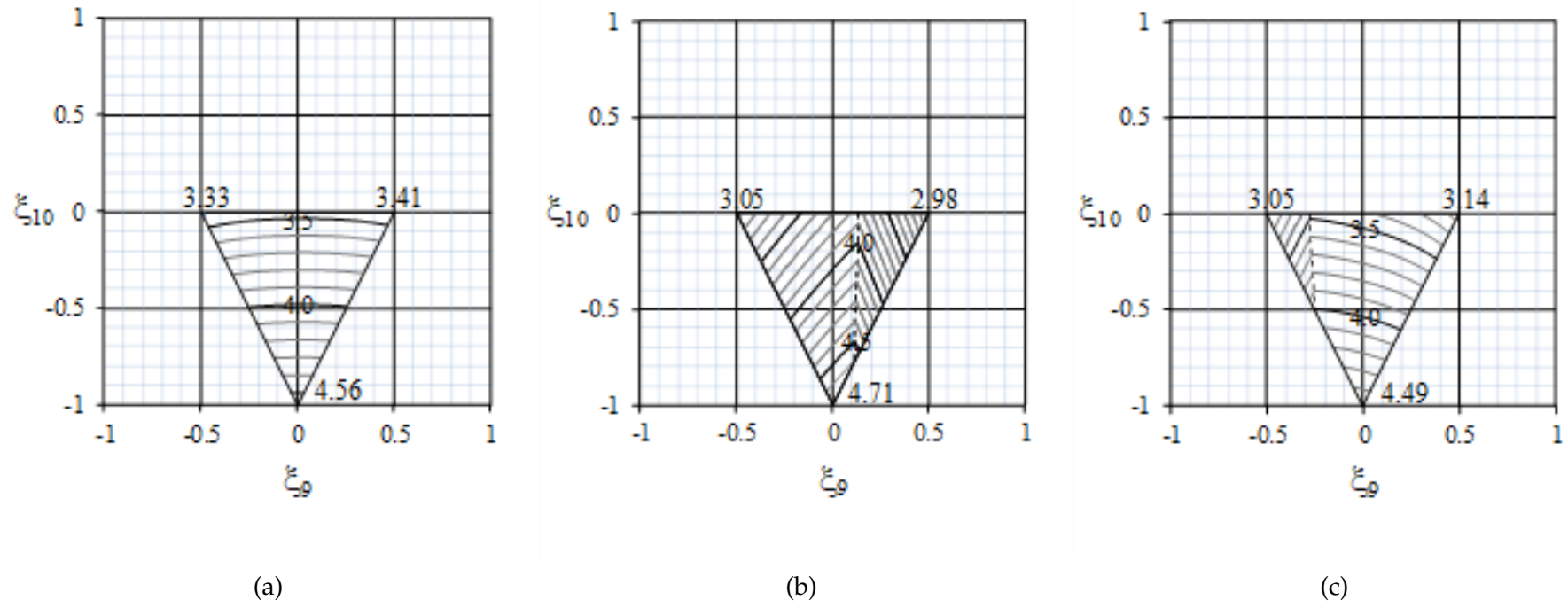


FIGURE 3.7: Compression buckling contours, $k_x (= N_x b^2 / \pi^2 D_{Iso})$, for $\xi_{11} = 0.5$ with: (a) $a/b = 1.0$; (b) $a/b = 1.5$ and (c) $a/b = 2.0$.

3.3.2 CONTOUR MAPPING FOR SHEAR BUCKLING

Equations for shear loaded plates are obtained using the same procedure adopted for compression buckling. However, the finite element analysis software ABAQUS [100] must now be used for uncoupled as well as coupled designs to generate buckling factors. The plate axis system, positive shear load, positive fibre orientation with respect to the x-axis, and aspect ratio (a/b) are also defined in the thumbnail sketch in Fig. 3.8.

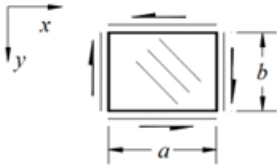


FIGURE 3.8: Illustration of the plate axis system, positive shear load, positive fibre orientation with respect to the x-axis, and aspect ratio (a/b).

For the uncoupled laminates, positive and negative shear give identical buckling load factors. The shear buckling factors are obtained by substituting the calculated coefficients into Eqn. 1.18. In this case, k_{xy} is defined by:

$$K_{xy} = \frac{N_{xy}b^2}{\pi^2 D_{Iso}} \quad (3.5)$$

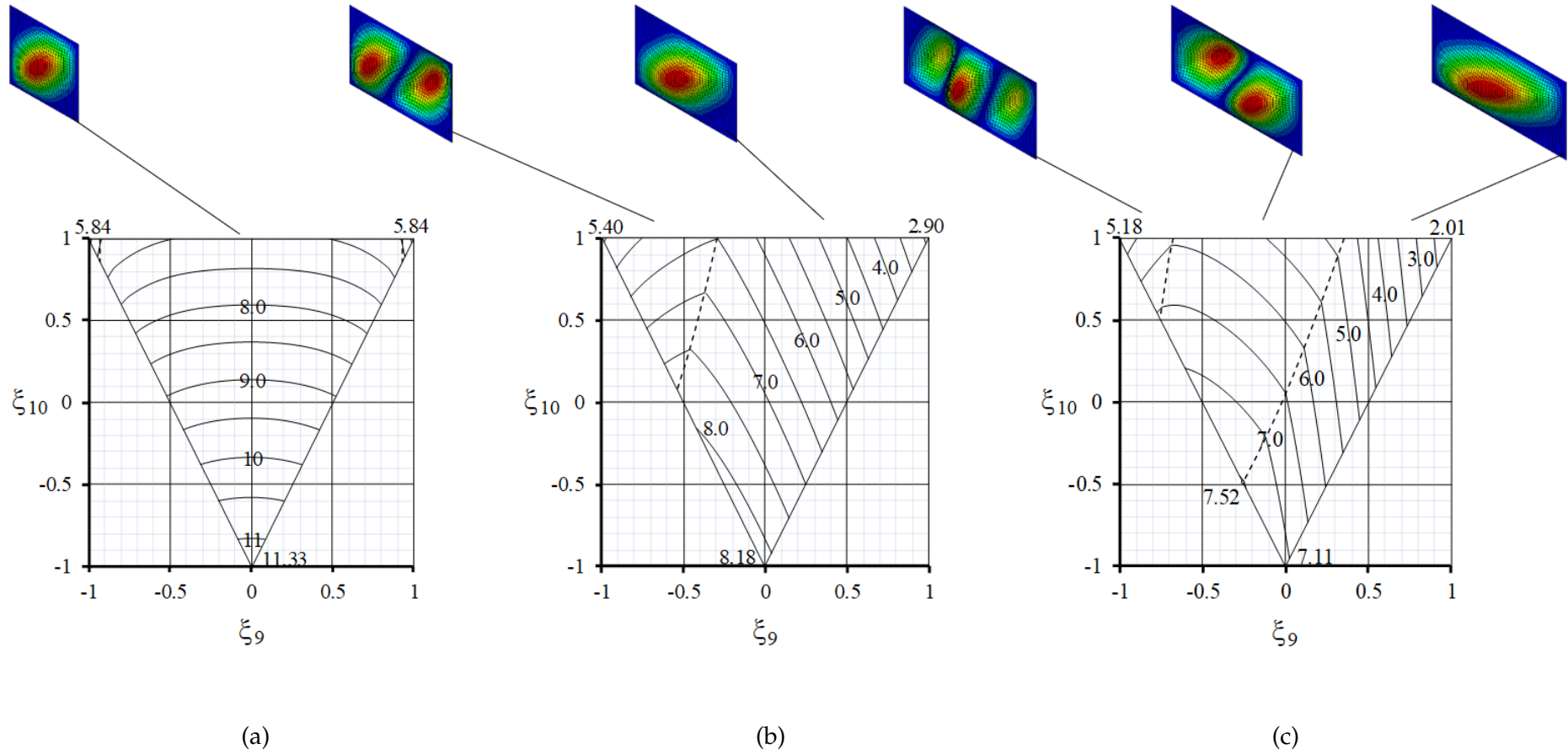


FIGURE 3.9: Positive and Negative Shear buckling factor contours, $k_{xy}(= N_{xy}b^2/\pi^2D_{Iso})$, for $\zeta_{11} = 0.0$ with: (a) $a/b = 1.0$; (b) $a/b = 1.5$, and (c) $a/b = 2.0$.

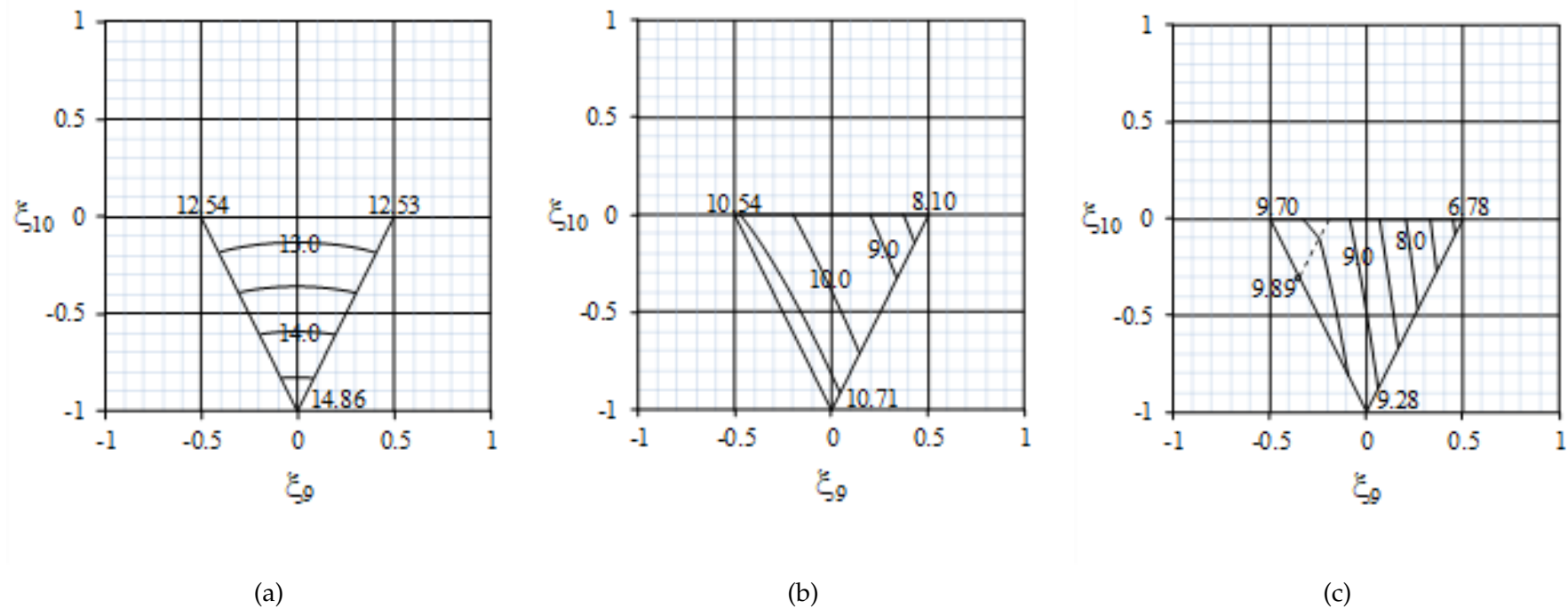


FIGURE 3.10: Negative Shear buckling factor contours, $k_{xy}(= N_{xy}b^2/\pi^2D_{Iso})$, for $\zeta_{11} = 0.5$ with: (a) $a/b = 1.0$; (b) $a/b = 1.5$ and (c) $a/b = 2.0$.

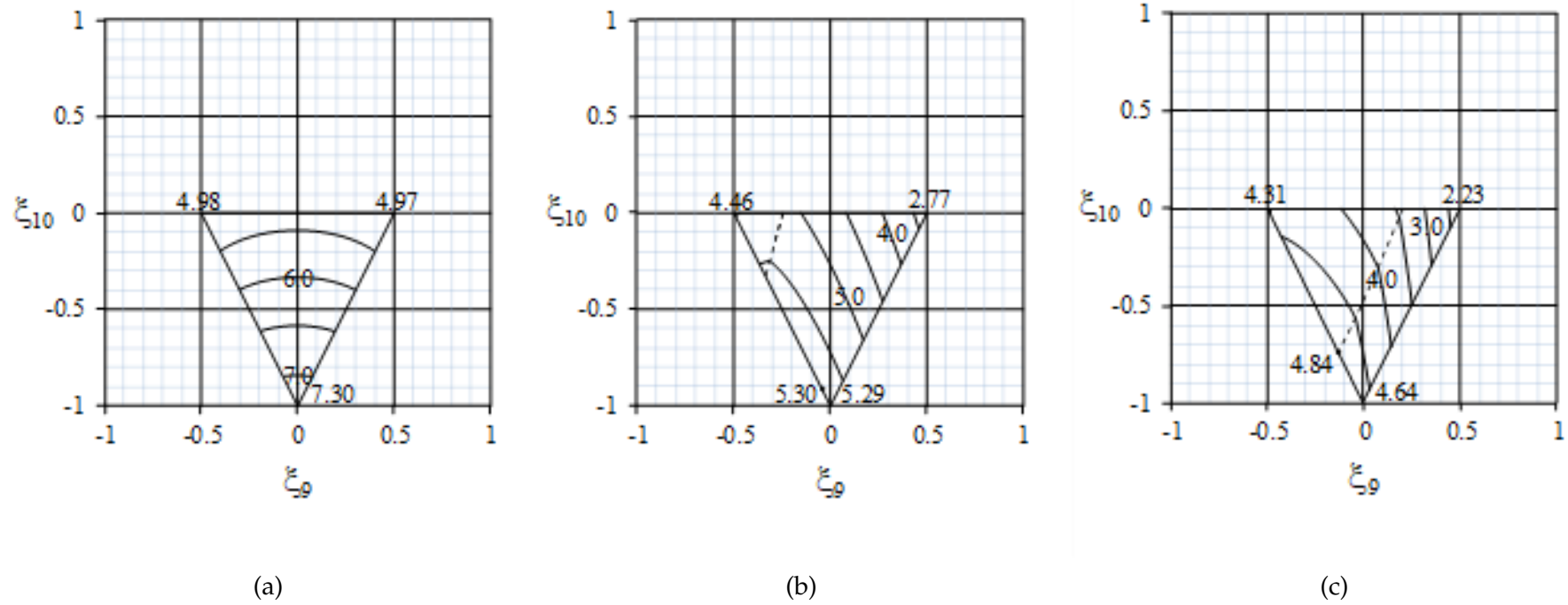


FIGURE 3.11: Positive Shear buckling factor contours, $k_{xy}(= N_{xy}b^2/\pi^2D_{Iso})$, for $\zeta_{11} = 0.5$ with: (a) $a/b = 1.0$; (b) $a/b = 1.5$ and (c) $a/b = 2.0$.

The resulting contour maps are presented in Figs. 3.10a - 3.10c, showing isolines of constant buckling load factor across the lamination parameter design space for aspect ratios $a/b = 1.0$, 1.5 and 2.0, respectively. Positive shear direction (N_{xy}) is defined together with positive fibre angle direction in Fig. 3.8. For uncoupled rectangular plates, there is no difference in the shear buckling results for positive shear or negative shear loading. However, for *Bend-Twist* coupled rectangular plates with $\xi_{11} = 0.5$, Fig. 3.10 and Fig. 3.11 demonstrate marked differences due to shear load reversal. This can be appreciated by the fact that shear loading and *Bend-Twist* coupling ($\xi_{11} \neq 0$) both give rise to skewed nodal lines in the buckling mode shapes [86]. Figure 3.10 and 3.11 represent the equivalent series of negative and positive shear buckling factor contour maps, respectively. In both cases, minima and maxima are on the sloping boundary of the feasible design space, which often coincide with dotted lines indicating a change in buckling mode. The maximum negative shear buckling factors, $k_{xy} = 14.86$ and 10.71 , are both located at $(\xi_9, \xi_{10}, \xi_{11}) = (0, -1, 0.5)$ for $a/b = 1.0$ and 1.5 , whilst for $a/b = 2.0$, $k_s = 9.89$ at $(\xi_9, \xi_{10}, \xi_{11}) = (-0.35, -0.31, 0.5)$. By contrast, only the maximum positive shear buckling factor, $k_{xy} = 7.30$, for coupled laminates with $a/b = 1.0$, is located at $(\xi_9, \xi_{10}, \xi_{11}) = (0, -1, 0.5)$. For $a/b = 1.5$ and 2.0 , $(\xi_9, \xi_{10}, \xi_{11}) = (0.41, -0.92, 0.5)$ and $(-0.13, -0.74, 0.5)$, with $k_{xy} = 5.30$ and 4.84 , respectively.

Shear buckling results from the literature [54] represent optimised lamination parameters for hypothetical or non-standard designs. For aspect ratio $a/b = 2.0$ they correspond to $(\xi_9, \xi_{10}) = (-0.39, -0.7)$ for orthotropic designs and $(\xi_9, \xi_{10}, \xi_{11}, \xi_{12}) = (-0.42, -0.64, -0.91, 0.77)$ for *Bend-Twist* coupled designs, representing buckling factor results, $k_{xy} = 7.94$ and 12.51 , respectively. By contrast, the maximum shear buckling factor for practical designs corresponds to $k_{xy} = 7.52$, at $(\xi_9, \xi_{10}) = (-0.26, -0.49)$ on Fig. 3.9c, for which stacking sequence $[45/-45_2/90/45/90_3/0]_S$, with matching lamination parameter coordinates, is readily extracted from the laminate database. Similarly, stacking sequence $[45_2/90_2/-45/90/0/-45]_S$ corresponds to the maximum shear buckling factor, $k_{xy} = 9.89$, at $(\xi_9, \xi_{10}, \xi_{11}) = (-0.35, -0.31, 0.5)$ on Fig. 3.10c. Practical designs clearly offer more modest performance benefits than optimised solutions would suggest.

Note that the optimized lamination parameters for shear buckling [54], with $a/b = 1$ and 2 , were virtually the same for both simply supported and clamped conditions. The degrading influence of a *Bend-Twist* coupling on compression buckling load was also found to be similar for both simply supported and clamped boundary conditions [25].

3.3.3 SURFACE CONTOUR MAPPING FOR COMPRESSION AND SHEAR BUCKLING

Contour mapping is applied to external surfaces of the feasible domain of lamination parameters for each of the aspect ratios $a/b = 1.0, 1.5$ and 2.0 as illustrated in Figs 3.12 - 3.14 for compression buckling and Figs. 3.15 - 3.17 for (positive) shear buckling, respectively. The design space is a tetrahedron shape identical to Fig. 3.1c, the surface contours start from the left surface, which is the $\zeta_{10} - \zeta_{11}$ plane with $\zeta_{11} = 1$ on the left. These reveal the bounds on buckling performance for all hypothetical designs, as well as local optima away from the edges of the design space.

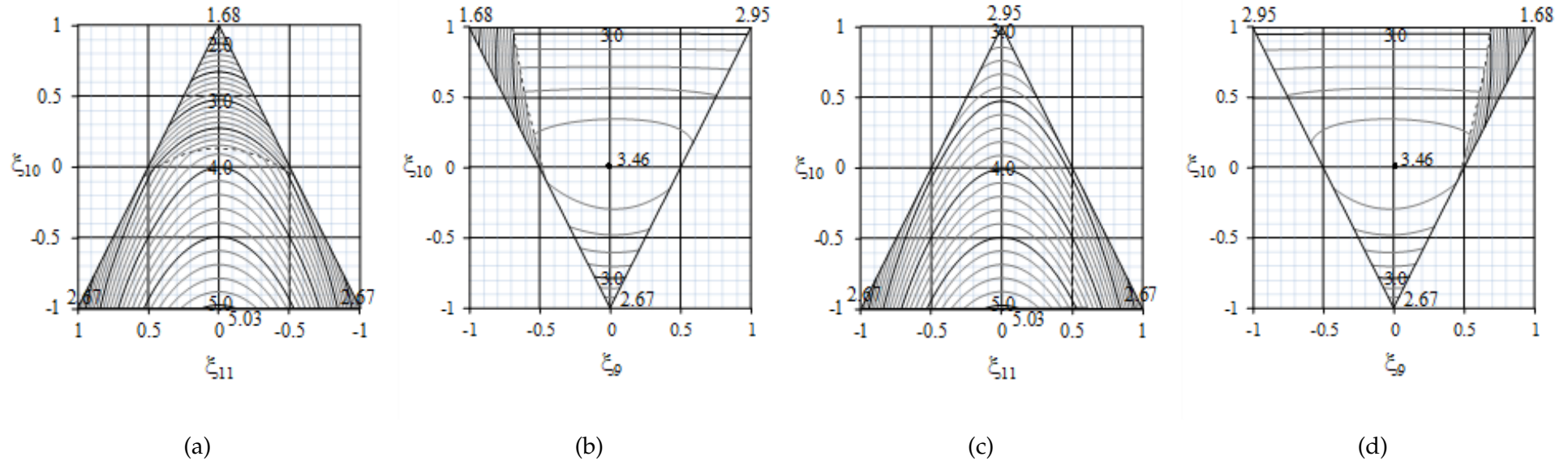


FIGURE 3.12: Lamination parameter design space surface contours for Compression buckling factor, $k_x (= N_x b^2 / \pi^2 D_{Iso})$, with $a/b = 1$, corresponding to: (a) Left (sloping) face; (b) Front (sloping) face; (c) Right (sloping) face and; Rear (sloping) face.

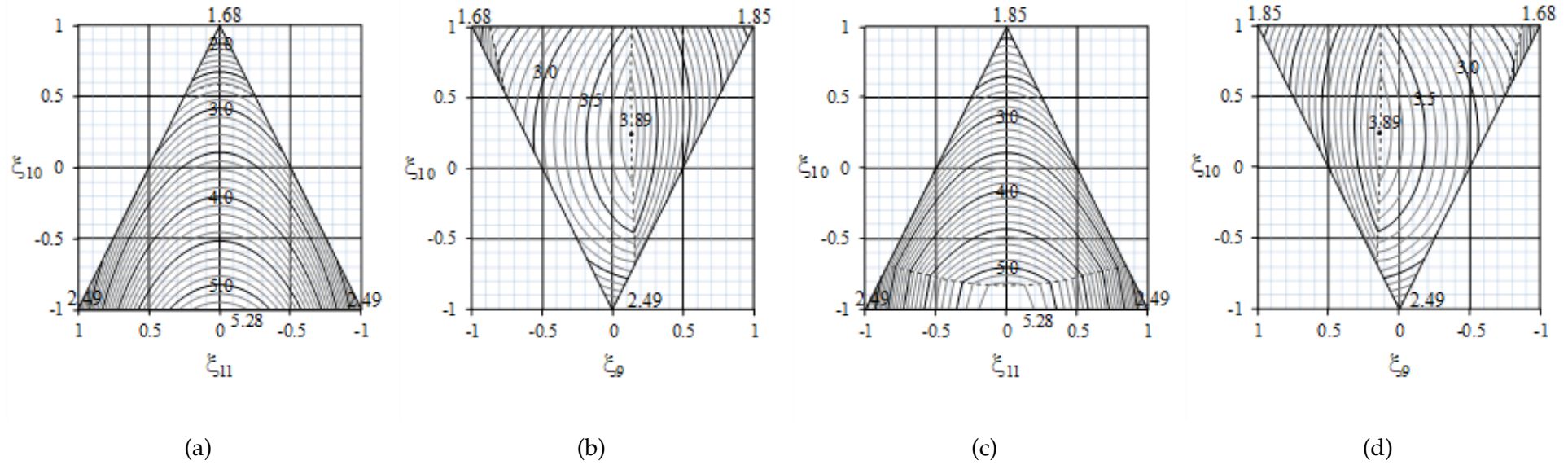


FIGURE 3.13: Lamination parameter design space surface contours for Compression buckling factor, $k_x (= N_x b^2 / \pi^2 D_{Iso})$, with $a/b = 1.5$, corresponding to: (a) Left (sloping) face; (b) Front (sloping) face; (c) Right (sloping) face and; Rear (sloping) face.

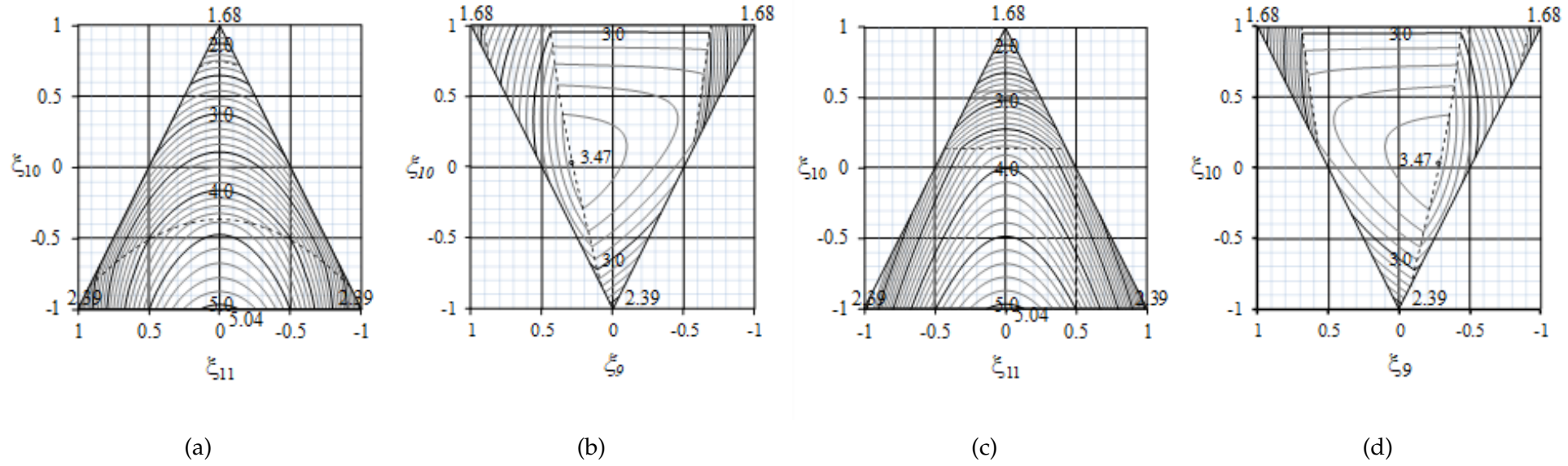


FIGURE 3.14: Lamination parameter design space surface contours for Compression buckling factor, $k_x (= N_x b^2 / \pi^2 D_{Iso})$, with $a/b = 2$, corresponding to: (a) Left (sloping) face; (b) Front (sloping) face; (c) Right (sloping) face and; (d) Rear (sloping) face.

Figures 3.12 - 3.14 show all four surfaces of the design space, represented by a regular tetrahedron, onto which compression buckling contours for aspect ratios $a/b = 1.0, 1.5$ and 2.0 are superimposed. The mode changes are denoted by dotted lines, which once again disrupt the continuity of the isolines of constant buckling load factor, as was seen in cross-sections through the design space. The effect of *Bend-Twist* coupling, arising from $\xi_{11} \neq 0$, now introduces significant curvature into the boundaries between different mode regions, as illustrated in Fig. 3.12a. The local optimum at the centre of the front and rear sloping faces represents the hypothetical limit of the pseudo quasi-homogeneous quasi-isotropic laminate, with $\xi_{11} = \pm 0.5$ and $k_x = 3.46$. The maximum buckling load factor, $k_x = 5.03$, can be found along the bottom edge of the design space, on Fig. 3.12a and 3.12c, but this corresponds to a fully uncoupled design. The local optimum at the centre of the front and rear sloping faces shift position with changes in aspect ratio, and corresponds to a mode change boundary in Figs. 3.12 and 3.14. The variation in the optimum buckling factor for the three aspect ratios of Figs. 3.15 to 3.17 can be explained by observing the behaviour of the highest Garland curve across Fig. 3.4 at the same aspect ratios.

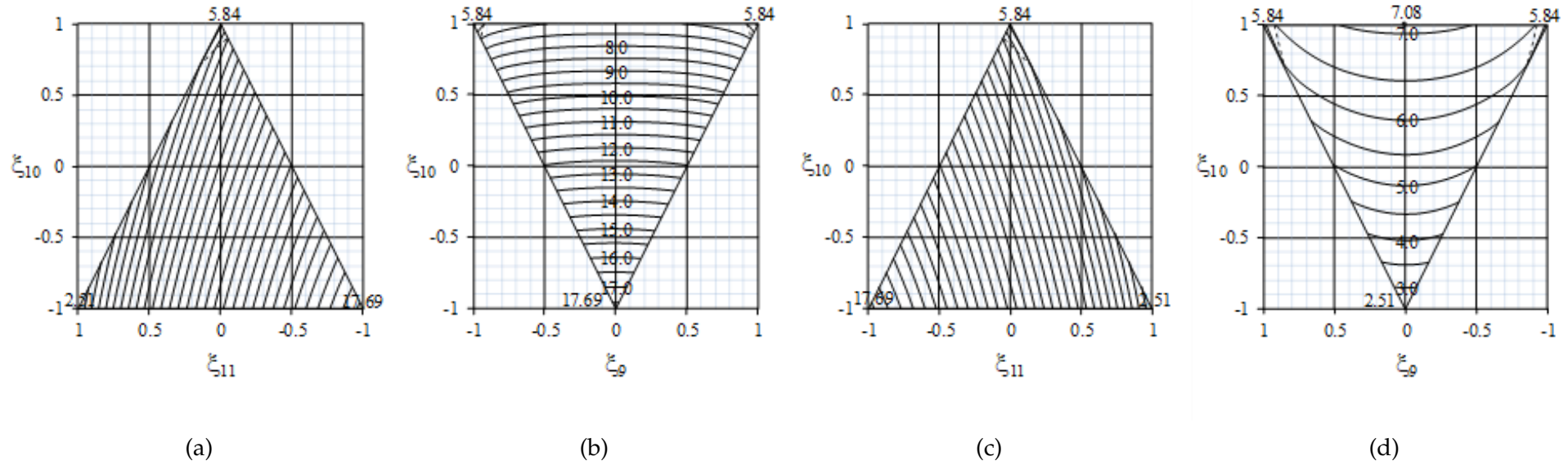


FIGURE 3.15: Lamination parameter design space surface contours for Positive Shear buckling factor, $k_{xy}(= N_{xy}b^2/\pi^2D_{Iso})$, with $a/b = 1$, corresponding to: (a) Left (sloping) face; (b) Front (sloping) face; (c) Right (sloping) face and; Rear (sloping) face.

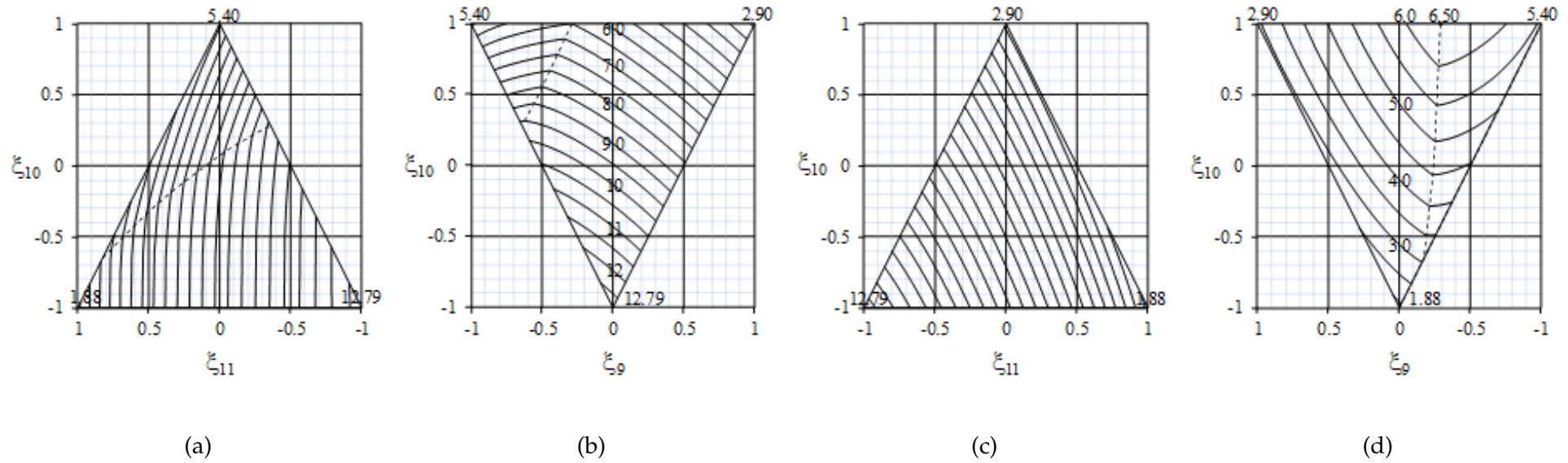


FIGURE 3.16: Lamination parameter design space surface contours for Positive Shear buckling factor, $k_{xy}(= N_{xy}b^2/\pi^2D_{Iso})$, with $a/b = 1.5$, corresponding to: (a) Left (sloping) face; (b) Front (sloping) face; (c) Right (sloping) face and; Rear (sloping) face.

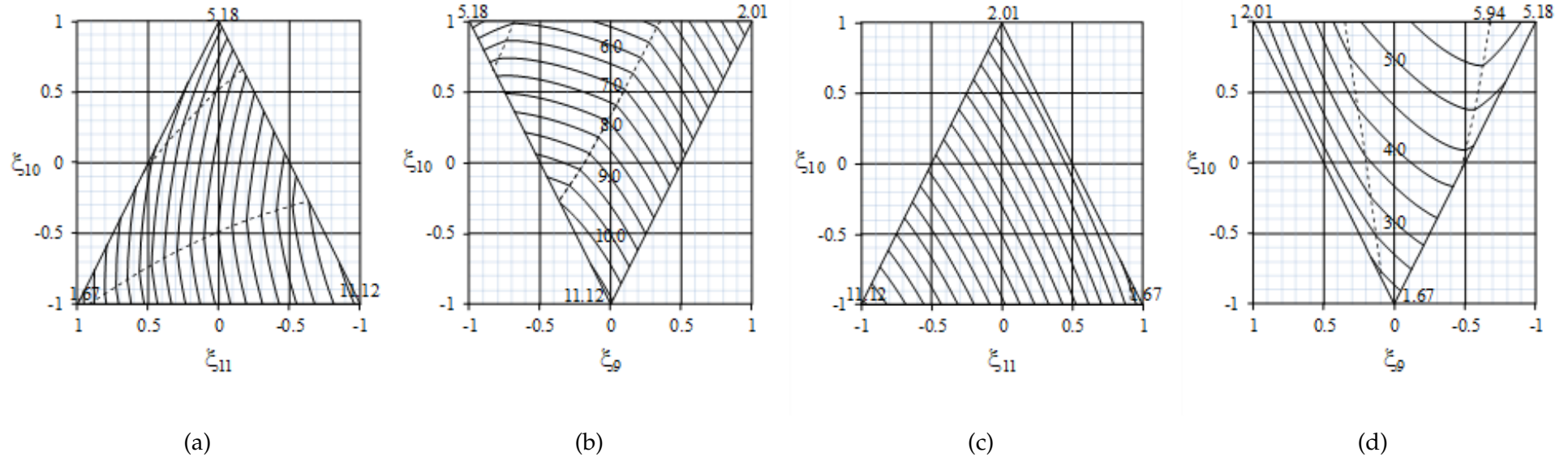


FIGURE 3.17: Lamination parameter design space surface contours for Positive Shear buckling factor, $k_{xy}(= N_{xy}b^2/\pi^2D_{Iso})$, with $a/b = 2$, corresponding to: (a) Left (sloping) face; (b) Front (sloping) face; (c) Right (sloping) face and; Rear (sloping) face.

Figures 3.15 - 3.17 illustrate the surface contours for shear buckling with $a/b = 1.0, 1.5$ and 2.0 , respectively. Lines traced from the apex of the tetrahedron, across these surfaces, differ significantly from those of the cross section of Figs. 3.9, at $\zeta_{11} = 0$. Similarly, surface mode changes can be compared to the cross sections of Figs. 3.10 and 3.11 for negative shear (front surface) and positive shear (rear surface) at $\zeta_{11} = 0.5$, respectively, and reveal the influence on mode change with increasing magnitude of *Bend-Twist* coupling. The number and position of these mode changes also vary significantly with aspect ratio. Indeed, no mode changes are present in the surface contours for the infinitely long case [86], in which local optima were also found in locations that are non-intuitive, i.e. the optimum shear buckling factor $k_{xy,\infty} = 9.06$ at $(\zeta_9, \zeta_{10}, \zeta_{11}) = (-0.18, -0.64, -0.82)$, which exceeds $k_{xy,\infty} = 8.84$ at $(\zeta_9, \zeta_{10}, \zeta_{11}) = (0, -1, -1)$. For finite length plates, the hypothetical optima for $a/b = 1.0, 1.5$, and 2.0 correspond to $k_{xy} = 17.69, 12.79$ and 11.12 , respectively, and all occur at $(\zeta_9, \zeta_{10}, \zeta_{11}) = (0, -1, -1)$.

Collectively, the cross-section and surface contour maps demonstrate the added complexity associated with laminate selection from a design space in which buckling factor is a non-continuous function (i.e. the buckling mode changes across the design space). They also demonstrate that the isolines of constant buckling factor become increasingly curved as the aspect ratio tends towards an infinitely long plate, and/or the magnitude of ζ_{11} (i.e. the *Bend-Twist* coupling) increases. However, for practical designs, the limits of ζ_{11} are more realistically represented through cross sections at $\zeta_{11} = 0$ and $\zeta_{11} = 0.5$, which reveal optima that are non-intuitive.

These design charts can also be used in conjunction with the data in Table A4 of the electronic annexe, containing 16-ply quasi-isotropic symmetric stacking sequence listings with associated lamination parameter coordinates, grouped to aid design selection for minimising the degrading influence of *Bend-Twist* coupling.

3.4 CONCLUSION

- Insights have been given for maximising compression and shear buckling load for simply supported finite length plates with $0^\circ, 90^\circ$ and $\pm 45^\circ$ ply orientations, through the superposition of contour maps onto the lamination parameter design space for practical laminate designs with *Bend-Twist* coupling. The non-intuitive location of local as well as global

optima are revealed by inspection.

- Contour maps representing cross sections through the design space demonstrate the added complexity associated with laminate selection when buckling factor is a non-continuous function. This is due to mode changes that are dependent both on bending stiffness properties (or lamination parameter coordinate) as well as plate aspect ratio.
- The contour maps represent practical limits on buckling performance by accounting for common laminate design rules, including symmetry, standard ply angles, minimum ply percentages and maximum ply contiguity rules.
- Contour maps representing the outer surfaces of the design space demonstrate the limits on both compression and shear buckling performance as a result of the presence of Bend-Twist coupling, noting that significant improvements in shear buckling load, are largely beyond those achievable in design practice.

The raw and processed data required to reproduce these findings are available to download at
doi: [10.17632/rys232ynhf.2](https://doi.org/10.17632/rys232ynhf.2)

CHAPTER 4

DOUBLE ANGLE-PLY (DD) LAMINATES

4.1 INTRODUCTION AND MOTIVATION TO DOUBLE ANGLE-PLY LAMINATES AND OFF-AXIS ALIGNMENT

Previous chapters explored the buckling performance of uncoupled and Bend-Twist coupled laminates with standard fibre configurations. The aim of the work in this chapter is to apply knowledge from Chapters 1 to 3 to explore the first ply failure (FPF) performance of composite laminates with double-angle, as opposed to standard angle-ply configurations.

Small plates are likely to fail by material failure, i.e. first ply failure, as their small size makes buckling unlikely. As size increases, buckling becomes more likely; plates with large aspect ratios are likely to fail by buckling. Consequently, there is a certain plate size where the FPF and buckling loads are identical. For such laminates, neither buckling nor material failure occurs until the structure fails by both mechanisms simultaneously. This leads to the other goal of this chapter, to design laminates that possess equal buckling and first ply failure (FPF) strengths using the lamination parameter optimisation approach introduced in previous chapters.

The first part of this chapter involves applying the same lamination parameter design space contour mapping technique used in the previous chapter, but this time to double angle-ply or 'Double-double' (DD) laminates. The latter contains 2 distinct pairs of plies with fibre orientations $(\pm\psi, \pm\phi)$, that are repeated numerous times through the laminate, instead of the more usual $(0^\circ, 90^\circ$ and $\pm 45^\circ)$ layup configuration. The DD configuration offers an extended design space in which to identify a laminate with the same weight but higher buckling and/or FPF strength, or alternatively, a laminate with the same buckling and/or FPF strength, but of lower weight. A stiffness matching technique is then used to design DD laminates and 'feasible' design regions

(i.e. those subject to the applied design constraints) of the DD laminate designs are plotted. Off-axis rotations are applied to laminates and the FPF performance is compared to laminates with standard fibre orientations. Polar plots of the FPF performance of the laminates subject to off-axis alignments are presented, to compare the various laminate designs. The final objective involves predicting the optimum size of the laminate plates, in which the aspect ratios are typical of the width between stiffeners in a stiffened panel wing skin.

Aero-elastic tailoring of composite wings is expected to lead to a valuable drag reduction mechanism in conventional swept back wings [110], by reducing any fluctuation away from the optimized static cruise configuration, i.e., reducing the magnitude of wing-twist as it bends. Drag reduction can be achieved by introducing passive *Bend-Twist* coupling behaviour (a so-called passive-adaptive wing), to maintain a constant angle of attack across the wing, irrespective of the magnitude of the bending deflection [14]. This has been demonstrated for a number of competing laminate tailoring techniques. To create a *Bend-Twist* coupled behaviour Extension-Shear coupled properties are usually required and achieved by including off-axis fibre orientations in the layup. Off-axis alignment (β) refers to an angle away from the x-y axes, where the latter are defined by the direction of loading, as illustrated in Fig. 4.1. The focus of the previous chapters has, thus far, been restricted to buckling behaviour. The effect of such tailoring on laminate first ply failure performance is now also considered to examine the feasibility of this tailoring method. This is assessed by combining buckling predictions with material strength constraints.

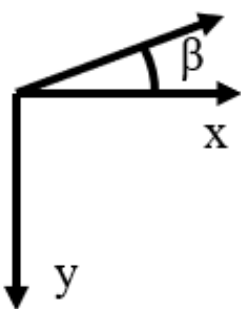


FIGURE 4.1: Illustration of the off-axis alignment on the x-y axis.

Studies on buckling optimisation of composite laminates subject to material strength constraints are summarised elsewhere [39]. Their purpose is to reduce the feasible design region and obtain stacking sequences for specific design applications. Material strength constraints are applied either through a maximum limit on laminate strain or via individual ply stresses [111].

This includes methods for determining optimal stacking sequences to maximise buckling load [112]. This includes methods for determining optimal stacking sequences to maximise buckling load [28].

Very few studies have previously been conducted on the assessment of buckling, subject to material strength constraints, for off-axis aligned laminates possessing *Extension-Shear* coupling behaviour [113]. The objective of this study is therefore to explore the available design space for a number of design solutions, including both DD and standard laminates. Off-axis orientation (with respect to the loading direction) is applied to both types of laminate to introduce Extension-Shear coupling, and also to standard designs that already possess an Extension-Shear coupling without the requirement for off-axis alignment. Laminate designs are matched for buckling load, with off-axis alignments that give maximum *Extension-Shear* coupling, and material strength assessment is then made.

The introduction of passive *Bend-Twist* coupling at the wing-box level has been demonstrated [110] Shear coupling at the laminate level, i.e., in the wing skins. However, there is a limited design space for standard ply laminates with *Extension-Shearing* coupling [104] (with 0° , $\pm 45^\circ$ and 90° ply orientations). By contrast, a substantial design space exists for laminates that possess both *Extension-Shearing and Bending-Twisting* coupling [102], yet care must be exercised since the presence of Bend-Twist coupling leads to a significant reduction in buckling load [25].

DD laminates have been shown to offer potential improvements in material strength [88], together with ease of manufacturability [89], when compared to standard ply laminates. However, little consideration has been given to bending stiffness.

The normal practice of choosing the extensional stiffness first, typically by applying certain ply percentages, offers the possibility of shuffling the stacking sequence, within the constraints of the symmetric design rule for standard laminates, to optimise the buckling performance. However, this usually leads to the introduction of a Bend-Twist coupling behaviour which, more often than not, leads to a penalty in the buckling load. The methodology adopted here instead imposes a desired buckling load to match a required laminate strength target.

4.2 METHODOLOGY

This chapter follows on from a recent study focusing on bending stiffness matching [97], and the development of a new database of DD laminate configurations containing specific mechanical coupling characteristics. The stiffness matching approach is used to develop laminate designs with bending isotropy, i.e. where the bending stiffness lamination parameters (ξ_{9-12}) are zero, to which off-axis loading orientations can then be applied to introduce Extension-Shear coupling for first ply failure assessment. This is to ensure that the buckling performance is not affected by the introduction of off-axis alignment.

The development of a passive adaptive *Bend-Twist* coupled wing requires Extension-Shear coupled laminate skins [14], these can be achieved in several ways. The following types of laminates are used for the design process:

1. off-axis fibre alignment (β) of otherwise balanced and symmetric laminates with standard ply orientations (0° , $\pm 45^\circ$ and 90°)
2. Off-axis orientation of double angle-ply (DD) ($\pm\phi^\circ$ and $\pm\psi^\circ$) laminates, with otherwise *Uncoupled* properties
3. *Extension-Shear* coupled (only) laminates with standard ply orientations

A non-symmetric isotropic laminate configuration with standard ply orientations is also used as a datum to compare against the coupled designs, as this laminate is fully isotropic, i.e. $\xi_{1-12} = 0$ and has a classic compressive buckling factor of 4.0.

$$[45/90/0/-45/0/-45/90/-45/45/0/45/90/45/90/-45/90/0/45/0/-45/0/-45/45/90]_T \quad (4.1)$$

where the subscript T represents a complete laminate stacking sequence, as mentioned in Chapter 1.

The designs are fixed to 24-ply, which represents the minimum ply number grouping for $\pi/4$ bending isotropy [114, 96].

The balanced and symmetric design has the stacking sequence:

$$[-45/45/0_3/45/0/-45/0/90/0/90]_S \quad (4.2)$$

This stacking sequence is selected from the 24-ply laminate database, since it produces the highest *Extension-Shear* coupling, measured as $A_{16}/A_{11} = 21.9\%$ at off-axis orientation of $\beta = 37.3^\circ$. Note that the application of off-axis alignment also introduces the non-zero lamination parameters, ξ_3 and ξ_4 , giving $(\xi_1, \xi_2, \xi_3, \xi_4) = (0.09, -0.29, 0.32, 0.17)$. Without off-axis alignment, the lamination parameters $(\xi_1, \xi_2) = (0.33, 0.33)$. The lamination parameter and extensional stiffnesses, A_{ij} , are related through Eqn. 2.7 from Chapter 1.

For the DD designs, a new design methodology is adopted [97]. A technique to match the bending stiffness between standard ply laminates (with 0° , $\pm 45^\circ$ and 90° fibre directions) and DD laminates (with $\pm\phi^\circ$ and $\pm\psi^\circ$ fibre directions) is used. The conventional fibre directions, 0° , 90° and $\pm 45^\circ$ are replaced with $\pm\phi_\gamma$ and $\pm\psi_{1-\gamma}$ pairs, where γ represents the proportion of $\pm\phi$, and $(1 - \gamma)$ represents the proportion of $\pm\psi$. For extension stiffness matching, these proportions correspond to the $\pm\phi$ and $\pm\psi$ ply percentages. For bending stiffness matching, the proportions correspond to the relative contribution to bending stiffness of $\pm\phi$ and $\pm\psi$ plies in the laminate. The formulation of stiffness matching was explained in section 1.2.9, only a short recap is provided here. The relative contribution to bending stiffness of the $\pm\phi$ ply sub-laminate in terms of lamination parameters is given by:

$$\zeta_{\pm\phi} = (\zeta_9 - \beta)(\alpha - \beta) \quad (4.3)$$

$$\alpha = \cos 2\phi \quad \beta = \cos 2\psi \quad (4.4)$$

where α and β can be expressed in the form of a quadratic equation:

$$\beta = -\frac{\zeta_{10} + 1 - 2\alpha^2}{4(\alpha - \zeta_9)} + \sqrt{\left(\frac{\zeta_{10} + 1 - 2\alpha^2}{4(\alpha - \zeta_9)}\right)^2 - \frac{2\alpha^2\zeta_9 - \alpha - \zeta_{10}\alpha}{2(\alpha - \zeta_9)}} \quad (4.5)$$

which leads to a solution for angle ϕ from Eqn. 4.4 (solved iteratively), then Eqns. 4.3 and 4.5 are matched for the desired lamination parameters (ζ_9, ζ_{10}) . Finally, a solution for angle ψ is obtained directly from Eqn. 4.4, once the iterative process has converged.

Stacking sequences, lamination parameters and angles ϕ and ψ from a previous study [97] are listed in Table 4.1. The angles were derived from Eqns. 4.3 – 4.5 for $(\zeta_9, \zeta_{10} = (0, 0))$.

TABLE 4.1: Stacking sequences for fully uncoupled double angle-ply laminates with 24 layers. The listed angles (ϕ, ψ) produce bending isotropy.

Design	Stacking Sequence	ψ°, ϕ°	ζ_1, ζ_2
<i>a</i>	$[\psi/-\psi/-\phi/\phi/\phi/-\phi/\phi/-\phi/\phi/-\psi/\psi/-\psi/\psi/\phi/-\phi/-\phi/\phi/-\phi/\phi/\phi/-\phi/\psi/-\psi]_T$	63.78, 17.44	-0.13, -0.06
<i>b</i>	$[\psi/-\psi/-\phi/-\phi/-\phi/\phi/-\phi/\phi/-\psi/\psi/\phi/-\phi/\phi/-\phi/-\psi/\psi/-\phi/\phi/-\phi/\phi/\phi/-\phi/\psi/-\psi]_T$	65.08, 19.58	-0.17, -0.04
<i>c</i>	$[\psi/-\psi/-\phi/\phi/\phi/-\phi/-\psi/\psi/\phi/-\phi/-\phi/\phi/\phi/-\phi/-\phi/\phi/-\psi/\psi/-\phi/\phi/\phi/-\phi/\psi/-\psi]_T$	68.08, 23.04	-0.25, 0.01
<i>d</i>	$[\psi/-\psi/-\phi/\phi/-\psi/\psi/\phi/-\phi/\phi/-\phi/\phi/-\phi/-\phi/\phi/-\phi/\phi/-\phi/\phi/-\psi/\psi/\phi/-\phi/\psi/-\psi]_T$	74.28, 27.06	-0.37, 0.20
<i>e</i>	$[\psi/-\psi/\phi/-\phi/-\phi/\phi/\psi/-\psi/-\psi/\psi/-\psi/\psi/-\psi/\psi/-\psi/\psi/\psi/-\psi/-\phi/\phi/\phi/-\phi/\psi/-\psi]_T$	70.46, 24.95	0.17, -0.05
<i>f</i>	$[\psi/-\psi/\phi/-\phi/\psi/-\psi/-\phi/\phi/-\psi/\psi/-\psi/\psi/-\psi/\psi/-\psi/-\psi/-\phi/\phi/\psi/-\psi/\phi/-\phi/\psi/-\psi]_T$	78.64, 28.59	0.05, -0.04

The *Extension-Shearing* coupled laminate with standard ply orientations:

$$[-45/0/45/90/90/0/45/45/-45/45/90/45/45/90/45/-45/45/90/45/0/45/0/90/-45]_T \quad (4.6)$$

was derived using an algorithm developed previously [104]. The design has a maximum A_{16}/A_{11} of 16.7%, without off-axis alignment, β , and shares the same compression buckling load, N_x , as the isotropic plate, as can be readily confirmed from the closed form solution of Eqn. 1.18 in Chapter 1, given that the design is fully uncoupled in bending, i.e., $D_{16} = D_{26} = 0$. For convenience, the equation is provided here again:

$$N_x = \pi^2 [D_{11} \left(\frac{m}{a}\right)^2 + 2(D_{11} + 2D_{66}) \left(\frac{n^2}{b^2}\right) + D_{22} \left(\frac{n^4}{b^4}\right) \left(\frac{a}{m}\right)^2]$$

where a and b are the length and width of the laminate, m is the number of half-waves of the

buckling mode along the plate length and D_{ij} are the elements of the bending stiffness matrix [D]. The lamination parameter is generally given by Eqn. 2.7 in Chapter 1,), though for double angle-ply, the equation is adjusted slightly to:

$$\begin{aligned}\bar{\zeta}_1 &= \frac{n_\phi \cos 2\theta_\phi + n_\psi \cos 2\theta_\psi}{n} & \bar{\zeta}_2 &= \frac{n_\phi \cos 4\theta_\phi + n_\psi \cos 4\theta_\psi}{n} \\ \bar{\zeta}_3 &= \frac{n_\phi \sin 2\theta_\phi + n_\psi \sin 2\theta_\psi}{n} & \bar{\zeta}_4 &= \frac{n_\phi \sin 4\theta_\phi + n_\psi \sin 4\theta_\psi}{n} \\ \bar{\zeta}_9 &= \frac{\zeta_\phi \cos 2\theta_\phi + \zeta_\psi \cos 2\theta_\psi}{\zeta} & \bar{\zeta}_{10} &= \frac{\zeta_\phi \cos 4\theta_\phi + \zeta_\psi \cos 4\theta_\psi}{\zeta} \\ \bar{\zeta}_{11} &= \frac{\zeta_\phi \sin 2\theta_\phi + \zeta_\psi \sin 2\theta_\psi}{\zeta} & \bar{\zeta}_{12} &= \frac{\zeta_\phi \sin 4\theta_\phi + \zeta_\psi \sin 4\theta_\psi}{\zeta}\end{aligned}\quad (4.7)$$

where $\zeta = n^3$.

The Tsai-Wu failure criteria 1.27 is used for the strength assessment and is defined by:

$$F_1\sigma_1 + 2F_2\sigma_2 + F_{11}\sigma_1^2 + F_{22}\sigma_2^2 + F_{66}\tau_{12}^2 - \sqrt{F_{11}F_{22}}\sigma_1\sigma_2 = 1 \quad (4.8)$$

where

$$\begin{aligned}F_1 &= \frac{1}{\sigma_1^T} + \frac{1}{\sigma_1^C} & F_2 &= \frac{1}{\sigma_2^T} + \frac{1}{\sigma_2^C} \\ F_{11} &= -\frac{1}{\sigma_1^T\sigma_1^C} & F_{22} &= -\frac{1}{\sigma_2^T\sigma_2^C} & F_{66} &= \left(\frac{1}{\tau_{12}^F}\right)^2\end{aligned}\quad (4.9)$$

Individual terms correspond to the strength data listed in Table 4.2 for the T300/5208 graphite/epoxy material adopted in this study.

TABLE 4.2: Engineering properties of T300/5208 graphite/epoxy.

E_1 (GPa)	181.0	σ_1^T	1500
E_2 (GPa)	10.3	σ_1^C	-1500
G_{12} (GPa)	7,17	σ_2^T	40
ν_{12}	0.28	σ_2^C	-246
		τ_{12}	68

where σ_{1T} , σ_{1C} , σ_{2T} and σ_{2C} represent the allowable tensile and compression stress values in the principal coordinate system, and τ_{12F} represents the allowable in-plane shear stress value.

The stiffness matching approach is now extended to simultaneously match both first ply failure and buckling load constraints, for a chosen DD laminate with maximised *Extension-Shear* coupling.

The results presented are based on compression buckling load, N_x , of a rectangular, simply supported plate with fixed aspect ratios, a/b , which for the uncoupled designs adopted here, allows the use of the closed form buckling solution given by Eqn. 1.18. The procedure involves simultaneously matching the load for both buckling and first ply failure, from which the physical plate dimensions a and b can be determined.

4.3 DESIGN SPACES OF DOUBLE ANGLE-PLY LAMINATE DESIGNS

Only six laminate designs for fully uncoupled DD laminates with 24 layers produce bending isotropy, these are listed in Table 4.1. These six DD laminate designs share two unique sets of extension stiffness properties, hence there are only two points on the lamination parameter design spaces for extensional stiffness. Designs *a*, *b*, *c* and *d* share one of the unique points and *e* and *f* share the other.

The DD laminate designs (listed in Table 4.1) are far from the in-plane lamination parameters (ξ_1, ξ_2) for typical aircraft components. For example, a Spar (0, -0.6), a Skin (0.32, 0.12) and a Stiffener (0.5, 0.4), which correspond to the following ply percentages for 0° , $\pm 45^\circ$ and 90° ply orientations: Spar (10/80/10), Skin (44/44/12) and Stiffener (60/30/10). However, if the angles are switched, where the outer plies of the laminates become ϕ rather than ψ the design space becomes a mirror image of the design space that was generated before switching the angles, and the new solutions are found to be in close proximity to a typical Skin component, for which buckling load and FPF strength constraints coincide at some point along a wing structure.

The results are therefore reported with the ϕ and ψ in the DD laminate design stacking sequence switched. However, for bending isotropy to be maintained in the designs reported in Table 4.1, the values of ϕ and ψ must be modified as follows:

$$\phi_{\text{switched}} = 90^\circ - \psi \quad (4.10)$$

$$\psi_{\text{switched}} = 90^\circ - \phi$$

Figure 4.2a and 4.2b represent the lamination parameter design spaces, for extensional (4.2a) and bending stiffness (4.2b), for DD laminate design case *d*. The latter was chosen for illustration in Fig. 4.5 as it was found to have the lowest first ply failure (FPF) load (i.e. 605.3 N/mm) among all the standard and DD laminate designs, in which the FPF load is used as the input load for all the laminate design analyses. Referring to Fig. 4.5, the fine grey lines indicate isolines along which the percentage of ψ and ϕ ply orientations in the laminate layup are constant (the percentage values are given in Fig. 4.2a in green font colour for the psi ply angle and brown font colour for the phi ply angle). The red bold lines indicate values of the laminate parameters that predict constant buckling factors for a square plate (i.e. $k_x = 4.0$, the classical value for a square plate manufactured from an isotropic material such as aluminium or a QI laminate) superimposed on the design spaces, varying from 0° at the top right to 90° at the top left and $\pm 45^\circ$ at the bottom of the design space, as shown in Fig. 4.2a that are in grey font colour. The dashed guidance line is used to read off the values of the ψ and ϕ ply angles for the DD design indicated by the blue point (laminate design *d*) by using its intersection values with the bold purple line. In the example shown in Fig. 4.2a, the values of ψ and ϕ are 74.28 and 27.06, as listed in Table 4.1. Note that for any given point in the graphs, the dashed guidance line must be recalculated using the method outlined in Section 4.2.

The overall compression for aspect ratio (a/b) = 1 and 1.5 are superimposed onto the bending stiffness design spaces of laminate design *d* on Fig. 4.2c and 4.2d, respectively.

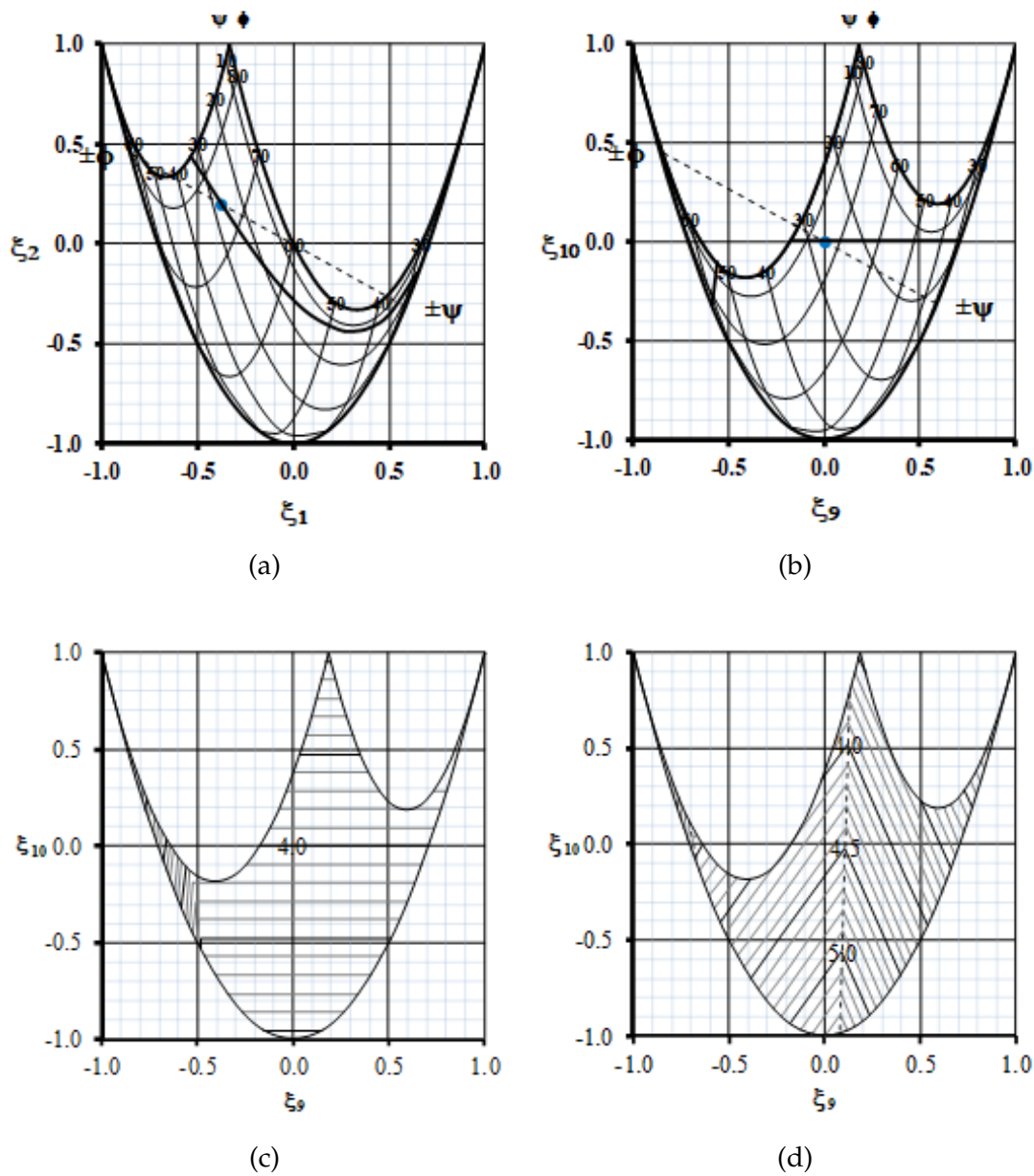


FIGURE 4.2: Lamination parameter design spaces for laminate *d* from Table 4.1 corresponding to (a) extension stiffness and; (b) bending stiffness, with the lines of constant compression buckling factor $k_x = 4.0$. Compression buckling contour maps for aspect ratio (c) $a/b = 1.0$ and; (d) $a/b = 1.5$.

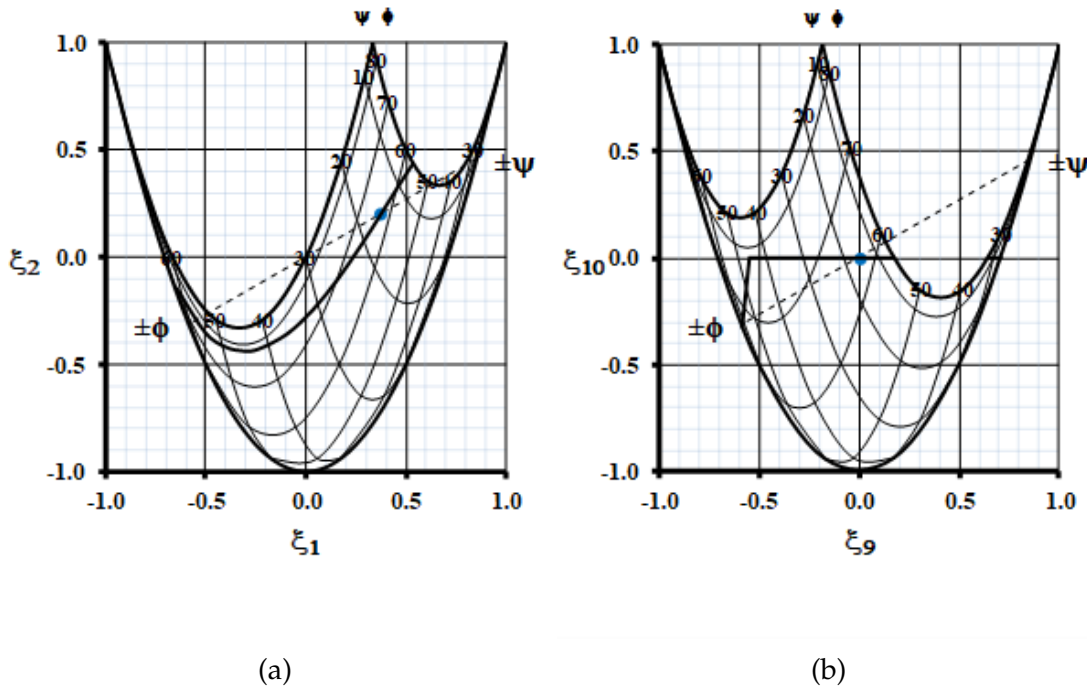


FIGURE 4.3: Feasible design space for (a) extension stiffness and; (b) bending stiffness, for the angles switched DD laminate *d* with bold lines that pass through the blue points representing constant compression buckling factor, $k_x = 4.0$.

Figure 4.3 represents the extension and bending stiffness design spaces with a superimposed compression buckling line of $k_x = 4.0$ for the angles switched DD laminate design *d*. Figure 4.2a, 4.2b and Figure 4.3 illustrate that it is possible to design double angle-ply laminates with the classical buckling factor of 4.0.

The compressive load (N_x), given by Eqn. 1.18, corresponding to the minimum first ply failure after off-axis orientation, is used to normalise all the polar plots that follow.

The first ply failure strength across the lamination parameter design spaces for extensional stiffness DD laminate design *d* is presented as a bubble plot in Figure 4.4a, which will be used later on to show the potential improvements for other designs. The size of the bubble is proportional to the FPF strength value, which is normalised against the FPF load of ϕ and $\psi = 0^\circ$ degree (5027 N/mm), i.e. a unidirectional laminate. This means that the stronger the design is in terms of FPF, the larger the bubble is. The full-size bubble (= 1.0) of the 0° laminate (i.e. with $\xi_1, \xi_2 = (1, 1)$) in the top right corner of Figure is shown for comparison. Figure 4.4b represents a conversion of the bubble to a 3-D plot for an alternative method of illustrating the data, where the lines in the z direction represent the FPF strength of the point with the length proportional to the magnitude. Maximum first ply failure strength using Tsai-Wu failure criterion occurs at $(\psi, \phi) = (\pm 6^\circ, \pm 6^\circ)$,

approximately 3.5% higher than 0° . Figure 4.4c shows a plot of the FPF strength for various failure criteria (Tsai-Wu, Tsai-Hill, Maximum Stress, Maximum Strain Puck and Puppo-Evensen) with (ψ, ϕ) ranged from 0° to 12° to investigate the prediction of Tsai-Wu model that the ply orientation with highest FPF strength does not occur at 0° but elsewhere. Only the Tsai-Wu failure criterion shows an increase in strength from 2° to 8° while all the other criteria have a decreasing trend, showing that the Tsai-Wu failure criterion gives a different prediction to the other criteria. This is important since the observation suggests that uni-directional laminate is not the strongest in terms of FPF strength according to Tsai-Wu failure criterion, where 0° laminates is usually expected to be the strongest under compressive loading. Since different failure criteria predict failure differently, experimental tests are needed to verify which failure criterion gives the best prediction for the laminate designs.

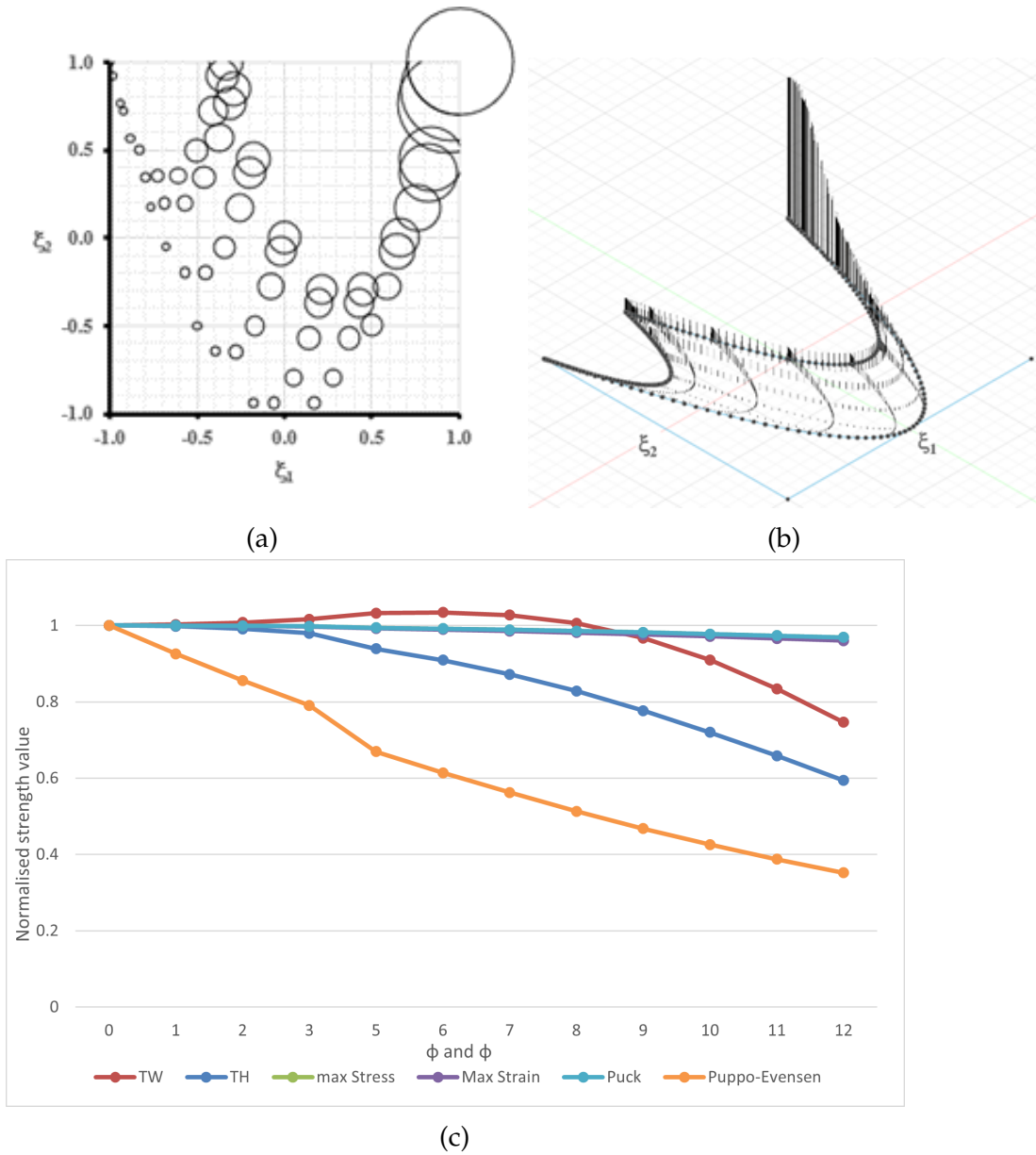


FIGURE 4.4: Illustration of: (a) a bubble plot with comparison of a full size bubble at $(\xi_1, \xi_2) = (1, 1)$; (b) a 3-D conversion of the bubble plot for laminate *d* and (c) comparisons between 6 failure criteria with ψ , and ϕ ranging from 0° to 12° .

Figure 4.5a and 4.5b represent bubble plots of the first ply failure strength of DD laminates *a* to *d*, in 10° increments across the design space for both normal and switched angles, while Fig. 4.5c and 4.5d represent the bubble plots for laminate *e* and *f*. The black bold lines in the design spaces representing $k_x = 4.0$ is superimposed on Figs. 4.5a to 4.5d. Figures 4.5e and 4.5f show bubble plots of standard ply angles with the 10% rule applied and onto which the 6 DD laminate designs are superimposed for comparisons. The Tsai-Wu failure criterion is used to assess uniaxial compression strength, which is proportional to bubble area and is normalized with respect to the 0° ply laminate, which has the highest failure strength of 1. Only the results

for DD laminates *a* to *d* are given in Figs. 4.5a and 4.5b. The location of typical aircraft wing skin designs is also plotted on the lamination design space of Figs. 4.5b, 4.5c, 4.5e and 4.5f for comparison with the DD laminates. The colour of the bubbles corresponds to the colours of the DD Designs *a*, *b*, *c*, *d*, *e* and *f*.

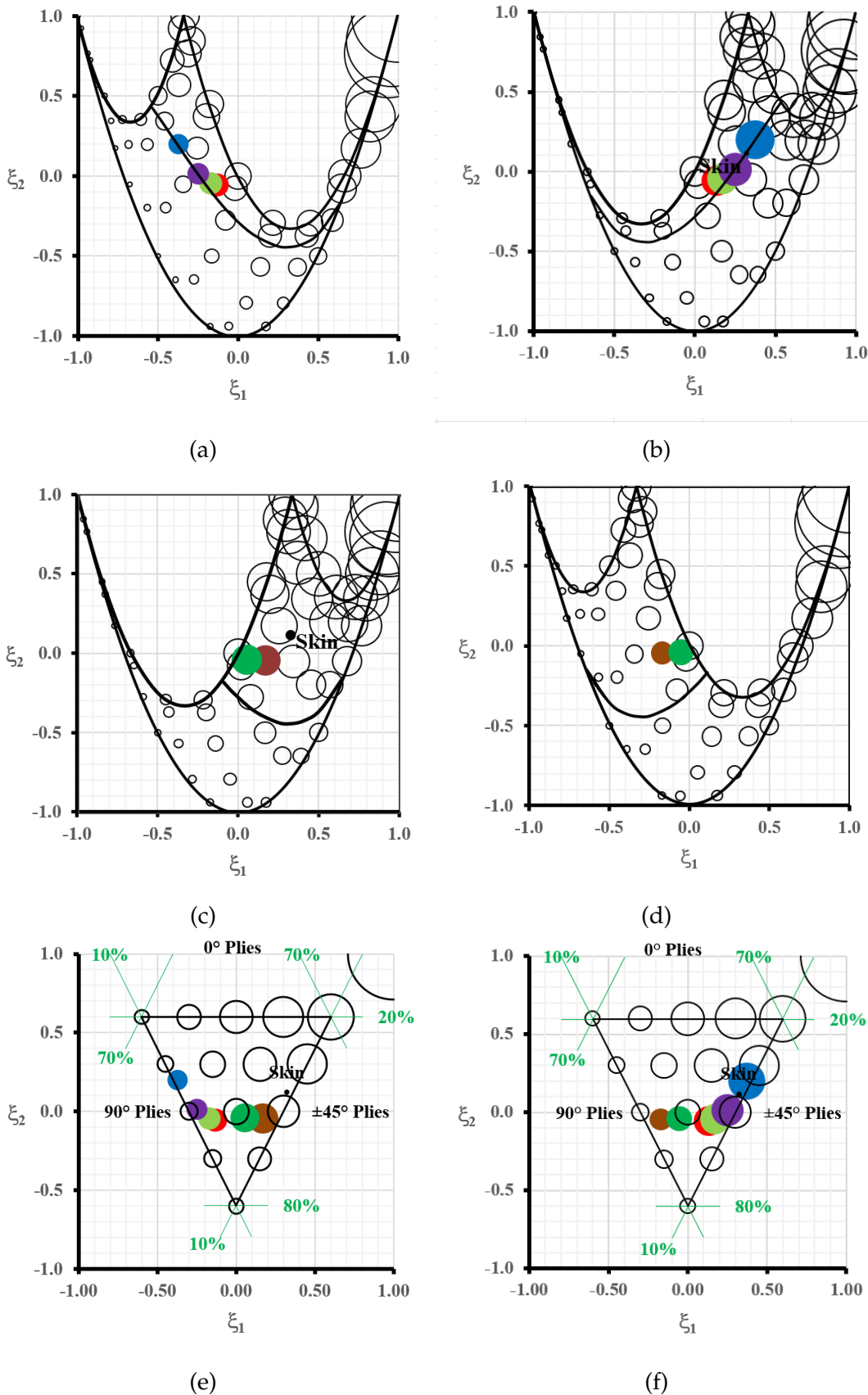


FIGURE 4.5: Strength comparisons for fully uncoupled Standard laminates (satisfying 10% rule) and DD laminates for stacking sequences *a* to *d* with angles: (a) as listed in Table 4.1; (b) switched; stacking sequences *e* and *f* with angles: (c) as listed in Table 4.1; (d) switched. Standard laminates are superimposed on designs *a* to *f* with angles: (e) listed in Table 4.1 and; (f) switched. Strength values are indicated by bubble area, normalized against maximum (100%) strength for 0° ply laminate shown at $(\xi_1, \xi_2) = (1, 1)$.

Figure 4.5a and 4.5b illustrate the potential to optimize laminates for FPF strength without degrading the buckling load, by choosing designs along the buckling line indicated in bold in Fig. 4.3. This implies that the strength of composite laminates can be improved without a reduction in buckling load. The equivalent line of constant buckling factor, $k_x = 4.0$, is plotted in Figs. 4.5a and 4.5b, revealing that the line on Fig. 4.5b is very close to the typical location of aircraft wing skin configuration. From Fig. 4.6e, it can be seen that the designs *e* and *f*, with $(\xi_1, \xi_2) = (0.17, -0.05)$ and $(0.05, -0.04)$ respectively, have higher failure strength than designs *a* to *d*, but with angles switched using Eqn. 4.10 in Fig. 4.6f, design *d* has the highest strength compared to the other designs.

Strength values are indicated by bubble area, normalized against maximum (100%) strength for a 0° ply laminate shown at $(\xi_1, \xi_2) = (1, 1)$. This was chosen to reflect the test procedure for determining laminate strength data. Laminate *d* has a normalised strength of 6.2%, in Figure 4.5a, and with angles switched has a normalised strength of 10.3%, in Figure 4.5b.

Only 2 extensional stiffness design spaces are presented here for the 6 laminates, as laminates with the same ply percentages share the same extensional stiffness design space, i.e. *a* to *d* and *e* and *f*. In contrast, the bending stiffness design space is different for each design, which is shown in Figs. 4.6 and 4.7, the former for normal angle and the latter for angle-switched designs.

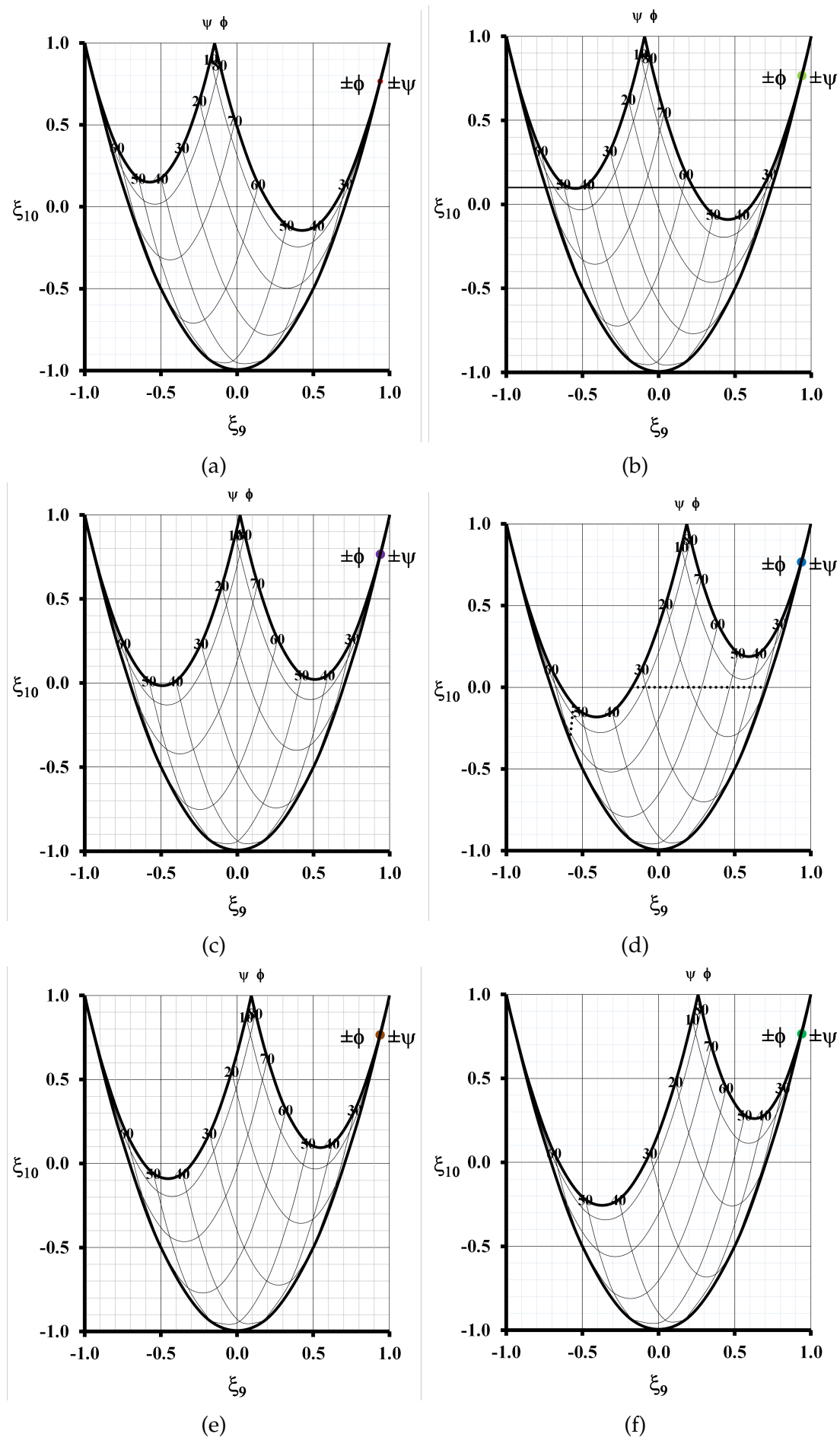


FIGURE 4.6: The bending stiffness design space for the laminates with normal angle configurations (a): *a*; (b): *b*; (c): *c*; (d): *d*; (e): *e* and (f): *f*.

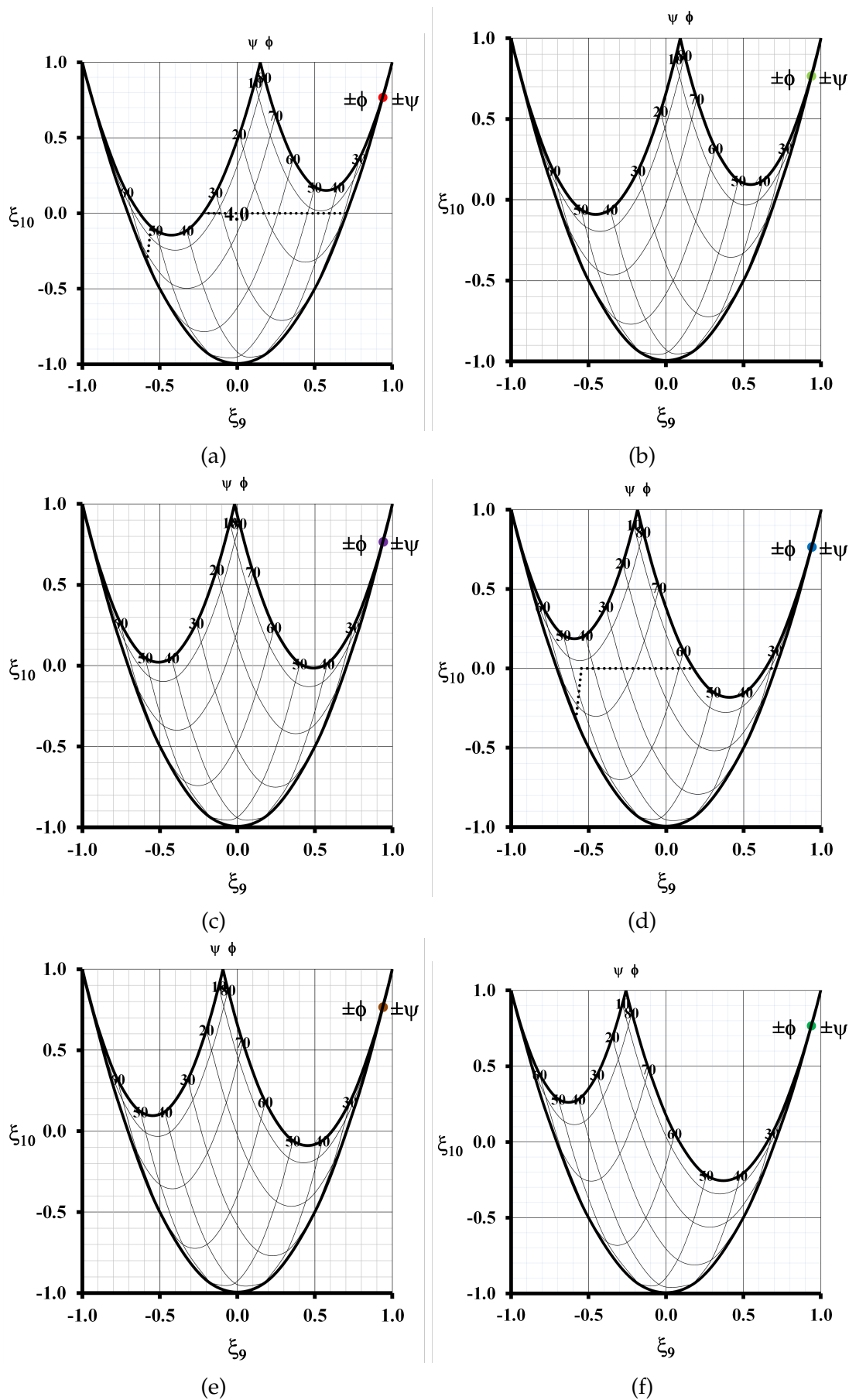
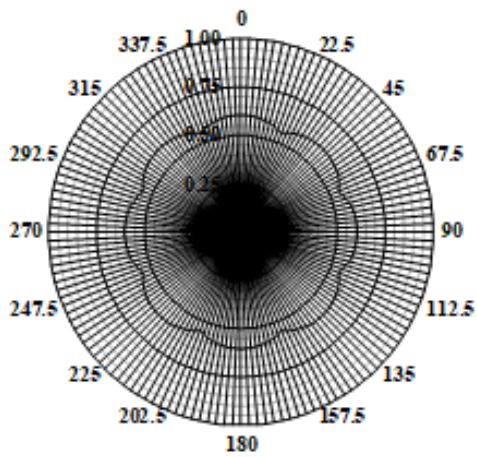


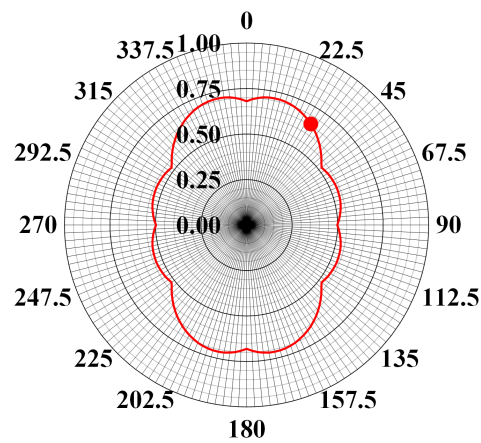
FIGURE 4.7: The bending stiffness design space for the laminate with angle switched configurations (a): *a*; (b): *b*; (c): *c*; (d): *d*; (e): *e* and (f): *f*.

4.4 OFF-AXIS ALIGNMENT

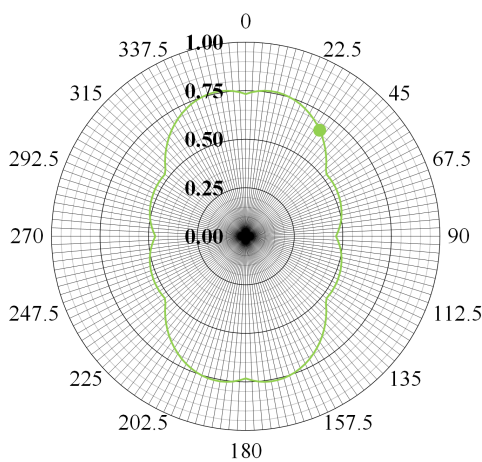
Off-axis alignments from 0° to 360° are introduced to the laminate designs listed above, and the resulting first ply failure performance, predicted using the Tsai-Wu failure criterion, is presented using polar plots. Fig. 4.8 represents polar plots of first ply failure with applied off-axis orientation, including the 6 DD laminates, balanced and symmetric, isotropic and Extension-Shear coupled only laminates. All the designs are normalized against DD laminate d which has the lowest first ply failure load. The point on each figure, denoted by the value of β , gives the maximum value of A_{16}/A_{11} .



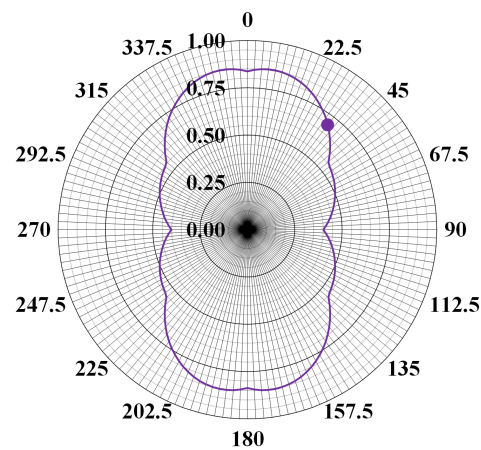
(a) Max $A_{16}/A_{11} = 8.3\%$ at $\beta = 32.5^\circ$



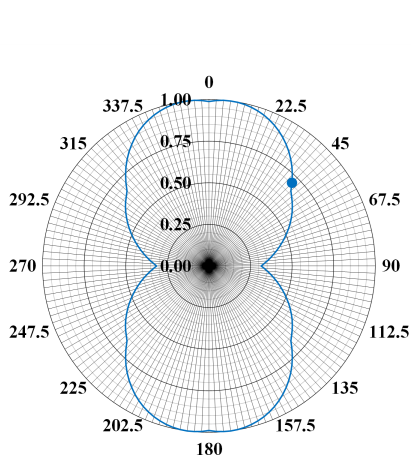
(b) Max $A_{16}/A_{11} = 8.3\%$ at $\beta = 32.5^\circ$



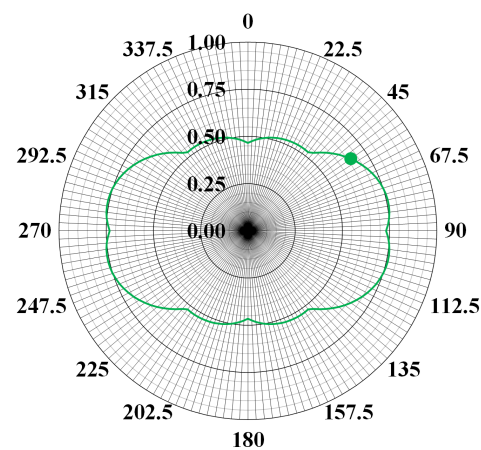
(c) Max $A_{16}/A_{11} = -10.4\%$ at $\beta = 33.8^\circ$



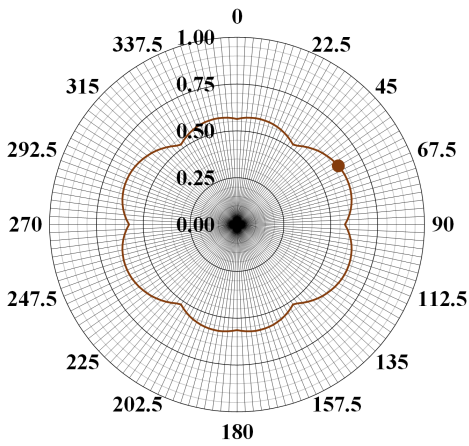
(d) Max $A_{16}/A_{11} = -14.4\%$ at $\beta = 38.3^\circ$



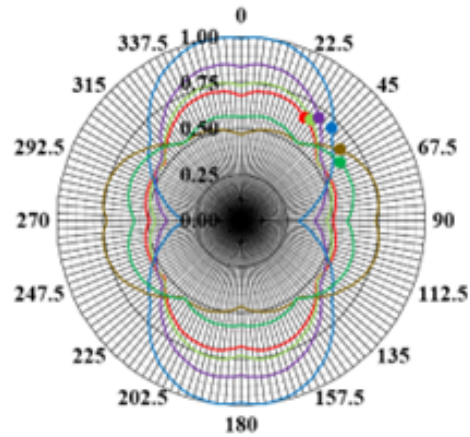
(e) Max $A_{16}/A_{11} = -22.1\%$ at $\beta = 46.1^\circ$



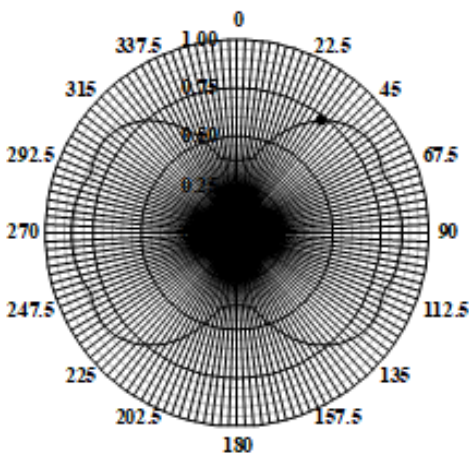
(f) Max $A_{16}/A_{11} = 10.3\%$ at $\beta = 56.2^\circ$



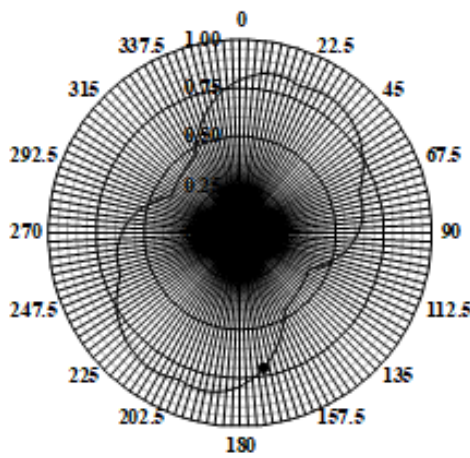
(g) Max $A_{16}/A_{11} = 3.6\%$ at $\beta = 59.1^\circ$



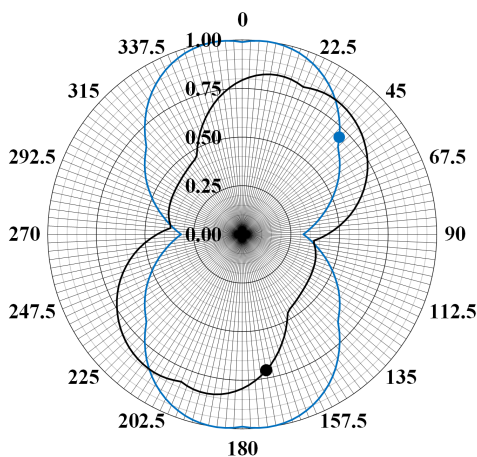
(h) Laminates *a* to *f* out envelopes



(i) $A_{16}/A_{11} = 16.3\%$ at $\beta = 0^\circ$ and Max $A_{16}/A_{11} = 18.0\%$ at $\beta = 170.1^\circ$



(j) Laminate *d* and *E-S* coupled outer envelopes

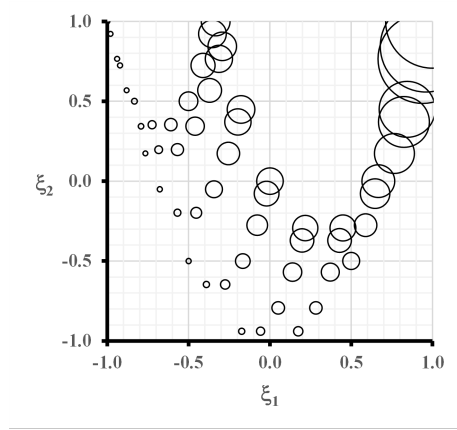


(k)

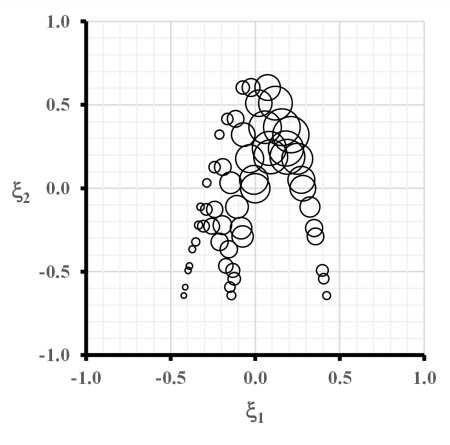
FIGURE 4.8: Strength comparisons for off-axis orientation β between a full envelope of 24 plies: (a) Isotropic laminate; DD laminate design: (b) *a*; (c) *b*; (d) *c*; (e) *d*; (f) *e* and (g) *f*; (h) superimposed laminates *a* to *f*; (i) Balanced and symmetric; (j) Extension-Shearing coupled (only) design and; (k) Superimposed laminate *d* and Extension-Shearing coupled design, all subject to equal compressive force resultant (N_x).

Laminate **d** has the highest maximum A_{16}/A_{11} among all the DD designs. The angles switched laminates gives the same maximum A_{16}/A_{11} as their non-switched angles counter laminates. Normalised against the first ply failure load for laminate **d** (100% at $\beta = \pm 7.1^\circ$), the balanced and symmetric design is at 37.5% of its material strength constraint and the *Extension-Shear* coupled only laminate is at 79.3% (at $\beta = 0^\circ$). However, at off-axis alignment, corresponding to maximum A_{16}/A_{11} , laminate **d** and the balanced and symmetric designs are at 68.9% (at $\beta = 46.1^\circ$) and 73.1% (at $\beta = 37.3^\circ$) of their material strength constraint, respectively. This shows that the FPF of the laminate designs can be improved by implementing off-axis alignments.

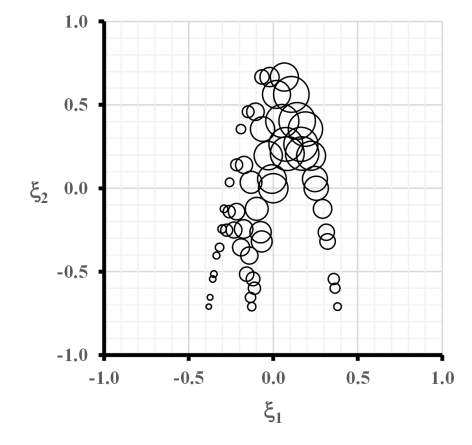
Figure 4.9 shows the design spaces of the 6 DD laminates. The initial graphs in this figure are plotted with the off-axis alignment of each laminate orientated to give the max value of A_{16}/A_{11} applied (as indicated in the top row of the Figure) the subsequent graphs in Fig. 4.9 are without off-axis alignment. Figure 4.10 presents the similar design spaces for the angle switched version. ϕ and ψ are swept from 0° to 90° to investigate the effect of off-axis alignment on both the design space and the material strength. The design space shrinks as β increases from 0° to 45° and expands from 45° to 90° .



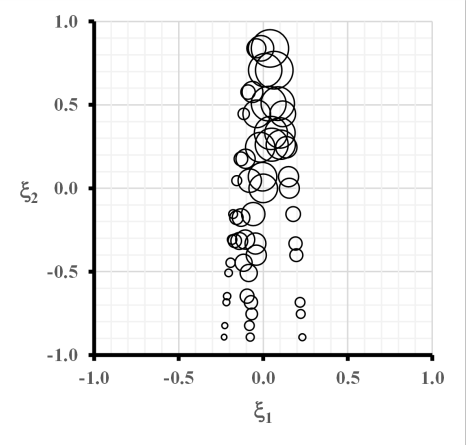
(a) Laminate *a* - *d* without off-axis alignment β



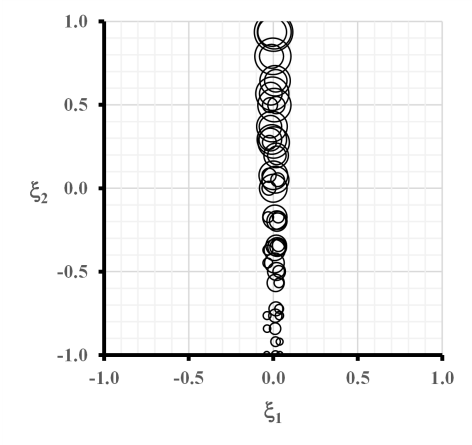
(b) Laminate *a* (Max $A_{16}/A_{11} = 8.3\%$ at $\beta = 32.5^\circ$)



(c) Laminate *b* (Max $A_{16}/A_{11} = 10.4\%$ at $\beta = 33.8^\circ$)



(d) Laminate *c* (Max $A_{16}/A_{11} = 14.4\%$ at $\beta = 38.3^\circ$)



(e) Laminate *d* (Max $A_{16}/A_{11} = 22.1\%$ at $\beta = 46.1^\circ$)

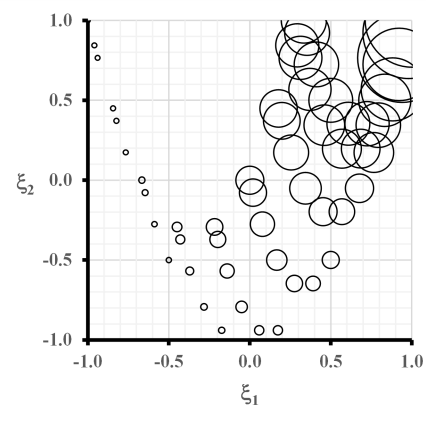
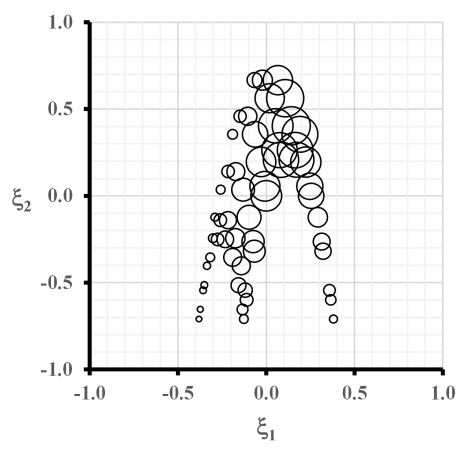
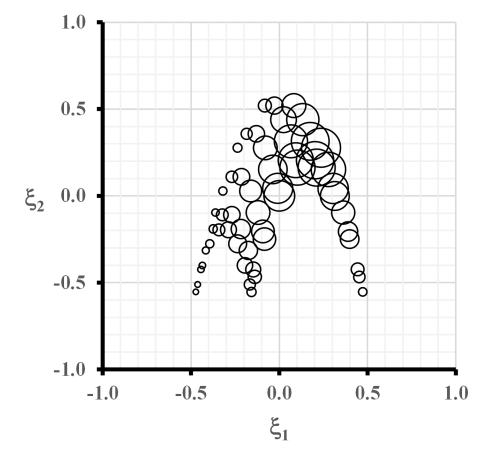
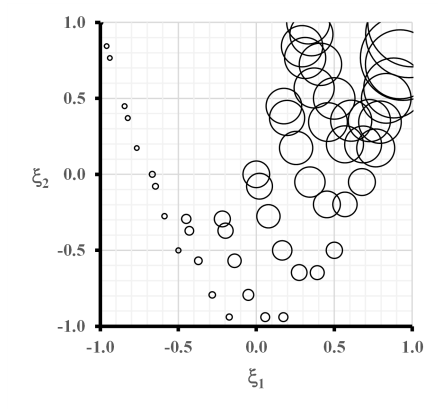
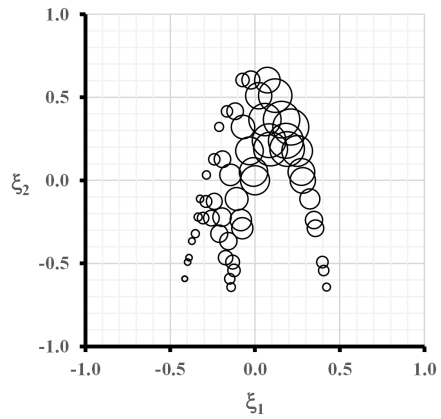
(f) Laminate $e - f$ without off-axis alignment β (g) Laminate e (Max $A_{16}/A_{11} = 10.3\%$ at $\beta = 56.2^\circ$)(h) Laminate f (Max $A_{16}/A_{11} = 3.6\%$ at $\beta = 59.1^\circ$)

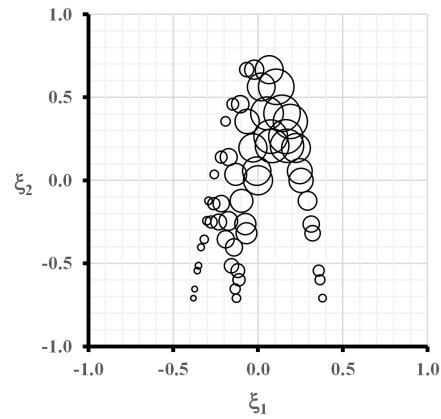
FIGURE 4.9: Illustration of the extensional stiffness design spaces of the 6 DD laminate designs with and without off-axis alignment, and bubbles indicating the normalized FPF strength



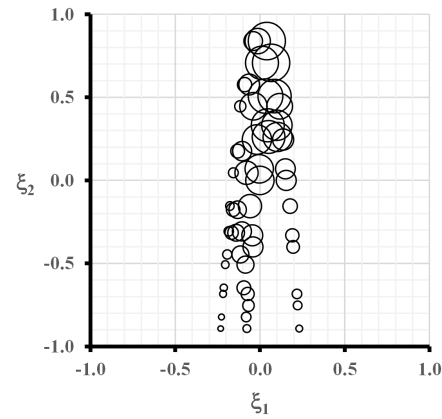
(a) Laminate *a* - *d* without off-axis alignment β



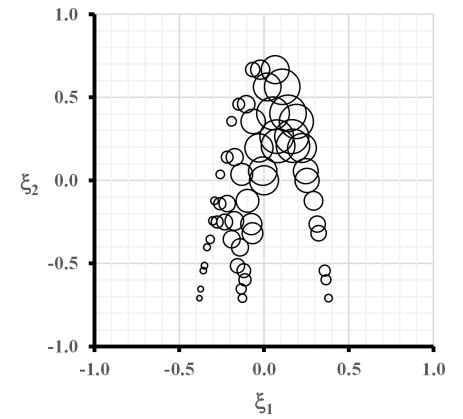
(b) Laminate *a* (Max $A_{16}/A_{11} = 8.3\%$ at $\beta = 32.5^\circ$)



(c) Laminate *b* (Max $A_{16}/A_{11} = 10.4\%$ at $\beta = 33.8^\circ$)



(d) Laminate *c* (Max $A_{16}/A_{11} = 14.4\%$ at $\beta = 38.3^\circ$)



(e) Laminate *d* (Max $A_{16}/A_{11} = 22.1\%$ at $\beta = 46.1^\circ$)

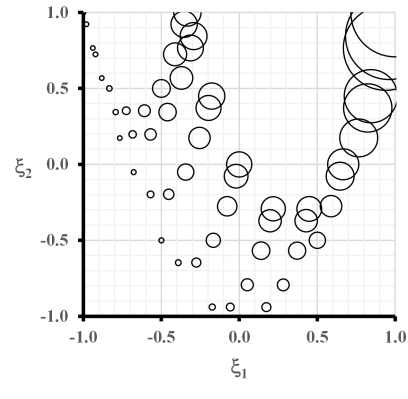
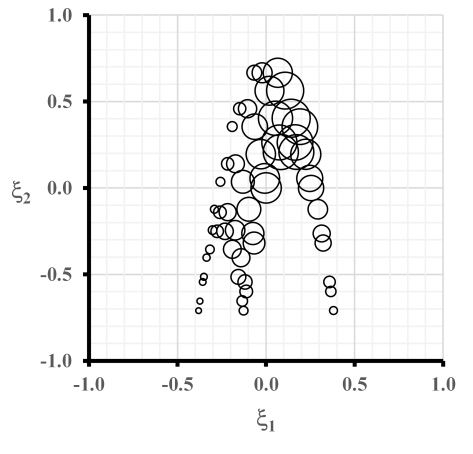
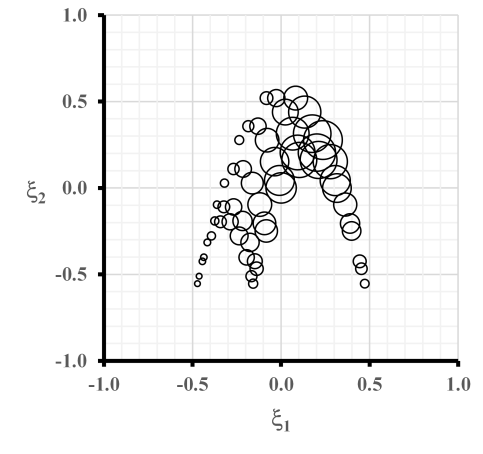
(f) Laminate *e* - *f* without off-axis alignment β (g) Laminate *e* (Max $A_{16}/A_{11} = 10.3\%$ at $\beta = 56.2^\circ$)(h) Laminate *f* (Max $A_{16}/A_{11} = 3.6\%$ at $\beta = 59.1^\circ$)

FIGURE 4.10: Illustration of the extension stiffness design spaces of the 6 angle switched DD laminate designs with and without off-axis alignment, and bubbles indicating the normalized FPF strength

Figure 4.11 shows a series of polar plots showing the normalised first ply failure load, using the FPF load of a 24-ply unidirectional laminate containing all 0° laminate with FPF strength of 5027N. In mathematical representation, is given as N_x/N_{X_0} .

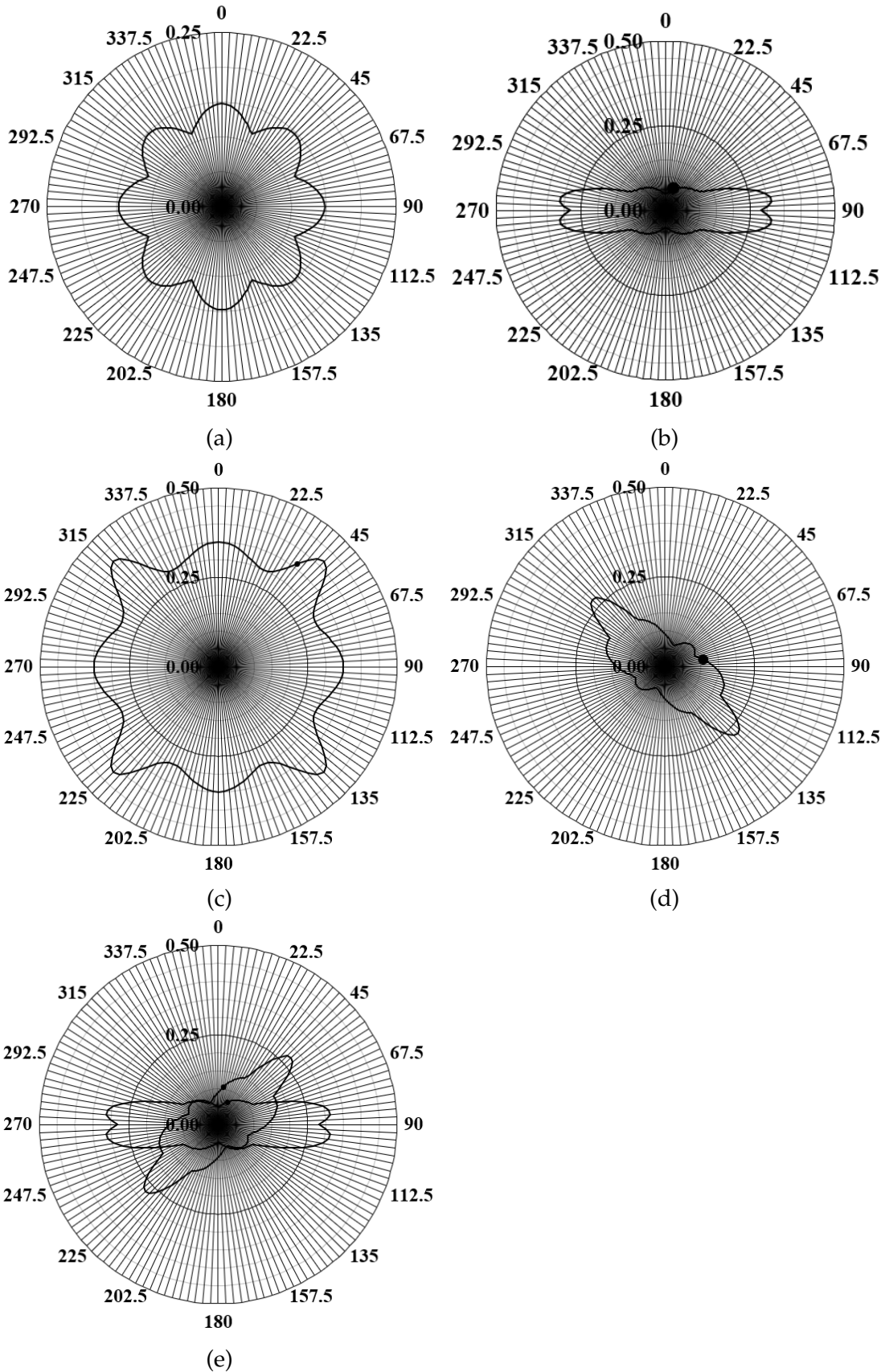
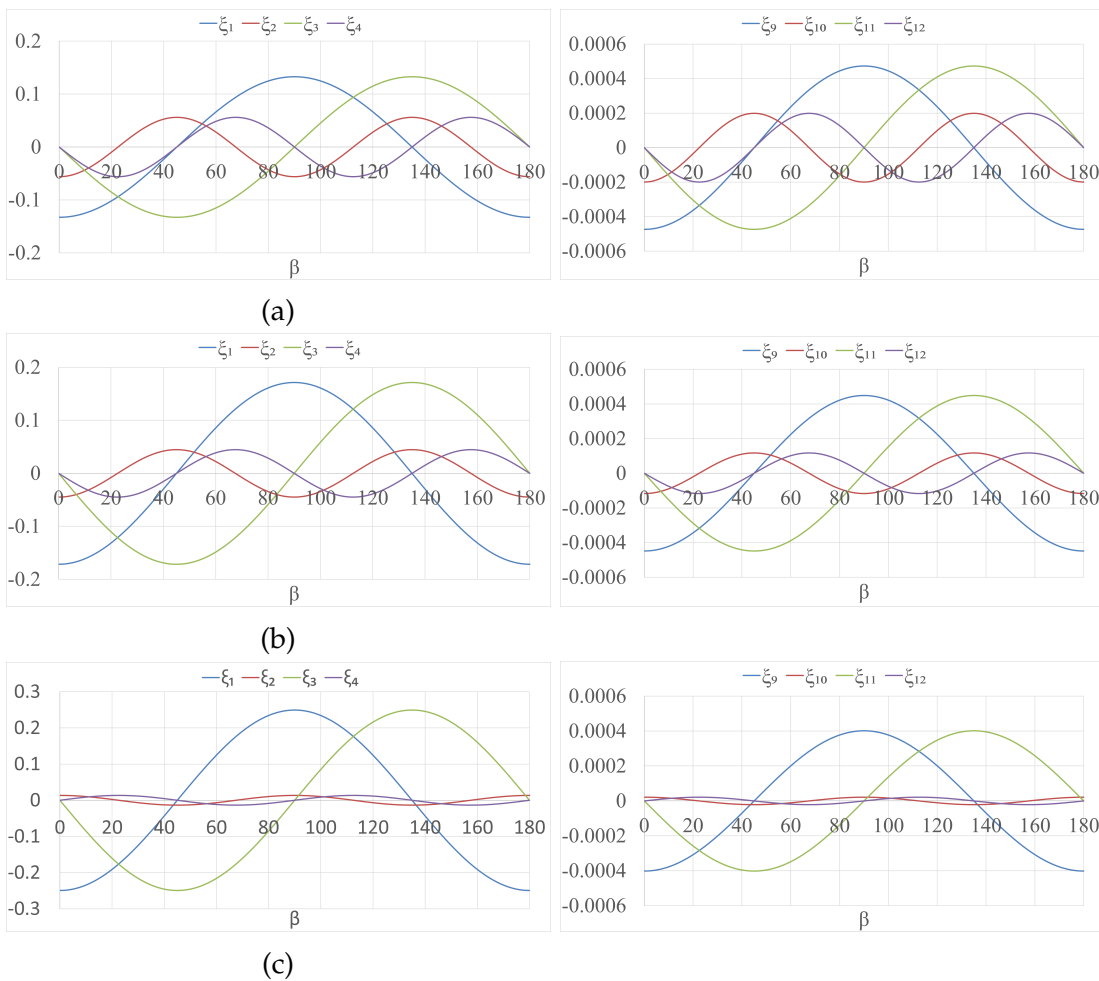


FIGURE 4.11: Strength comparisons for off-axis orientation β between a full envelope of 24 ply: (a) Isotropic laminate; (b) DD laminate design d ; (c) Balanced and symmetric; (d) E - S coupled (only) design and; (e) Superimposed laminate d and E - S coupled design, normalised to equal compressive force resultant (N_x) of 5027N.

The FPF load (N_x) of a 0° laminate (5027N) is applied to all the designs as the input compressive load, and off-axis alignment is then introduced to calculate the Tsai-Wu FPF strength using Eqn. 1.27. As the FPF load for 0° off-axis alignment is the highest, all the Tsai-Wu values of the designs with off-axis alignment must be larger than 1.0. Therefore, the reciprocal values are used to generate the polar plots, meaning that 1.0 is the highest strength.

Normalising against the first ply failure load for a 0° ply laminate, the Isotropic laminate has 8.5% of the FPF strength and the E - S coupled only laminate has 5.5% (at $\beta = 0^\circ$). For off-axis alignment, corresponding to maximum A_{16}/A_{11} , laminate d and the balanced and symmetric designs are at 6.2% (at $\beta = 46.1^\circ$) and 5.8% (at $\beta = 37.3^\circ$) of the first ply failure strength, respectively.

However, off-axis alignment introduces extra terms in both extensional and bending stiffness lamination parameters i.e. $\xi_{3,4}$ and $\xi_{11,12}$, changing the design space from 2-D to 4-D. The relationship between the lamination parameters and off-axis alignment for the DD designs is presented in Fig. 4.12. Note that for ξ_{1-4} and ξ_{9-12} with the same relationship against β (laminate a, b, c and d), the laminate is considered as Quasi Homogenous, where $D_{ij} = A_{ij}H^2/12$.



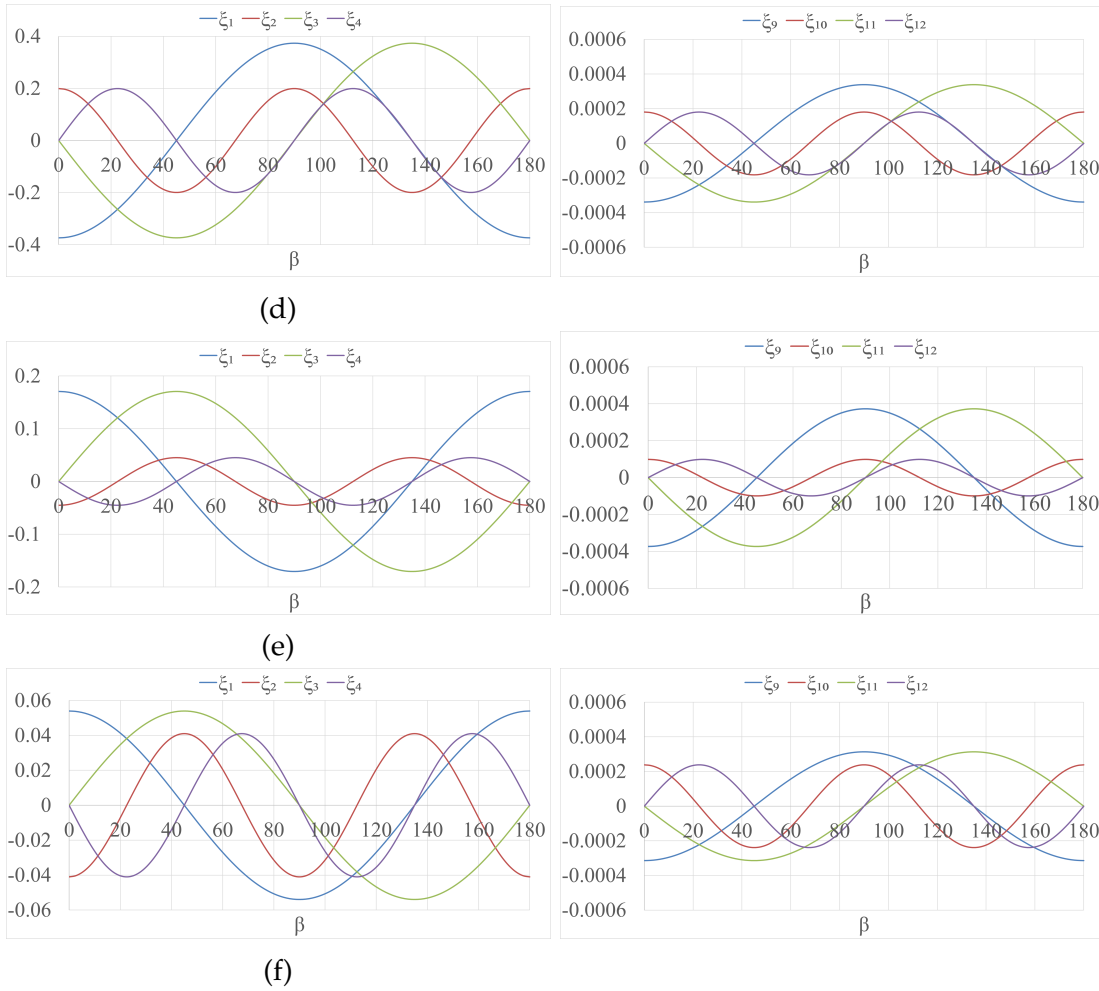


FIGURE 4.12: The relationship between the extensional ζ_{1-4} and bending stiffness lamination parameters ζ_{9-12} and β for DD laminate designs: (a) *a*; (b) *b*; (c) *c*; (d) *d*; (e) *e* and (f) *f*.

Figure 4.12 demonstrated that the values of ζ_{1-4} can increase up to almost ± 0.4 , while the values of ζ_{9-12} ranged between ± 0.0006 . However, the the relationship between the lamination parameters and off-axis alignment and the influence are generally not understood, more thorough explanation is required. Therefore, Chapter 5 will focus on the influence of the coupling terms and 4-D design spaces.

Table 4.3 presents the required laminate width, b , for coincident buckling and first ply failure under compression load of the DD laminate designs for aspect ratios $a/b = 1.0, 1.5, 2.0$ and 2.5 . The dimensions are typical of the width between stiffeners in a stiffened panel wing skin. Table 4.4 shows the width-to-total thickness ratio, b/H , of the optimal designs in Table 4.3. Note that results of $a/b = 1$ and 2 are shown in the same row as the two ratios share identical dimensions.

TABLE 4.3: Plate width (mm), b , corresponding to 24-ply DD design with coincident buckling and first ply failure.

AR	Laminate Design					
	a	b	c	d	e	f
1 and 2	107.7	107.7	116.5	124.5	92.0	98.6
1.5	112.1	115.3	121.4	129.6	95.8	102.7
2.5	109.4	112.6	118.5	126.5	93.5	100.2

TABLE 4.4: Width-to-thickness ratio, b/H , corresponding to optimal 24 ply DD designs in Table 4.3.

AR	Laminate Design					
	a	b	c	d	e	f
1 and 2	32.1	33.0	34.8	37.1	27.4	29.4
1.5	33.4	34.4	36.2	38.7	28.6	30.6
2.5	32.6	33.6	35.3	37.7	27.9	29.9

4.5 COMPRESSION TEST

The final section of this chapter involves compression tests. The main objective of the tests is to characterise the compression behaviour of the material including compression stiffness, evaluate predictions made in this chapter and investigate the failure strength of the laminate designs discussed in this chapter. Due to COVID-19, I was not able to perform the manufacture and test process myself, but Prof. Christopher York and Dr Periyasamy Manikandan kindly helped carry out the processes at the Singapore Institution of Technology. Double angle-ply laminate design, d with $\beta = -46.1^\circ$, isotropic, E - S coupled and balanced and symmetric (BS) laminates with $\beta = 37.3^\circ$ were manufactured, with 3 specimens tested for each design. The stacking sequences are listed in Chapter 4.2. SE 84LV low temperature cure carbon fibre epoxy prepreg was used [14], the designed length, width and thickness of the laminates were: 150 mm, 25 mm and 3.30 mm, and a cross sectional area, A , of 82.5 mm².

The unidirectional (UD) prepreg tape was rolled out and cut manually to the required fibre orientations and the plies were manually stacked according to the specified stacking sequences. To

remove any voids or air gaps between plies during the lay-up process, debulking was performed in every 6 plies of stacking. Stacked laminates were then cured using an autoclave programmed to the recommendations given by the material supplier, where pressure and temperature are 1 bar and 80 °C.

The laminates are then cut into the desired size as shown in Fig. 4.13.



FIGURE 4.13: Manufactured DD laminates.

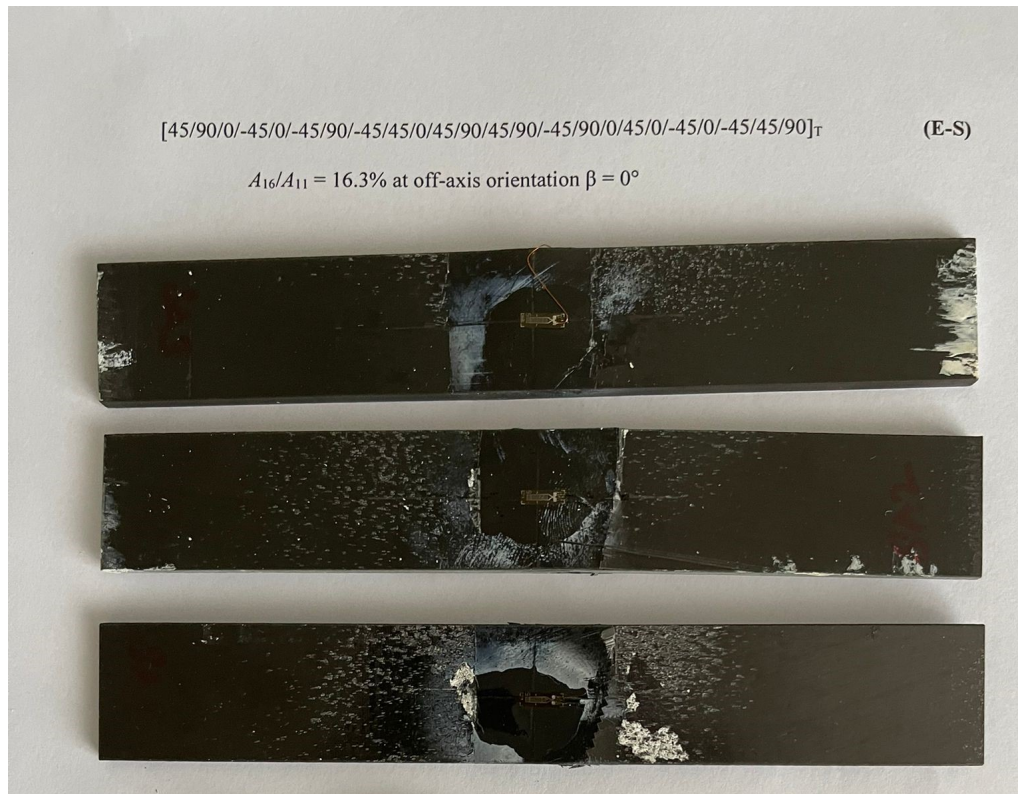
- v The coupon was loaded to 1 kN and returned to 0 to monitor the strain readings, where the strains were usually about 100 to 200 micro-strain, which is negligible.
- vi The compression test was started, and the samples were loaded until failure.

The measured values of the manufactured laminates are shown in Table 4.5, where DD, ES, BS and ISO represent the double angle-ply, *Extension-Shear coupled*, balance and symmetric and fully isotropic designs.

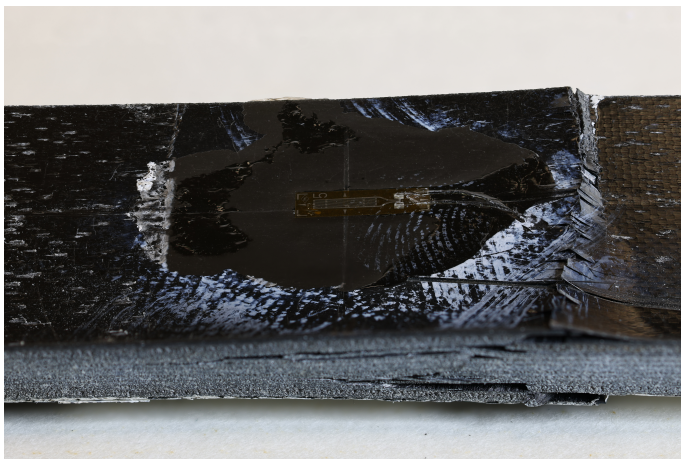
TABLE 4.5: Measured dimensions of manufactured laminate designs.

Specimen	l (mm)	w (mm)	t (mm)	A (mm ²)
DD-1	150	24.72	3.29	81.31
DD-2	150	24.00	3.40	81.60
DD-3	150	24.97	3.41	85.02
ES-1	150	23.95	3.39	81.19
ES-2	150	24.04	3.38	81.24
ES-3	150	24.57	3.38	83.05
BS-1	150	23.94	3.39	81.14
BS-2	150	24.17	3.39	81.94
BS-3	150	24.42	3.41	85.27
ISO-1	150	24.64	3.27	80.48
ISO-2	150	23.99	3.38	81.07
ISO-3	150	24.02	3.35	80.45

Examples of the laminates after failure are shown in Fig. 4.15.



(a)



(b)

FIGURE 4.15: Samples after failure for (a) all *E-S* laminates and (b) a zoomed in capture of one of the laminates after failure.

The resulting compressive stress is given as:

$$\sigma_i = \frac{P_i}{A} \quad (4.11)$$

where P_i represents the compressive load at a particular point. Finally, the chord modulus of

elasticity, E_{chord} , is given as:

$$E = \frac{\delta\sigma}{\delta\epsilon} \quad (4.12)$$

A range of strain from 1000 to 3000 μ strain is used for modulus calculations, which is recommended by ASTM standards [115]. Strain gauges were attached to the front and back surfaces of the test specimens, one on each surface. A compression load was applied until the specimens failed. The resulting failure strength, maximum stress, strain and modulus obtained using both the measured dimension and design dimensions are summarised in Tables 4.6 and 4.7. The resulting stress-strain graphs of the specimens are presented in Fig. 4.16. While FPF predictions are made using Tsai-Wu failure criteria for comparisons, which are given in Table 4.8, since the engineering properties of the SE 84LV material is not given by the material supplier, T300/5208 is used for the prediction and the predictions are used to compare to the test results.

TABLE 4.6: Resulted failure strength, maximum stress, strain and modulus obtained from using measured dimensions.

Property	P_{max} (kN)				σ_{max} (kN)			
Sample	Iso	DD	ES	BS	ISO	DD	ES	BS
1	22.70	28.56	22.83	30.72		351.30	281.15	378.66
2	29.32	29.73	24.58	23.32	361.68	364.36	302.56	284.62
3	31.06	21.95	22.42	26.22	386.08	258.17	269.99	314.85
Average	30.19	26.75	23.28	26.75	373.88	324.61	284.57	326.04
Property	ϵ_{av}^u (%)				E (GPa)			
Sample	ISO	DD	ES	BS	ISO	DD	ES	BS
1		0.86	0.62	1.05		42.99	38.66	40.13
2	0.74	1.01	0.81	0.87	51.19	39.07	38.72	39.67
3	0.70	0.68	0.75	0.87	48.88	40.78	37.85	36.40
Average	0.72	0.85	0.73	0.93	50.03	40.95	38.41	38.74

TABLE 4.7: Resulted failure strength, maximum stress, strain and modulus obtained from using designed dimensions.

Property	P_{\max} (kN)				σ_{\max} (kN)			
Sample	Iso	DD	ES	BS	ISO	DD	ES	BS
1	22.70	28.56	22.83	30.72		346.24	276.69	372.41
2	29.32	29.73	24.58	23.32	355.41	360.38	297.93	282.67
3	31.06	21.95	22.42	26.22	376.48	266.07	271.78	317.79
Average	330.19	26.75	23.28	26.75	365.95	324.23	282.13	324.29
Property	ϵ_{av}^u (%)				E (GPa)			
Sample	ISO	DD	ES	BS	ISO	DD	ES	BS
1		0.86	0.62	1.05		42.99	38.66	40.13
2	0.74	1.01	0.81	0.87	51.19	39.07	38.72	39.67
3	0.70	0.68	0.75	0.87	48.88	40.78	37.85	36.40
Average	0.72	0.85	0.73	0.93	50.04	40.95	38.41	38.74

TABLE 4.8: First ply Failure load predictions of the fully isotropic, DD design d with $\beta=-46.1^\circ$, E - S coupled and balanced and symmetric designs $\beta=37.3^\circ$ under compressive load.

FPF Strength Prediction (N)			
ISO	DD laminate design d ($\beta = -46.1$)	ES	BS ($\beta=37.3^\circ$)
22,780	19,977	18,059	19,279

Note that one of the strain gauges for ES-1 specimens malfunctioned during the test and no strain gauges were installed for ISO-1. Therefore, the results for these 2 test samples are simply discarded.

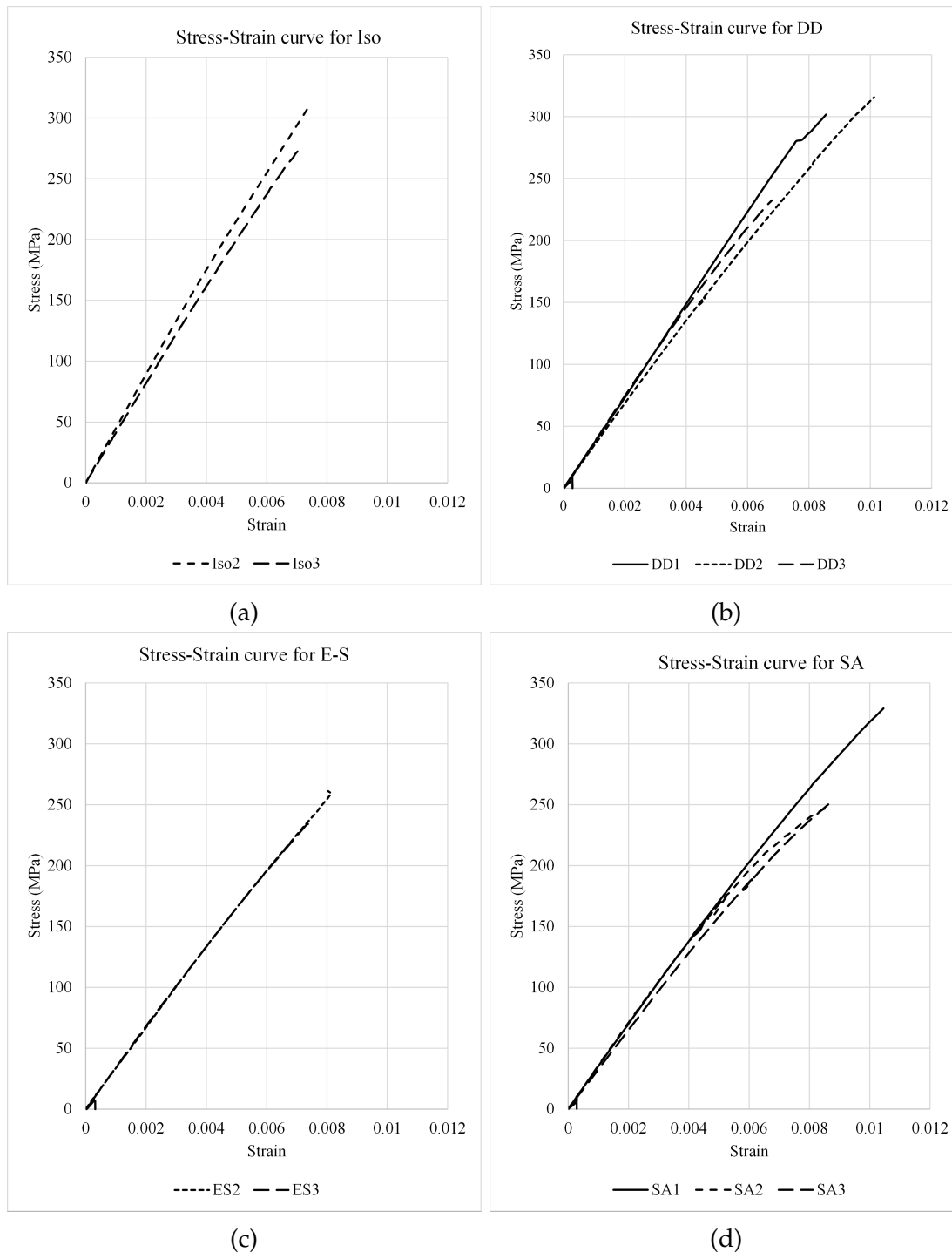


FIGURE 4.16: Stress-strain curves of specimens for (a): Isotropic; (b): DD design *d*; (c): *Extension-Shear* and; (d): Balanced and Symmetric laminates.

Table 4.8 shows the numerical predictions of FPF for the 4 different designs. It can be seen that the isotropic design has the highest predicted FPF load, the *E-S* coupled design has the lowest failure strength and the DD design has a similar performance as the balanced and symmetric design. The compression test results for the 4 designs in Tables 4.6 and 4.7 show a similar relationship but with higher values. The isotropic design has the highest failure load, while the *E-S* design is the first to fail and the DD and balanced and symmetric designs lie in the middle

with very similar failure strengths. Figure 4.16 presents the stress and strain relationships of the samples for the 4 different designs. The results show that *E-S* coupled laminates have the most consistent results, but only 2 samples were available for comparison. The *E-S* coupled design does not show any favourable improvement compared to the other designs, while DD laminate with off-axis alignment gives a similar failure strength as the balanced and symmetric design with standard fibre orientation. Laminate design *d* was chosen as the weakest without off-axis alignment, other DD designs (which have stronger FPF strength without off-axis alignment) with their beta that gives their responding maximum *E-S* can be manufactured and tested.

This is a preliminary experiment, only 3 specimens were manufactured and tested for each design, which cannot conclude the findings reliably, therefore more specimens should be manufactured and tested with 155 mm length that provides more accurate results. The failure load of the predictions is on average 3,000 N lower than the test results, the difference between the prediction and test results is due to the difference in material used for the predictions and actual test. For future experiment, the engineering properties should be characterised for better predictions and direct comparisons with the test. The difference in failure load can also be associated with the prediction tool, predictions were made with the Tsai-Wu failure criterion, but failure is predicted slightly differently according to the failure criteria, as discussed in Chapter 1. Therefore, predictions should be done with other failure criteria and compared to the experimental results to find out the criterion that has the closest fit to the test results.

Moreover, the recommended length of the specimen is 140 to 155 mm, and the actual size of the specimen is 150 mm, which is within the suggested range. However, the sample is subjected to shear deformation soon after the load is not pure axial compression load. After 50 tests, it was concluded that specimens with 155 mm length provided more accurate modulus and strength values compared to the data provided by the supplier, than 150 mm samples. Moreover, specimens of 155 mm were able to be slotted within the wedges more firmly, reducing the chance of in-plane shear motion occurring under axial compression loads.

In terms of potential future work, buckling and first ply failure tests can also be performed, which would act as validations for all the numerical and analytical work performed in the past 4 years.

4.6 CONCLUSION

This chapter has explored the design spaces of DD laminate designs, which match the equivalent ply percentages of typical aircraft skin designs. The effect of off-axis alignment on the first ply failure performance of laminates is demonstrated. Moreover, this chapter has attempted to predict the optimum dimensions of the DD laminates by matching the structural buckling and material strength constraints.

Polar plots of first ply failure have demonstrated that DD designs offer comparable strength to standard laminates when off-axis orientation is applied in order to maximise anisotropy or *Extension-Shear* coupling.

Preliminary experimental tests have shown that the DD designs with off-axis alignment offer comparable failure strength to standard laminates when aligned to the prediction by the Tsai-Wu failure criterion.

The design approach used to achieve optimised material strength and anisotropy has been shown to be possible without degrading the buckling performance of various standard and DD laminate designs.

CHAPTER 5

COUPLING EFFECTS

5.1 INTRODUCTION

Chapter 3 explored the buckling performance of uncoupled and *Bend-Twist* (*B-T*) coupled laminates with standard fibre orientations. Chapter 4 introduced the new double angle-ply or ‘double-double’ (DD) configuration where the first ply failure (FPF) of DD laminates was assessed and discussed. This chapter follows the previous 2 chapters, applying knowledge of coupling behaviour to DD laminate technology. The goal of this chapter is to combine the knowledge from chapters 3 & 4 to explore the design space of fully *B-T* coupled DD laminates to and design laminates with potential improvements in buckling or FPF performance with Tsai-Wu failure criteria [58, 32].

The first objective of this chapter involves the investigation of the effect of fully coupled bending stiffness parameters, ζ_{11} and ζ_{12} , on the buckling performance of laminates with standard quad and DD orientations. The second objective is to assess the buckling and first-ply failure performance of DD laminates with full *B-T* coupling, using a stiffness matching technique. To do this, a 4-dimensional design space for fully coupled *B-T* designs is presented. Another objective is to design fully *B-T* coupled laminates with improved FPF performance without degradation in buckling performance. The final objective of the chapter is to investigate the performance of tapered DD laminates that possess *B-T* coupling, the effect of the direction of tapering on buckling performance is also examined.

Optimisation of composite laminates using lamination parameters allows the design process to be simplified. The introduction of coupling behaviour, such as Extension-Shear (*E-S*) and *B-T* coupling, leads to extra design variables such as ζ_3 and ζ_4 or ζ_{11} and ζ_{12} and results in a

more complicated 3, or even 4-dimensional design space. However, the increase in size of the design space increases the possibility of designing composite structures with improved material properties or failure performance.

Earlier studies attempted to design composite laminates using lamination parameters and investigated the relationships between the different lamination parameters [46, 43, 37]. The relationships between the lamination parameters were also developed [43, 44, 40, 41] and projections of 6 planes of bending stiffness was demonstrated [40]. The relationship between the bending stiffness lamination parameters for standard quads and DD laminates in 2 and 3 dimensions are summarised in Table 1. However, no prior studies have successfully fully illustrated the entire 4-dimensional design space.

TABLE 5.1: The bending stiffness lamination parameters relationships of standard and DD laminates in 2-D and 3-D design spaces.

	Standard Quads	Double angle-ply
2-D	$\zeta_2 = 2\zeta_1 - 1$ or $\zeta_2 = -2\zeta_1 - 1$	$\zeta_2 = 2\zeta_1^2 - 1$
	$\zeta_{10} = 2\zeta_9 - 1$ or $\zeta_{10} = -2\zeta_9 - 1$	$\zeta_{10} = 2\zeta_9^2 - 1$
3-D	$\zeta_2 = 2\zeta_1 - 1$ or $\zeta_2 = -2\zeta_1 - 1$	$\zeta_2 = -2\zeta_1^2 + 1$
	$\zeta_3 = \zeta_1 + 1$ or $\zeta_3 = \zeta_1 - 1$	$\zeta_1^2 + \zeta_3^2 = 1$
	$\zeta_{10} = 2\zeta_9 - 1$ or $\zeta_{10} = -2\zeta_9 - 1$	$\zeta_{10} = -2\zeta_9^2 + 1$
	$\zeta_{11} = \zeta_9 + 1$ or $\zeta_{11} = \zeta_9 - 1$	$\zeta_9^2 + \zeta_{11}^2 = 1$

Bend-Twist coupled laminates are known to have reduced compressive buckling load, in contrast to fully uncoupled laminates even through stiffness matching. The effect is often ignored in practice as it can be dissipated by thick laminates containing a lot of plies [116]. However, this can cause predictions to be unsafe even when following design guidance [103] and using closed form solutions [50]. This is especially true in thin plate laminates, where buckling performance is affected by *B-T* -coupling and can be overestimated if the effect is ignored. The effect of *B-T* coupling on buckling performance has been studied previously in terms of lamination parameter design space [86].

As discussed in the literature review in Chapter 1, researchers have attempted to illustrate the 4-D design spaces for fully coupled laminates. Previous chapters explored the 2-D and 3-D design

space of standard Quads and DD laminates. This chapter explores the 4-D world of coupled laminates, focusing on the effect of B - T coupling. A laminate database from [117] containing fully uncoupled standard quad laminates with balanced and symmetric configurations is used for this part of the project using newly developed datasets. First, the effect of B - T coupling is investigated. Stiffness matching between quads and DD designs is performed to determine the double angle that gives matching lamination parameters values of standard laminates. Laminates with different thicknesses are examined, and compressive buckling and FPF performance comparisons are provided.

5.2 BENDING-TWISTING COUPLING

The first part of this chapter involves the investigation of the specific effect of bending stiffness ζ_{11} and ζ_{12} on buckling performance for laminates aspect ratios 1, 1.5 and 2 with standard quads and DD orientations. A database (Appendix 1: Balanced and Symmetric Standard-Ply Designs) from York [96] is used, which contains fully uncoupled laminate designs for 12 to 24-ply balanced and symmetric layups, with standard angles. All the balanced and symmetric designs are subject to the 10% rule design constraint, where each ply angle contributes at least 10% towards the whole laminate; and ply continuity of 3, where the maximum number of repeating plies with the same angle orientation, occurring consecutively, is limited to 3. Laminate designs including 12, 16, 20 and 24 plies are selected from the database. Designs closest to the point $(\zeta_9, \zeta_{10}) = (0, -1)$ on a bending stiffness lamination parameters (ζ_9, ζ_{10}) design space are chosen. The stacking sequences of the different laminate thickness designs are listed Table 5.2, where $(+, -, \circ, \bullet) = (+45^\circ, -45^\circ, 0^\circ$ and $90^\circ)$. Note that all the designs with standard fibre orientations are fully uncoupled, with ζ_{11} and $\zeta_{12} = 0$ and with 0 in the $[B]$ matrix, which means the laminate is immune to thermal warping. While the DD laminate designs are shown in Table 5.3, with their bending stiffnesses matched to the standard fibre orientation counterpart of the same thickness. Note that there are multiple stacking sequences of the same thickness that share the same point on a bending stiffness lamination parameter (ζ_9, ζ_{10}) design space, as mentioned in chapter 3, but only one is shown here for demonstration purposes.

TABLE 5.2: Thickness, stacking sequence and the bending stiffness of the standard quads laminates.

Number of ply	Stacking Sequences	(ξ_9, ξ_{10})
12	$[+/-/-/\bullet/+/\circ/\circ/+/\bullet/-/-/+]\text{T}$	$(-0.083, -0.815)$
16	$[+/-/-/+/\bullet/-/+/\circ/\circ/+/-/\bullet/+/-/-/+]\text{T}$	$(-0.070, -0.852)$
20	$[+/-/-/\bullet/+/\circ/\circ/\bullet/\bullet/\circ/\circ/-/+/\bullet/-/-/+]\text{T}$	$(-0.102, -0.692)$
24	$[-/+/\circ/\circ/\bullet/\bullet/\circ/\circ/\bullet/+/-/-/+/-/+/-/+]\text{T}$	$(-0.007, -0.926)$

TABLE 5.3: Thickness, stacking sequence and the bending stiffness of the DD laminates with equivalent ξ_9 and ξ_{10} .

Number of ply	Stacking Sequences	(ξ_9, ξ_{10})
12	$[\psi/-\psi/-\phi/\phi/-\phi/\phi/\phi/-\phi/\phi/-\phi/-\psi/\psi]\text{T}$	$(-0.083, -0.815)$
16	$[\psi/-\psi/-\phi/\phi/-\psi/\psi/-\psi/\psi/-\psi/\psi/\psi/-\psi/\phi/-\phi/\psi/-\psi]\text{T}$	$(-0.070, -0.852)$
20	$[\psi/-\psi/\phi/-\phi/-\psi/\psi/-\phi/\phi/-\phi/\phi/-\phi/\phi/\phi/-\phi/\psi/-\psi/\phi/-\phi/-\psi/\psi]\text{T}$	$(-0.102, -0.692)$
24	$[\psi/-\psi/-\psi/\psi/-\phi/\phi/-\psi/\psi/-\phi/\phi/-\phi/\phi/\phi/-\phi/\phi/-\phi/-\psi/\psi/\phi/-\phi/\psi/-\psi/\psi/-\psi]\text{T}$	$(-0.007, -0.926)$

To investigate the effect of the B - T coupling terms, the ξ_9 and ξ_{10} are fixed and arbitrarily ξ_{11} and ξ_{12} are introduced in different combinations since the designs from the database are uncoupled. FEA predictions of buckling performance (where the simulation model was discussed in Chapter 2) are made with various combinations of the coupling terms introduced, as listed in Table 5.4. The same set of combinations is applied to the DD laminate designs to examine the effect of coupling behaviour.

TABLE 5.4: List of combination of arbitrary B - T coupling applied to the standard and DD laminate designs.

Combination	1	2	3	4	5	6	7	8	9
ξ_{11}	0	0.25	-0.25	0.25	0	-0.25	0	0.25	-0.25
ξ_{12}	0	0.25	-0.25	0	0.25	0	-0.25	-0.25	0.25

The resulting buckling factors for laminates of aspect ratios (AR) 1.0, 1.5 and 2.0 are presented

below, the buckling performance for standard and DD configurations are identical, therefore only one set of results is presented here.

TABLE 5.5: Buckling factors of standard quads and DD designs under the ζ_{11} and ζ_{12} combinations listed in Table 5.4 for AR = 1.0.

No. of Ply	Combination								
	1	2	3	4	5	6	7	8	9
12	4.84	4.71	4.71	4.72	4.83	4.72	4.83	4.71	4.71
16	4.87	4.74	4.74	4.75	4.87	4.75	4.87	4.75	4.75
20	4.70	4.57	4.57	4.58	4.70	4.58	4.70	4.58	4.58
24	4.93	4.81	4.81	4.81	4.93	4.81	4.93	4.81	4.81

TABLE 5.6: Buckling factors of standard quads and DD designs under the ζ_{11} and ζ_{12} combinations listed in Table 5.4 for AR = 1.5.

No. of Ply	Combination								
	1	2	3	4	5	6	7	8	9
12	4.99	4.87	4.87	4.85	4.99	4.85	4.99	4.83	4.83
16	5.04	4.90	4.90	4.90	5.03	4.90	5.03	4.88	4.88
20	4.84	4.70	4.70	4.70	4.84	4.70	4.84	4.69	4.69
24	5.19	5.05	5.05	5.04	5.18	5.04	5.18	5.02	5.02

TABLE 5.7: Buckling factors of standard quads and DD designs under the ζ_{11} and ζ_{12} combinations listed in Table 5.4 for AR = 2.0.

No. of Ply	Combination								
	1	2	3	4	5	6	7	8	9
12	4.84	4.73	4.73	4.70	4.83	4.70	4.83	4.66	4.66
16	4.87	4.77	4.77	4.74	4.87	4.74	4.87	4.70	4.70
20	4.71	4.60	4.60	4.57	4.70	4.57	4.70	4.53	4.53
24	4.94	4.83	4.83	4.80	4.95	4.80	4.95	4.76	4.76

The introduction of B - T coupling leads to a very small decrease in buckling performance, with at worst, almost 4% reduction. The buckling performance of laminate designs with only ξ_{12} is about 0.1% lower than the fully uncoupled case, this indicate that ξ_{12} has a bigger effect on buckling performance than ξ_{11} . As the design spaces expand with the introduction of coupling behaviour, more designs are available to be explored. More flexible structures can potentially be manufactured with coupling properties and non-symmetric stacking sequence instead of standard Quads laminates without degrading the buckling performance.

5.3 STIFFNESS MATCHING

The purpose of this section is to examine the buckling and first-ply failure performance of DD laminates with *Bending-Twist* coupling when using a stiffness matching technique. Laminate designs from 3 datasets are used, the first dataset is the same set of uncoupled data provided in York [96]. The second and third datasets are extensions of the first dataset. The second dataset was derived in the same fashion as the first dataset but contains only 24 ply laminates, while the third dataset is derived in the same fashion as the uncoupled dataset while relaxing the constraint for the Bending-Twist coupling, the latter dataset includes 12, 16, 20 and 24 plies designs. The reason for developing the new datasets (2 & 3) is that there were relatively few uncoupled solutions in the first dataset, where B-T coupling is present in virtually all symmetric designs, which is tolerated because of manufacturing simplicity, despite the knock-down in buckling load discussed in previous chapters. Standard designs are fully uncoupled ($A_S B_0 D_S$), meaning that the A_{16} , A_{26} terms of the $[A]$ matrix, all the elements in $[B]$ and D_{16} and D_{26} are all zero. In contrast, the DD designs are all B - T coupled ($A_S B_0 D_F$).

In this section, DD laminates are designed with improved FPF strength without degrading their buckling performance compared to standard quad laminates. A two-level design process is used; the first level investigates the FPF strength of B - T coupled DD laminate designs in the database, for the 4 different laminate thicknesses. Firstly, the fully coupled laminate designs with standard orientations (listed in Table 5.2) are used as a target for subsequent comparisons. The DD designs of each number of ply are divided into different groups in terms of ply percentages, for example, the 12-ply designs are grouped into $[\pm\psi/\pm\phi] = [4/8]$ and $[8/4]$, where all the designs in each group give the same extensional stiffness for any given pair of angles. Each

group has designs that produce the same bending stiffness lamination parameters ξ_9 and ξ_{10} for a given value of $\pm\psi$ and $\pm\phi$, but the values of ξ_{11} and ξ_{12} differs between each design. A stiffness matching technique is applied, which the tailoring was discussed in Chapter 4. The bending stiffness ξ_9 and ξ_{10} of the DD designs are matched to the standard quad design of the same ply number. Each ply percentage group has the same values of $\pm\psi$ and $\pm\phi$ that produce the target bending stiffness, and the group that gives the highest FPF strength is found. The fully uncoupled designs with bending stiffness lamination parameters (ξ_9, ξ_{10}) closest to $(0, -1)$ are selected because the point $(0, -1)$ has the highest compressive buckling load and close to the highest shear buckling load, as was shown in Chapter 3.

Next, the second level attempts to design laminates with the highest buckling load, here the group that gives the highest FPF strength for each laminate thickness is used. The buckling load of each design in the group is found using FEA to determine which has the highest buckling load.

The database contains *B-T* coupled laminate designs ranging from 12, 16, 20 and 24 plies, the number of designs for each laminate thickness is shown in Table 5.8. Although there are over 15,000 designs in total, there are only 14 different extensional stiffnesses (ξ_{1-4}) , where all designs have zero $\xi_{3,4}$, while the bending stiffnesses (ξ_{9-12}) differ for each design. This means that for a given bending stiffness, there are only 14 different $[A]$ matrices throughout.

TABLE 5.8: Number of DD laminate designs that match the design constraints for each laminate thickness.

Number of plies	24	20	16	12
Number of designs	14,134	1,430	146	18

The buckling performance of the designs is predicted using Abaqus, while the FPF is assessed using the Tsai-Wu failure criterion, which is given by Eqn. 1.27 in Chapter 1.2.7. The buckling and FPF strengths of the fully uncoupled designs with standard quad orientations are listed in Table 5.9. These values are used to compare against the *B-T* coupled DD designs (with matched stiffnesses).

TABLE 5.9: Buckling and first ply failure performances of the fully uncoupled laminate designs with standard configurations listed in Table 5.2.

Ply number	AR	Buckling load (N)	First ply failure load (FPF), N_x (N)
24	1	38927	229,951
	1.5	40,940	
	2	39,005	
20	1	21467	208,577
	1.5	22,123	
	2	21,494	
16	1	11,384	134,573
	1.5	11,786	
	2	11,394	
12	1	4,770	114,925
	1.5	4,924	
	2	4,772	

5.3.1 FIRST PLY FAILURE OF DD LAMINATES WITH BENDING-TWISTING COUPLING

The values of ψ and ϕ of double angle-ply laminate designs that can produce matched bending stiffness lamination parameters, ξ_9 and ξ_{10} , to the standard laminates are calculated, where the approach was introduced in Chapter 4. Although the number of designs available is large, the number of designs that give the matching target lamination parameters $\xi_{9,10}$ is significantly reduced since not every configuration can produce the same lamination parameters.

24-PLY

The 24 plies DD designs are divided into 5 different sub-groups, according to the number of plies for ψ and ϕ respectively, which are: $[\psi/\phi] = [4/20], [8/16], [12/12], [16/8]$ and $[20/4]$. There are in total 14,134 designs that fit the stacking sequence constraints (10% rule and contiguity = 3), but the number of designs that contain a combination of $\pm\psi$ and $\pm\phi$ that matches the target bending stiffness values of $(\xi_9, \xi_{10}) = (-0.045, -0.967)$ is greatly reduced. All the designs are normalised

against the FPF value of the standard quad benchmark. The FPF strengths are normalised against their quad counterparts of the same thickness. DD designs from the same sub-groups within the same thickness group, have identical FPF strength. One design from each sub-groups with the lowest normalised FPF strength from each ply percentage group is shown in Table 5.10, while the full list of all the sub-groups that give a different FPF value can be found in Appendix A5. The first column shows the number of plies for $\pm\psi$ and $\pm\phi$ within the 24-ply laminate and the subscript represent the design number. The first column shows the number of plies for $\pm\psi$ and $\pm\phi$ within the 24-ply laminate and the subscript represents the design number. The second column shows the stacking sequences of the designs, and the third column shows the ψ and ϕ angle that gives the matching bending stiffness to the fully uncoupled design with the same number of plies. The final column shows the FPF performances in comparison to their bending stiffness matched Quad design. A more detailed list showing one design from each sub-group can be found in A5.

TABLE 5.10: 24-ply designs, stacking sequences and ψ_{\pm} , ϕ_{\pm} values that produce bending stiffness that matches $(\xi_9, \xi_{10}) = (-0.045, -0.967)$.

Design	Stacking sequence	$(\pm\psi, \pm\phi)$	Normalised FPF strength
Quad	$[-/+/-/-/+/-/+/-/+/\bullet/\circ/\circ/\bullet/\bullet/\circ/\circ/\bullet/+/-/-/+/-/+/-/+/-]_{\text{T}}$	-	1
$[4/20]_1$	$[\psi/-\psi/-\phi/\phi/-\phi/\phi/-\phi/\phi/-\phi/\phi/-\phi/\phi/\phi/-\phi/\phi/-\phi/\phi/-\phi/\phi/-\psi/\psi]_{\text{T}}$	$(\pm 51.7^\circ, \pm 40.5^\circ)$	2.292
$[8/16]_{10}$	$[\psi/-\psi/-\psi/\psi/-\phi/\phi/-\phi/\phi/-\phi/\phi/-\phi/\phi/\phi/-\phi/\phi/-\phi/\phi/-\psi/\psi/\psi/-\psi]_{\text{T}}$	$(\pm 48.8^\circ, \pm 36.6^\circ)$	1.658
$[12/12]_{17}$	$[\psi/-\psi/-\psi/\psi/-\psi/\psi/-\phi/\phi/-\phi/\phi/-\phi/\phi/\phi/-\phi/\phi/-\phi/\phi/-\psi/\psi/\psi/-\psi/\psi/-\psi]_{\text{T}}$	$(\pm 47.3^\circ, \pm 29.9^\circ)$	1.014
$[16/8]_{15}$	$[\psi/-\psi/\psi/-\psi/\psi/-\psi/\psi/-\psi/\phi/-\phi/\phi/-\phi/-\phi/\phi/-\phi/\phi/-\psi/\psi/-\psi/\psi/-\psi/\psi]_{\text{T}}$	$(\pm 46.3^\circ, \pm 6.58^\circ)$	0.456
$[20/4]_3$	$[\psi/-\psi/-\psi/\psi/-\psi/\psi/-\phi/\phi/-\psi/\psi/-\psi/\psi/-\psi/\psi/\psi/-\psi/\phi/-\phi/\psi/-\psi/\psi/-\psi/\psi/-\psi]_{\text{T}}$	$(\pm 46.9^\circ, \pm 26.1^\circ)$	1.749

The FPF strength of the designs is normalised against the quad design, with the quad design

being 1. Designs with a FPF strength value larger than 1 indicates that the design has a lower FPF load than the standard design and a lower value means the design has a better FPF performance. Although most designs show higher first ply failure value when compare with the standard quad design, design $[16/8]_{15}$ has a normalised FPF strength of 0.456. This means that the design is at around 45% of its failure strength when the failure load of the quad design (766.5N) is applied. This shows that some DD laminates offer the potential for improvement in FPF strength, without any decrease in buckling performance. The 2-D extensional stiffness and 4-D design spaces of design $[16/8]_{15}$ are plotted and shown in Fig. 5.2 (where the laminate parameters ξ_{9-12} represent the 4 different dimensions of the design space). Figures 5.2a, 5.2b and 5.2d in Fig. 5.2 shows the usual 3-D design space that was shown in chapter 3 and 4, and the other 3 sub-figures show the relationships between the 3 bending stiffness and the additional ξ_{12} .

A 4-D design space offers an extra dimension of potential feasible designs to be explored, which can potentially be used for optimisation with buckling factors superimposed on the design space like the ones shown in Chapters 3 and 4. However, relationships between each 2 of the 4 stiffnesses cannot be described with simple formulations like the ones in Table 1, so overall general design space (which 2-D and 3-D design spaces were drawn in previous chapters) was not able to draw.

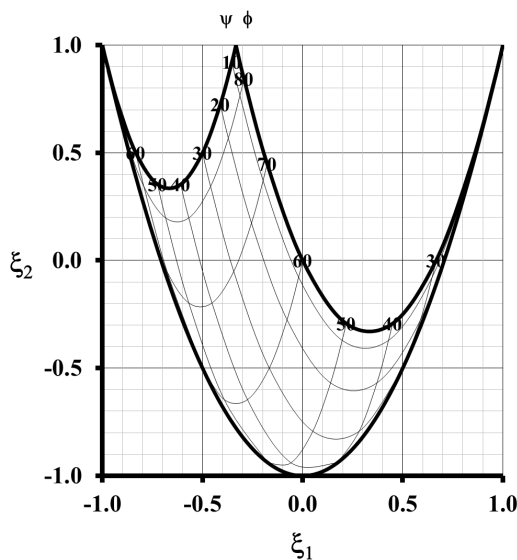


FIGURE 5.1: Illustration of the 2-D extensional stiffness design space of 24-ply design sub-group $[16/8]_{15}$.

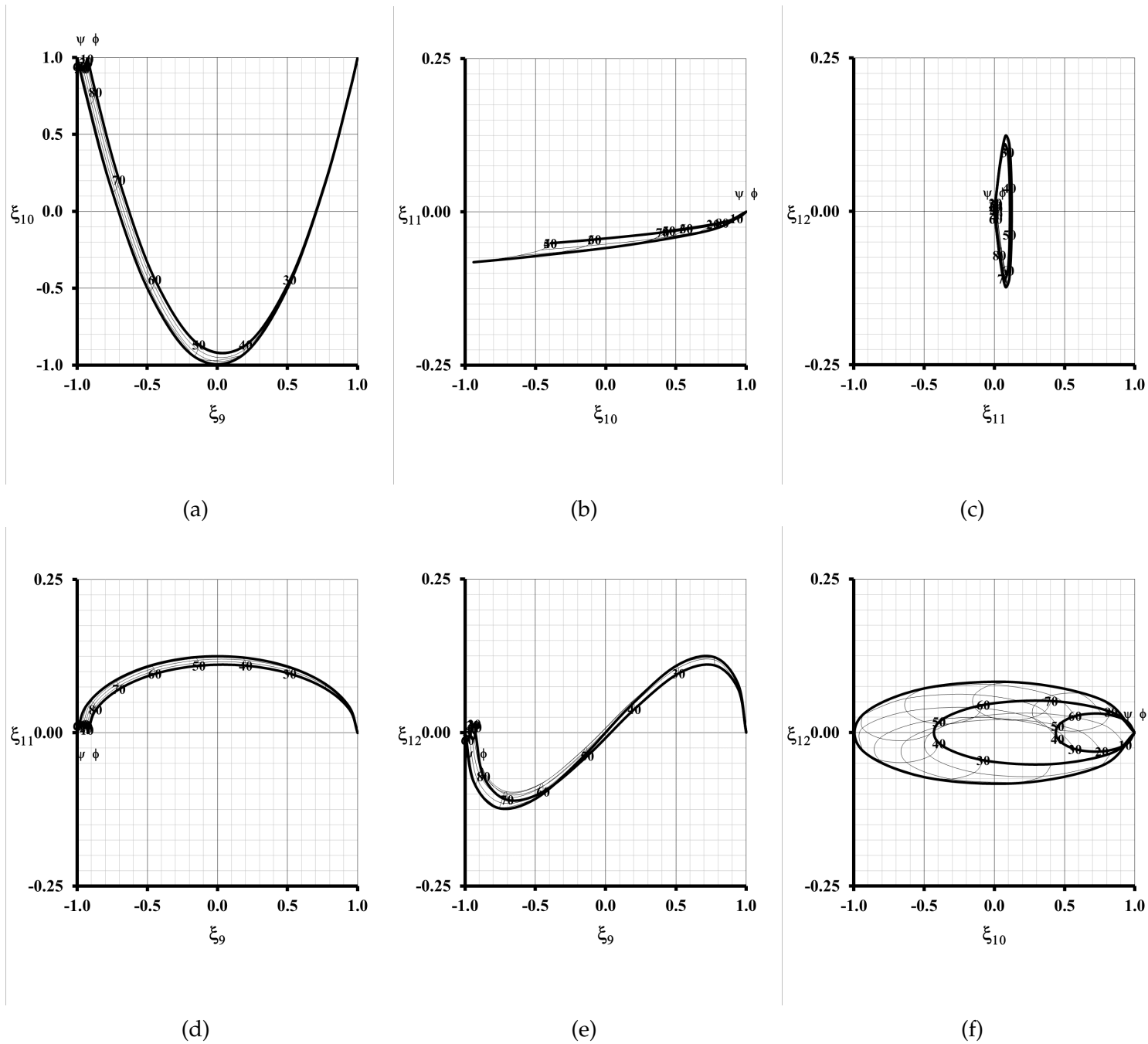


FIGURE 5.2: Illustration of the 4-D bending stiffness design space of 24-ply design sub-group $[16/8]_{15}$.

20-PLY

The 20 plies DD laminate designs are divided into 4 different groups, according to the number of ψ and ϕ plies respectively. These include: $[\psi/\phi] = [4/16], [8/12], [12/8]$ and $[16/4]$. There are in total 1,430 designs that fit the stacking sequence constraints (10% rule and contiguity = 3), only 17 designs with combinations of $\pm\psi$ and $\pm\phi$ are found that match the target bending stiffness values of $(\xi_9, \xi_{10}) = (-0.102, -0.692)$. Again, the design with the lowest normalised FPF strength from each sub-group for each ply percentage group of the 20 plies DD laminate designs are shown in Table 5.11, together with the normalised FPF value. A more detailed list showing one design from each sub-group can be found in A6.

TABLE 5.11: 20-ply designs, stacking sequences and ψ_{\pm}, ϕ_{\pm} values that produce bending stiffness that matches $(\xi_9, \xi_{10}) = (-0.102, -0.692)$.

Design	Stacking sequence	$(\pm\psi, \pm\phi)$	Normalised FPF strength
Quad	$[+/-/-/\bullet/+/+/-/\circ/\circ/\bullet/\bullet/\circ/\circ/-/+ +/+/\bullet/-/-/+]_{\Gamma}$	-	1
$[4/16]_1$	$[\psi/-\psi/-\phi/\phi/-\phi/\phi/-\phi/\phi/-\phi/\phi/\phi/-\phi/\phi/-\phi/\phi/-\psi/\psi]_{\Gamma}$	$(\pm 59.7^{\circ}, \pm 37.2^{\circ})$	1.690
$[8/12]_6$	$[\psi/-\psi/\psi/-\psi/\phi/-\phi/\phi/-\phi/\phi/-\phi/-\phi/\phi/-\phi/\phi/-\psi/\psi/-\psi/\psi]_{\Gamma}$	$(\pm 53.8^{\circ}, \pm 25.8^{\circ})$	0.743
$[12/8]_8$	$[\psi/-\psi/-\psi/\psi/-\phi/\phi/-\psi/\psi/-\phi/\phi/\phi/-\phi/-\psi/\psi/\phi/-\phi/\psi/-\psi/\psi/-\psi]_{\Gamma}$	$(\pm 52.8^{\circ}, \pm 20.0^{\circ})$	0.806
$[16/4]_2$	$[\psi/-\psi/-\psi/\psi/-\phi/\phi/-\psi/\psi/-\psi/\psi/-\psi/\psi/\psi/-\psi/\phi/-\phi/\psi/-\psi/\psi/-\psi]_{\Gamma}$	$(\pm 52.6^{\circ}, \pm 18.8^{\circ})$	1.331

Table 5.11 shows that for the 20-ply designs, there are 2 sub-groups with improved FPF performance, namely $[8/12]_6$ and $[12/8]_8$, with normalised FPF values of 0.743 and 0.806. The 2-D and 4-D extensional and bending stiffness design spaces of both designs $[12/8]_8$ and $[8/12]_6$ are shown in Figs. 5.3, 5.4, 5.5 and 5.6.

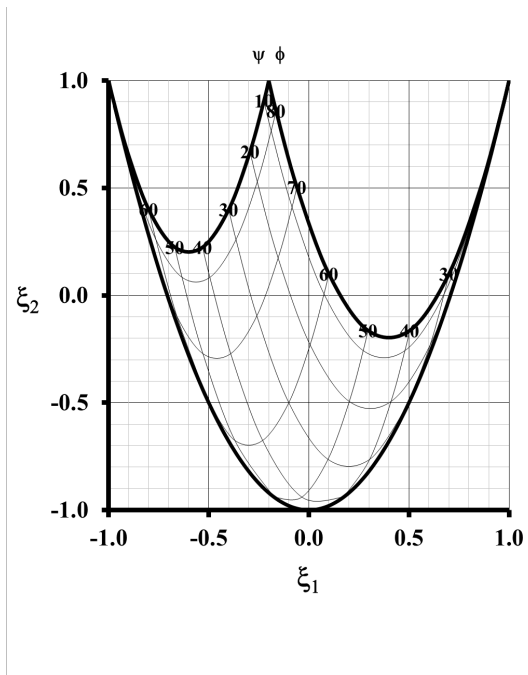


FIGURE 5.3: Illustration of the 2-D extensional stiffness design space of 20-ply design sub-group $[12/8]_{13}$.

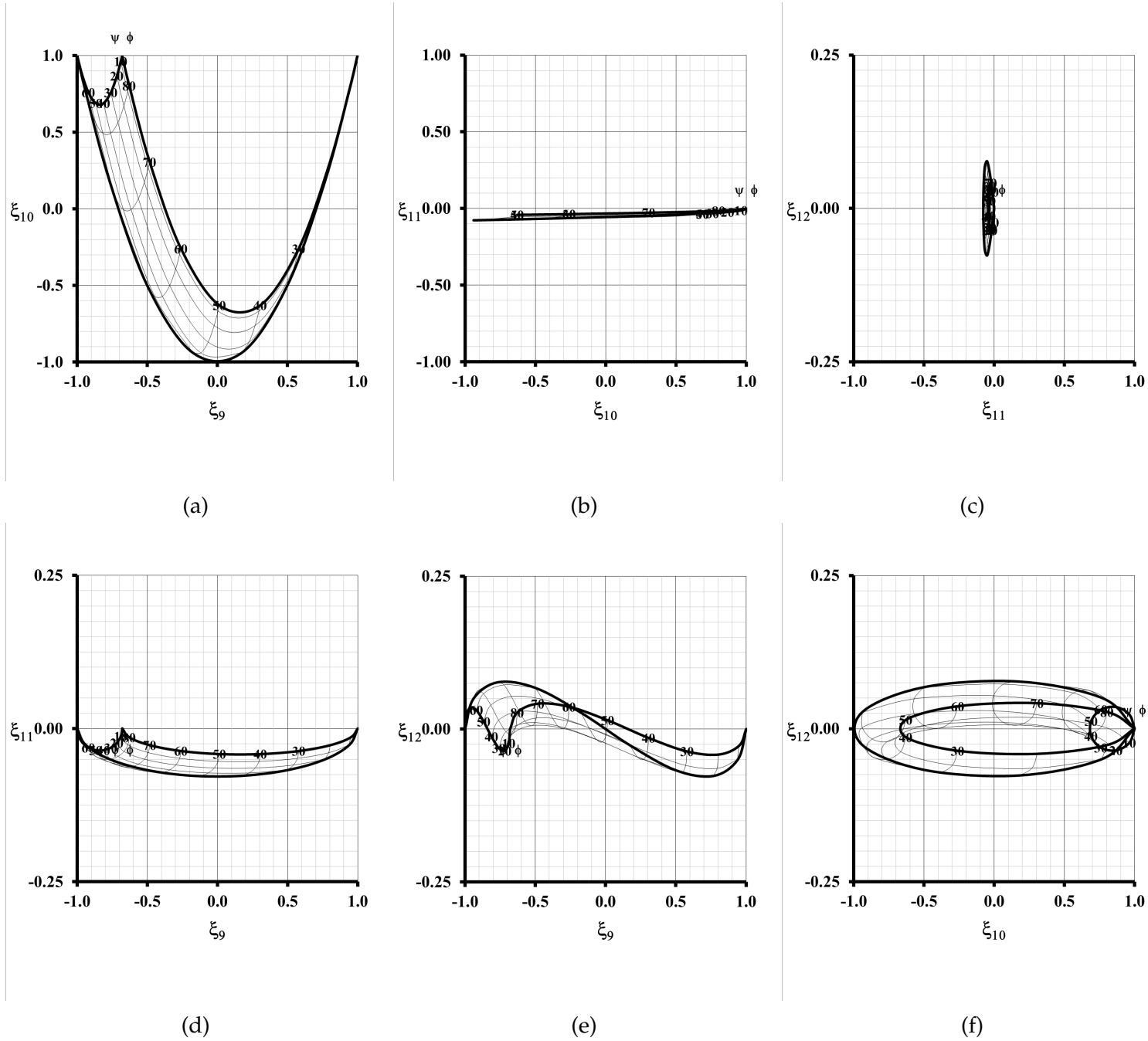


FIGURE 5.4: Illustration of the 4-D bending stiffness design space of the 20-ply design sub-group $[12-8]_6$.

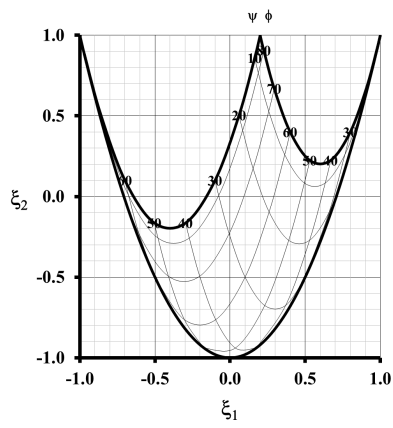
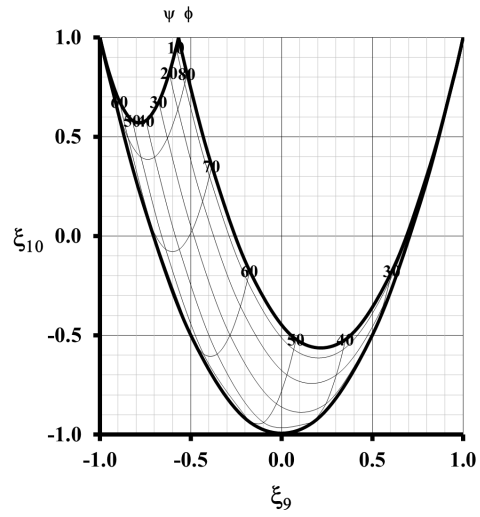
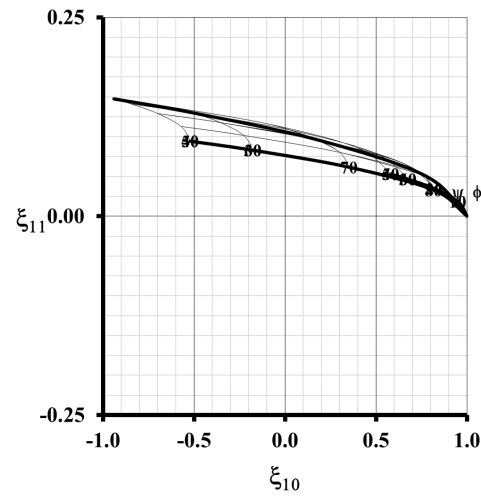


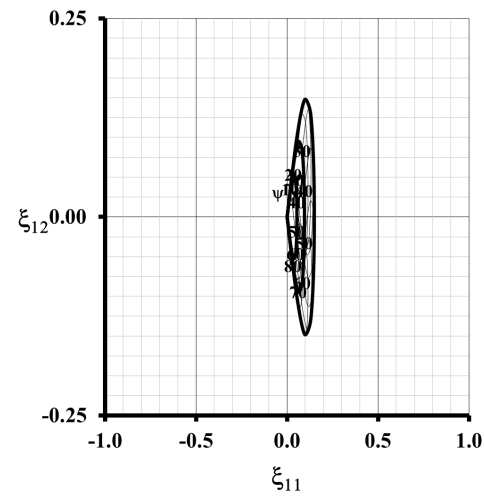
FIGURE 5.5: Illustration of the 2-D extensional stiffness design space of 20-ply design sub-group $[8/12]_6$.



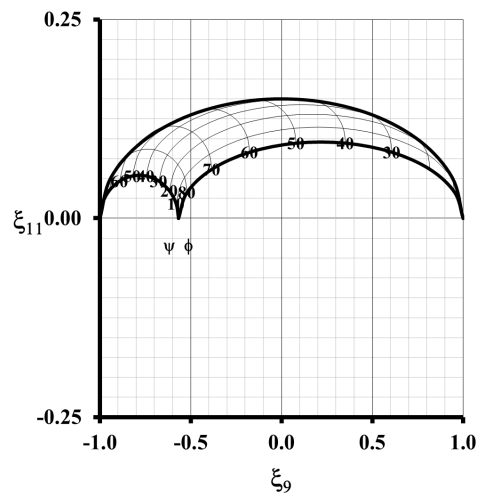
(a)



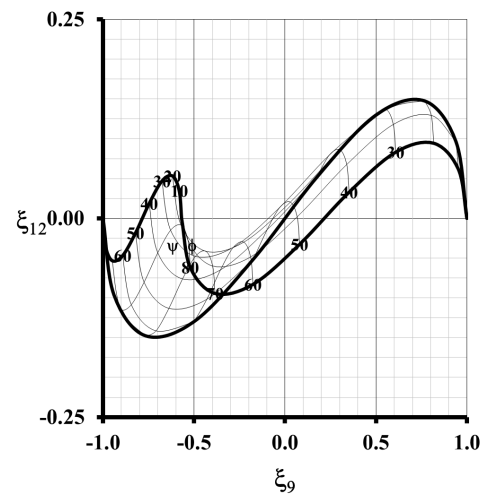
(b)



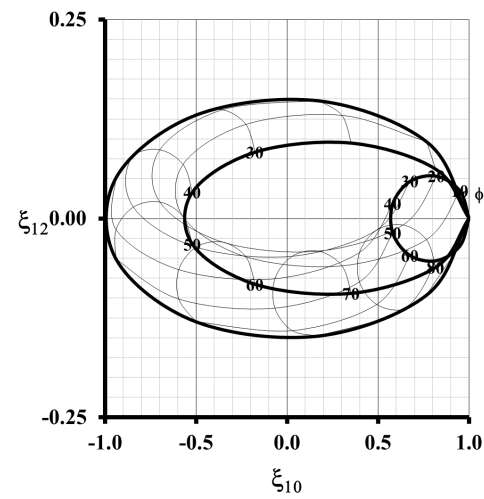
(c)



(d)



(e)



(f)

FIGURE 5.6: Illustration of the 4-D bending stiffness design space of the 20-ply design sub-group $[8-12]_6$.

16-PLY

The 16-ply DD laminates are divided into 4 different groups, according to the number of ψ and ϕ respectively, which are: $[\psi/\phi] = [4/12]$, $[8/8]$ and $[12/4]$. There are in total 146 designs that fit the stacking sequence constraints (10% rule and contiguity = 3). All the 16-ply sub-groups of B - T coupled DD laminates that match the target bending stiffness of $(\xi_9, \xi_{10}) = (-0.070, -0.852)$ with different first ply failure strengths are shown in Table 5.12. In this case, just one sub-group with improved FPF performance is found, i.e. $[8/8]_4$ with a normalised FPF value of 0.589. The extensional and bending design spaces of design $[8/8]_4$ is plotted and shown in Figs. 5.7 and 5.8.

TABLE 5.12: 16-ply designs, stacking sequences and ψ_{\pm} , ϕ_{\pm} values that produce bending stiffness that matches $(\xi_9, \xi_{10}) = (-0.070, -0.852)$.

Design	Stacking sequence	$(\pm\psi, \pm\phi)$	Normalised FPF strength
Quad	$[+/-/-/+/\bullet/-/+/\circ/\circ/+/-/\bullet/+/-/-/+]\Gamma$	-	1
$[4/12]_1$	$[\psi/-\psi/-\phi/\phi/-\phi/\phi/-\phi/\phi/\phi/-\phi/\phi/-\phi/\phi/-\phi/\psi/-\psi]\Gamma$	$(\pm 53.6^\circ, \pm 38.1^\circ)$	1.426
$[8/8]_1$	$[\psi/-\psi/-\phi/\phi/-\phi/\phi/-\psi/\psi/\phi/-\phi/-\psi/\psi/\psi/-\psi/\phi/-\phi]\Gamma$	$(\pm 54.7^\circ, \pm 39.4^\circ)$	1.717
$[8/8]_2$	$[\psi/-\psi/-\phi/\phi/-\phi/\phi/-\psi/\psi/-\psi/\psi/\phi/-\phi/\phi/-\phi/\psi/-\psi]\Gamma$	$(\pm 53.4^\circ, \pm 37.8^\circ)$	1.675
$[8/8]_3$	$[\psi/-\psi/-\phi/\phi/-\psi/\psi/-\phi/\phi/\phi/-\phi/-\psi/\psi/\phi/-\phi/\psi/-\psi]\Gamma$	$(\pm 52.2^\circ, \pm 35.7^\circ)$	1.391
$[8/8]_4$	$[\psi/-\psi/\psi/-\psi/\phi/-\phi/\phi/-\phi/-\phi/\phi/-\phi/\phi/-\psi/\psi/-\psi/\psi]\Gamma$	$(\pm 49.9^\circ, \pm 25.6^\circ)$	0.589
$[12/4]_1$	$[\psi/-\psi/-\phi/\phi/-\psi/\psi/-\psi/\psi/-\psi/\psi/\psi/-\psi/\phi/-\phi/\psi/-\psi]\Gamma$	$(\pm 52.0^\circ, \pm 35.2^\circ)$	2.042
$[12/4]_2$	$[\psi/-\psi/-\psi/\psi/-\phi/\phi/-\psi/\psi/-\psi/\psi/\phi/-\phi/\psi/-\psi/\psi/-\psi]\Gamma$	$(\pm 49.7^\circ, \pm 23.6^\circ)$	1.004

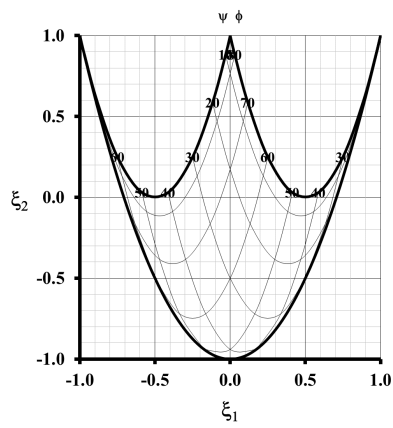
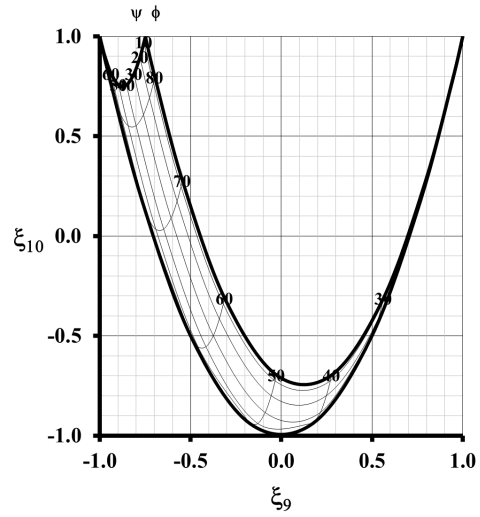
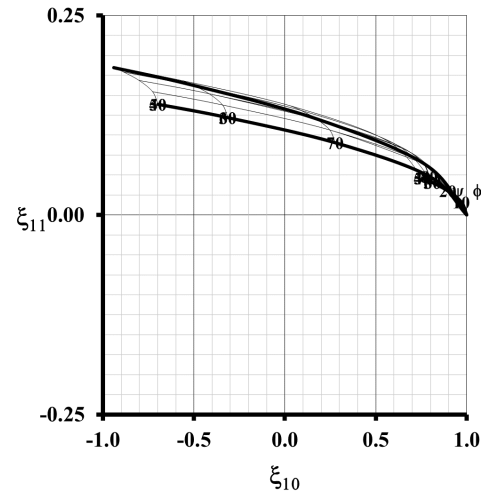


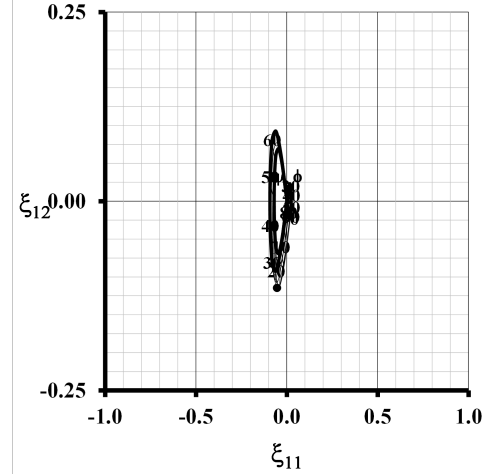
FIGURE 5.7: Illustration of the 2-D extensional stiffness design space of 16-ply design sub-group $[8/8]_4$.



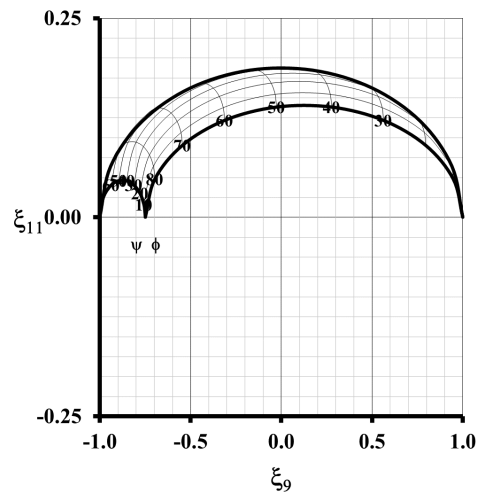
(a)



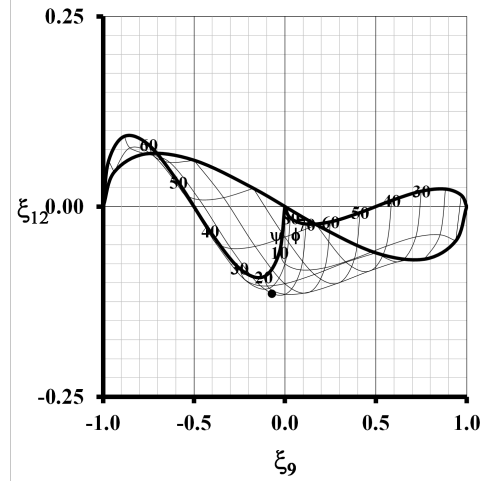
(b)



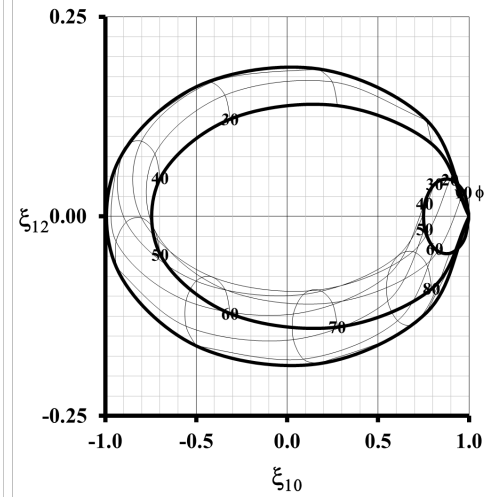
(c)



(d)



(e)



(f)

FIGURE 5.8: Illustration of the 4-D bending stiffness design space of the 16-ply design sub-group $[8-8]_4$.

12-PLY LAMINATE DESIGNS

The 12 plies DD laminates are divided into 2 different groups according to the number of ψ and ϕ , namely $[\psi/\phi] = [4/8]$, and $[8/4]$. There are in total 18 designs that fit the stacking sequence constraints (10% rule and contiguity = 3). All the 12-ply sub-groups of B-T coupled DD laminates that match the target bending stiffness of $(\zeta_9, \zeta_{10}) = (-0.083, -0.815)$ with different FPF strengths are shown in Table 5.13. However, there are no design with improved FPF performances are found. The extensional and bending stiffness design spaces of design $[4/8]_1$ are plotted and shown in Figs. 5.9 and 5.10.

TABLE 5.13: 12-ply designs, stacking sequences and ψ_{\pm}, ϕ_{\pm} values that produce bending stiffness that matches $(\zeta_9, \zeta_{10}) = (-0.083, -0.815)$.

Design	Stacking sequence	$(\pm\psi, \pm\phi)$	Normalised FPF strength
Quad	$[+/-/-/\bullet/+/\circ/\circ/+/\bullet/-/-/+]_T$	-	1
$[4/8]_1$	$[\psi/-\psi/-\phi/\phi/-\phi/\phi/\phi/-\phi/\phi/-\psi/\psi]_T$	$(\pm 52.9^\circ, \pm 34.2^\circ)$	1.255
$[8/4]_1$	$[\psi/-\psi/-\phi/\phi/-\psi/\psi/-\psi/\psi/\phi/-\phi/\psi/-\psi]_T$	$(\pm 52.4^\circ, \pm 32.9^\circ)$	1.823

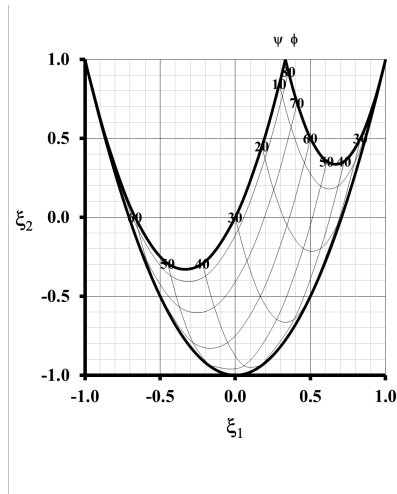
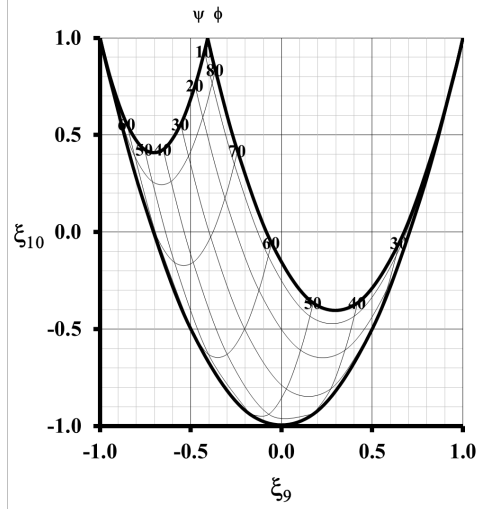
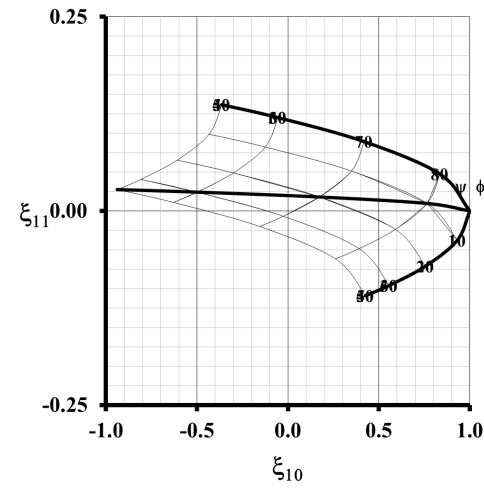


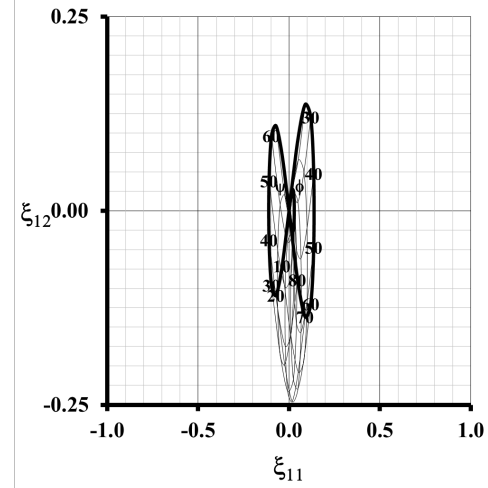
FIGURE 5.9: Illustration of the 2-D extensional stiffness design space of 12-ply design sub-group $[4/8]_1$.



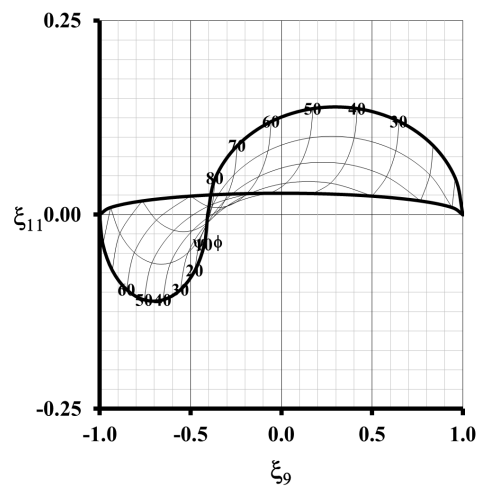
(a)



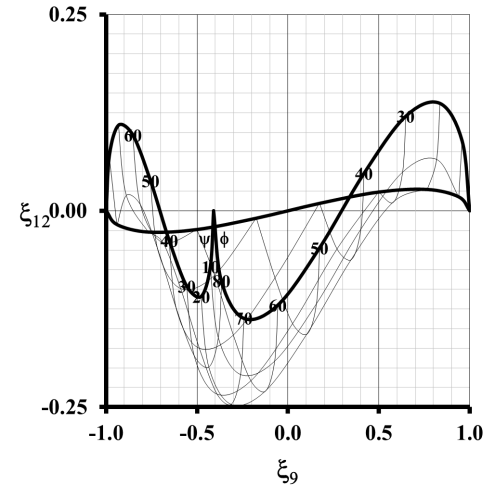
(b)



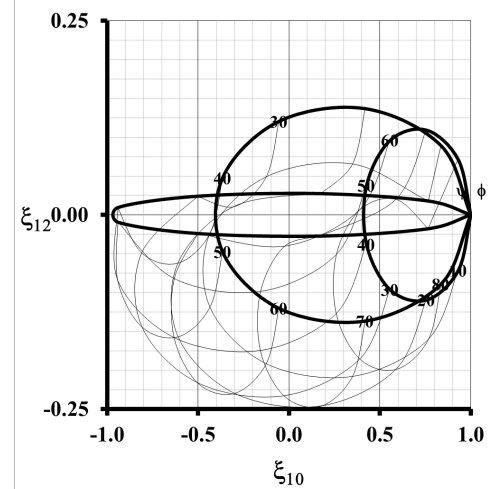
(c)



(d)



(e)



(f)

FIGURE 5.10: Illustration of the 4-D bending stiffness design space of the 12-ply design sub-group $[4-8]_1$.

5.4 COMPRESSION BUCKLING

Section 5.3 of this chapter investigated the FPF performance of the B-T coupled designs, and sub-groups with improved FPF for each laminate thickness were found. This section explores the buckling performance of the designs. Buckling analysis is performed on the sub-groups that showed improvements in FPF using FEA. From Section 5.3, improvements in FPF were found for 16, 20 and 24 plies *B-T* coupled designs, therefore FEA is conducted on the designs from the sub-groups that show improvements for these 3 laminate thicknesses. The sub-groups are $[16/8]_{15}$ from 24-ply, $[8/12]_6$ and $[12/8]_8$ from 16-ply laminates, the number of designs in these sub-groups is listed below:

TABLE 5.14: Number of individual designs from sub-groups of 24, 20 and 16 plies laminate with improved FPF strength.

Sub-Group	$[16/8]_{16}$	$[12/8]_6$	$[8/12]_8$	$[8/8]_4$
Number of design	202	60	60	16

As this is a preliminary study on the database, a selection of random designs are picked from each sub-groups, and buckling simulations are performed. The stacking sequence of designs that are selected from each sub-group is listed in Table 5.15 to 5.16. All the designs from the same sub-group have identical extensional stiffness $\tilde{\zeta}_{1-4}$ and bending stiffness $\tilde{\zeta}_9$ and $\tilde{\zeta}_{10}$, the difference is in the bending stiffness terms associated with *B-T* coupling, where the notations 1 = ψ , 2 = $-\psi$, 3 = ϕ and 4 = ϕ .

TABLE 5.15: List of stacking sequences of 10 designs from 24-ply B - T coupled DD laminate design sub-group $[16/8]_{15}$. All designs possess identical extensional stiffness $(\zeta_1, \zeta_2, \zeta_3, \zeta_4) = (0.295, -0.365, 0, 0)$ and bending stiffness $(\zeta_9, \zeta_{10}) = (-0.007, -0.926)$.

Design	Stacking Sequence	(ζ_{11}, ζ_{12})
$[16/8]_{5a}$	$[\psi/-\psi/-\psi/\psi/-\psi/\psi/-\psi/\psi/-\phi/\phi/-\phi/\phi/\phi/-\phi/\phi/-\phi/-\psi/\psi/\psi/-\psi/\psi/-\psi/\psi/-\psi]_{\Gamma}$	$(-0.059, -0.001)$
$[16/8]_{5b}$	$[\psi/-\psi/-\psi/\psi/-\psi/\psi/-\psi/\psi/-\phi/\phi/\phi/-\phi/\phi/-\phi/-\phi/\phi/\psi/-\psi/\psi/-\psi/\psi/-\psi/-\psi/\psi]_{\Gamma}$	$(-0.035, 0.003)$
$[16/8]_{5c}$	$[\psi/-\psi/-\psi/\psi/\psi/-\psi/-\psi/\psi/\phi/-\phi/\phi/-\phi/-\phi/\phi/-\phi/\phi/-\psi/\psi/-\psi/\psi/\psi/-\psi/\psi/-\psi]_{\Gamma}$	$(-0.004, 0.007)$
$[16/8]_{5d}$	$[\psi/-\psi/-\psi/\psi/\psi/-\psi/-\psi/\psi/-\phi/\phi/-\phi/\phi/\phi/-\phi/\phi/-\phi/-\psi/\psi/\psi/-\psi/\psi/-\psi/-\psi/\psi]_{\Gamma}$	$(0.004, -0.007)$
$[16/8]_{5e}$	$[\psi/-\psi/-\psi/\psi/\psi/-\psi/-\psi/\psi/\phi/-\phi/\phi/-\phi/-\phi/\phi/-\phi/\phi/-\psi/\psi/\psi/-\psi/\psi/-\psi/-\psi/\psi]_{\Gamma}$	$(0.010, 0.006)$
$[16/8]_{5f}$	$[\psi/-\psi/-\psi/\psi/\psi/-\psi/-\psi/\psi/\phi/-\phi/-\phi/\phi/\phi/-\phi/-\phi/\phi/\psi/-\psi/-\psi/\psi/\psi/-\psi/-\psi/\psi]_{\Gamma}$	$(0.015, 0.002)$
$[16/8]_{5g}$	$[\psi/-\psi/\psi/-\psi/-\psi/\psi/-\psi/\psi/-\phi/\phi/\phi/-\phi/\phi/-\phi/-\phi/\phi/\psi/-\psi/\psi/-\psi/-\psi/\psi/-\psi/\psi]_{\Gamma}$	$(0.028, -0.002)$
$[16/8]_{5h}$	$[\psi/-\psi/\psi/-\psi/-\psi/\psi/\psi/-\psi/\phi/-\phi/\phi/-\phi/-\phi/\phi/-\phi/\phi/-\psi/\psi/-\psi/\psi/-\psi/\psi/\psi/-\psi]_{\Gamma}$	$(0.052, 0.002)$
$[16/8]_{5i}$	$[\psi/-\psi/\psi/-\psi/\psi/-\psi/-\psi/\psi/-\phi/\phi/-\phi/\phi/\phi/-\phi/\phi/-\phi/-\psi/\psi/-\psi/\psi/\psi/-\psi/-\psi/\psi]_{\Gamma}$	$(0.059, -0.012)$
$[16/8]_{5j}$	$[\psi/-\psi/\psi/-\psi/\psi/-\psi/\psi/-\psi/\phi/-\phi/\phi/-\phi/-\phi/\phi/-\phi/\phi/-\psi/\psi/-\psi/\psi/-\psi/\psi/-\psi/\psi]_{\Gamma}$	$(0.114, -0.004)$

TABLE 5.16: List of stacking sequences of 10 designs from 20-ply B - T coupled DD laminate design sub-group $[8/12]_6$. All designs possess identical extensional stiffness $(\zeta_1, \zeta_2, \zeta_3, \zeta_4) = (0.252, -0.466, 0, 0)$ and bending stiffness $(\zeta_9, \zeta_{10}) = (-0.102, -0.692)$.

Design	Stacking Sequence	(ζ_{11}, ζ_{12})
$[8/12]_{6a}$	$[\psi/-\psi/-\psi/\psi/-\phi/\phi/\phi/-\phi/-\phi/\phi/\phi/-\phi/-\phi/\phi/\phi/-\phi/-\psi/\psi/\psi/-\psi]_T$	$(-0.014, -0.018)$
$[8/12]_{6b}$	$[\psi/-\psi/-\psi/\psi/\phi/-\phi/-\phi/\phi/-\phi/\phi/\phi/-\phi/\phi/-\phi/-\phi/\phi/-\psi/\psi/\psi/-\psi]_T$	$(0.005, 0.006)$
$[8/12]_{6c}$	$[\psi/-\psi/-\psi/\psi/\phi/-\phi/\phi/-\phi/-\phi/\phi/-\phi/\phi/\phi/-\phi/-\phi/\phi/-\psi/\psi/\psi/-\psi]_T$	$(0.024, 0.029)$
$[8/12]_{6d}$	$[\psi/-\psi/-\psi/\psi/-\phi/\phi/\phi/-\phi/-\phi/\phi/-\phi/\phi/\phi/-\phi/\phi/-\phi/\psi/-\psi/-\psi/\psi]_T$	$(-0.012, -0.036)$
$[8/12]_{6e}$	$[\psi/-\psi/-\psi/\psi/\phi/-\phi/\phi/-\phi/-\phi/\phi/-\phi/\phi/-\phi/\phi/-\phi/\psi/-\psi/-\psi/\psi]_T$	$(0.007, -0.013)$
$[8/12]_{6f}$	$[\psi/-\psi/-\psi/\psi/\phi/-\phi/\phi/-\phi/-\phi/\phi/-\phi/\phi/-\phi/\phi/-\phi/\psi/-\psi/-\psi/\psi]_T$	$(0.026, 0.011)$
$[8/12]_{6g}$	$[\psi/-\psi/\psi/-\psi/-\phi/\phi/-\phi/\phi/\phi/-\phi/-\phi/\phi/\phi/-\phi/\phi/-\phi/-\psi/\psi/-\psi/\psi]_T$	$(0.059, -0.096)$
$[8/12]_{6h}$	$[\psi/-\psi/\psi/-\psi/-\phi/\phi/\phi/-\phi/-\phi/\phi/\phi/-\phi/\phi/-\phi/-\phi/\phi/-\psi/\psi/-\psi/\psi]_T$	$(0.087, -0.061)$
$[8/12]_{6i}$	$[\psi/-\psi/\psi/-\psi/-\phi/\phi/\phi/-\phi/\phi/-\phi/\phi/-\phi/-\phi/\phi/-\phi/\phi/-\psi/\psi/-\psi/\psi]_T$	$(0.106, -0.038)$
$[8/12]_{6j}$	$[\psi/-\psi/\psi/-\psi/\phi/-\phi/\phi/-\phi/\phi/-\phi/-\phi/\phi/-\phi/\phi/-\phi/\phi/-\psi/\psi/-\psi/\psi]_T$	$(0.134, -0.003)$

TABLE 5.17: List of stacking sequences of 10 designs from 20-ply B - T coupled DD laminate design sub-group $[12/8]_8$. All designs possess identical extensional stiffness $(\zeta_1, \zeta_2, \zeta_3, \zeta_4) = (0.252, -0.466, 0, 0)$ and bending stiffness $(\zeta_9, \zeta_{10}) = (-0.102, -0.692)$.

Design	Stacking Sequence	(ζ_{11}, ζ_{12})
$[12/8]_{8a}$	$[\psi/-\psi/-\psi/\psi/-\phi/\phi/-\psi/\psi/-\phi/\phi/\phi/-\phi/-\psi/\psi/\phi/-\phi/\psi/-\psi/-\psi]_T$	$(-0.064, -0.014)$
$[12/8]_{8b}$	$[\psi/-\psi/-\psi/\psi/\phi/-\phi/-\psi/\psi/\phi/-\phi/-\phi/\phi/\psi/-\psi/-\phi/\phi/-\psi/\psi/\psi/-\psi]_T$	$(0.006, 0.045)$
$[12/8]_{8c}$	$[\psi/-\psi/-\psi/\psi/\phi/-\phi/-\psi/\psi/\phi/-\phi/-\phi/\phi/\psi/-\psi/-\phi/\phi/\psi/-\psi/-\psi/\psi]_T$	$(0.017, 0.039)$
$[12/8]_{8d}$	$[\psi/-\psi/-\psi/\psi/\phi/-\phi/\psi/-\psi/\phi/-\phi/-\phi/\phi/-\psi/\psi/-\phi/\phi/-\psi/\psi/\psi/-\psi]_T$	$(0.040, 0.026)$
$[12/8]_{8e}$	$[\psi/-\psi/-\psi/\psi/\phi/-\phi/\psi/-\psi/\phi/-\phi/-\phi/\phi/-\psi/\psi/-\phi/\phi/\psi/-\psi/-\psi/\psi]_T$	$(0.052, 0.020)$
$[12/8]_{8f}$	$[\psi/-\psi/\psi/-\psi/\phi/-\phi/-\psi/\psi/\phi/-\phi/-\phi/\phi/-\psi/\psi/-\phi/\phi/-\psi/\psi/\psi/-\psi]_T$	$(0.064, 0.014)$
$[12/8]_{8g}$	$[\psi/-\psi/\psi/-\psi/\phi/-\phi/-\psi/\psi/-\phi/\phi/-\phi/\phi/-\psi/\psi/\phi/-\phi/\psi/-\psi/-\psi/\psi]_T$	$(0.052, -0.028)$
$[12/8]_{8h}$	$[\psi/-\psi/-\psi/\psi/\phi/-\phi/\psi/-\psi/\phi/-\phi/-\phi/\phi/\psi/-\psi/-\phi/\phi/-\psi/\psi/-\psi/\psi]_T$	$(0.075, 0.008)$
$[12/8]_{8i}$	$[\psi/-\psi/\psi/-\psi/\phi/-\phi/-\psi/\psi/\phi/-\phi/-\phi/\phi/\psi/-\psi/-\phi/\phi/-\psi/\psi/-\psi/\psi]_T$	$(0.098, -0.005)$
$[12/8]_{8j}$	$[\psi/-\psi/\psi/-\psi/\phi/-\phi/\psi/-\psi/\phi/-\phi/-\phi/\phi/-\psi/\psi/-\phi/\phi/-\psi/\psi/-\psi/\psi]_T$	$(0.133, -0.023)$

TABLE 5.18: List of stacking sequences of 10 designs from 16 ply *B-T* coupled DD laminate design sub-group $[4/8]_4$. All designs possess identical extensional stiffness $(\zeta_1, \zeta_2, \zeta_3, \zeta_4) = (0.228, -0.579, 0, 0)$ and bending stiffness $(\zeta_9, \zeta_{10}) = (-0.070, -0.850)$.

Design	Stacking Sequence	(ζ_{11}, ζ_{12})
$[8/8]_{4a}$	$[\psi/-\psi/-\psi/\psi/-\phi/\phi/-\phi/\phi/\phi/-\phi/\phi/-\phi/-\psi/\psi/\psi/-\psi]_T$	$(-0.037, -0.046)$
$[8/8]_{4b}$	$[\psi/-\psi/-\psi/\psi/\phi/-\phi/-\phi/\phi/\phi/-\phi/-\phi/\phi/-\psi/\psi/\psi/-\psi]_T$	$(0.018, 0.023)$
$[8/8]_{4c}$	$[\psi/-\psi/-\psi/\psi/\phi/-\phi/\phi/-\phi/-\phi/\phi/-\phi/\phi/-\psi/\psi/\psi/-\psi]_T$	$(0.037, 0.046)$
$[8/8]_{4d}$	$[\psi/-\psi/-\psi/\psi/-\phi/\phi/-\phi/\phi/\phi/-\phi/\phi/-\phi/\psi/-\psi/-\psi/\psi]_T$	$(-0.013, -0.054)$
$[8/8]_{4e}$	$[\psi/-\psi/-\psi/\psi/-\phi/\phi/\phi/-\phi/\phi/-\phi/-\phi/\phi/\psi/-\psi/-\psi/\psi]_T$	$(0.023, -0.008)$
$[8/8]_{4f}$	$[\psi/-\psi/-\psi/\psi/\phi/-\phi/-\phi/\phi/\phi/-\phi/-\phi/\phi/\psi/-\psi/-\psi/\psi]_T$	$(0.041, 0.015)$
$[8/8]_{4g}$	$[\psi/-\psi/\psi/-\psi/-\phi/\phi/-\phi/\phi/\phi/-\phi/\phi/-\phi/-\psi/\psi/-\psi/\psi]_T$	$(0.102, -0.093)$
$[8/8]_{4h}$	$[\psi/-\psi/\psi/-\psi/-\phi/\phi/\phi/-\phi/\phi/-\phi/-\phi/\phi/-\psi/\psi/-\psi/\psi]_T$	$(0.139, -0.047)$
$[8/8]_{4i}$	$[\psi/-\psi/\psi/-\psi/\phi/-\phi/-\phi/\phi/\phi/-\phi/-\phi/\phi/-\psi/\psi/-\psi/\psi]_T$	$(0.157, -0.024)$
$[8/8]_{4j}$	$[\psi/-\psi/\psi/-\psi/\phi/-\phi/\phi/-\phi/-\phi/\phi/-\phi/\phi/-\psi/\psi/-\psi/\psi]_T$	$(0.175, -0.001)$

The buckling results of the designs for aspect ratios (a/b) 1.0, 1.5 and 2.0 are listed in Table 5.19 to 5.22, with the percentage change compared to their standard quad counterparts of the same thickness.

TABLE 5.19: Buckling and first ply failure performance comparison between 24-ply standard quad and 10 designs from $[16/8]_{15}$ *Bend-Twist* coupled double angle-ply sub-group.

Design	k_x (with percentage change compared to quad)					
	$a/b = 1$		$a/b = 1.5$		$a/b = 2$	
Quad	4.933		5.188		4.943	
$[16/8]_{15a}$	4.927	-0.13%	5.180	-0.15%	4.935	-0.15%
$[16/8]_{15b}$	4.931	-0.05%	5.185	-0.06%	4.940	-0.05%
$[16/8]_{15c}$	4.933	0%	5.188	0%	4.943	0%
$[16/8]_{15d}$	4.933	0%	5.188	0%	4.943	0%
$[16/8]_{15e}$	4.933	-0.01%	5.188	-0.01%	4.943	0%
$[16/8]_{15f}$	4.933	-0.01%	5.187	-0.01%	4.943	-0.01%
$[16/8]_{15g}$	4.932	-0.03%	5.186	-0.04%	4.941	-0.04%
$[16/8]_{15h}$	4.928	-0.10%	5.182	-0.12%	4.937	-0.12%
$[16/8]_{15i}$	4.927	-0.13%	5.180	-0.16%	4.935	-0.16%
$[16/8]_{15j}$	4.909	-0.49%	5.158	-0.59%	4.914	-0.59%

TABLE 5.20: Buckling and first ply failure performance comparison between 20-ply standard quad and 10 designs from $[8/12]_6$ *Bend-Twist* coupled double angle-ply sub-group.

Design	k_x (with percentage change compared to quad)					
	$a/b = 1$		$a/b = 1.5$		$a/b = 2$	
Quad	4.701		4.844		4.707	
$[8/12]_{6a}$	4.700	-0.01%	4.844	-0.01%	4.706	-0.01%
$[8/12]_{6b}$	4.701	0%	4.844	0%	4.707	0%
$[8/12]_{6c}$	4.700	-0.03%	4.843	-0.03%	4.706	-0.02%
$[8/12]_{6d}$	4.700	-0.01%	4.844	-0.01%	4.706	-0.01%
$[8/12]_{6e}$	4.701	0%	4.844	0%	4.707	0%
$[8/12]_{6f}$	4.700	-0.03%	4.843	-0.03%	4.705	-0.03%
$[8/12]_{6g}$	4.694	-0.15%	4.835	-0.19%	4.695	-0.24%
$[8/12]_{6h}$	4.686	-0.31%	4.826	-0.38%	4.688	-0.41%
$[8/12]_{6i}$	4.680	-0.45%	4.818	-0.54%	4.681	-0.55%
$[8/12]_{6j}$	4.667	-0.73%	4.803	-0.85%	4.669	-0.81%

TABLE 5.21: Buckling and first ply failure performance comparison between 20-ply standard quad and 10 designs from $[12/8]_8$ *Bend-Twist* coupled double angle-ply sub-group.

Design	k_x (with percentage change compared to quad)					
	$a/b = 1$		$a/b = 1.5$		$a/b = 2$	
Quad	4.701		4.844		4.707	
$[12/8]_{8a}$	4.693	-0.17%	4.835	-0.19%	4.699	-0.17%
$[12/8]_{8b}$	4.701	-0.01%	4.844	-0.01%	4.707	0%
$[12/8]_{8c}$	4.700	-0.02%	4.844	-0.02%	4.706	-0.01%
$[12/8]_{8d}$	4.698	-0.07%	4.839	-0.12%	4.704	-0.06%
$[12/8]_{8e}$	4.696	-0.11%	4.838	-0.13%	4.702	-0.11%
$[12/8]_{8f}$	4.693	-0.17%	4.835	-0.19%	4.699	-0.17%
$[12/8]_{8g}$	4.696	-0.11%	4.838	-0.13%	4.700	-0.14%
$[12/8]_{8h}$	4.690	-0.23%	4.832	-0.27%	4.695	-0.25%
$[12/8]_{8i}$	4.682	-0.39%	4.822	-0.46%	4.686	-0.44%
$[12/8]_{8j}$	4.667	-0.73%	4.803	-0.85%	4.669	-0.81%

TABLE 5.22: Buckling and first ply failure performance comparison between 16-ply standard quad and 10 designs from $[8/8]_4$ *Bend-Twist* coupled double angle-ply sub-group.

Design	k_x (with percentage change compared to quad)					
	$a/b = 1$		$a/b = 1.5$		$a/b = 2$	
Quad	4.869		5.041		4.873	
$[8/8]_{4a}$	4.866	-0.06%	5.038	-0.06%	4.871	-0.05%
$[8/8]_{4b}$	4.868	-0.01%	5.040	-0.02%	4.873	-0.01%
$[8/8]_{4c}$	4.866	-0.06%	5.038	-0.06%	4.871	-0.05%
$[8/8]_{4d}$	4.868	-0.01%	5.040	-0.01%	4.873	-0.01%
$[8/8]_{4e}$	4.868	-0.02%	5.040	-0.03%	4.872	-0.02%
$[8/8]_{4f}$	4.866	-0.07%	5.037	-0.08%	4.870	-0.07%
$[8/8]_{4g}$	4.849	-0.41%	5.015	-0.52%	4.845	-0.58%
$[8/8]_{4h}$	4.833	-0.74%	4.996	-0.90%	4.828	-0.92%
$[8/8]_{4i}$	4.823	-0.95%	4.984	-1.14%	4.818	-1.13%
$[8/8]_{4j}$	4.811	-1.19%	4.970	-1.40%	4.807	-1.35%

The majority of the DD laminate designs have less than a 1% decrease in buckling load compared to the standard quad design of the same number of ply. This result shows that B-T coupled DD laminates are capable of providing FPF improvements of more than 200%, with almost no degradation in buckling load. For example, a 24-ply B-T coupled DD laminate with stacking sequence $[\psi/-\psi/-\psi/\psi/\psi/-\psi/-\psi/\psi/\phi/-\phi/\phi/-\phi/-\phi/\phi/-\phi/\phi/-\psi/\psi/-\psi/\psi/\psi/-\psi/\psi/-\psi]_T$ has a normalised FPF strength of 0.456 when the FPF compressive load of a 24-ply standard quad laminate is applied. This shows the potential of B-T coupled laminates to replace traditional quad laminates in applications where buckling performance is the main concern.

This is a preliminary view of the 4-D design space of the DD designs, the stacking sequences were chosen by stiffness matching to the standard quad designs. Fully coupled laminates are never the major focus of composite laminates and it is not well understood, as it adds another degree of complications to the design space, etc. In the future, 4-D design spaces can potentially be used as an optimisation tool like the way used in Chapters 3 and 4 to design fully coupled laminates with improved buckling and/ or FPF performances depending on the applications.

5.5 CONCLUSION

This chapter explored the effect of *Bend-Twist* coupling on the buckling and FPF performance of laminates with standard and DD ply configurations, focusing on the individual lamination parameter terms associated with B-T coupling.

The FPF performance of laminate designs that possess B-T coupling is assessed and compared with standard quad laminates. Results show the potential of DD laminates in improving FPF strength with minimal reduction in buckling load. The 4-dimensional design spaces of B-T coupled DD laminates with improved FPF were drawn.

In this preliminary study of the datasets, random designs were selected manually. Future work should focus on developing a method to analyse the designs more efficiently. Using a more efficient approach, DD designs with B-T coupled behaviour can be optimised to maximise FPF strength. As a next step, the shear buckling performance of DD, B-T coupled laminates could also be studied.

CHAPTER 6

CONCLUSION AND FUTURE WORK

This chapter presents conclusions of the work discussed in Chapters 3 - 5. Potential future work that could be conducted, following on from the work are then presented.

6.1 CONCLUSION

The overall aim of this research was to enhance the buckling and first-ply failure (FPF) performances of composite laminates that possess mechanically coupled behaviours. Traditionally, composite laminates used in industry are mainly standard quad laminates without any coupling behaviour; popular as these kinds of laminates are guaranteed to be warp-free. However, this means that typically the full potential of composite laminates is not utilised, as the design space is limited. This research therefore aimed to demonstrate that the new types of laminate have greater potential than traditional designs. A less common approach (lamination parameters), is used to design and analyse laminates with both standard and double angle-ply (DD) orientations. The potential of DD laminate designs in terms of buckling and FPF performances, more specifically their first ply failure and the effect of mechanical coupling behaviour on the performance of both standard and DD composite laminates were explored.

Chapter 1 of this work discussed the history, background knowledge and previous studies on composite laminates, including numerical and experimental work that focused on buckling and first-ply failure analysis. Lamination parameters, which can be used as an optimisation tool, were introduced, and were discussed in relation to previous research on composite laminate optimisation using lamination parameters. Unlike the traditional optimisation method that uses genetic algorithm (GA) to find the optimal ply angle for a particular stacking sequence, lamination parameters combine the usual design variables like ply angle, ply percentages, thickness etc

into a single set of design variables, allowing the optimisation problem to be linear for single part structures. New ply orientation technology, variable angle tow (VAT) laminate, was also discussed, which allows the laminate properties to be changed continuously across the laminate. Research had shown potential in buckling, but the technology also causes the thickness of the laminate to fluctuate throughout the laminate. An alternative ply orientation layout, double angle ply laminates, was introduced, in which every ply within the laminate is straight while the ply angle can be any arbitrary value. This increases the size of the design space and the potential to improve the performances compared to standard orientation laminates. The numerical models should be accurate therefore multiple approaches to calculate the ABD matrix were presented to ensure all the equations were implemented correctly. Since buckling prediction of coupled laminates must be done by FEA, the FEA model was presented in Chapter 2, demonstrating that predictions from FEA and numerical formulas were identical. As double angle-ply laminates are more complicated than standard laminates, standard quad laminates must first be understood and then built upon. Chapter 3 implemented classical laminate theory, here the ABD matrix was used to conduct buckling and first ply failure analysis. Compressive and shear buckling mode shapes were predicted and contour maps of lamination parameter designs spaces for various aspect ratio plates were drawn in terms of buckling factors, for both compression and shear buckling. Design spaces of coupled laminates were also discussed.

Chapter 4 discussed improved laminate performance relating to both in-plane properties (e.g. first ply failure) and out-of-plane properties (e.g. initial buckling) using double angle-ply laminates (with $\pm\psi$ and $\pm\phi$ ply orientations). The DD laminates were stiffness matched to standard laminate configurations. The values of ψ and ϕ required to produce specific values of extensional or bending stiffnesses. An original procedure for producing isotropic laminates in bending was employed. The design space of DD laminates was explored and compared to standard quad laminates. Bubble plots presenting the first ply failure strength of the DD designs were also presented. Off-axis orientation was then applied to these designs to maximise Extension-Shear coupling; bending isotropy is unaffected by off-axis alignment, hence buckling performance is also unchanged. Polar plots of first ply failure illustrated that DD laminate designs offer comparable strength to standard laminates when off-axis orientation is applied to maximise anisotropy or Extension-Shear coupling. It was also shown that first ply failure strength can be increased and optimised without affecting the buckling performance of both the standard and DD

designs. Preliminary compressive tests showed similar findings when compared to the numerical predictions.

The design space was expanded to 4-dimensions in Chapter 5, and the effect of bending stiffness on the buckling performance of DD laminates was explored. Double angle-ply designs were stiffness matched to standard laminates for various thickness designs. Buckling and first ply failure performance were compared between standard and DD designs, and the 4-D design space of the DD designs were plotted. Results showed that improving first-ply failure is possible with negligible reductions in buckling performance. It was demonstrated that, with the introduction of *Bend-Twist* coupling behaviour for double angle-ply designs, the reduction in buckling load was very small. Preliminary research on tapering with DD laminates with *Bend-Twist* coupling was also performed with an example.

Key conclusions of this thesis are summarised here:

- Compressive and shear buckling mode shapes were predicted and contour maps of lamination parameter designs spaces were drawn
- Polar plots of first ply failure illustrated that DD laminate designs with Extension-Shear coupling offer comparable strength to standard laminates
- First ply failure strength can be increased without affecting the buckling performance of both the standard and DD designs
- Results showed that *Bend-Twist* coupling has a small impact on the buckling performance for both standard and DD laminates
- Preliminary design showed that first-ply failure of fully coupled DD laminates can be improved with very small reductions in buckling performance

Suggestions for future follow-up work are made in the next section. These include potential research on developing a more effective approach to generating design spaces and contour maps, shear buckling performance analysis of double angle-ply laminates and tapered laminates, investigating first ply failure strength with different failure criteria and finally practical experiments to validate all the predictions made from this research.

6.2 FUTURE WORK

6.2.1 DESIGN SPACES AND CONTOUR MAPS

Previous chapters discussed design spaces and contour maps representing buckling factors. The general approach to drawing the contour plots was discussed in Chapter 3, which involves a polynomial surface equation using 15 points of a triangular zone. However, this method becomes less accurate as the design space becomes more complicated. For example, when the shape of the contour changes to non-triangular as the angle configuration changes from standard to double angle, or if the region lies close to a buckling mode-change boundary, these regions on the design space map are too complex to be well-described by a relatively simple 15 coefficients polynomial equation. Also, when the triangular region is too small, the polynomial equation is inaccurate. To cover the gaps and produce more accurate polynomial equations, the area can be split into multiple smaller regions, with multiple polynomial equations zones to reduce the uncovered area.

For standard quad laminates, the increase in complexity near the mode shape regions can be overcome by finding the polynomial equation of each mode (e.g. $m = 1$ and 2 etc) across the entire design space surface or cross section. The line of change in the buckling mode can be obtained by finding the points where the isolines for the different buckling modes intercept (for example, $m_1=m_2$). This approach can be applied to double angle-ply laminate design spaces. However, the issue with this approach is that regions close to a mode change line or parabola are difficult to be solved by this method, since there is always area that cannot be covered by the 15 points polynomial equation. Therefore, a possible future work may involve the development of a more effective approach to generating design spaces and contour maps.

Moreover, bubble plots were introduced in Chapter 4, here the size of the bubble represents the value of the first ply failure strength. Attempts were made to convert the bubble plots into contour maps like the ones in Chapter 3 (see, for example, Fig. 4.4a). However, the attempts were unsuccessful as the change in the first-ply failure values could not be described using the 15-point polynomial equation. Instead, another approach was to present the strength values in a 3-D plot, where the values are shown in terms of straight lines in the z -direction, see Fig. 4.4b. This figure is a 3-D design space plot generated with a CAD model, which was intended to present the bubble plot in an alternative way. Here the length of the lines is proportional to the strength

values. However, drawing the line using a CAD model was extremely time-consuming, and the software became unstable as the number of lines increased, which led to software crashes. A computer with better hardware performance might solve the problem of crashing, but the major problem was the method of generating the 3-D design space. Developing a more convenient way to generate design spaces and contour maps could also aid to generate a better representation of 3-D design space plotting.

As mentioned in previous chapters, lamination parameters can be used as an optimisation tool. By applying stiffness matching to a database of laminate designs, first ply failure strength of DD laminates can be improved without degradation in buckling performance when compared to standard quad laminates, which was shown in Chapter 5. One of the motivations of this project was to examine DD laminates as an alternative approach to VAT laminates to design composite laminates with potential improvements in buckling and FPF performance. It would be interesting and sensible to compare the performance of DD and VAT laminates directly, hence another potential future topic could focus on a comparison of the buckling and/or FPF performance of laminate designs optimised using the lamination parameter design approach for both DD and VAT laminates.

It would be useful to assess the knockdown for the most extreme cases for this set of designs, but this may have to be relegated to future work.

6.2.2 BOUNDARY CONDITION

This project primarily focused on simply supported laminates. However, there are many more alternative boundary conditions, such as clamped and free, that are used in industry for different applications. Future work could assess the performance of composite laminates subject to different boundary conditions.

6.2.3 SHEAR BUCKLING

This project primarily focused on compressive buckling. Chapter 3 looked into the shear buckling design spaces of 24-ply laminates with standard quad configurations. Chapter 4, 5 and ?? only considered compressive buckling due to its popularity, as it is more commonly encountered in structural designs. Shear buckling is more important for structures like web sections on an 'T

beam. Therefore, exploring the shear buckling performance of straight and tapered laminates for standard and DD orientations could be beneficial and might be considered for potential future work.

6.2.4 FIRST PLY FAILURE STRENGTH

This project considered the first ply failure strength of both standard quad and DD laminates. Various types of failure criteria were used, including independent, partially interactive and fully interactive. Chapter 4 compared the results obtained from different failure criteria, but the majority of this project uses the Tsai-Wu failure criterion as it is one of the most popular models used in industry. Another possible topic for future work could focus on the effect of using different failure criteria on DD-orientated laminates and tapered laminates, to explore the difference in their predictions. Ideally, with the help of experimental work, the failure criterion that best fits the predictions could be identified.

6.2.5 EXPERIMENTAL WORK

All the buckling and FPF analysis in this project was based on simulations produced by finite element analysis and equations mentioned in Chapter 1. During the early stages of the project, a visit to the Singapore Institution of Technology was planned to manufacture laminate for buckling and FPF testing. The buckling tests were aimed to validate and compare the results obtained from FEA and numerical calculations, with experimental results. The FPF test was intended to see which failure criterion would be closest to the test results. This would then be used for the rest of the project. However, the trip did not happen because of COVID-19.

Towards to end of the project, an attempt was made to manufacture simple composite laminates. A 12-ply woven fabric laminate was produced (see Fig. 6.1). The laminate was manufactured by manually stacking each ply, then the stacked fabric was cured in an oven. Due to the lack of time, no follow-up work was performed on the manufactured laminate.



(a)

(b)

FIGURE 6.1: (a) Top view and; (b) bottom view of the 12-ply laminate made from woven fabric.

BIBLIOGRAPHY

- [1] C. Soutis, "Carbon fiber reinforced plastics in aircraft construction," *Materials Science and Engineering A*, vol. 412, pp. 171–176, 2005.
- [2] G. Hellard, "Composites in airbus - a long story of innovations and experiences," 2008.
- [3] F. A. S. Technology(FAST), "A350xwb special edition," *Airbus technical magazine*, p. 25, 2013.
- [4] J. Hale, "Boeing 787 from ground up," *Boeing Comercial Aeromagazine*, p. 9, 2012.
- [5] L. Ilcewicz, D. Hoffman, and A. Fawcett, "Composite applications in commercial airframe structures," *Comprehensive Composite Materials*, pp. 87–119, 2000.
- [6] R. M. Jones, *Mechanics of Composite Materials*. Talyer Francis, 2nd ed., 1999.
- [7] J. L. Grenestedt, "A study on the effect of bending-twisting coupling on buckling strength," *Composite Structures*, vol. 12, pp. 271–290, 1989.
- [8] O. R. Gürdal, Z, "In-plane response of laminates wuth spatially varying fibre orientations variable stiffness concept," *AIAA Journal*, vol. 31, pp. 751–758, 1993.
- [9] B. C. Kim, K. Potter, and P. M. Weaver, "Continuous tow shearing for manufacturing variable angle tow composites," *Composites Part A*, vol. 43, pp. 1347–1356, 2012.
- [10] M. W. Hyer, *Stress analysis of fibre-reinforced composite materials*. DEStech Publications, uodated ed., 1998.
- [11] C. B. York, "Stacking sequences for extensionally isotropic, fully isotropic and quasi-homogeneous orthotropic laminates," pp. 1–40, 2008.
- [12] D. Cui, D. Li, and S. Zhou, "Solution of coupled mechanical behavior of bending-twisting coupled box structure based on multi-coupled laminates," *Composite Structures*, vol. 301, 12 2022.

- [13] D. Cui and D. Li, "Bending-twisting coupled structures based on composite laminates with extension-shear coupling effect," *Composite Structures*, vol. 209, pp. 434–442, 2 2019.
- [14] C. B. York, Y. B. Murta, and S. F. Almeida, "A passive-adaptive wing for drag reduction," 2018.
- [15] D. J. Baker, "Response of damaged and undamaged tailored extension-shear-coupled composite panels," *Journal of Aircraft*, vol. 43, pp. 517–527, 2006.
- [16] C. B. York and K. K. Lee, "Test validation of extension-twisting coupled laminates with matched orthotropic stiffness," *Composite Structures*, vol. 242, 6 2020.
- [17] C. B. York, "On composite laminates with extensional-anisotropy," 2008.
- [18] E. S. D. Unit, "Stiffnesses of laminated flat plates." 1994.
- [19] C. B. York, "Extension-twist coupled laminates for aero-elastic compliant blade design," pp. 23–26, 2012.
- [20] C. B. York, "Influence of bending–twisting coupling on compression and shear buckling strength," 2015.
- [21] J. Li and D. Li, "Extension-shear coupled laminates with immunity to hygro-thermal shearing distortion," *Composite Structures*, vol. 123, pp. 401–407, 2015.
- [22] A. Baucke and C. Mittelstedt, "Closed-form analysis of the buckling loads of composite laminates under uniaxial compressive load explicitly accounting for bending-twisting-coupling," *Composite Structures*, vol. 128, pp. 437–454, 2015.
- [23] C. B. York, "Characterization of nonsymmetric forms of fully orthotropic laminates," *Journal of Aircraft*, vol. 46, pp. 1114–1125, 2009.
- [24] C. B. York, "Unbalanced and symmetric laminates: New perspectives on a less common design rule," pp. 6627–6638, 2013.
- [25] C. B. York, "On bending-twisting coupled laminates," *Composite Structures*, vol. 160, pp. 887–900, 2017.
- [26] E. S. D. Unit, "Laminate stacking sequences for special orthotropy (applications to fibre reinforced composites)," *ESDU Data Items*, 1982.

- [27] N. R. Ball, P. M. Sargent, and D. O. Ige, "Genetic algorithm representations for laminate layups," *Artificial Intelligence in Engineering*, vol. 8, pp. 99–108, 1993.
- [28] R. H. Lopez, M. A. Luersen, and E. S. Cursi, "Optimization of laminated composites considering different failure criteria," *Composites Part B: Engineering*, vol. 40, pp. 731–740, 2009.
- [29] S. F. Hwang, Y. C. Hsu, and Y. Chen, "A genetic algorithm for the optimization of fiber angles in composite laminates," *Journal of Mechanical Science and Technology*, vol. 28, pp. 3163–3169, 2014.
- [30] R. L. Riche and R. T. Haftka, "Optimization of laminate stacking sequence for buckling load maximization by genetic algorithm," *AIAA Journal*, vol. 31, pp. 951–956, 1993.
- [31] T. S.W., H. J.C., and P. N.J., *Composite materials workshop*. CT: Technomic Publishing Co., Inc., 1968.
- [32] S. W. Tsai and H. T. Hahm, *Introduction to Composite Materials*. 1980.
- [33] S. Setoodeh, M. M. Abdalla, and Z. Gürdal, "Design of variable-stiffness laminates using lamination parameters," *Composites Part B: Engineering*, vol. 37, pp. 301–309, 2006.
- [34] V. B. Hammer, M. P. Bendsøe, R. Lipton, and P. Pedersen, "Parametrization in laminate design for optimal compliance," *International Journal of Solids and Structures*, vol. 34, pp. 415–434, 1997.
- [35] M. W. Bloomfield, C. G. Diaconu, and P. M. Weaver, "On feasible regions of lamination parameters for lay-up optimization of laminated composites," *Proceedings of the Royal Society A: Mathematical, Physical and Engineering Sciences*, vol. 465, pp. 1123–1143, 2009.
- [36] Z. Wu, G. Raju, S. White, and P. M. Weaver, "Optimal design of postbuckling behaviour of laminated composite plates using lamination parameters," *55th AIAA/ASME/ASCE/AHS/SC Structures, Structural Dynamics, and Materials Conference*, 2014.
- [37] H. Fukunaga and H. Sekine, "A laminate design for elastic properties of symmetric laminates with extension-shear or bending-twisting coupling," *Journal of Composite Materials*, vol. 28, pp. 708–731, 1994.

- [38] G. Raju, Z. Wu, and P. M. Weaver, "On further developments of the feasible region of lamination parameters for composite laminates," *55th AIAA/ASMe/ASCE/AHS/SC Structures, Structural Dynamics, and Materials Conference*, 2014.
- [39] Z. Gürdal, R. T. Haftka, and P. Hajela, *Design and Optimization of Laminated Composite Materials*. Wiley-Interscience, 1999.
- [40] J. Grenestedt and P. Gudmundson, "Layup optimization of composite material structures," *Optimal Design with Advanced Materials*, pp. 311–336, 1993.
- [41] M. Miki, "Material design of composite laminates with required in-plane elastic properties," pp. 1725–1731, 1982.
- [42] M. Miki and Y. Sugiyama, "Optimum design of laminated composite plates using lamination parameters," *AIAA Journal*, vol. 31, pp. 921–922, 1993.
- [43] H. Fukunaga and S. Hideki, "Stiffness design method of symmetric laminates using lamination parameters," *AIAA Journal*, vol. 30, pp. 2791–2793, 1992.
- [44] C. G. Diaconu, M. Sato, and H. Sekine, "Feasible region in general design space of lamination parameters for laminated composites," *AIAA Journal*, vol. 40, pp. 559–565, 2002.
- [45] J. Foldager, J. S. Hansen, and N. Olhoff, "A general approach forcing convexity of ply angle optimization in composite laminates," *Structural Optimization*, vol. 16, pp. 201–211, 1998.
- [46] J. L. Grenestedt, "Layup optimization against buckling of shear panels," *Structural Optimization*, vol. 3, pp. 115–120, 1991.
- [47] B. Liu, R. T. Haftka, and P. Trompette, "Maximization of buckling loads of composite panels using flexural lamination parameters," *Structural and Multidisciplinary Optimization*, vol. 26, pp. 28–36, 2004.
- [48] M. A. Albazzan, R. Harik, B. F. Tatting, and Z. Gürdal, "Efficient design optimization of nonconventional laminated composites using lamination parameters: A state of the art," *Composite Structures*, vol. 209, pp. 362–374, 2019.
- [49] U. Kuhlmann, B. Braun, A. Detzel, M. Feldmann, J. Naumes, M. Oppe, Y. Galea, M. P. O., J. Raoul, L. Davaine, M. G. J. Johansson, B. Clarin, R. Maquoi, H. Degee, N. Boissonnade, F. G. J. Chica, J. Espiga, F. Rey, G. Uria, G. Nusse, and F. Schroter, *Competitive steel and*

composite bridges by innovative steel-plated structures, RFSR-CT-2003-00018. Research Fund for Coal and Steel, 2008.

- [50] J. E. Herencia, P. M. Weaver, and M. I. Friswell, "Closed-form solutions for buckling of long anisotropic plates with various boundary conditions under axial compression," *Journal of Engineering Mechanics*, vol. 136, pp. 1105–1114, 2010.
- [51] P. M. Weaver, "On optimisation of long anisotropic flat plates subject to shear buckling loads," vol. 7, pp. 5638–5648, 2004.
- [52] C. B. York, "Elastic buckling design curves for isotropic rectangular plates with continuity or elastic edge restraint against rotation," *Aeronautical Journal*, vol. 104, pp. 175–182, 2000.
- [53] M. Stein and J. Neff, "Buckling stresses of simply supported rectangular flat plates in shear," *NACA TN 1222*, 1947.
- [54] H. Fukunaga, H. Sekine, M. Sato, and A. Iino, "Buckling design of symmetrically laminated plates using lamination parameters," *Computers and Structures*, vol. 57, pp. 643–649, 1995.
- [55] C. D. Kim and C. W. Bert, "Critical speed analysis of laminated composite, hollow drive shafts," *Composites Engineering*, vol. 3, pp. 633–643, 1993.
- [56] H. S. Lee and C. B. York, "Compression and shear buckling performance of finite length plates with bending-twisting coupling," *Composite Structures*, vol. 241, p. 112069, 2020.
- [57] C. B. York and P. Weaver, "Balanced and symmetric laminates - new perspectives on," 2010.
- [58] E. S. D. Unit, "Failure criteria for an individual layer of a fibre reinforced composite laminate under in-plane loading." 1983.
- [59] A. Puck, J. Kopp, and M. Knops, "Guidelines for the determination of the parameters in puck's action plane strength criterion," *Composites Science and Technology*, vol. 62, pp. 371–378, 2002.
- [60] A. Puck and H. Schürmann, "Failure analysis of frp laminates by means of physically based phenomenological models," *Failure Criteria in Fibre-Reinforced-Polymer Composites*, vol. 3538, pp. 832–876, 2004.

- [61] Z. Hashin and A. Rotem, "A fatigue failure criterion for fiber reinforced materials," *Journal of Composite Materials*, vol. 7, pp. 448–464, 1973.
- [62] Z. Hashin, "Failure criteria for unidirectional fiber composites," *Journal of Applied Mechanics, Transactions ASME*, vol. 47, pp. 329–334, 1980.
- [63] A. H. Puppo and H. A. Evensen, "Strength of anisotropic materials under combined stresses," *AIAA Journal*, vol. 10, pp. 468–474, 1972.
- [64] S. W. Tsai and J. D. D. Melo, "A unit circle failure criterion for carbon fiber reinforced polymer composites," *Composites Science and Technology*, vol. 123, pp. 71–78, 2016.
- [65] R. C. Burk, "Standard failure criteria needed for advanced composites," *AIAA Journal*, vol. 21, pp. 58–62, 1983.
- [66] C. Sun, B. Quinn, and J. Tao, "Comparative evaluation of failure analysis methods for composite laminates," *U.S. Department of Transportation*, p. 133, 1996.
- [67] F. Paris, "A study of failure criteria of fibrous composite materials," 2001.
- [68] M. J. Hinton, A. S. Kaddour, and P. D. Soden, *A comparison of the predictive capabilities of current failure theories for composite laminates, judged against experimental evidence*, vol. 62. 2002.
- [69] R. Narayanaswami and H. M. Adelman, "Evaluation of the tensor polynomial and hoffman strength theories for composite materials," *Journal of Composite Materials*, vol. 11, pp. 366–377, 1977.
- [70] W. C. Cui, M. R. Wisnom, and M. Jones, "A comparison of failure criteria to predict delamination of unidirectional glass/epoxy specimens waisted through the thickness," *Composites*, vol. 23, pp. 158–166, 1992.
- [71] P. M. Weaver, K. D. Potter, K. Hazra, M. A. Saverymuthapulle, and M. T. Hawthorne, "Buckling of variable angle tow plates: From concept to experiment," pp. 1–10, 2009.
- [72] G. Raju, Z. Wu, B. C. Kim, and P. M. Weaver, "Prebuckling and buckling analysis of variable angle tow plates with general boundary conditions," *Composite Structures*, vol. 94, pp. 2961–2970, 2012.

- [73] R. M. Groh and P. M. Weaver, "Buckling analysis of variable angle tow, variable thickness panels with transverse shear effects," *Composite Structures*, vol. 107, pp. 482–493, 2014.
- [74] S. Setoodeh, M. M. Abdalla, S. T. Ijsselmuiden, and Z. Gürdal, "Design of variable-stiffness composite panels for maximum buckling load," *Composite Structures*, vol. 87, pp. 109–117, 2009.
- [75] Z. Gürdal, B. F. Tatting, and C. K. Wu, "Variable stiffness composite panels: Effects of stiffness variation on the in-plane and buckling response," *Composites Part A: Applied Science and Manufacturing*, vol. 39, pp. 911–922, 2008.
- [76] Z. Wu, P. M. Weaver, G. Raju, and B. C. Kim, "Buckling analysis and optimisation of variable angle tow composite plates," *Thin-Walled Structures*, vol. 60, pp. 163–172, 2012.
- [77] B. H. Coburn, Z. Wu, and P. M. Weaver, "Buckling analysis of stiffened variable angle tow panels," *Composite Structures*, vol. 111, pp. 259–270, 2014.
- [78] Z. Wu, G. Raju, and P. M. Weaver, "Optimization of variable angle tow plates with one free edge using lamination parameters," pp. 5344–5351, 2013.
- [79] G. Raju, Z. Wu, and P. M. Weaver, "Postbuckling analysis of variable angle tow plates using differential quadrature method," *Composite Structures*, vol. 106, pp. 74–84, 2013.
- [80] Z. Wu, P. M. Weaver, and G. Raju, "Postbuckling optimisation of variable angle tow composite plates," *Composite Structures*, vol. 103, pp. 34–42, 2013.
- [81] Z. Wu, G. Raju, and P. M. Weaver, "Feasible region of lamination parameters for optimization of variable angle tow (vat) composite plates," 2013.
- [82] P. T. Langley, "Finite element modeling of tow-placed variable-stiffness composite laminates," *Virginia Polytechnic Institute and State University*, p. 137, 1999.
- [83] B. C. Kim, K. Hazra, P. Weaver, and K. Potter, "Limitations of fibre placement techniques for variable angle tow composites and their process-induced defects," 2011.
- [84] Z. Xiao and P. Harrison, "Buckling analysis of variable stiffness panels manufactured by fabric steering technology," pp. 11–19, 2019.

- [85] J. A. Bailie, R. P. Ley, and A. Pasricha, "A summary and review of composite laminate design guidelines," *NASA Contract NAS1-19347*, 1997.
- [86] C. B. York and S. F. M. de Almeida, "Effect of bending-twisting coupling on the compression and shear buckling strength of infinitely long plates," *Composite Structures*, vol. 184, pp. 18–29, 2018.
- [87] S. W. Tsai, J. D. D. Melo, S. Shin, A. Arteiro, and R. Rainsberger, *Composite Laminates: Theory and practice of analysis, design and automated layup*. Stanford University Composites Design Group, 2017.
- [88] S. W. Tsai, "Keynote: design of composite laminates," 2017.
- [89] M. W. Nielsen, K. J. Johnson, A. T. Rhead, and R. Butler, "Laminate design for optimised in-plane performance and ease of manufacture," *Composite Structures*, vol. 177, pp. 119–128, 2017.
- [90] B. Vermes, S. W. Tsai, T. Massard, G. S. Springer, and T. Czigany, "Design of laminates by a novel "double–double" layup," *Thin-Walled Structures*, vol. 165, p. 107954, 2021.
- [91] B. Vermes, S. W. Tsai, A. Riccio, F. D. Caprio, and S. Roy, "Application of the tsai's modulus and double-double concepts to the definition of a new affordable design approach for composite laminates," *Composite Structures*, vol. 259, p. 113246, 2021.
- [92] S. W. Tsai, "Double–double: New family of composite laminates," *AIAA Journal*, vol. 59, pp. 4293–4305, 2021.
- [93] S. W. Tsai, N. Sharma, A. Arteiro, S. Roy, and B. Rainsberger, *Composite double-double and grid/skin structures - low weight/low cost design and manufacturing*. 2019.
- [94] B. P. Kristinsdottir, Z. B. Zabinsky, M. E. Tuttle, and S. Neogi, "Optimal design of large composite panels with varying loads," *Composite Structures*, vol. 51, pp. 93–102, 2001.
- [95] S. Shrivastava, N. Sharma, S. W. Tsai, and P. M. Mohite, "D and dd-drop layup optimization of aircraft wing panels under multi-load case design environment," *Composite Structures*, vol. 248, p. 112518, 2020.
- [96] C. B. York, "Laminate stiffness tailoring for improved buckling performance," *Thin-Walled Structures*, vol. 161, p. 107482, 2021.

- [97] C. B. York, "New insights into stiffness matching between standard and double angle-ply laminates.," 2018.
- [98] C. B. York, "On tapered warp-free laminates with single-ply terminations," *Composites Part A: Applied Science and Manufacturing*, vol. 72, pp. 127–138, 2015.
- [99] E. S. D. Unit, "Buckling of rectangular specially orthotropic plates." 1995.
- [100] D. Systemes, *Abaqus 6.14 Analysis User's Guide*. Dassault Systèmes Simulia Corp. Providence, RI, 2014.
- [101] E. S. D. Unit, "Estimation of the stiffnesses and apparent elastic properties of laminated flat plate." 2012.
- [102] C. B. York and S. F. M. de Almeida, "On extension-shearing bending-twisting coupled laminates," *Composite Structures*, vol. 164, pp. 10–22, 2017.
- [103] M. P. Nemeth, "Importance of anisotropy on buckling of compression-loaded symmetric-composite plates," *AIAA Journal*, vol. 24, pp. 1831–1835, 1986.
- [104] C. B. York, "On extension-shearing coupled laminates," *Composite Structures*, vol. 120, pp. 472–482, 2015.
- [105] M. S. Anderson and W. J. Stroud, "M. s. anderson and w. j. stroud. general panel sizing computer code and its application to composite structural panels," *AIAA Journal*, vol. 17, pp. 892–897, 1979.
- [106] C. B. York, F. W. Williams, D. Kennedy, and R. Butler, "A parametric study of optimum designs for benchmark stiffened wing panels," *Composites Engineering*, vol. 3, pp. 619–632, 1993.
- [107] I. plane Bending and M. P. Nemeth, "Buckling of symmetrically laminated plates with compression, shear, and in-plane bending," *AIAA Journal*, vol. 30, 1992.
- [108] J. Loughlan, "Shear buckling behaviour of thin composite plates with particular reference to the effects of bend-twist coupling," *International Journal of Mechanical Sciences*, vol. 43, pp. 771–792, 2001.

- [109] A. Standard, "Standard test method for compressive residual strength properties of damaged polymer matrix composite plates," *ASTM International*, vol. i, pp. 1–16, 2012.
- [110] C. Jutte and B. K. Stanford, "Aeroelastic tailoring of transport aircraft wings: State-of-the-art and potential enabling technologies," *Nasa*, p. 34, 2014.
- [111] C. B. York, "Buckling analysis and minimum-mass design procedures for composite wing-box structures," *Journal of Aircraft*, vol. 43, pp. 528–536, 2006.
- [112] H. A. Deveci, L. Aydin, and H. S. Artem, "Buckling optimization of composite laminates using a hybrid algorithm under puck failure criterion constraint," *Journal of Reinforced Plastics and Composites*, vol. 35, pp. 1233–1247, 2016.
- [113] O. Stodieck, J. E. Cooper, P. M. Weaver, and P. Kealy, "Aeroelastic tailoring of a representative wing-box using tow-steered composites," *AIAA Journal*, vol. 55, pp. 1425–1439, 2017.
- [114] P. Vannucci and G. Verchery, "A new method for generating fully isotropic laminates," *Composite Structures*, vol. 58, pp. 75–82, 2002.
- [115] A. Standard, "Standard test method for compressive properties of polymer matrix composite materials," *Annual Book of ASTM Standards*, vol. 03, pp. 1–13, 2016.
- [116] F. X. Irisarri, A. Lasseigne, F. H. Leroy, and R. L. Riche, "Optimal design of laminated composite structures with ply drops using stacking sequence tables," *Composite Structures*, vol. 107, pp. 559–569, 2014.
- [117] C. B. York, "Laminate stiffness tailoring for improved buckling performance - appendix 1," 2020.

APPENDIX

A1 ABAQUS INPUT CODES FOR COMPRESSION BUCKLING WITH ABD MATRIX INPUT

*HEADING

Compression loaded laminate with ABD matrix

**RESTART,WRITE

Creating nodes for corners

*NODE

1001, 0.,0.

1061,300.,0.

61001,0,300

61061,300,300

Define the top and bottom edges

*NGEN,NSET=BOT

1001,1061

*NGEN,NSET=TOP

61001,61061

Generating and grouping nodes

*NFILL,NSET=ALLN

BOT, TOP, 60, 1000

*NSET,NSET=LEFT, GENERATE

2001, 60001, 1000

*NSET,NSET=LEFTS, GENERATE

1001, 61001, 60000

*NSET,NSET=LEFTD,GENERATE

3001,59001,2000

*NSET,NSET=LEFTQ,GENERATE

2001,60001,2000

*NSET,NSET=RIGHT,GENERATE

2061,60061,1000

*NSET,NSET=RIGHTS,GENERATE

1061,61061,60000

*NSET,NSET=RIGHTD,GENERATE

3061,59061,2000

*NSET,NSET=RIGHTQ,GENERATE

2061,60061,2000

Generating elements

*ELEMENT,TYPE=S8R5

1001, 1001,1003,3003,3001,1002,2003,3002,2001

*ELGEN,ELSET=ALLE

1001, 30,2,1, 30,2000,1000

Apply material properties

*MATERIAL, NAME=CFRP

*SHELL GENERAL SECTION, ELSET=ALLE, OFFSET=0.5

256047.4, 75797.9, 256047.4, 0, 0, 90124.7, 0, 0,

0, 239858.1, 0, 0, 0, 71005.4, 239858.1, 0,

0, 0, 0, 0, 84426.3

Boundary conditions

*BOUNDARY

**Simply supported boundary conditions.

TOP,3

TOP,5,6

BOT,3

BOT,5,6

DIAG,3

```
DIAG,6
1001,1,2
61001,1
*STEP
1
**Conduct buckling analysis**
*BUCKLE
2,2,5,40
*CLOAD
**Applying compression load**
LEFTS,1,0.01673722
LEFTQ,1,0.066948883
LEFTD,1,0.033474441
RIGHTS,1,-0.01673722
RIGHTQ,1,-0.066948883
RIGHTD,1,-0.033474441
*ENDSTEP
```

A2 EXTRACTS OF ABAQUS INPUT CODES FOR COMPRESSION BUCKLING WITH STACKING SEQUENCE

```
**Apply material properties**
*ELASTIC, TYPE=LAMINA
181000,10300,0.28,7170,7170,7170
*SHELL GENERAL SECTION, ELSET=ALLE, COMPOSITE
** AsB0Di 24-ply
0.1397,,CFRP,-45
0.1397,,CFRP,90
0.1397,,CFRP,0
0.1397,,CFRP,45
0.1397,,CFRP,0
```

0.1397,,CFRP,45
0.1397,,CFRP,90
0.1397,,CFRP,45
0.1397,,CFRP,-45
0.1397,,CFRP,0
0.1397,,CFRP,-45
0.1397,,CFRP,90
0.1397,,CFRP,-45
0.1397,,CFRP,90
0.1397,,CFRP,45
0.1397,,CFRP,90
0.1397,,CFRP,0
0.1397,,CFRP,-45
0.1397,,CFRP,0
0.1397,,CFRP,45
0.1397,,CFRP,0
0.1397,,CFRP,45
0.1397,,CFRP,-45
0.1397,,CFRP,90

A3 EXTRACTS OF ABAQUS INPUT CODES FOR SHEAR LOADING

**Applying shear load

LEFTS,2,0.01673722

LEFTQ,2,0.066948883

LEFTD,2,0.033474441

RIGHTS,2,-0.01673722

RIGHTQ,2,-0.066948883

RIGHTD,2,-0.033474441

BOTS,1,0.01673722

BOTQ,1,0.066948883

BOTD,1,0.033474441

TOPS,1,-0.01673722

TOPQ,1,-0.066948883

A4 STACKING SEQUENCES

TABLE A1: Stacking sequences and Lamination Parameter coordinates for Quasi Isotropic laminates for 16 ply laminates, i.e. $(\zeta_1, \zeta_2) = (0, 0)$. Here the 10% rule has been applied, which corresponds to the minimum number of plies in each of the standard ply orientations. Ply contiguity constraints have also been applied, which limits the maximum of number of adjacent plies with the same orientation to 3, as is now common design practice. The listings are grouped by matching orthotropic bending stiffness (ζ_9, ζ_{10}) and ordered by increasing Bending-Twisting coupling, ζ_{11} . Symbols +, - \circ and \bullet represent standard ply angles 0° , 90° and $\pm 45^\circ$, respectively.

Stacking Sequence	ζ_9	ζ_{10}	ζ_{11}
+ \bullet \bullet - - \circ + \circ \circ + \circ - - \bullet \bullet +	-0.39	-0.07	0.15
+ \bullet \bullet - + \circ - \circ \circ - \circ + - \bullet \bullet +	-0.39	-0.07	0.27
+ \bullet \bullet + - \circ - \circ \circ - \circ - + \bullet \bullet +	-0.39	-0.07	0.36
+ \bullet \bullet - - \circ \circ + + \circ \circ - - \bullet \bullet +	-0.38	-0.05	0.14
+ \bullet \bullet - + \circ \circ - - \circ \circ + - \bullet \bullet +	-0.38	-0.05	0.28
+ \bullet \bullet + - \circ \circ - - \circ \circ - + \bullet \bullet +	-0.38	-0.05	0.38
+ \bullet \bullet - \circ - + \circ \circ + - \circ - \bullet \bullet +	-0.35	0.00	0.19
+ \bullet \bullet - \circ + - \circ \circ - + \circ - \bullet \bullet +	-0.35	0.00	0.23
+ \bullet \bullet + \circ - - \circ \circ - - \circ + \bullet \bullet +	-0.35	0.00	0.40
+ \bullet \bullet - \circ - \circ + + \circ - \circ - \bullet \bullet +	-0.34	0.02	0.18
+ \bullet \bullet - \circ + \circ - - \circ + \circ - \bullet \bullet +	-0.34	0.02	0.25
+ \bullet \bullet + \circ - \circ - - \circ - \circ + \bullet \bullet +	-0.34	0.02	0.41
+ \bullet - \bullet - \circ + \circ \circ + \circ - \bullet - \bullet +	-0.33	-0.19	0.09
+ \bullet - \bullet + \circ - \circ \circ - \circ + \bullet - \bullet +	-0.33	-0.19	0.21
+ \bullet + \bullet - \circ - \circ \circ - \circ - \bullet + \bullet +	-0.33	-0.19	0.42
+ \bullet \bullet - \circ \circ - + + - \circ \circ - \bullet \bullet +	-0.32	0.07	0.20
+ \bullet \bullet - \circ \circ + - - + \circ \circ - \bullet \bullet +	-0.32	0.07	0.22
+ \bullet - \bullet - \circ \circ + + \circ \circ - \bullet - \bullet +	-0.32	-0.16	0.08
+ \bullet - \bullet + \circ \circ - - \circ \circ + \bullet - \bullet +	-0.32	-0.16	0.22
+ \bullet + \bullet - \circ \circ - - \circ \circ - \bullet + \bullet +	-0.32	-0.16	0.43
+ \bullet \bullet \circ - - + \circ \circ + - - \circ \bullet \bullet +	-0.30	0.09	0.23
+ \bullet \bullet \circ - + - \circ \circ - + - \circ \bullet \bullet +	-0.30	0.09	0.28
+ \bullet \bullet \circ + - - \circ \circ - - + \circ \bullet \bullet +	-0.30	0.09	0.35
+ \bullet - \bullet \circ - + \circ \circ + - \circ \bullet - \bullet +	-0.29	-0.12	0.13
+ \bullet - \bullet \circ + - \circ \circ - + \circ \bullet - \bullet +	-0.29	-0.12	0.18
+ \bullet + \bullet \circ - \circ \circ - \circ \bullet + \bullet +	-0.29	-0.12	0.46

+ ● -- ● ○ + ○ ○ + ○ ● -- ● +	-0.28	-0.28	0.05
+ ● - + ● ○ - ○ ○ - ○ ● + - ● +	-0.28	-0.28	0.26
+ ● + - ● ○ - ○ ○ - ○ ● - + ● +	-0.28	-0.28	0.38
+ ● ● ○ - ○ - + + - ○ - ○ ● ● +	-0.27	0.16	0.25
+ ● ● ○ - ○ + - - + ○ - ○ ● ● +	-0.27	0.16	0.27
+ ● -- ● ○ ○ + + ○ ○ ● -- ● +	-0.27	-0.26	0.04
+ ● - + ● ○ ○ - - ○ ○ ● + - ● +	-0.27	-0.26	0.27
+ ● + - ● ○ ○ - - ○ ○ ● - + ● +	-0.27	-0.26	0.39
+ ● - ● ○ ○ - + + - ○ ○ ● - ● +	-0.26	-0.05	0.14
+ ● - ● ○ ○ + - - + ○ ○ ● - ● +	-0.26	-0.05	0.16
+ - ● ● - ○ + ○ ○ + ○ - ● ● - +	-0.26	-0.33	0.02
+ - ● ● + ○ - ○ ○ - ○ + ● ● - +	-0.26	-0.33	0.14
+ + ● ● - ○ - ○ ○ - ○ - ● ● + +	-0.26	-0.33	0.49
+ - ● ● - ○ ○ + + ○ ○ - ● ● - +	-0.25	-0.30	0.01
+ - ● ● + ○ ○ - - ○ ○ + ● ● - +	-0.25	-0.30	0.15
+ + ● ● - ○ ○ - - ○ ○ - ● ● + +	-0.25	-0.30	0.50
+ ● ● ○ ○ - - + + - - ○ ○ ● ● +	-0.23	0.23	0.28
+ ● ● ○ ○ - + - - + - ○ ○ ● ● +	-0.23	0.23	0.30
+ ● -- + ○ ● ○ ○ ● ○ + - - ● +	-0.22	-0.40	0.11
+ ● - + - ○ ● ○ ○ ● ○ - + - ● +	-0.22	-0.40	0.20
+ ● + - - ○ ● ○ ○ ● ○ - - + ● +	-0.22	-0.40	0.32
+ - ● ● ○ - + ○ ○ + - ○ ● ● - +	-0.22	-0.26	0.06
+ - ● ● ○ + - ○ ○ - + ○ ● ● - +	-0.22	-0.26	0.11
+ + ● ● ○ - - ○ ○ - - ○ ● ● + +	-0.22	-0.26	0.53
+ - ● - ● ○ + ○ ○ + ○ ● - ● - +	-0.21	-0.42	-0.02
+ - ● + ● ○ - ○ ○ - ○ ● + ● - +	-0.21	-0.42	0.19
+ + ● - ● ○ - ○ ○ - ○ ● - ● + +	-0.21	-0.42	0.45
+ ● -- ○ ● + ○ ○ + ● ○ - - ● +	-0.21	-0.28	0.05
+ ● - + ○ ● - ○ ○ - ● ○ + - ● +	-0.21	-0.28	0.26
+ ● + - ○ ● - ○ ○ - ● ○ - + ● +	-0.21	-0.28	0.38
+ - ● ● ○ - ○ + + ○ - ○ ● ● - +	-0.21	-0.23	0.05
+ - ● ● ○ + ○ - - ○ + ○ ● ● - +	-0.21	-0.23	0.12
+ + ● ● ○ - ○ - - ○ - ○ ● ● + +	-0.21	-0.23	0.54

+ ● -- ○ ● ○ + + ○ ● ○ -- ● +	-0.20	-0.26	0.04
+ ● - + ○ ● ○ -- ○ ● ○ + - ● +	-0.20	-0.26	0.27
+ ● + - ○ ● ○ -- ○ ● ○ - + ● +	-0.20	-0.26	0.39
+ ● - ○ ● - ○ + + ○ - ● ○ - ● +	-0.19	-0.09	0.12
+ ● - ○ ● + ○ -- ○ + ● ○ - ● +	-0.19	-0.09	0.19
+ ● + ○ ● - ○ -- ○ - ● ○ + ● +	-0.19	-0.09	0.47
+ ● ○ ● -- + ○ ○ + -- ● ○ ● +	-0.19	0.09	0.23
+ ● ○ ● - + - ○ ○ - + - ● ○ ● +	-0.19	0.09	0.28
+ ● ○ ● + - - ○ ○ - - + ● ○ ● +	-0.19	0.09	0.35
+ ● -- ○ + ● ○ ○ ● + ○ -- ● +	-0.19	-0.33	0.07
+ ● - + ○ - ● ○ ○ ● - ○ + - ● +	-0.19	-0.33	0.23
+ ● + - ○ - ● ○ ○ ● - ○ - + ● +	-0.19	-0.33	0.35
+ - ● ● ○ ○ - + + - ○ ○ ● ● - +	-0.19	-0.19	0.07
+ - ● ● ○ ○ + - - + ○ ○ ● ● - +	-0.19	-0.19	0.09
+ ● ○ ● -- ○ + + ○ -- ● ○ ● +	-0.18	0.12	0.22
+ ● ○ ● - + ○ -- ○ + - ● ○ ● +	-0.18	0.12	0.29
+ ● ○ ● + - ○ -- ○ - + ● ○ ● +	-0.18	0.12	0.36
+ ● - ○ ● ○ - + + - ○ ● ○ - ● +	-0.16	-0.05	0.14
+ ● - ○ ● ○ + - - + ○ ● ○ - ● +	-0.16	-0.05	0.16
+ ● -- ○ + ○ ● ● ○ + ○ -- ● +	-0.16	-0.33	0.07
+ ● - + ○ - ○ ● ● ○ - ○ + - ● +	-0.16	-0.33	0.23
+ ● + - ○ - ○ ● ● ○ - ○ - + ● +	-0.16	-0.33	0.35
+ ● - ○ - ● + ○ ○ + ● - ○ - ● +	-0.16	-0.19	0.09
+ ● - ○ + ● - ○ ○ - ● + ○ - ● +	-0.16	-0.19	0.21
+ ● + ○ - ● - ○ ○ - ● - ○ + ● +	-0.16	-0.19	0.42
+ ● - ○ - ● ○ + + ○ ● - ○ - ● +	-0.15	-0.16	0.08
+ ● - ○ + ● ○ -- ○ ● + ○ - ● +	-0.15	-0.16	0.22
+ ● + ○ - ● ○ -- ○ ● - ○ + ● +	-0.15	-0.16	0.43
+ ● ○ ● - ○ - + + - ○ - ● ○ ● +	-0.15	0.16	0.25
+ ● ○ ● - ○ + - - + ○ - ● ○ ● +	-0.15	0.16	0.27
+ - - ● ● ○ + ○ ○ + ○ ● ● - - +	-0.15	-0.54	-0.08
+ - ● - + ○ ● ○ ○ ● ○ + - ● - +	-0.15	-0.54	0.04
+ - ● + - ○ ● ○ ○ ● ○ - + ● - +	-0.15	-0.54	0.13

+ ● ○ - ● - + ○ ○ + - ● - ○ ● +	-0.14	0.00	0.19
+ ● ○ - ● + - ○ ○ - + ● - ○ ● +	-0.14	0.00	0.23
+ ● ○ + ● - - ○ ○ - - ● + ○ ● +	-0.14	0.00	0.40
+ - - ● ● ○ ○ + + ○ ○ ● ● - - +	-0.14	-0.52	-0.09
+ - + ● ● ○ ○ - - ○ ○ ● ● + - +	-0.14	-0.52	0.26
+ + - ● ● ○ ○ - - ○ ○ ● ● - + +	-0.14	-0.52	0.40
+ - ● - ○ ● + ○ ○ + ● ○ - ● - +	-0.14	-0.42	-0.02
+ - ● + ○ ● - ○ ○ - ● ○ + ● - +	-0.14	-0.42	0.19
+ + ● - ○ ● - ○ ○ - ● ○ - ● + +	-0.14	-0.42	0.45
+ ● - - ○ ○ + ● ● + ○ ○ - - ● +	-0.14	-0.28	0.05
+ ● - + ○ ○ - ● ● - ○ ○ + - ● +	-0.14	-0.28	0.26
+ ● + - ○ ○ - ● ● - ○ ○ - + ● +	-0.14	-0.28	0.38
+ ● - ○ - + ● ○ ○ ● + - ○ - ● +	-0.14	-0.23	0.12
+ ● - ○ + - ● ○ ○ ● - + ○ - ● +	-0.14	-0.23	0.19
+ ● + ○ - - ● ○ ○ ● - - ○ + ● +	-0.14	-0.23	0.40
+ ● ○ - ● + ○ - - ○ + ● - ○ ● +	-0.13	0.02	0.25
+ ● ○ + ● - ○ - - ○ - ● + ○ ● +	-0.13	0.02	0.41
+ ● ○ - ● - ○ + + ○ - ● - ○ ● +	-0.13	0.02	0.18
+ - ● - + ○ ○ ● ● ○ ○ + - ● - +	-0.13	-0.54	0.04
+ - ● + - ○ ○ ● ● ○ ○ - + ● - +	-0.13	-0.54	0.13
+ + ● - - ○ ○ ● ● ○ ○ - - ● + +	-0.13	-0.54	0.39
+ - ● - ○ ● ○ + + ○ ● ○ - ● - +	-0.13	-0.40	-0.04
+ - ● + ○ ● ○ - - ○ ● ○ + ● - +	-0.13	-0.40	0.20
+ + ● - ○ ● ○ - - ○ ● ○ - ● + +	-0.13	-0.40	0.46
+ - ● ○ ● - + ○ ○ + - ● ○ ● - +	-0.13	-0.26	0.06
+ - ● ○ ● + - ○ ○ - + ● ○ ● - +	-0.13	-0.26	0.11
+ + ● ○ ● - - ○ ○ - - ● ○ ● + +	-0.13	-0.26	0.53
+ ● ○ ● ○ - - + + - - ○ ● ○ ● +	-0.12	0.23	0.28
+ ● ○ ● ○ - + - - + - ○ ● ○ ● +	-0.12	0.23	0.30
+ - ● ○ ● - ○ + + ○ - ● ○ ● - +	-0.12	-0.23	0.05
+ - ● ○ ● + ○ - - ○ + ● ○ ● - +	-0.12	-0.23	0.12
+ ● - ○ - + ○ ● ● ○ + - ○ - ● +	-0.12	-0.23	0.12
+ ● - ○ + - ○ ● ● ○ - + ○ - ● +	-0.12	-0.23	0.19

+ ● ○ - ● ○ - + + - ○ ● - ○ ● +	-0.11	0.07	0.20
+ ● ○ - ● ○ + - - + ○ ● - ○ ● +	-0.11	0.07	0.22
+ - ● ○ ● ○ - + + - ○ ● ○ ● - +	-0.09	-0.19	0.07
+ - ● ○ ● ○ + - - + ○ ● ○ ● - +	-0.09	-0.19	0.09
+ ● - ○ - ○ + ● ● + ○ - ○ - ● +	-0.09	-0.19	0.09
+ ● - ○ + ○ - ● ● - ○ + ○ - ● +	-0.09	-0.19	0.21
+ ● + ○ - ○ - ● ● - ○ - ○ + ● +	-0.09	-0.19	0.42
+ ● ○ - - ● ○ + + ○ ● - - ○ ● +	-0.09	-0.05	0.14
+ ● - ○ ○ ● - + + - ● ○ ○ - ● +	-0.09	-0.05	0.14
+ ● - ○ ○ ● + - - + ● ○ ○ - ● +	-0.09	-0.05	0.16
+ ● ○ - + ● ○ - - ○ ● + - ○ ● +	-0.09	-0.05	0.28
+ ● ○ + - ● ○ - - ○ ● - + ○ ● +	-0.09	-0.05	0.38
+ - ● + ○ - ○ ● ● ○ - ○ + ● - +	-0.09	-0.47	0.16
+ + ● - ○ - ○ ● ● ○ - ○ - ● + +	-0.09	-0.47	0.42
+ - ● ○ - ● + ○ ○ + ● - ○ ● - +	-0.09	-0.33	0.02
+ - ● ○ + ● - ○ ○ - ● + ○ ● - +	-0.09	-0.33	0.14
+ + ● ○ - ● - ○ ○ - ● - ○ ● + +	-0.09	-0.33	0.49
+ - - ● + ○ ● ○ ○ ● ○ + ● - - +	-0.09	-0.66	-0.02
+ - + ● - ○ ● ○ ○ ● ○ - ● + - +	-0.09	-0.66	0.19
+ + - ● - ○ ● ○ ○ ● ○ - ● - + +	-0.09	-0.66	0.33
+ - ● ○ - ● ○ + + ○ ● - ○ ● - +	-0.08	-0.30	0.01
+ - ● ○ + ● ○ - - ○ ● + ○ ● - +	-0.08	-0.30	0.15
+ + ● ○ - ● ○ - - ○ ● - ○ ● + +	-0.08	-0.30	0.50
+ ● ○ - - + ● ○ ○ ● + - - ○ ● +	-0.08	-0.12	0.18
+ ● ○ - + - ● ○ ○ ● - + - ○ ● +	-0.08	-0.12	0.25
+ ● ○ + - - ● ○ ○ ● - - + ○ ● +	-0.08	-0.12	0.34
+ - - ● ○ ● + ○ ○ + ● ○ ● - - +	-0.08	-0.54	-0.08
+ - + ● ○ ● - ○ ○ - ● ○ ● + - +	-0.08	-0.54	0.25
+ + - ● ○ ● - ○ ○ - ● ○ ● - + +	-0.08	-0.54	0.39
+ - ● - ○ ○ ● + + ● ○ ○ - ● - +	-0.08	-0.40	-0.04
+ - ● + ○ ○ ● - - ● ○ ○ + ● - +	-0.08	-0.40	0.20
+ + ● - ○ ○ ● - - ● ○ ○ - ● + +	-0.08	-0.40	0.46
+ ● - ○ ○ - ● + + ● - ○ ○ - ● +	-0.07	-0.09	0.12

+ - ● ○ - + ● ○ ○ ● + - ○ ● - +	-0.07	-0.38	0.05
+ - ● ○ + - ● ○ ○ ● - + ○ ● - +	-0.07	-0.38	0.12
+ + ● ○ - - ● ○ ○ ● - - ○ ● + +	-0.07	-0.38	0.47
+ - - ● + ○ ○ ● ● ○ ○ + ● - - +	-0.07	-0.66	-0.02
+ - + ● - ○ ○ ● ● ○ ○ - ● + - +	-0.07	-0.66	0.19
+ + - ● - ○ ○ ● ● ○ ○ - ● - + +	-0.07	-0.66	0.33
+ ● - ○ ○ - + ● ● + - ○ ○ - ● +	-0.06	-0.12	0.13
+ ● ○ - - + ○ ● ● ○ + - - ○ ● +	-0.06	-0.12	0.18
+ ● - ○ ○ + - ● ● - + ○ ○ - ● +	-0.06	-0.12	0.18
+ ● ○ - + - ○ ● ● ○ - + - ○ ● +	-0.06	-0.12	0.25
+ ● ○ + - - ○ ● ● ○ - - + ○ ● +	-0.06	-0.12	0.34
+ ● + ○ ○ - - ● ● - - ○ ○ + ● +	-0.06	-0.12	0.46
+ - - ● ○ + ● ○ ○ ● + ○ ● - - +	-0.06	-0.59	-0.06
+ - + ● ○ - ● ○ ○ ● - ○ ● + - +	-0.06	-0.59	0.22
+ + - ● ○ - ● ○ ○ ● - ○ ● - + +	-0.06	-0.59	0.36
+ ○ ● ● - - + ○ ○ + - - ● ● ○ +	-0.05	0.09	0.23
+ ○ ● ● - + - ○ ○ - + - ● ● ○ +	-0.05	0.09	0.28
+ ○ ● ● + - - ○ ○ - - + ● ● ○ +	-0.05	0.09	0.35
+ ● ○ - - ○ ● + + ● ○ - - ○ ● +	-0.05	-0.05	0.14
+ ● ○ - + ○ ● - - ● ○ + - ○ ● +	-0.05	-0.05	0.28
+ ● ○ + - ○ ● - - ● ○ - + ○ ● +	-0.05	-0.05	0.38
+ - - + ● ○ ● ○ ○ ● ○ ● + - - +	-0.05	-0.75	0.02
+ - + - ● ○ ● ○ ○ ● ○ ● - + - +	-0.05	-0.75	0.14
+ + - - ● ○ ● ○ ○ ● ○ ● - - + +	-0.05	-0.75	0.28
+ - ● ○ - + ○ ● ● ○ + - ○ ● - +	-0.05	-0.38	0.05
+ - ● ○ + - ○ ● ● ○ - + ○ ● - +	-0.05	-0.38	0.12
+ + ● ○ - - ○ ● ● ○ - - ○ ● + +	-0.05	-0.38	0.47
+ ○ ● ● - - ○ + + ○ - - ● ● ○ +	-0.04	0.12	0.22
+ ○ ● ● - + ○ - - ○ + - ● ● ○ +	-0.04	0.12	0.29
+ ○ ● ● + - ○ - - ○ - + ● ● ○ +	-0.04	0.12	0.36
+ - ● ○ - ○ ● + + ● ○ - ○ ● - +	-0.04	-0.30	0.01
+ - ● ○ + ○ ● - - ● ○ + ○ ● - +	-0.04	-0.30	0.15
+ + ● ○ - ○ ● - - ● ○ - ○ ● + +	-0.04	-0.30	0.50

+ ● ○ ○ ● - - + + - - ● ○ ○ ● +	-0.02	0.23	0.28
+ ● ○ ○ ● - + - - + - ● ○ ○ ● +	-0.02	0.23	0.30
+ - ● ○ - ○ + ● ● + ○ - ○ ● - +	-0.02	-0.33	0.02
+ - ● ○ + ○ - ● ● - ○ + ○ ● - +	-0.02	-0.33	0.14
+ + ● ○ - ○ - ● ● - ○ - ○ ● + +	-0.02	-0.33	0.49
+ - ● ○ ○ ● - + + - ● ○ ○ ● - +	-0.02	-0.19	0.07
+ - ● ○ ○ ● + - - + ● ○ ○ ● - +	-0.02	-0.19	0.09
+ - - ● ○ ○ ● + + ● ○ ○ ● - - +	-0.02	-0.52	-0.09
+ - + ● ○ ○ ● - - ● ○ ○ ● + - +	-0.02	-0.52	0.26
+ + - ● ○ ○ ● - - ● ○ ○ ● - + +	-0.02	-0.52	0.40
+ - - + ● ○ ○ ● ● ○ ○ ● + - - +	-0.02	-0.75	0.02
+ - + - ● ○ ○ ● ● ○ ○ ● - + - +	-0.02	-0.75	0.14
+ + - - ● ○ ○ ● ● ○ ○ ● - - + +	-0.02	-0.75	0.28
+ ○ ● ● - ○ - + + - ○ - ● ● ○ +	-0.01	0.16	0.25
+ ○ ● ● - ○ + - - + ○ - ● ● ○ +	-0.01	0.16	0.27
+ - ○ ● ● - + ○ ○ + - ● ● ○ - +	-0.01	-0.26	0.06
+ - ○ ● ● + - ○ ○ - + ● ● ○ - +	-0.01	-0.26	0.11
+ + ○ ● ● - - ○ ○ - - ● ● ○ + +	-0.01	-0.26	0.53
+ - - ● ○ ○ + ● ● + ○ ○ ● - - +	-0.01	-0.54	-0.08
+ - + ● ○ ○ - ● ● - ○ ○ ● + - +	-0.01	-0.54	0.25
+ + - ● ○ ○ - ● ● - ○ ○ ● - + +	-0.01	-0.54	0.39
+ ● ○ - ○ + ● - - ● + ○ - ○ ● +	-0.01	0.02	0.25
+ ● ○ + ○ - ● - - ● - ○ + ○ ● +	-0.01	0.02	0.41
+ ● ○ - ○ - ● + + ● - ○ - ○ ● +	-0.01	0.02	0.18
+ - ● ○ ○ - ● + + ● - ○ ○ ● - +	0.00	-0.23	0.05
+ - ○ ● ● - ○ + + ○ - ● ● ○ - +	0.00	-0.23	0.05
+ - ● ○ ○ + ● - - ● + ○ ○ ● - +	0.00	-0.23	0.12
+ - ○ ● ● + ○ - - ○ + ● ● ○ - +	0.00	-0.23	0.12
+ + ○ ● ● - ○ - - ○ - ● ● ○ + +	0.00	-0.23	0.54
+ + ● ○ ○ - ● - - ● - ○ ○ ● + +	0.00	-0.23	0.54
+ ○ ● - ● - + ○ ○ + - ● - ● ○ +	0.00	0.00	0.19
+ ● ○ - ○ - + ● ● + - ○ - ○ ● +	0.00	0.00	0.19
+ ○ ● - ● + - ○ ○ - + ● - ● ○ +	0.00	0.00	0.23

+ - - ○ ● ● + ○ ○ + ● ● ○ - - +	0.01	-0.54	-0.08
+ - + ○ ● ● - ○ ○ - ● ● ○ + - +	0.01	-0.54	0.25
+ + - ○ ● ● - ○ ○ - ● ● ○ - + +	0.01	-0.54	0.39
+ ○ ● - ● + ○ - - ○ + ● - ● ○ +	0.01	0.02	0.25
+ ○ ● + ● - ○ - - ○ - ● + ● ○ +	0.01	0.02	0.41
+ ○ ● - ● - ○ + + ○ - ● - ● ○ +	0.01	0.02	0.18
+ ○ ● ● ○ - - + + - - ○ ● ● ○ +	0.02	0.23	0.28
+ ○ ● ● ○ - + - - + - ○ ● ● ○ +	0.02	0.23	0.30
+ - ○ ● - ● + ○ ○ + ● - ● ○ - +	0.02	-0.33	0.02
+ - ○ ● + ● - ○ ○ - ● + ● ○ - +	0.02	-0.33	0.14
+ + ○ ● - ● - ○ ○ - ● - ● ○ + +	0.02	-0.33	0.49
+ - ○ ● ● ○ - + + - ○ ● ● ○ - +	0.02	-0.19	0.07
+ - ○ ● ● ○ + - - + ○ ● ● ○ - +	0.02	-0.19	0.09
+ - - + ○ ● ● ○ ○ ● ● ○ + - - +	0.02	-0.75	0.02
+ - + - ○ ● ● ○ ○ ● ● ○ - + - +	0.02	-0.75	0.14
+ + - - ○ ● ● ○ ○ ● ● ○ - - + +	0.02	-0.75	0.28
+ - - ○ ● ● ○ + + ○ ● ● ○ - - +	0.02	-0.52	-0.09
+ - + ○ ● ● ○ - - ○ ● ● ○ + - +	0.02	-0.52	0.26
+ + - ○ ● ● ○ - - ○ ● ● ○ - + +	0.02	-0.52	0.40
+ ● ○ ○ - - ● + + ● - - ○ ○ ● +	0.04	0.12	0.22
+ ● ○ ○ - + ● - - ● + - ○ ○ ● +	0.04	0.12	0.29
+ ● ○ ○ + - ● - - ● - + ○ ○ ● +	0.04	0.12	0.36
+ - ○ ● - ● ○ + + ○ ● - ● ○ - +	0.04	-0.30	0.01
+ - ○ ● + ● ○ - - ○ ● + ● ○ - +	0.04	-0.30	0.15
+ + ○ ● - ● ○ - - ○ ● - ● ○ + +	0.04	-0.30	0.50
+ - - ○ ● + ● ○ ○ ● + ● ○ - - +	0.04	-0.59	-0.06
+ - + ○ ● - ● ○ ○ ● - ● ○ + - +	0.04	-0.59	0.22
+ + - ○ ● - ● ○ ○ ● - ● ○ - + +	0.04	-0.59	0.36
+ ○ ● - - ● + ○ ○ + ● - - ● ○ +	0.04	-0.07	0.15
+ ○ ● - + ● - ○ ○ - ● + - ● ○ +	0.04	-0.07	0.27
+ ○ ● + - ● - ○ ○ - ● - + ● ○ +	0.04	-0.07	0.36
+ ○ ● - ● ○ - + + - ○ ● - ● ○ +	0.04	0.07	0.20
+ ○ ● - ● ○ + - - + ○ ● - ● ○ +	0.04	0.07	0.22

+ - ○ ● - + ● ○ ○ ● + - ● ○ - +	0.05	-0.38	0.05
+ - ○ ● + - ● ○ ○ ● - + ● ○ - +	0.05	-0.38	0.12
+ + ○ ● - - ● ○ ○ ● - - ● ○ + +	0.05	-0.38	0.47
+ ○ ● - - ● ○ + + ○ ● - - ● ○ +	0.05	-0.05	0.14
+ ○ ● - + ● ○ - - ○ ● + - ● ○ +	0.05	-0.05	0.28
+ ○ ● + - ● ○ - - ○ ● - + ● ○ +	0.05	-0.05	0.38
+ - - ○ ● + ○ ● ● ○ + ● ○ - - +	0.06	-0.59	-0.06
+ - + ○ ● - ○ ● ● ○ - ● ○ + - +	0.06	-0.59	0.22
+ + - ○ ● - ○ ● ● ○ - ● ○ - + +	0.06	-0.59	0.36
+ ○ - ● ● - + ○ ○ + - ● ● - ○ +	0.06	-0.12	0.13
+ ○ ● - - + ● ○ ○ ● + - - ● ○ +	0.06	-0.12	0.18
+ ○ - ● ● + - ○ ○ - + ● ● - ○ +	0.06	-0.12	0.18
+ ○ ● - + - ● ○ ○ ● - + - ● ○ +	0.06	-0.12	0.25
+ ○ ● + - - ● ○ ○ ● - - + ● ○ +	0.06	-0.12	0.34
+ ○ + ● ● - - ○ ○ - - ● ● + ○ +	0.06	-0.12	0.46
+ - - ○ + ● ● ○ ○ ● ● + ○ - - +	0.07	-0.66	-0.02
+ - + ○ - ● ● ○ ○ ● ● - ○ + - +	0.07	-0.66	0.19
+ + - ○ - ● ● ○ ○ ● ● - ○ - + +	0.07	-0.66	0.33
+ - - ○ ● ○ ● + + ● ○ ● ○ - - +	0.07	-0.52	-0.09
+ - + ○ ● ○ ● - - ● ○ ● ○ + - +	0.07	-0.52	0.26
+ + - ○ ● ○ ● - - ● ○ ● ○ - + +	0.07	-0.52	0.40
+ - ○ - ● ● + ○ ○ + ● ● - ○ - +	0.07	-0.42	-0.02
+ - ○ + ● ● - ○ ○ - ● ● + ○ - +	0.07	-0.42	0.19
+ + ○ - ● ● - ○ ○ - ● ● - ○ + +	0.07	-0.42	0.45
+ - ○ ● - + ○ ● ● ○ + - ● ○ - +	0.07	-0.38	0.05
+ - ○ ● + - ○ ● ● ○ - + ● ○ - +	0.07	-0.38	0.12
+ + ○ ● - - ○ ● ● ○ - - ● ○ + +	0.07	-0.38	0.47
+ ○ - ● ● - ○ + + ○ - ● ● - ○ +	0.07	-0.09	0.12
+ ○ - ● ● + ○ - - ○ + ● ● - ○ +	0.07	-0.09	0.19
+ ○ + ● ● - ○ - - ○ - ● ● + ○ +	0.07	-0.09	0.47
+ - ○ ● - ○ ● + + ● ○ - ● ○ - +	0.08	-0.30	0.01
+ - ○ ● + ○ ● - - ● ○ + ● ○ - +	0.08	-0.30	0.15
+ + ○ ● - ○ ● - - ● ○ - ● ○ + +	0.08	-0.30	0.50

+ - ○ ● - ○ + ● ● + ○ - ● ○ - +	0.09	-0.33	0.02
+ - ○ ● + ○ - ● ● - ○ + ● ○ - +	0.09	-0.33	0.14
+ + ○ ● - ○ - ● ● - ○ - ● ○ + +	0.09	-0.33	0.49
+ - - ○ + ● ○ ● ● ○ ● + ○ - - +	0.09	-0.66	-0.02
+ - + ○ - ● ○ ● ● ○ ● - ○ + - +	0.09	-0.66	0.19
+ + - ○ - ● ○ ● ● ○ ● - ○ - + +	0.09	-0.66	0.33
+ - ○ + ● - ● ○ ○ ● - ● + ○ - +	0.09	-0.47	0.16
+ + ○ - ● - ● ○ ○ ● - ● - ○ + +	0.09	-0.47	0.42
+ - ○ ● ○ ● - + + - ● ○ ● ○ - +	0.09	-0.19	0.07
+ ○ - ● - ● + ○ ○ + ● - ● - ○ +	0.09	-0.19	0.09
+ - ○ ● ○ ● + - - + ● ○ ● ○ - +	0.09	-0.19	0.09
+ ○ - ● + ● - ○ ○ - ● + ● - ○ +	0.09	-0.19	0.21
+ ○ + ● - ● - ○ ○ - ● - ● + ○ +	0.09	-0.19	0.42
+ ○ ● - - ○ ● + + ● ○ - - ● ○ +	0.09	-0.05	0.14
+ ○ - ● ● ○ - + + - ○ ● ● - ○ +	0.09	-0.05	0.14
+ ○ - ● ● ○ + - - + ○ ● ● - ○ +	0.09	-0.05	0.16
+ ○ ● - + ○ ● - - ● ○ + - ● ○ +	0.09	-0.05	0.28
+ ○ ● + - ○ ● - - ● ○ - + ● ○ +	0.09	-0.05	0.38
+ ○ - ● - ● ○ + + ○ ● - ● - ○ +	0.11	-0.16	0.08
+ ○ - ● + ● ○ - - ○ ● + ● - ○ +	0.11	-0.16	0.22
+ ○ + ● - ● ○ - - ○ ● - ● + ○ +	0.11	-0.16	0.43
+ ○ ● - - ○ + ● ● + ○ - - ● ○ +	0.11	-0.07	0.15
+ ○ ● - + ○ - ● ● - ○ + - ● ○ +	0.11	-0.07	0.27
+ ○ ● + - ○ - ● ● - ○ - + ● ○ +	0.11	-0.07	0.36
+ ○ ● - ○ ● - + + - ● ○ - ● ○ +	0.11	0.07	0.20
+ ○ ● - ○ ● + - - + ● ○ - ● ○ +	0.11	0.07	0.22
+ ○ ● ○ ● - - + + - - ● ○ ● ○ +	0.12	0.23	0.28
+ ○ ● ○ ● - + - - + - ● ○ ● ○ +	0.12	0.23	0.30
+ - ○ + ● - ○ ● ● ○ - ● + ○ - +	0.12	-0.47	0.16
+ + ○ - ● - ○ ● ● ○ - ● - ○ + +	0.12	-0.47	0.42
+ - ○ ● ○ - ● + + ● - ○ ● ○ - +	0.12	-0.23	0.05
+ ○ - ● - + ● ○ ○ ● + - ● - ○ +	0.12	-0.23	0.12
+ - ○ ● ○ + ● - - ● + ○ ● ○ - +	0.12	-0.23	0.12

+ - ○ ● ○ - + ● ● + - ○ ● ○ - +	0.13	-0.26	0.06
+ - ○ ● ○ + - ● ● - + ○ ● ○ - +	0.13	-0.26	0.11
+ + ○ ● ○ - - ● ● - - ○ ● ○ + +	0.13	-0.26	0.53
+ ○ ● - ○ + ● - - ● + ○ - ● ○ +	0.13	0.02	0.25
+ ○ ● + ○ - ● - - ● - ○ + ● ○ +	0.13	0.02	0.41
+ ○ ● - ○ - ● + + ● - ○ - ● ○ +	0.13	0.02	0.18
+ - - ○ ○ ● ● + + ● ● ○ ○ - - +	0.14	-0.52	-0.09
+ - + ○ ○ ● ● - - ● ● ○ ○ + - +	0.14	-0.52	0.26
+ + - ○ ○ ● ● - - ● ● ○ ○ - + +	0.14	-0.52	0.40
+ - ○ - ● ○ + ● ● + ○ ● - ○ - +	0.14	-0.42	-0.02
+ - ○ + ● ○ - ● ● - ○ ● + ○ - +	0.14	-0.42	0.19
+ + ○ - ● ○ - ● ● - ○ ● - ○ + +	0.14	-0.42	0.45
+ ○ - - ● ● + ○ ○ + ● ● - - ○ +	0.14	-0.28	0.05
+ ○ - + ● ● - ○ ○ - ● ● + - ○ +	0.14	-0.28	0.26
+ ○ + - ● ● - ○ ○ - ● ● - + ○ +	0.14	-0.28	0.38
+ ○ - ● - + ○ ● ● ○ + - ● - ○ +	0.14	-0.23	0.12
+ ○ - ● + - ○ ● ● ○ - + ● - ○ +	0.14	-0.23	0.19
+ ○ + ● - - ○ ● ● ○ - - ● + ○ +	0.14	-0.23	0.40
+ ○ ● - ○ - + ● ● + - ○ - ● ○ +	0.14	0.00	0.19
+ ○ ● - ○ + - ● ● - + ○ - ● ○ +	0.14	0.00	0.23
+ ○ ● + ○ - - ● ● - - ○ + ● ○ +	0.14	0.00	0.40
+ ○ ● ○ - ● - + + - ● - ○ ● ○ +	0.15	0.16	0.25
+ ○ ● ○ - ● + - - + ● - ○ ● ○ +	0.15	0.16	0.27
+ - - ○ ○ ● + ● ● + ● ○ ○ - - +	0.15	-0.54	-0.08
+ - ○ - + ● ○ ● ● ○ ● + - ○ - +	0.15	-0.54	0.04
+ - ○ + - ● ○ ● ● ○ ● - + ○ - +	0.15	-0.54	0.13
+ - + ○ ○ ● - ● ● - ● ○ ○ + - +	0.15	-0.54	0.25
+ + ○ - - ● ○ ● ● ○ ● - - ○ + +	0.15	-0.54	0.39
+ + - ○ ○ ● - ● ● - ● ○ ○ - + +	0.15	-0.54	0.39
+ ○ - - ● ● ○ + + ○ ● ● - - ○ +	0.15	-0.26	0.04
+ ○ - + ● ● ○ - - ○ ● ● + - ○ +	0.15	-0.26	0.27
+ ○ + - ● ● ○ - - ○ ● ● - + ○ +	0.15	-0.26	0.39
+ ○ - ● - ○ ● + + ● ○ - ● - ○ +	0.15	-0.16	0.08

+ ○ ● ○ -- ● + + ● -- ○ ● ○ +	0.18	0.12	0.22
+ ○ ● ○ - + ● -- ● + - ○ ● ○ +	0.18	0.12	0.29
+ ○ ● ○ + - ● -- ● - + ○ ● ○ +	0.18	0.12	0.36
+ ○ ● ○ -- + ● ● + -- ○ ● ○ +	0.19	0.09	0.23
+ ○ ● ○ - + - ● ● - + - ○ ● ○ +	0.19	0.09	0.28
+ ○ ● ○ + -- ● ● -- + ○ ● ○ +	0.19	0.09	0.35
+ ○ -- ● + ○ ● ● ○ + ● -- ○ +	0.19	-0.33	0.07
+ ○ - + ● - ○ ● ● ○ - ● + - ○ +	0.19	-0.33	0.23
+ ○ + - ● - ○ ● ● ○ - ● - + ○ +	0.19	-0.33	0.35
+ - ○ ○ ● ● - + + - ● ● ○ ○ - +	0.19	-0.19	0.07
+ - ○ ○ ● ● + -- + ● ● ○ ○ - +	0.19	-0.19	0.09
+ ○ - ● ○ - ● + + ● - ○ ● - ○ +	0.19	-0.09	0.12
+ ○ - ● ○ + ● -- ● + ○ ● - ○ +	0.19	-0.09	0.19
+ ○ + ● ○ - ● -- ● - ○ ● + ○ +	0.19	-0.09	0.47
+ - ○ - ○ ● ● + + ● ● ○ - ○ - +	0.20	-0.40	-0.04
+ ○ -- + ● ● ○ ○ ● ● + -- ○ +	0.20	-0.40	0.11
+ ○ - + - ● ● ○ ○ ● ● - + - ○ +	0.20	-0.40	0.20
+ - ○ + ○ ● ● -- ● ● ○ + ○ - +	0.20	-0.40	0.20
+ ○ + -- ● ● ○ ○ ● ● -- + ○ +	0.20	-0.40	0.32
+ + ○ - ○ ● ● -- ● ● ○ - ○ + +	0.20	-0.40	0.46
+ ○ -- ● ○ ● + + ● ○ ● -- ○ +	0.20	-0.26	0.04
+ ○ - + ● ○ ● -- ● ○ ● + - ○ +	0.20	-0.26	0.27
+ ○ + - ● ○ ● -- ● ○ ● - + ○ +	0.20	-0.26	0.39
+ ○ - ● ○ - + ● ● + - ○ ● - ○ +	0.20	-0.12	0.13
+ ○ - ● ○ + - ● ● - + ○ ● - ○ +	0.20	-0.12	0.18
+ ○ + ● ○ -- ● ● -- ○ ● + ○ +	0.20	-0.12	0.46
+ - ○ - ○ ● + ● ● + ● ○ - ○ - +	0.21	-0.42	-0.02
+ - ○ + ○ ● - ● ● - ● ○ + ○ - +	0.21	-0.42	0.19
+ + ○ - ○ ● - ● ● - ● ○ - ○ + +	0.21	-0.42	0.45
+ ○ -- ● ○ + ● ● + ○ ● -- ○ +	0.21	-0.28	0.05
+ ○ - + ● ○ - ● ● - ○ ● + - ○ +	0.21	-0.28	0.26
+ ○ + - ● ○ - ● ● - ○ ● - + ○ +	0.21	-0.28	0.38
+ - ○ ○ ● - ● + + ● - ● ○ ○ - +	0.21	-0.23	0.05

+ ○ ○ ● ● - - + + - - ● ● ○ ○ +	0.23	0.23	0.28
+ ○ ○ ● ● - + - - + - ● ● ○ ○ +	0.23	0.23	0.30
+ - ○ ○ - ● ● + + ● ● - ○ ○ - +	0.25	-0.30	0.01
+ - ○ ○ + ● ● - - ● ● + ○ ○ - +	0.25	-0.30	0.15
+ + ○ ○ - ● ● - - ● ● - ○ ○ + +	0.25	-0.30	0.50
+ - ○ ○ - ● + ● ● + ● - ○ ○ - +	0.26	-0.33	0.02
+ - ○ ○ + ● - ● ● - ● + ○ ○ - +	0.26	-0.33	0.14
+ + ○ ○ - ● - ● ● - ● - ○ ○ + +	0.26	-0.33	0.49
+ ○ - ○ ● ● - + + - ● ● ○ - ○ +	0.26	-0.05	0.14
+ ○ - ○ ● ● + - - + ● ● ○ - ○ +	0.26	-0.05	0.16
+ ○ ○ ● - ● - + + - ● - ● ○ ○ +	0.27	0.16	0.25
+ ○ ○ ● - ● + - - + ● - ● ○ ○ +	0.27	0.16	0.27
+ ○ - - ○ ● ● + + ● ● ○ - - ○ +	0.27	-0.26	0.04
+ ○ - + ○ ● ● - - ● ● ○ + - ○ +	0.27	-0.26	0.27
+ ○ + - ○ ● ● - - ● ● ○ - + ○ +	0.27	-0.26	0.39
+ ○ - - ○ ● + ● ● + ● ○ - - ○ +	0.28	-0.28	0.05
+ ○ - + ○ ● - ● ● - ● ○ + - ○ +	0.28	-0.28	0.26
+ ○ + - ○ ● - ● ● - ● ○ - + ○ +	0.28	-0.28	0.38
+ ○ - ○ ● - ● + + ● - ● ○ - ○ +	0.28	-0.09	0.12
+ ○ - ○ ● + ● - - ● + ● ○ - ○ +	0.28	-0.09	0.19
+ ○ + ○ ● - ● - - ● - ● ○ + ○ +	0.28	-0.09	0.47
+ ○ ○ ● - - ● + + ● - - ● ○ ○ +	0.29	0.12	0.22
+ ○ ○ ● - + ● - - ● + - ● ○ ○ +	0.29	0.12	0.29
+ ○ ○ ● + - ● - - ● - + ● ○ ○ +	0.29	0.12	0.36
+ ○ - ○ ● - + ● ● + - ● ○ - ○ +	0.29	-0.12	0.13
+ ○ - ○ ● + - ● ● - + ● ○ - ○ +	0.29	-0.12	0.18
+ ○ + ○ ● - - ● ● - - ● ○ + ○ +	0.29	-0.12	0.46
+ ○ ○ ● - - + ● ● + - - ● ○ ○ +	0.30	0.09	0.23
+ ○ ○ ● - + - ● ● - + - ● ○ ○ +	0.30	0.09	0.28
+ ○ ○ ● + - - ● ● - - + ● ○ ○ +	0.30	0.09	0.35
+ ○ - ○ - ● ● + + ● ● - ○ - ○ +	0.32	-0.16	0.08
+ ○ - ○ + ● ● - - ● ● + ○ - ○ +	0.32	-0.16	0.22
+ ○ + ○ - ● ● - - ● ● - ○ + ○ +	0.32	-0.16	0.43

+ ○ ○ - ● + ● - - ● + ● - ○ ○ +	0.34	0.02	0.25
+ ○ ○ + ● - ● - - ● - ● + ○ ○ +	0.34	0.02	0.41
+ ○ ○ - ● - ● + + ● - ● - ○ ○ +	0.34	0.02	0.18
+ ○ ○ - ● - + ● ● + - ● - ○ ○ +	0.35	0.00	0.19
+ ○ ○ - ● + - ● ● - + ● - ○ ○ +	0.35	0.00	0.23
+ ○ ○ + ● - - ● ● - - ● + ○ ○ +	0.35	0.00	0.40
+ ○ ○ - - ● ● + + ● ● - - ○ ○ +	0.38	-0.05	0.14
+ ○ ○ - + ● ● - - ● ● + - ○ ○ +	0.38	-0.05	0.28
+ ○ ○ + - ● ● - - ● ● - + ○ ○ +	0.38	-0.05	0.38
+ ○ ○ - - ● + ● ● + ● - - ○ ○ +	0.39	-0.07	0.15
+ ○ ○ - + ● - ● ● - ● + - ○ ○ +	0.39	-0.07	0.27
+ ○ ○ + - ● - ● ● - ● - + ○ ○ +	0.39	-0.07	0.36

[12/12] ₁	$[\psi/-\psi/-\phi/\phi/-\phi/\phi/-\phi/\phi/-\psi/\psi/-\psi/\psi/\phi/-\phi/-\psi/\psi/\psi/-\psi/\psi/-\psi/\phi/-\phi/\phi/-\phi]_{\Gamma}$	$(\pm 52.4^{\circ}, \pm 40.9^{\circ})$	2.765
[12/12] ₂	$[\psi/-\psi/-\phi/\phi/-\phi/\phi/-\psi/\psi/-\phi/\phi/\phi/-\phi/-\psi/\psi/-\psi/\psi/\psi/-\psi/\psi/-\psi/\phi/-\phi/\phi/-\phi]_{\Gamma}$	$(\pm 52.0^{\circ}, \pm 40.7^{\circ})$	2.713
[12/12] ₃	$[\psi/-\psi/-\phi/\phi/-\phi/\phi/-\phi/\phi/-\psi/\psi/-\psi/\psi/-\psi/\psi/\phi/-\phi/\psi/-\psi/\phi/-\phi/\psi/-\psi/\phi/-\phi]_{\Gamma}$	$(\pm 51.8^{\circ}, \pm 40.5^{\circ})$	2.685
[12/12] ₄	$[\psi/-\psi/-\phi/\phi/-\phi/\phi/-\phi/\phi/-\psi/\psi/-\psi/\psi/-\psi/\psi/\psi/-\psi/\phi/-\phi/\phi/-\phi/\psi/-\psi]_{\Gamma}$	$(\pm 51.2^{\circ}, \pm 40.1^{\circ})$	2.599
[12/12] ₅	$[\psi/-\psi/-\phi/\phi/-\phi/\phi/-\psi/\psi/-\phi/\phi/-\psi/\psi/-\psi/\psi/\phi/-\phi/\phi/-\phi/\psi/-\psi/\psi/-\psi/\phi/-\phi]_{\Gamma}$	$(\pm 50.9^{\circ}, \pm 39.8^{\circ})$	2.537
[12/12] ₆	$[\psi/-\psi/-\phi/\phi/-\psi/\psi/-\phi/\phi/-\phi/\phi/\phi/-\phi/-\psi/\psi/-\psi/\psi/\psi/-\psi/\phi/-\phi/\psi/-\psi/\phi/-\phi]_{\Gamma}$	$(\pm 50.7^{\circ}, \pm 39.7^{\circ})$	2.505
[12/12] ₇	$[\psi/-\psi/-\phi/\phi/-\phi/\phi/-\psi/\psi/-\psi/\psi/-\phi/\phi/\phi/-\phi/-\psi/\psi/\psi/-\psi/\phi/-\phi/\phi/-\phi/\psi/-\psi]_{\Gamma}$	$(\pm 50.6^{\circ}, \pm 39.5^{\circ})$	2.404
[12/12] ₈	$[\psi/-\psi/-\phi/\phi/-\phi/\phi/-\psi/\psi/-\psi/\psi/-\phi/\phi/-\psi/\psi/\phi/-\phi/\phi/-\phi/\psi/-\psi/\phi/-\phi/\psi/-\psi]_{\Gamma}$	$(\pm 50.0^{\circ}, \pm 38.8^{\circ})$	2.331
[12/12] ₉	$[\psi/-\psi/-\phi/\phi/-\psi/\psi/-\phi/\phi/-\psi/\psi/-\phi/\phi/\phi/-\phi/\phi/-\phi/-\psi/\psi/\psi/-\psi/\psi/-\psi/\phi/-\phi]_{\Gamma}$	$(\pm 49.9^{\circ}, \pm 38.6^{\circ})$	2.294
[12/12] ₁₀	$[\psi/-\psi/-\phi/\phi/-\psi/\psi/-\phi/\phi/-\phi/\phi/-\psi/\psi/-\psi/\psi/\phi/-\phi/\phi/-\phi/\psi/-\psi/\phi/-\phi/\psi/-\psi]_{\Gamma}$	$(\pm 49.7^{\circ}, \pm 38.4^{\circ})$	2.255
[12/12] ₁₁	$[\psi/-\psi/-\phi/\phi/-\phi/\phi/-\psi/\psi/-\psi/\psi/-\psi/\psi/-\psi/\psi/\phi/\phi/\phi/-\phi/\phi/-\phi/\phi/-\phi/\psi/-\psi/\psi/-\psi]_{\Gamma}$	$(\pm 49.5^{\circ}, \pm 38.0^{\circ})$	2.173
[12/12] ₁₂	$[\psi/-\psi/-\phi/\phi/-\psi/\psi/-\phi/\phi/-\psi/\psi/-\phi/\phi/-\psi/\psi/\phi/-\phi/\phi/-\phi/\phi/-\phi/\psi/-\psi/\psi/-\psi]_{\Gamma}$	$(\pm 49.1^{\circ}, \pm 37.3^{\circ})$	2.040
[12/12] ₁₃	$[\psi/-\psi/-\phi/\phi/-\psi/\psi/-\psi/\psi/-\phi/\phi/-\phi/\phi/\phi/-\phi/\phi/-\phi/-\psi/\psi/\psi/-\psi/\phi/-\phi/\psi/-\psi]_{\Gamma}$	$(\pm 49.0^{\circ}, \pm 37.1^{\circ})$	1.992
[12/12] ₁₄	$[\psi/-\psi/-\psi/\psi/-\phi/\phi/-\phi/\phi/-\phi/\phi/-\psi/\psi/-\psi/\psi/\phi/-\phi/\phi/-\phi/\phi/-\phi/\psi/-\psi/\psi/-\psi]_{\Gamma}$	$(\pm 48.7^{\circ}, \pm 36.5^{\circ})$	1.891
[12/12] ₁₅	$[\psi/-\psi/-\psi/\psi/-\phi/\phi/-\phi/\phi/-\psi/\psi/-\phi/\phi/\phi/-\phi/-\psi/\psi/\phi/-\phi/\phi/-\phi/\psi/-\psi/\psi/-\psi]_{\Gamma}$	$(\pm 48.5^{\circ}, \pm 35.8^{\circ})$	1.780
[12/12] ₁₆	$[\psi/-\psi/-\psi/\psi/-\phi/\phi/-\psi/\psi/-\phi/\phi/-\phi/\phi/\phi/-\phi/\phi/-\phi/-\psi/\psi/\phi/-\phi/\psi/-\psi/\psi/-\psi]_{\Gamma}$	$(\pm 48.0^{\circ}, \pm 34.2^{\circ})$	1.525

[12/12] ₁₇	$[\psi/-\psi/-\psi/\psi/-\psi/\psi/-\phi/\phi/-\phi/\phi/-\phi/\phi/\phi/-\phi/\phi/-\phi/\phi/-\psi/\psi/\psi/-\psi/\psi/-\psi]_{\Gamma}$	($\pm 47.3^{\circ}$, $\pm 29.9^{\circ}$)	1.014
[16/8] ₁	$[\psi/-\psi/-\psi/\psi/-\psi/\psi/-\phi/\phi/-\phi/\phi/-\phi/\phi/\phi/-\phi/\phi/-\phi/\phi/-\psi/\psi/\psi/-\psi/\psi/-\psi]_{\Gamma}$	($\pm 50.5^{\circ}$, $\pm 39.4^{\circ}$)	2.899
[16/8] ₂	$[\psi/-\psi/-\phi/\phi/-\phi/\phi/-\psi/\psi/-\psi/\psi/-\psi/\psi/-\psi/\psi/\psi/-\psi/\psi/-\psi/\phi/-\phi/\phi/-\phi/\psi/-\psi]_{\Gamma}$	($\pm 50.2^{\circ}$, $\pm 39.1^{\circ}$)	2.826
[16/8] ₃	$[\psi/-\psi/-\phi/\phi/-\psi/\psi/-\phi/\phi/-\psi/\psi/-\psi/\psi/-\psi/\psi/\psi/\phi/-\phi/\psi/-\psi/\psi/-\psi/\psi/-\psi/\phi/-\phi]_{\Gamma}$	($\pm 49.8^{\circ}$, $\pm 38.6^{\circ}$)	2.709
[16/8] ₄	$[\psi/-\psi/-\phi/\phi/-\psi/\psi/-\phi/\phi/-\psi/\psi/-\psi/\psi/-\psi/\psi/\psi/-\psi/\phi/-\phi/\psi/-\psi/\phi/-\phi/\psi/-\psi]_{\Gamma}$	($\pm 49.4^{\circ}$, $\pm 37.9^{\circ}$)	2.583
[16/8] ₅	$[\psi/-\psi/-\psi/\psi/-\phi/\phi/-\phi/\phi/-\psi/\psi/-\psi/\psi/\phi/-\phi/\psi/-\psi/-\psi/\psi/\psi/-\psi/\psi/-\psi/\phi/-\phi]_{\Gamma}$	($\pm 49.2^{\circ}$, $\pm 37.5^{\circ}$)	2.493
[16/8] ₆	$[\psi/-\psi/-\psi/\psi/-\phi/\phi/-\psi/\psi/-\phi/\phi/\phi/-\phi/-\psi/\psi/-\psi/\psi/\psi/-\psi/\psi/-\psi/\psi/-\psi/\phi/-\phi]_{\Gamma}$	($\pm 48.9^{\circ}$, $\pm 37.0^{\circ}$)	2.396
[16/8] ₇	$[\psi/-\psi/-\phi/\phi/-\psi/\psi/-\psi/\psi/-\phi/\phi/-\psi/\psi/-\psi/\psi/\psi/-\psi/\phi/-\phi/\phi/-\phi/\psi/-\psi/\psi/-\psi]_{\Gamma}$	($\pm 48.7^{\circ}$, $\pm 36.4^{\circ}$)	2.291
[16/8] ₈	$[\psi/-\psi/-\psi/\psi/-\phi/\phi/-\phi/\phi/-\psi/\psi/-\psi/\psi/-\psi/\psi/\psi/-\psi/\phi/-\phi/\phi/-\phi/\psi/-\psi/\psi/-\psi]_{\Gamma}$	($\pm 48.5^{\circ}$, $\pm 35.7^{\circ}$)	2.176
[16/8] ₉	$[\psi/-\psi/-\psi/\psi/-\phi/\phi/-\psi/\psi/-\phi/\phi/-\psi/\psi/\phi/-\phi/-\psi/\psi/\psi/-\psi/\psi/-\psi/\phi/-\phi/\psi/-\psi]_{\Gamma}$	($\pm 48.3^{\circ}$, $\pm 35.4^{\circ}$)	2.115
[16/8] ₁₀	$[\psi/-\psi/-\phi/\phi/-\psi/\psi/-\psi/\psi/-\psi/\psi/-\psi/\psi/-\psi/\psi/\phi/\phi/\phi/-\phi/\phi/-\phi/\psi/-\psi/\psi/-\psi/\psi/-\psi]_{\Gamma}$	($\pm 48.0^{\circ}$, $\pm 34.0^{\circ}$)	1.909
[16/8] ₁₁	$[\psi/-\psi/-\psi/\psi/-\phi/\phi/-\psi/\psi/-\psi/\psi/-\psi/\psi/\phi/\phi/\phi/-\phi/-\psi/\psi/\psi/-\psi/\phi/-\phi/\psi/-\psi/\psi/-\psi]_{\Gamma}$	($\pm 47.7^{\circ}$, $\pm 32.9^{\circ}$)	1.749
[16/8] ₁₂	$[\psi/-\psi/-\psi/\psi/-\phi/\phi/-\psi/\psi/-\psi/\psi/-\phi/\phi/-\psi/\psi/\phi/-\phi/\phi/-\phi/\psi/-\psi/\psi/-\psi/\psi/-\psi]_{\Gamma}$	($\pm 47.5^{\circ}$, $\pm 31.5^{\circ}$)	1.566
[16/8] ₁₃	$[\psi/-\psi/-\psi/\psi/-\psi/\psi/-\phi/\phi/-\phi/\phi/-\psi/\psi/-\psi/\psi/\phi/-\phi/\phi/-\phi/\psi/-\psi/\psi/-\psi/\psi/-\psi]_{\Gamma}$	($\pm 47.2^{\circ}$, $\pm 29.6^{\circ}$)	1.352

[16/8] ₁₄	$[\psi/-\psi/-\psi/\psi/-\psi/\psi/-\phi/\phi/-\psi/\psi/-\phi/\phi/-\phi/-\psi/\psi/\phi/-\phi/\psi/-\psi/\psi/-\psi/\psi/-\psi/\psi/-\psi]_{\Gamma}$	(±47.0°, ±26.7°)	1.098
[16/8] ₁₅	$[\psi/-\psi/\psi/-\psi/\psi/-\psi/\psi/-\psi/\phi/-\phi/\phi/-\phi/-\phi/\phi/-\phi/\phi/-\psi/\psi/-\psi/\psi/-\psi/\psi/-\psi/\psi]_{\Gamma}$	(±46.3°, ±6.58°)	0.456
[20/4] ₁	$[\psi/-\psi/-\phi/\phi/-\psi/\psi/-\psi/\psi/-\psi/\psi/-\psi/\psi/-\psi/\psi/-\psi/\psi/\psi/-\psi/\psi/-\psi/\psi/-\psi/\phi/-\phi/\psi/-\psi]_{\Gamma}$	(±48.7°, ±36.3°)	2.976
[20/4] ₂	$[\psi/-\psi/-\psi/\psi/-\phi/\phi/-\psi/\psi/-\psi/\psi/-\psi/\psi/-\psi/\psi/-\psi/\psi/\psi/-\psi/\psi/-\psi/\phi/-\phi/\psi/-\psi/\psi/-\psi]_{\Gamma}$	(±47.7°, ±32.7°)	2.447
[20/4] ₃	$[\psi/-\psi/-\psi/\psi/-\psi/\psi/-\phi/\phi/-\psi/\psi/-\psi/\psi/-\psi/\psi/-\psi/\psi/\psi/-\psi/\phi/-\phi/\psi/-\psi/\psi/-\psi/\psi/-\psi]_{\Gamma}$	(±46.9°, ±26.1°)	1.749

A6 20-PLY DD LAMINATES RESULTS

TABLE A3: 20-ply designs, stacking sequences and ψ_{\pm} , ϕ_{\pm} values that produce bending stiffness that matches that $(\zeta_9, \zeta_{10}) = (-0.102, -0.692)$.

Design	Stacking sequence	$(\pm\psi, \pm\phi)$	Normalised FPF strength
Quad	$[+/-/-/\bullet/+/+/-/\circ/\circ/\bullet/\bullet/\circ/\circ/-$ $/+/+/\bullet/-/-/+]_T$	-	1
$[4/16]_1$	$[\psi/-\psi/-\phi/\phi/-\phi/\phi/-\phi/\phi/-\phi/\phi/-\phi/\phi/-$ $\phi/\phi/-\phi/\phi/-\phi/-\psi/\psi]_T$	$(\pm 59.7^\circ, \pm 37.2^\circ)$	1.690
$[8/12]_1$	$[\psi/-\psi/-\phi/\phi/-\phi/\phi/-\phi/\phi/-\phi/\phi/-\phi/\phi/-$ $\phi/\phi/-\phi/\phi/-\phi/-\psi/\psi]_T$	$(\pm 64.0^\circ, \pm 39.9^\circ)$	2.160
$[8/12]_2$	$[\psi/-\psi/-\phi/\phi/-\phi/\phi/-\phi/\phi/-\psi/\psi/\phi/-\phi/-$ $\psi/\psi/\phi/-\phi/\psi/-\psi/\phi/-\phi]_T$	$(\pm 61.5^\circ, \pm 38.6^\circ)$	2.020
$[8/12]_3$	$[\psi/-\psi/-\phi/\phi/-\phi/\phi/-\phi/\phi/-\psi/\psi/-\psi/\psi/\phi/-$ $\phi/\phi/-\phi/\phi/-\phi/\psi/-\psi]_T$	$(\pm 59.5^\circ, \pm 37.1^\circ)$	1.833
$[8/12]_4$	$[\psi/-\psi/-\phi/\phi/-\phi/\phi/-\psi/\psi/-\phi/\phi/\phi/-\phi/-$ $\psi/\psi/\phi/-\phi/\phi/-\phi/\psi/-\psi]_T$	$(\pm 58.3^\circ, \pm 35.9^\circ)$	1.686
$[8/12]_5$	$[\psi/-\psi/-\psi/\psi/-\phi/\phi/-\phi/\phi/-\phi/\phi/\phi/-\phi/\phi/-$ $\phi/\phi/-\phi/-\psi/\psi/\psi/-\psi]_T$	$(\pm 56.4^\circ, \pm 33.1^\circ)$	1.345
$[8/12]_6$	$[\psi/-\psi/\psi/-\psi/\phi/-\phi/\phi/-\phi/\phi/-\phi/-\phi/\phi/-$ $\phi/\phi/-\phi/\phi/-\psi/\psi/-\psi/\psi]_T$	$(\pm 53.8^\circ, \pm 25.8^\circ)$	0.743
$[12/8]_1$	$[\psi/-\psi/-\phi/\phi/-\phi/\phi/-\psi/\psi/-\psi/\psi/-$ $\psi/\psi/\phi/-\phi/\psi/-\psi/\psi/-\psi/\phi/-\phi]_T$	$(\pm 59.3^\circ, \pm 36.9^\circ)$	2.372
$[12/8]_2$	$[\psi/-\psi/-\phi/\phi/-\phi/\phi/-\psi/\psi/-\psi/\psi/-$ $\psi/\psi/\psi/-\psi/\phi/-\phi/\phi/-\phi/\psi/-\psi]_T$	$(\pm 58.2^\circ, \pm 35.7^\circ)$	2.203
$[12/8]_3$	$[\psi/-\psi/-\phi/\phi/-\psi/\psi/-\phi/\phi/-\psi/\psi/\phi/-\phi/-$ $\psi/\psi/\psi/-\psi/\psi/-\psi/\phi/-\phi]_T$	$(\pm 57.6^\circ, \pm 35.1^\circ)$	2.111
$[12/8]_4$	$[\psi/-\psi/-\phi/\phi/-\psi/\psi/-\phi/\phi/-\psi/\psi/-$ $\psi/\psi/\phi/-\phi/\psi/-\psi/\phi/-\phi/\psi/-\psi]_T$	$(\pm 56.2^\circ, \pm 32.8^\circ)$	1.808
$[12/8]_5$	$[\psi/-\psi/-\phi/\phi/-\psi/\psi/-\psi/\psi/-\phi/\phi/\phi/-\phi/-$ $\psi/\psi/\psi/-\psi/\phi/-\phi/\psi/-\psi]_T$	$(\pm 55.3^\circ, \pm 30.9^\circ)$	1.582

[12/8] ₆	$[\psi/-\psi/-\phi/\phi/-\psi/\psi/-\psi/\psi/-\phi/\phi/-\psi/\psi/\phi/-\phi/\phi/-\phi/\psi/-\psi/\psi/-\psi]_{\Gamma}$	$(\pm 54.5^{\circ}, \pm 28.5^{\circ})$	1.337
[12/8] ₇	$[\psi/-\psi/-\psi/\psi/-\phi/\phi/-\phi/\phi/-\psi/\psi/-\psi/\psi/\phi/-\phi/\phi/-\phi/\psi/-\psi/\psi/-\psi]_{\Gamma}$	$(\pm 53.6^{\circ}, \pm 25.2^{\circ})$	1.076
[12/8] ₈	$[\psi/-\psi/-\psi/\psi/-\phi/\phi/-\psi/\psi/-\phi/\phi/\phi/-\phi/-\psi/\psi/\phi/-\phi/\psi/-\psi/\psi/-\psi]_{\Gamma}$	$(\pm 52.8^{\circ}, \pm 20.0^{\circ})$	0.806
[16/4] ₁	$[\psi/-\psi/-\phi/\phi/-\psi/\psi/-\psi/\psi/-\psi/\psi/-\psi/\psi/\psi/-\psi/\psi/-\psi/\phi/-\phi/\psi/-\psi]_{\Gamma}$	$(\pm 55.2^{\circ}, \pm 30.6^{\circ})$	2.669
[16/4] ₂	$[\psi/-\psi/-\psi/\psi/-\phi/\phi/-\psi/\psi/-\psi/\psi/-\psi/\psi/\psi/-\psi/\phi/-\phi/\psi/-\psi/\psi/-\psi]_{\Gamma}$	$(\pm 52.6^{\circ}, \pm 18.8^{\circ})$	1.531